UNIVERSITAT DE BARCELONA

Tectonic structure and formation kinematics of the Western Mediterranean basins

Marina Viñas Gaza

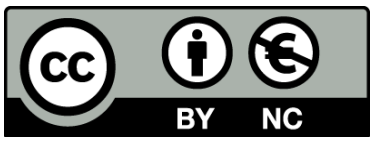

Tectonic structure and formation kinematics of the Western Mediterranean basins

Memòria presentada per

Marina Viñas Gaza

per optar al grau de Doctor per la Universitat de Barcelona

Aquesta memòria s'ha dut a terme dins del Programa de Doctorat de Ciències de la Terra de la Universitat de Barcelona sota la direcció del Dr. César Rodríguez Ranero i sota la tutela del Dr. Juanjo Ledo Fernández

Barcelona, novembre de 2016

Vinyes verdes vora el mar,
ara que el vent no remuga,
us feu més verdes i encar
teniu la fulla poruga,
vinyes verdes vora el mar.

Aquetes paraules van adreçades a totes les persones que d'una manera o altre han fet possible el desenvolupament i final d'aqueta tesi.

Al meu director *César Rodríguez Ranero* per ensenyar-me i guiar-me durant aquets quatre anys, per orientar-me durant la travessa pel desert del doctorand i animar-me quan aqueta es feia llarga.

Al *Ben De Mol* i a *l'Alcinoe Calahorrano* per la seva dedicació i paciència infinita a l'hora d'ensenyar-me les claus del processat sísmic.

Als meus supervisors durant les estades a l'estranger, a la *Dra. Paraskevi Nomikou* per fer-me sentir com a casa i al *Dr. Dirk Klaeschen* per fer de la física un món fascinant.

A mi compi de despacho, de sótano, de desayunos en silencio, de risas y muchos llantos, de siestas mirando al infinito, meriendas gochas y sábados en el TKmax, *Laura* te quiero.

A la *Clàudia*, l'*Estela*, el *Miquel* i el *Dani* companys de torn, de pis, de tertúlies de cafè, de viatges interiors, de sopars de reencuantro, de festes majors, de concerts de puta mare! La història amb vosaltres no s'acaba!

A tots els companys del *CMIMA*, els que hi són i els que han continuat camins ben lluny, gràcies.

A la meva *mare* i la meva *germana*, per ser tant fortes i valentes i al meu *pare*, que tot i no ser-hi sempre m'acompanya. Aqueta tesi ha estat possible gràcies a vosaltres, sóc tot el que m'heu ensenyat.

Finalment, a tu *Sergio*, gràcies per la teva ajuda, per la teva paciència, per la teva dedicació i sobretot, gràcies per pujar aquell avió i voler iniciar amb mi aquet llarg viatge.

A tots,

Gràcies.

Funding

The author of this thesis has benefited from a four-year Formación de Personal Investigador (FPI) fellowship (reference CTM2011-30400-C02-01) from Ministerio de Economía y Competitividad (MINECO) between 2012 and 2016. The author was also granted, within the framework of the FPI, with the following two stays: 2 months at the Laboratory of Research and Management of Natural Hazards of the National and Kapodistrian University of Athens (Athens-Greece) (reference EEBB-I-2014-08538), and 3 months at the Department of Marine Geodynamics of the GEOMAR Helmholtz-Centre for Ocean Research Kiel (Kiel-Germany) (reference EEBB-I-2015-10093). This work was carried out within the Grup de Recerca Consolidat de la Generalitat de Catalunya *Barcelona Centre for Subsurface Imaging* (B-CSI) (2014SGR940). The group computer and software facilities have been largely funded with the projects Kaleidoscope, CO-DOS, Geomargen-1, and CODOS-Phase2 funded by Repsol.

CONTENTS

Part VI: References

ANNEX

Summary

In this work we present a geophysical study of three Western Mediterranean basins: Valencia Trough, Gulf of Lions and Algero-Balearic Basin. The work aims to define the tectonic structure, nature of the basement, and to discuss the age, kinematics and mechanisms involved in basin formation. To study the basins we have gathered all deep penetrating seismic data available in the region consisting on several academic and industry data reprocessed and interpreted for this work.

To study the Valencia Trough Basin structure, we reprocessed from field data the 400 km-long multichannel seismic line ESCI-Valencia acquired in 1992 by Geco-Prakla's survey vessel M.V. Bin Hai supported by the Spanish "Plan Nacional de I+D" with reference projects GEO89-0858 and GEO90-0733. We reprocessed the stack of the 170 km-long VALSIS-819 multichannel seismic line acquired in 1988 by the Lamont-Doherty Earth Observatory Research Vessel (R/V) Robert D. Conrad. We have also interpreted an industry seismic grid SGV01 acquired in 2001 by the Fugro-Geoteam vessel R.V. Geo Baltic.

To study the Gulf of Lions Basin formation we interpreted an industry dataset SPBAL01 acquired in 2001 by Spectrum Energy with the Polar Princes vessel. Some amount of post-migration cosmetic processing was done on some of the lines of this data set for presentation purposes.

To study the tectonic structure of the Algero-Balearic Basin we processed a 97 km-long multichannel seismic line TOPOMED-26 acquired by our group and with my participation in 2011 on-board the Spanish R/V Sarmiento de Gamboa. In order to discuss the nature of the basement of the Algero-Balearic Basin, we also used the Vp model of the wide-angle seismic profile P03 from the WESTMED project. Moreover we have done "mirror imaging" with Ocean Bottom Seismometers along line P04 of WESTMED, and integrated the results of line ESCI-Valencia across the south-Balearic margin.

The analysis, processing and interpretation of all this dataset allows us to a novel interpretation of a series of aspects regarding the structure and nature of the crust, and to discuss some new proposals for the tectonic processes that have led to the current configuration of the main Western Mediterranean basins.

Seismic interpretation of the Valencia Trough reveals that this basin is possibly floored by continental crust and it is possibly the oldest Western Mediterranean basin. Contrary to what it is typically interpreted; we propose that the present day configuration of the Valencia Trough is strongly dominated by the tectonic activity of Mesozoic structures. During

Mesozoic times occurred the greatest thinning of the crust yielding a minimum crustal thickness of ~4.5 km under the Columbretes Basin (SW Valencia Trough). Multichannel seismic sections show that the main tectonic structures are Mesozoic in age and reveal that the Neogene extensional event is very limited comparatively and has had a minor influence in the formation of the current crustal structure of the Valencia Trough. We also found no evidence of any relevant crustal thickening during Paleogene times. Thus our interpretation supports that the extension leading to the crustal configuration of the Valencia Trough was largely formed during Mesozoic times.

Interpretation of a grid of multichannel seismic profiles in the Gulf of Lions supports the existence of three geological domains that are: 1) a continental domain formed by normal faults that tilted the continental basement with syn-rift sediment infill. 2) a ~100 km wide transition domain between continental and clear oceanic domain, characterized by a thin anomalous layer with high velocity (7.5 km s^{-1}) that has been debated in the literature and that we interpret as exhumed and serpentinized mantle peridotite and 3) an oceanic domain characterized by thin oceanic crust (~5 km) with little evidence of important faulting.

Multichannel seismic results from Algero-Balearic Basin have been complemented with information provided by a Vp wide-angle tomographic model coincident with one of the seismic reflection lines. A comparison of depth-velocity profiles of the tomographic model with existing 1D velocity-depth compilations of continental and oceanic crust (e.g. White *et al.*, 1992; Christensen and Mooney, 1995) gives clues on the nature of the basement. The results reveal the existence of three main geological and geophysical domains: 1) a continental domain, with little evidence of faulted and tilted blocks (which are common features on extensional margins), although the vertical velocity structure matches well the Vp compilation for continental crust (Christensen and Mooney, 1995). The Vp data, seismic images and previous works on the region available in literature support abundant magmatism (with volcanism) during extension of soon after. 2) A narrow continent-ocean domain with vertical velocities neither typically continental crust nor oceanic crust and 3) a clear oceanic domain characterized by 6 km thick oceanic crust, with a vertical velocity gradient of oceanic layer 2 and 3, even though in this case formed in a back-arc context.

A new kinematic model for the opening of the Western Mediterranean basins is beyond the scope of our work, and requires integration with other datasets from Tyrrhenian and Alboran Basins, and an extended study of the West Sardinia and Corsica margins. Also, to advance in such model, it requires a detailed reconstruction of submarine volcanic activity, imaged in the seismic data in all three basins but inadequately studied in available literature.

Nonetheless, the results of this work should be considered in the future for new reconstructions that we propose need to be reviewed.

Part I:

Introduction

Chapter 1: Introduction

1.1 Basic concepts

1.1.1 Fundaments of plate tectonics

The **lithosphere** is the hard and rigid outer layer of the Earth. It is composed by the crust and upper mantle (Figure 1.1) and it deforms fundamentally elastically. The lithosphere is thinnest in the oceanic regions (from 2-4 km at mid ocean ridges to about 100 km for old lithosphere) and generally thicker in continental regions (from tens to about 200-250 km in cratons and shields). The lithosphere is fragmented into a small number of nearly rigid plates, tectonic plates that move relative to one another as they ride on top of a hotter, more viscous material, the **asthenosphere** (Figure 1.1). This model is the premise for the plate tectonics theory that describes the large-scale motion of these tectonic plates, stating that most of the deformation that results from their motion is accommodated along the edge, or boundary of the plates. There are three types of plate boundaries:

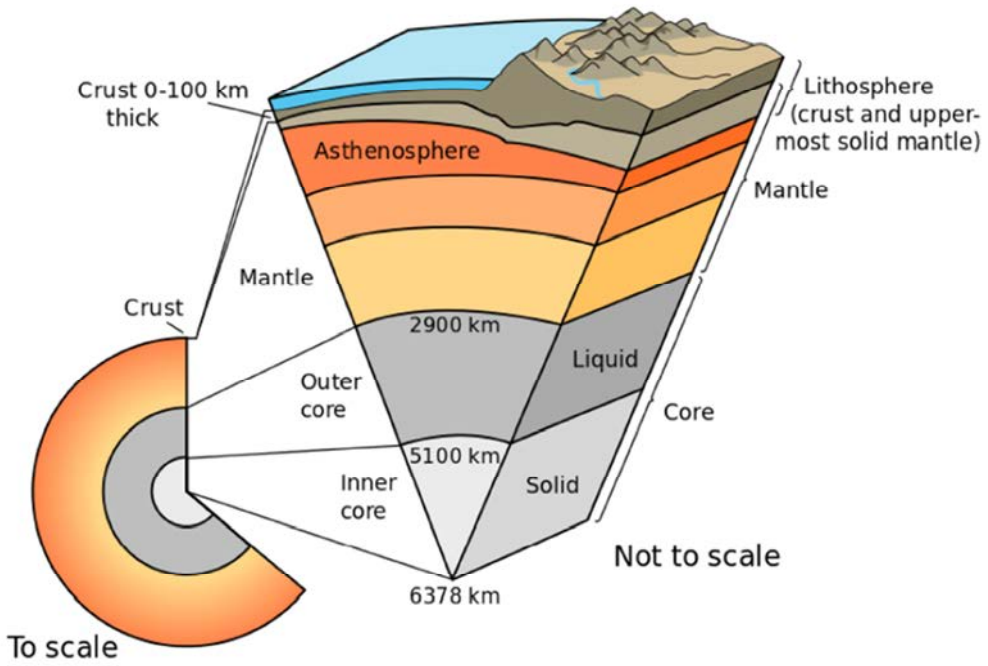

Figure 1.1. *Scheme of the Earth's internal structure showing the distribution of the crust, mantle and core. http://pubs.usgs.gov/gip/dynamic/inside.html*

1. **Divergent** (accretional or constructive), where plates are moving away from each other. At such boundaries new plate material is added to the lithosphere. They are normally represented by mid-ocean ridges or continental rifts (Figure 1.2).

2. **Convergent** (consuming or destructive), where plates approach each other. Most such boundaries are represented by oceanic trench, island-arc systems of subduction zones, where the denser plate of the two colliding plates descends into the mantle and is destroyed (Figure 1.2).

3. **Conservative**, where the tectonic plates move laterally to each other and are neither created nor destroyed, represented by transform or strike-slip fault systems (Figure 1.2).

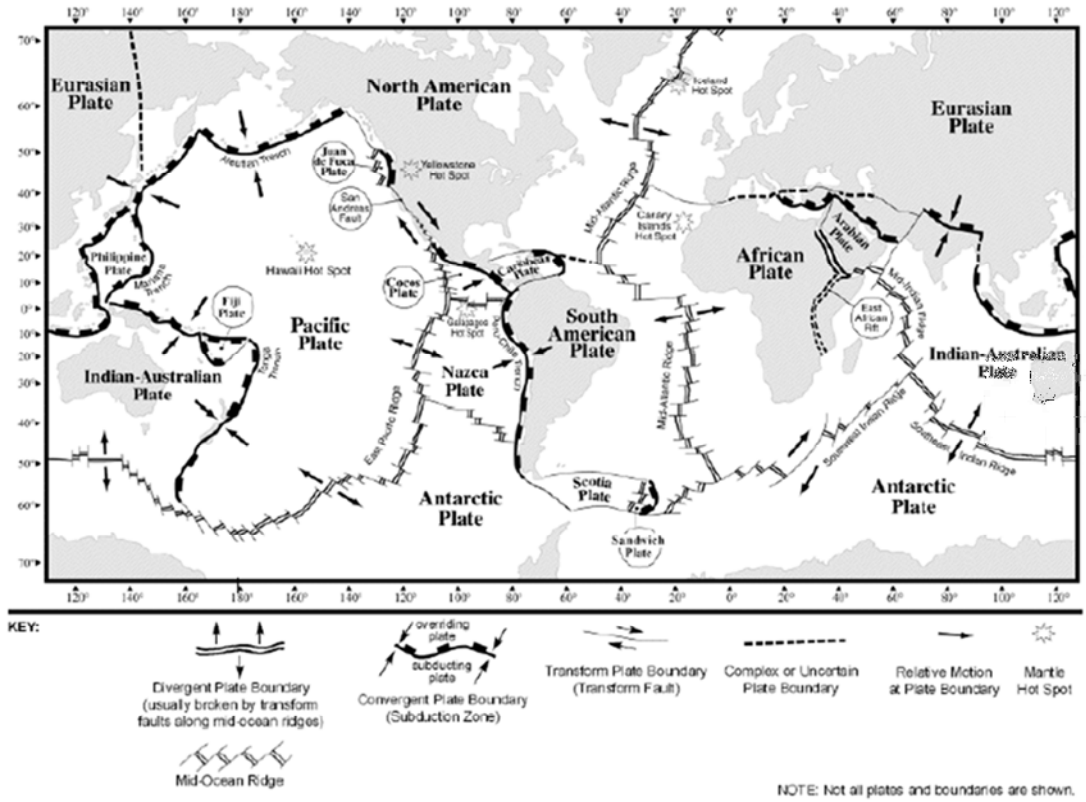

Figure 1.2. *Worldwide map showing the different types of plate boundary and the name of major tectonic plates. Black arrows indicate the relative movement between plates (Fowler, 1990)*

Based on geophysical and geological observations there are two kinds of crust: **continental crust** and **oceanic crust**.

The **continental crust** is composed by igneous, metamorphic and sedimentary rocks formed from mantle material typically involved in multiple episodes of melting, crystallization, accretion, subduction, erosion, metamorphism, plutonism and volcanism. Despite all this variability, the continental crust generally consists basically of two layers: the continental upper crust, with a composition close to granodiorite and the continental lower crust more close to granulite composition. In general, the average composition of the continental crust is more silica-rich than oceanic basalts. The average thickness and density is 35 km and 2.7 g/cm^3, respectively (Allaby, 2008). Christensen and Mooney (1995) global compilation indicates that in the upper crust P-wave seismic velocities usually range between 5.9-6.3 km/s and in the middle and lower crust the average velocity increases and ranges between 6.5 and 6.8 km/s. The difference between the felsic crust and the mantle peridotite is represented by a sharp velocity contrast, where velocities jump from ~6.8 km/s to 8.0-8.2 km/s (Fowler, 1990; Christensen and Mooney, 1995).

The **oceanic crust** is created at mid-ocean ridges when the plates move away from each other. The hot mantle rock flows upward to the gap created by the plate divergence and cools accreting to the base of the spreading plates. The oceanic crust sequence is commonly interpreted to be similar to the onland outcrops known as **"ophiolite complex**" with a large stratiform sequence of rock units, from top to bottom: basaltic pillow lavas, sheeted diabase dike complex, layered and non-layered gabbroic to ultramafic rocks. These ophiolitic rock units lay above melt-depleted peridotites, interpreted as residual upper mantle. The seismic structure of the oceanic crust is interpreted in terms of two velocity layers. **Layer 2** (extrusive basaltic pillows and sheeted lavas), is the region of oceanic crust in which the seismic velocity increases rapidly with depth from ~3.5 km/s to ~6.2 km/s in ~2 km of crust (gradients of 1-2 km s^{-1}) (Fowler, 1990; White *et al.*, 1992). It has been proposed that layer 2 can be subdivided into three layers, 2A, 2B and 2C, near the mid ocean ridge with P-wave velocities of 3.5, 4.8–5.5 and 5.8–6.2 km s^{-1}, respectively (Fowler, 1990). The average thickness of layer 2 is 1.5-2 km with a density between 1.6-2.7 g/cm^3 (Carlson and Herrick, 1990). **Layer 3** (gabbroic rocks) is the thickest oceanic layer, with an average thickness of 5 km (Allaby, 2008). Seismic velocities in Layer 3 range from ~6.5 km/s on top to ~7.2 km/s at the base of the crust, which means a velocity gradient of 0.1-0.2 s^{-1} (White *et al.*, 1992). The average density of this layer ranges from 2.9-3.0 g/cm^3 (Carlson and Herrick, 1990).

Finally, the **upper mantle** underlying the oceanic crust is composed by ultramafic rocks (peridotite) and has a density of 3.3 g/cm^3. Sometimes, the minerals forming the peridotites suffer a hydration and low temperature metamorphic transformation resulting in a new rock referred to as serpentinite. The alteration process is named **serpentinization**.

The crust is distinguished from the upper mantle by the change in chemical composition that takes place at the Moho or Mohorovicic discontinuity. Immediately above the Moho, the velocities of primary seismic waves (P-waves) are consistent with those through basalt (6.7–7.2 km/s), and below they are similar to those through peridotite (7.6–8.6 km/s). However, highly serpentinized mantle can have seismic velocities and densities similar to crustal rocks and it is often difficult to distinguish geophysically.

The formation and evolution of these different plate boundaries (divergent, convergent and conservative) are inter-related. This relationship between processes is especially evident in the Western Mediterranean basins where the continental extension (**rifting**) is originated in a **back-arc** context triggered by the retreat of the **subduction** slab. In the following section we present a revise of the fundaments of these processes.

1.1.2 Rifted margin

In the past, rifted margins have been classified as volcanic or non-volcanic margins. These terms are somewhat misleading as non-volcanic margins exhibit some limited magmatism, and therefore they are currently classified as rifted margins **"magma-poor"** or **"magma-dominated"** (e.g. so Reston, 2009) depending on whether less or more magmatism is observed than might be expected during the rifting above the normal asthenosphere (Figure 1.3).

Magma-dominated margins are characterized by thick wedges (up to 15 km) of volcanic flows manifested in seismic reflection data as seaward dipping reflectors (SDRs), and high velocity (Vp > 7.3 km/s) lower crust seaward of the continental rifted margin (e.g. Franke, 2013). Magma-dominated margins are often associated with the generation of large amounts of magmas during their formation, emplaced on top or at the base of the crust. The large amounts of magma produced in this type of margins cannot be explained only by decompression melting.

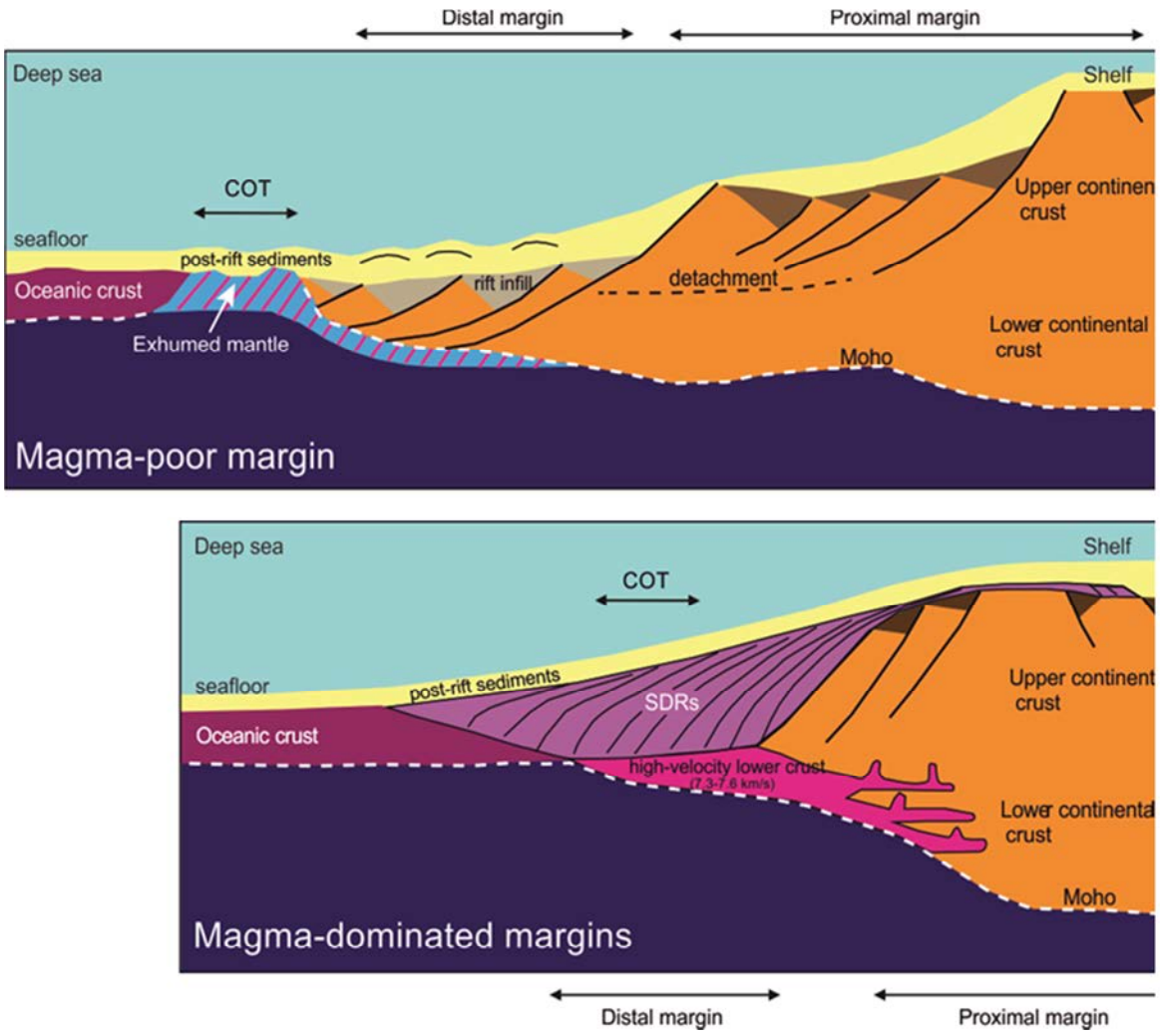

Figure 1.3. *Scheme of the two types of rifted margins, magma poor and magma dominated margins. The figure shows the position of the COT (continent-ocean transition zone) in both cases. SDRs: seaward dipping reflectors. After Doré and Ludin, 2015.*

There are several hypotheses regarding the origin for this excessive magmatism, these are: 1) mantle plume with elevated temperatures (White and McKenzie, 1989; White *et al*., 2008); 2) small-scale convection at the base of the lithosphere (Mutter *et al*., 1982; King and Anderson, 1995); and 3) heterogeneities in mantle source composition (Korenaga and Kelemen, 2000; Korenaga, 2004). Independently of the process involved in the formation of the margin, thinning of the magma-dominated margins typically occurs over a considerably short distance (50-100 km) and for that reason the Continent-Ocean transition (COT) is abrupt and narrow, located in the vicinity of the SDRs (e.g. Franke, 2013).

Magma-poor rifted margins do not present such features. Boillot *et al*. (1980) proposes that the margin is divided in a proximal and distal margin. The proximal margin is characterized

by the presence of high-angle and listric faults related to the fault-bounded rift basins while the distal margin is characterized by extremely thinned crust that is often separated from the oceanic crust by a domain of exhumed mantle. In this case, the COT occurs more progressively along a wide (~100-200 km) region where the mantle can eventually be exhumed without any associated melting due to the progressive extension (Boillot *et al*., 1980; Pérez-Gussinyé *et al*., 2001; Reston, 2009). In most models an intracrustal detachment is interpreted somewhere between the brittle upper crust and the mantle at the proximal margin, while at the distal margin brittle upper crust and upper mantle are separated by only a thin lower crustal layer or are juxtaposed. This leads to coupling and the formation of a detachment at the crust-mantle boundary, allowing the exhumation of the mantle further seaward (e.g. Franke, 2013). Figure 1.3 summarizes the overall crustal structure along magma-dominated and magma-poor rifted margins.

1.1.3 Subduction zones

The process of subduction starts when a newly created oceanic lithosphere moves away from an **ocean ridge**, it cools, thickens and becomes denser (Turcotte and Schubert, 2002). This cold and dense oceanic lithosphere becomes heavy enough to be gravitationally unstable with respect to the hot mantle rocks immediately underlying the lithosphere. As a result of this gravitational instability, the oceanic lithosphere founders and begins to sink into the mantle at the **ocean trenches** whereas the other plate, which is less dense, remains in the surface overriding the subducting lithosphere (Figure 1.4).

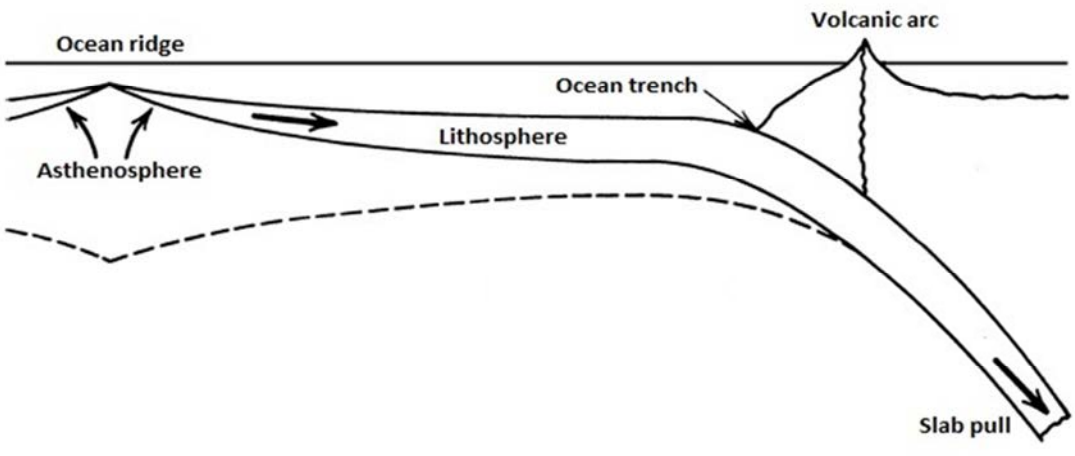

Figure 1.4. *Conceptual scheme of accretion of a lithospheric plate at mid-ocean ridges and its subduction at ocean trenches. After Turcotte and Schubert, 2002.*

Because the lithosphere behaves elastically, it can transmit stresses and act as a stress guide. **Slab pull** is the body force acting on the descending plate and transmitted to the surface plate, which is pulled toward the ocean trench (Figure 1.4). This driving force is considered to be the main mechanism causing plate tectonics and continental drift (Turcotte and Schubert, 2002). Ocean trenches are the sites of most of the greatest earthquakes. These earthquakes occur on the fault zone separating the descending lithosphere from the overriding lithosphere (1960 Chilean earthquake, 2004 Sumatra earthquake, 2011 Japan earthquake). Intraslab earthquakes within a cold subducting lithosphere are caused by a suite of mechanisms and extend to depths of ~660 km, defining the so-called Wadati-Benioff zone that in turn allows the definition of the location and geometry of the descending slab (Turcotte and Schubert, 2002).

Volcanism is also associated with subduction. In almost all cases, a line of regularly spaced volcanoes is present nearly parallel to the oceanic trench. This structure is known as the **volcanic arc** (Figure 1.4). Volcanic arcs lay 125 to 175 km above the descending plate and originates due to the fluids of the descending oceanic plate that induce melting in the overlaying mantle wedge and create sufficient buoyancy in the partially melted mantle wedge rock to generate an ascending flow (Figure 1.4) (Turcotte and Schubert, 2002).

1.1.4 Back-arc basins

In some trench systems, a secondary accretionary plate system lies behind the volcanic arc. This back-arc spreading is very similar to the seafloor spreading occurring at ocean ridges (Turcotte and Schubert, 2002). The evolution of back-arc basins has two main stages. In the first stage, the crust of the overriding plate is affected by extensional faulting forming a rift. If tensional stresses continue affecting the overriding plate, then the marginal rift evolves and the continental crust breaks off and a spreading centre similar to those found at ocean ridges is generated. Based on geological and geophysical observations of several well-known examples of bac-arc basins in the Western Pacific, Martinez *et al*. (2007) present two general models of back-arc basin formation (Figure 1.5). Although both cases develop in convergence contexts, the relative motion between the plates results in a divergent setting.

In one scenario, the velocity of subduction is higher than the velocity of convergence. In this case, the back-arc basin is assumed to be developed in a slab rollback setting (Figure 1.5 left-hand panels). Alternatively, a second scenario proposes that the overriding plate may be moving away from the trench (Figure 1.5 right-hand panels). In this model, the slab acts as a

sea anchor in the mantle resisting the migration of the oceanic trench with the retreating overriding plate (Martinez *et al.*, 2007).

Back-arc basins develop by a first stage of rifting that in subduction systems is typically near the volcanic arc front. Magmatism in volcanic arcs is strongly influenced by hydrous flux melting from the subducted slab. As the rifting evolves and separates from the arc through time, magma production changes towards a process referred as pressure release melting due to the decreasing pressure in the hot upwelling mantle that causes a partial melting (Martinez *et al.*, 2007). Therefore, crustal composition evolves from felsic composition with strong slab chemical influence, toward mafic mid-ocean ridge basalts MORB that characterize seafloor spreading in the open oceans (Gribble *et al.*, 1998).

Western Mediterranean basins are back-arc systems that show a change in behaviour through time, their present day geometry that appears to be the result of changes in the subduction system configuration. In the next section, we review the main studies that that influenced the theories of the evolution of the Western Mediterranean. In particular, we stress changes in techniques as seismic tomography and full-waveform inversion of the mantle, which produced a qualitative leap in understanding the processes that governed the formation and evolution of the Western Mediterranean basins.

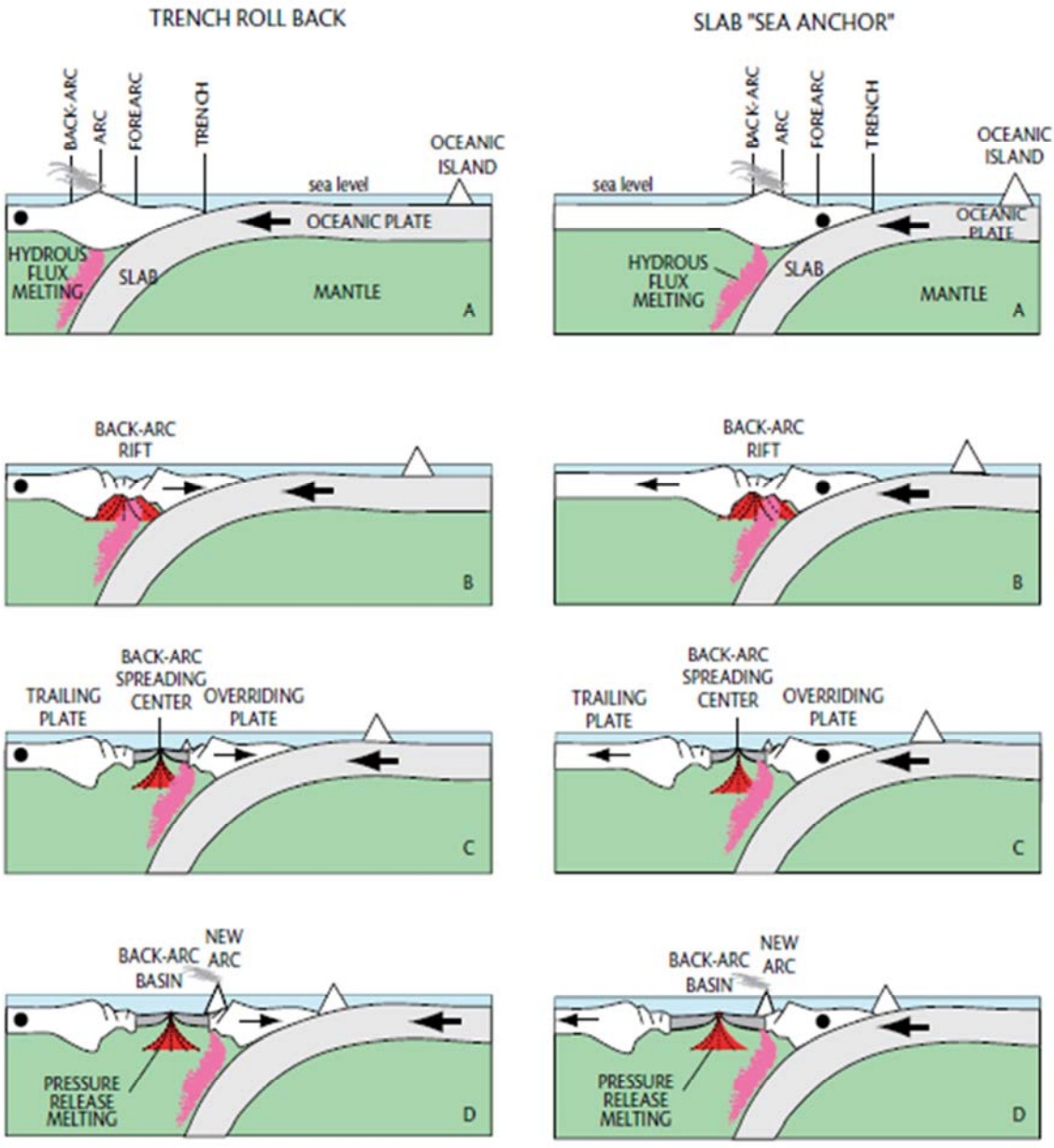

Figure 1.5. *Models of back-arc basin formation. Left panels show the back-arc opening with a slab rollback as a dredging mechanism. Note that the oceanic trench moves away from the fixed overriding plate (black dot). Right panels show the opening of a back-arc basin with a fixed trench (black dot). In this case, the overriding plate stretched away from the trench. Red areas define the back-arc spreading centre and pink areas the flux melting (Martinez et al., 2007).*

1.2 Western Mediterranean basins: a natural laboratory of Earth Sciences

The Western Mediterranean basins and surrounding areas constitute a natural laboratory for studying active geodynamic processes related to convergent boundaries, such as passive subduction of oceanic lithosphere, back-arc rifting and subduction-related volcanism. Progress in deep imaging, mantle tomography, and reflection and wide-angle seismic data during the last ~35 years have considerably improved our understanding of the lithospheric structure and the evolution of the Mediterranean basins and adjacent fold and thrust belts. To know about the deep architecture and the processes that have led to the present-day basins configuration is not only useful for hydrocarbon industry or academic research, but has also major social implications. A good knowledge of the interaction between deep geodynamic processes and surface processes is a requisite for risk assessment (e.g. earthquakes, volcanic eruptions, landslides) in highly populated areas as the Mediterranean shores and their hinterlands.

1.2.1 First kinematic models

Numerous reconstructions of the tectonic evolution of the Western Mediterranean basins have been published during last three decades. First geological evolution models (e.g. Rehault *et al*., 1984) are based on interpretations of geology, magnetic anomalies, paleomagnetic studies, volcanism and earthquake seismicity data (Rehault *et al*., 1984; Dewey *et al*., 1989; Lonergan and White, 1997; Gueguen *et al*., 1998; Frizon de Lamotte *et al*., 2000; Jolivet and Faccenna, 2000; Gelabert *et al*., 2002; Rosenbaum *et al*., 2002). Also, there were some studies combining tectonic reconstructions and the first results of mantle tomography, which were still limited because the uncertainties in delay-time tomography, but already suggested the presence of deep slabs in the Calabrian and Alboran regions (Blanco and Spakman, 1993; Carminati *et al*., 1998; Wortel and Spakman, 2000). These kinematic and geodynamic models differ in some aspects of regional scale interpretation, because data carry them to different interpretations. Possibly, the first Mediterranean-wide conceptual geodynamic model including the mantle structure is the seminal work of Wortel and Spakman (2000). All these models share the concept that slab rollback is the main process that triggered the opening of the Western Mediterranean basins. Rosenbaum *et al*. (2002) present a reconstruction of the tectonic evolution of the Western Mediterranean since Oligocene times taking into account all data mentioned above. Figure 1.6 shows a reconstruction of the opening of the Western Mediterranean basins accepted by most today, even though, timing and the style of slab movements through the mantle has been disputed. Rifting of continental plates probably started in the middle Oligocene (~30 Ma) northeast of

the Ligurian Sea extending southwestward through the Gulf of Lions (Séranne, 1990) and during the late Oligocene (~25 Ma) in the Valencia Trough (Roca *et al*., 1999). This first stage of subduction rollback resulted in a Balearic Islands and Corsica-Sardinia-Calabria block rotation. According to several authors, the extension in the Liguro-Provençal Basin and in the Valencia Trough ceased in the early Miocene (~21-18 Ma) with a collision between the Corsica-Sardinia and Calabria block with the Apennines (Burrus, 1989) and the jump in the subduction hinge south of the Balearic Islands (Bartrina *et al*., 1992; Watts & Torné, 1992). Between 18-15 Ma the Kabylies block was accreted to the African margin resulting in the formation of the Algerian Basin (Figure 1.6). During middle Miocene (~15 Ma) the westward rollback of the subduction hinge give rise to the formation of the Alboran Basin with the accretion of the Betic-Rif cordillera and the cessation of the back-arc extension in the Alboran Sea at ~10 Ma (Figure 1.6). Finally, in the Apennines region, a southeastward rollback of the subduction system took place during the Tortonian (~9 Ma) with the opening of the Tyrrhenian Basin. Two main stages characterized the formation of the Tyrrhenian Sea: a first stage during 9-5 Ma with the opening of the north Tyrrhenian Basin, and a second stage during the last 5-0 Ma with the opening of the south Tyrrhenian Basin (Figure 1.6).

The reconstruction showed in Figure 1.6 exemplifies a general evolutionary model that many scientists have used to explain the Western Mediterranean configuration (Rehault *et al*., 1984**;** Faccenna *et al*., 2004; Schettino and Turco, 2006; Jolivet *et al*., 2009; Carminati *et al*., 2012; Faccenna *et al*., 2014). This first model considers the subduction rollback of a unique and continuous slab from the north Apennines to the Betic-Rif region. However, this continuity had been challenged by the work published by Wortel and Spakman (2000) who presented new results from mantle tomography and introduced the concept of the slab detachment and lithosphere tearing to explain the evolution of the Western Mediterranean basins as the evolution of differentiated segmented slabs. In the next section, we review the main tomographic studies, which have contributed to a better understanding to the driving forces and to the kinematics of the Western Mediterranean basin formation.

Figure 1.6. *Reconstruction of the main steps during the opening and formation of the Western Mediterranean basins. The reconstruction starts at the Middle Oligocene (~30 Ma) with the opening of the Ligurian Sea and ends at the Late Pliocene with the opening of the south Tyrrhenian Basin (Rosenbaum et al., 2002).*

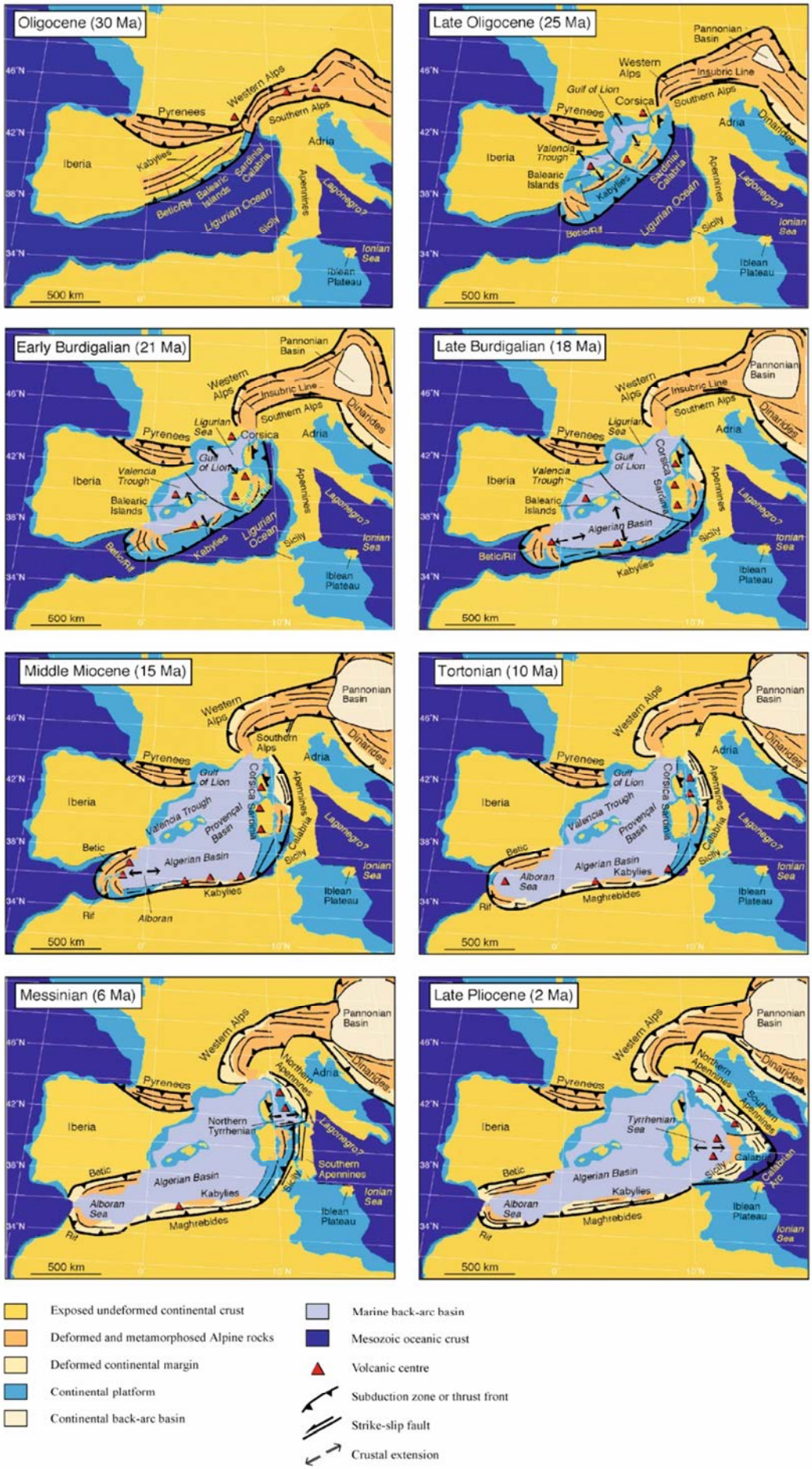
Oligocene (30 Ma)
Late Oligocene (25 Ma)
Early Burdigalian (21 Ma)
Late Burdigalian (18 Ma)
Middle Miocene (15 Ma)
Tortonian (10 Ma)
Messinian (6 Ma)
Late Pliocene (2 Ma)
Pyrenees
Western Alps
Southern Alps
Pannonian Basin
Insubric Line
Dinarides
Adria
Iberia
Kabylies
Balearic Islands
Sardinia/ Calabria
Apennines
Ligurian Ocean
Lagonegro?
Sicily
Ionian Sea
Iblean Plateau
Gulf of Lion
Corsica
Valencia Trough
Ligurian Sea
Betic/Rif
Algerian Basin
Provençal Basin
Betic
Rif
Alboran
Alboran Sea
Maghrebides
Northern Tyrrhenian
Northern Apennines
Southern Apennines
Tyrrhenian Sea
Calabrian Arc
500 km
46°N
42°N
38°N
34°N
Exposed undeformed continental crust
Deformed and metamorphosed Alpine rocks
Deformed continental margin
Continental platform
Continental back-arc basin
Marine back-arc basin
Mesozoic oceanic crust
Volcanic centre
Subduction zone or thrust front
Strike-slip fault
Crustal extension

1.2.2 Progress through tomographic studies

Traveltime tomography is a method for reconstructing the earth's velocity model from traveltimes of seismic arrivals picked on seismic records. These traveltimes can be measured from seismic data associated with a variety of source-receiver configurations, and can be used to extract velocity models of varying spatial resolution. Since the first tomographic studies based on arrivals of earthquakes on seismological networks around the Western Mediterranean, (e.g. Blanco and Spakman, 1993) high-velocity anomalies in seismic tomography has been interpreted as displaying the presence of subducted lithosphere in the Western Mediterranean mantle. Wortel and Spakman (2000) and Spakman and Wortel (2004) presented in their works the geodynamic interpretation of the results from mantle tomography from the Western Mediterranean region (Figure 1.7).

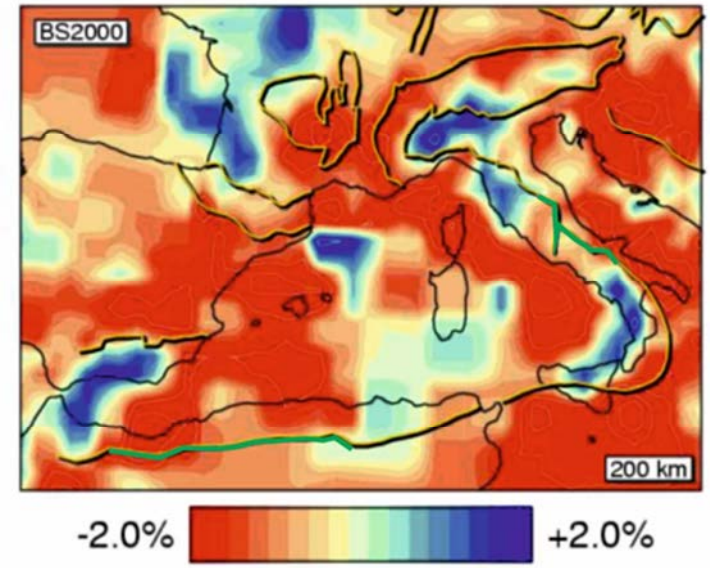

Figure 1.7. *Tomographic map view image at depth of 200 km of the Western Mediterranean and surrounding regions. Colours display the percentage deviation of seismic waves speed with respect to the 1-D reference model ak 135 (Kennet et al., 1995). Yellow lines indicate outlines of major tectonic features and green lines areas where the slab is supposedly detached. (Modified from Spakman and Wortel, 2004).*

They described the existence of a positive wave-speed anomalies located beneath the northern Apennines, Calabria and the Betic-Rif cordillera and interpreted these anomalies as different slabs. As the image 1.7 shows, there is not a visible continuous positive anomaly between northern Apennines and Calabria at 200 km-depth. The northern Apennines positive anomaly is interrupted in the central-southern Apennines and becomes visible again in the most southern Apennines and in the Calabrian region (Figure 1.7). However, the vertical

slices of the tomographic model displayed in Figure 1.8 show how the positive anomaly located below the northern Apennines and Calabrian arc is deepening sub-vertically up to 400 km depth (Figures 1.8a, c). From 400 km depth the positive anomaly is still deepening but becomes flat before 600 km depth (Figures 1.8a, c). In the central-southern Apennines (Figure 1.8b) this positive anomaly is not visible through the first 200 km depth, it appears from 260 km depth as a sub-vertical positive anomaly up to 400 km depth, whereas in the other images becomes flat between 400 km and 600 km depth (Figure 1.8c).

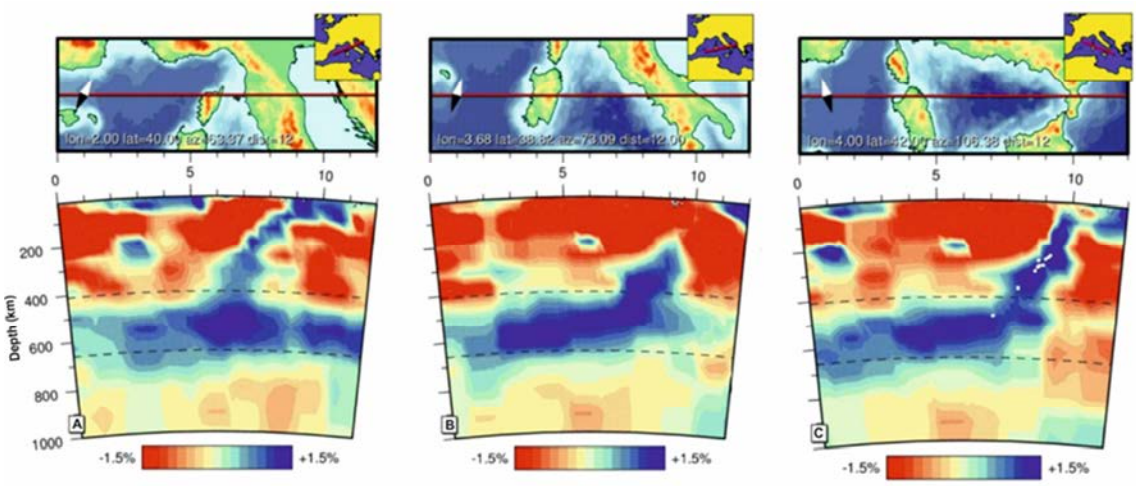

Figure 1.8. *Image of three cross sections through the first 1000 km of the Western Mediterranean mantle. A) Section through the northern Apennines and Liguro-Provençal Basin. B) Section through the central and southern Apennines and Tyrrhenian Basin. C) Section through the Tyrrhenian Basin and Calabria. White dots indicate major (magnitude > 4.8) earthquakes. The diamond symbol to the left in the map indicates a compass needle (white pointing north). Dashed lines in vertical sections represent the mantle discontinuities at 410 and 660 km depth. Note how the positive velocity anomaly interpreted as a subducting slab can be seen from the first km of crustal depth in the northern Apennines (A) and in the Calabrian arc (C), but, is not visible at ~200 km depth in the central southern Apennines (B) (Spakman and Wortel, 2004). For more information, see the text in this section.*

The existence of this gap located in the central-southern Apennines was discussed in previous works (e.g. Wortel and Spakman, 2000) with the introduction of the concept of slab detachment and lithospheric tearing. According to these authors, a small tear in the slab, originated by some lithospheric anomaly or mantle instability, may cause lateral rupture propagation (lithospheric tearing). The propagation of this tear is the consequence of the slab pull stress concentration. In a segment of a plate boundary where the slab is detached, the

stress concentration of the slab pull forces near the tip of the tear cause the propagation of it (Figure 1.9).

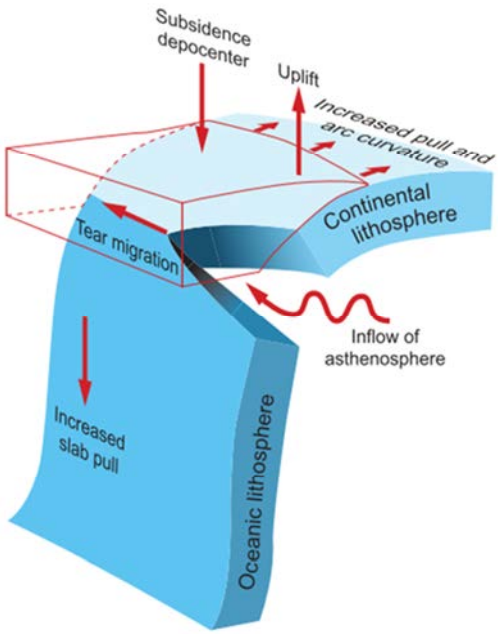

Figure 1.9. *Scheme of lateral migration of slab detachment developed into a large tear. Slab detachment most likely occurs episodically, in segments. The slab pull (the gravitational force associated with the cold, and hence, dense subducted lithosphere) causes a depocentre subsidence and uplift migrating along strike. It is also concentrated near the tip of the tear causing the tear propagation. Asthenospheric material flows replacing the gap resulting from the slab detachment (Wortel and Spakman, 2000).*

Beneath the Betic-Rif region a positive anomaly is also observed (Figure 1.7). An E-W cross section displayed in the Figure 1.10 through the Betic-Rif anomaly show that this positive anomaly is found from the base of the crust across the entire upper mantle down to 600 km depth. It presents an eastward dipping, almost vertical, configuration (Blanco and Spakman, 1993; Wortel and Spakman, 2000; Calvert *et al*., 2000; Spakman and Wortel, 2004). The interpretation of the Betic-Rif anomaly has been discussed by numerous authors. A variety of models have been proposed to explain the presence of a positive velocity anomaly beneath the Betic-Rif region, and the synchronous extension and contraction that occurred in the Alboran region and the surrounding Betic-Rif cordillera during the Early Miocene despite the continued convergence between Africa and Iberia. Each model has been associated with a different geodynamic process:

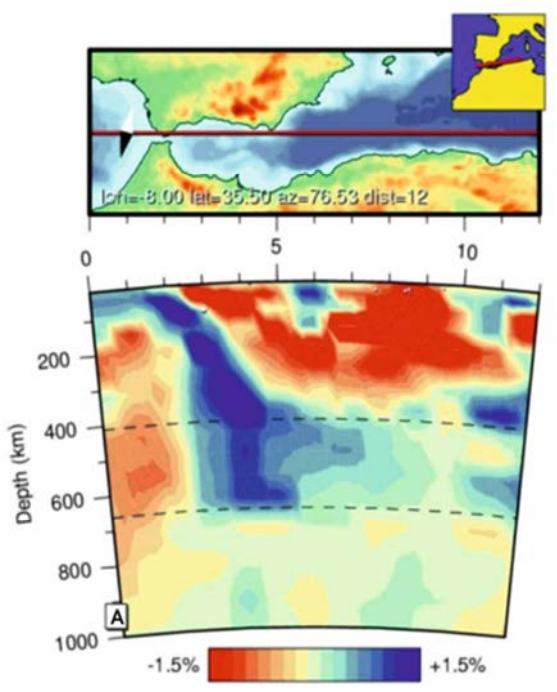

Figure 1.10. *Image of cross section through the first 1000 km of the Betic-Alboran region and Algerian Basin. White dots indicate major (magnitude > 4.8) earthquakes. The diamond symbol to the left in the map indicates a compass needle (white pointing north). Dashed lines in vertical section represent the mantle discontinuities at 410 and 660 km depth. Note how the positive velocity anomaly interpreted as the subducting slab is located below the Gibraltar arc and deepening almost vertically and slightly eastward to the 660 km mantle discontinuity (Spakman and Wortel, 2004).*

1) **Retreating subduction**. This model explains the migration of the Alboran block as a result of the westward rollback of the east dipping subducting slab in the Betic-Rif region (Figure 1.11). In this model, the presence of the positive velocity anomaly is related to the subducting slab, while the extension in the overriding plate is related to the rollback of the subducting slab (Lonergan and White, 1997). 2) **Slab break off**. This model presented by Zeck, 1997 considers a completely detached slab beneath the Betic-Rif region. This detached body could explain the presence of the positive velocity anomaly detected by seismic tomography and the extension of the overriding plate (Figure 1.11). 3) **Delamination**. Many authors hypothesized the process of delamination in the Alboran region as the detachment of a thickened lithosphere (Docherty and Banda, 1995; Seber *et al*., 1996; Tandon *et al*., 1998). The lithosphere was thickened due to the convergence between Africa and Iberia and it was detached from the overriding plate owing to gravitational instabilities (Figure 1.11) and 4) **Convective removal**. Convective removal is a process very similar to delamination. The main difference between both processes is that in the convective removal the thick lithosphere that becomes gravitationally unstable is removed by convective currents and replaced by asthenospheric material (Platt and Vissers, 1989). In both processes, the positive velocity anomaly is related to this thickened and removed lithospheric body and the extension of the overriding plate is related to the asthenospheric flow material (Figure 1.11).

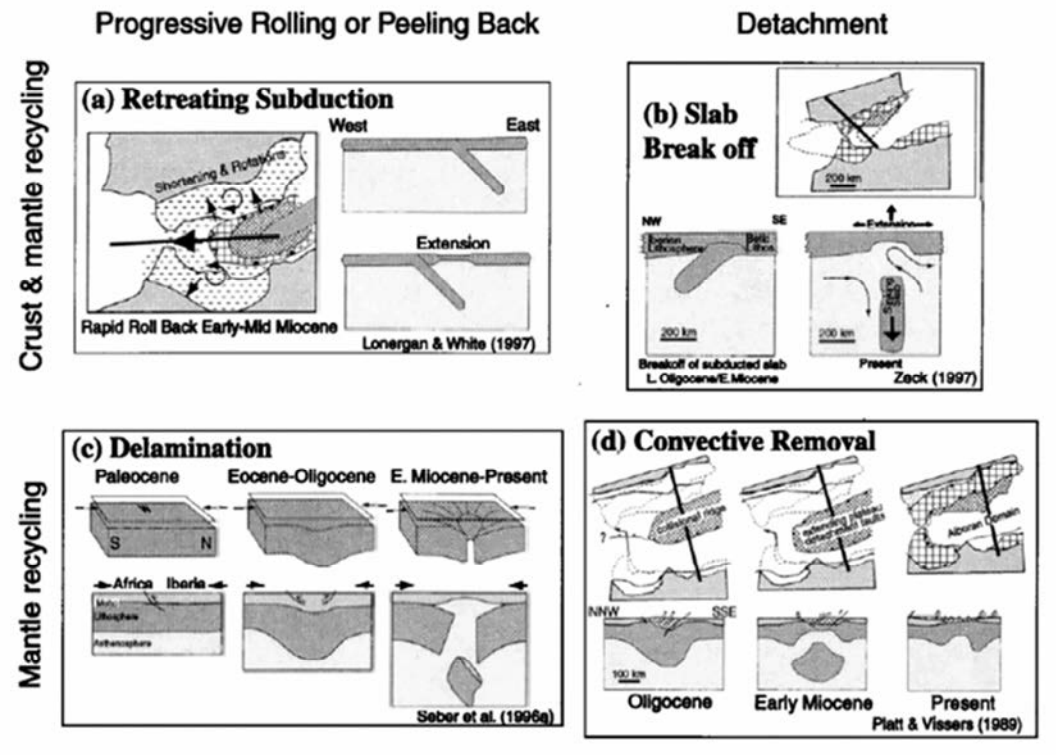

Figure 1.11. *Schematic models previously proposed to explain the geodynamic evolution of the Alboran region. These models may be categorized in terms of roll-back or detachment of the lithosphere and whether or not crust is involved in recycling of the lithosphere into the mantle (Calvert et al., 2000). (a) Retreat from east to west of an east dipping subducting slab during the Early Miocene (Lonergan and White, 1997). (b) Break-off of an NW dipping slab at the Oligocene-Miocene boundary perhaps subducted during eastward movement of Iberia relative to Eurasia (Zeck, 1997). (c) Delamination of lithosphere thickened during Paleogene convergence initiated during Early Miocene but still active today (Seber et al., 1996). (d) Convective removal during the Early Miocene of mantle lithosphere thickened during Paleogene convergence (Platt and Vissers, 1989).*

Calvert *et al.*, 2000 interpret that the positive velocity anomaly is a lithospheric body that has descended into the mantle but, it is not completely detached so that slab break off or convective removal are discarded. Those tomography results alone do not allow discrimination between retreating subduction or delamination process because both may present similar velocity features. However, new mantle tomography results from an increased coverage of stations supports a history in which slab rollback moved across the Alboran region with rapid east-west propagation along the African margin but slow along the Iberian margin, which is the cause of slab rotation under the Betics and Gibraltar region (Levander *et al.*, 2014). More recent studies combining tomography with GPS data, receiver functions and seismicity data suggest that the Alboran slab is still detaching or has recently

detached from the continental plate along the eastern Betics (Bezada *et al*., 2013; Mancilla *et al*., 2013; Palomeras *et al*., 2014; Thurner *et al*., 2014), but appears to be attached to the west (Levander *et al*., 2014; Mancilla *et al*., 2015; Villaseñor *et al*., 215). All this evidence suggests a combination of both retreating subduction and delamination processes similar to the model suggested for the Calabrian - Italy peninsula by Wortel and Spakmann (2000). The simultaneous occurrence of rollback and convergence between Africa and Iberia produced a lithospheric thickening because of the overthrusting of the crust to the west under the Gibraltar Arc and the detachment of the subducting oceanic lithosphere to the east under the Betic cordillera.

The integration of tomographic results and surface geology has led to the discussion of potential geodynamic evolutionary models explaining both sets of observations. Tomography images and seismicity data have confirmed the presence of different slabs partially detached in the Apennines region and in the Betic-Rif region, but the kinematics of each slab to its present position is still matter of debate. In one set of models different authors suggest that after the collision between the Kabylies block and North Africa, the Algerian Basin was formed as a result of approximately 500 km of an E-W motion of the Alboran domain (Figure 1.12). This westward motion is proposed to have been accommodated along the Emile Baudot and North Africa transforms (Lonergan and White, 1977; Mauffret *et al*., 2004; Spakman and Wortel, 2004; Gutscher *et al*., 2012; Chertova *et al*., 2014; van Hinsbergen *et al*., 2014). The model proposes that the slab of the Betic-Rif region detached faster from North Africa than from south Iberia and as a consequence the slab turned northward and eastward until its present position (Figure 1.12).

Figure 1.12. *Schematic tectonic map of the opening of the Western Mediterranean basins. LPB: Liguro-Provençal Basin. NBTZ: North Balearic Transform Zone. GoV: Gulf of Valencia. EBT: Emile Baudot Transform. NAT: North African transform. Note that the main difference between the first reconstruction model presented in section 1.2.1 and this models that in the latter the authors consider an east-west opening of the Algerian Basin, through a transform step faults located in the southern margin of the Balearic Islands (EBT) and the northern Africa (NAT), after the collision of the Kabylies block with Noth Africa (van Hinsbergen et al., 2014).*

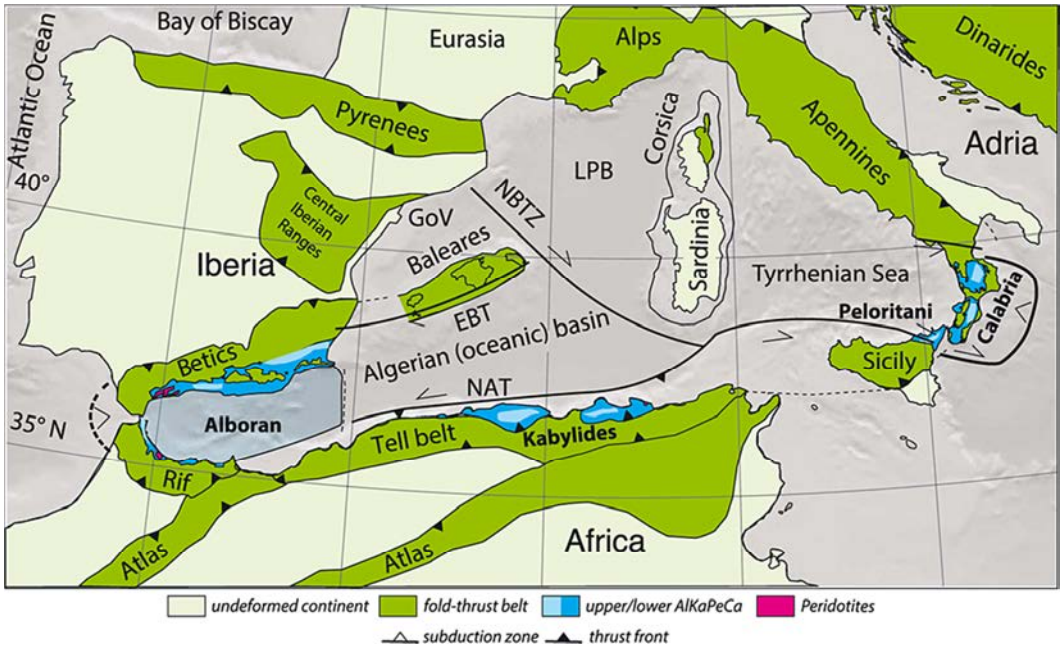

Another set of models (e.g. Vergés and Fernández, 2012) suggest a subduction and westward rollback scenario, but the main difference is that they argue that the subduction in the Alboran region was SE-directed under North Africa (Figure 1.13). They interpreted that the Alboran domain was attached to North Africa and retreated towards the northwest through a transform zone located between this southward dipping subduction zone and the northward dipping subduction zone below the Balearic Islands.

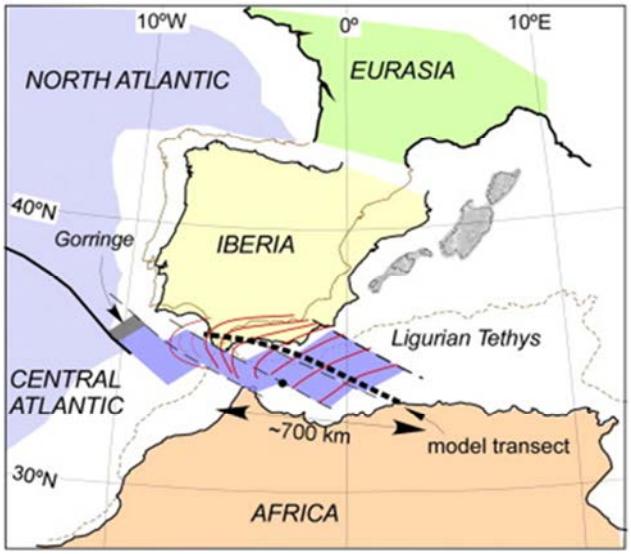

Figure 1.13. *Schematic tectonic reconstruction map of the Western Mediterranean region during Late Cretaceous. Thin continuous and dashed brown lines show the present position of Iberia and Africa respectively. Dashed black lines show the approximate trace of the proposed kinematic model. This model hypothesized a SE-directed subduction under North Africa. (Vergés and Fernández, 2012).*

Tomographic studies cannot sufficiently discern between both theories, the east dipping Alboran slab retreated westward and detached from North Africa and east Iberia, and the theory of a southward dipping subduction below North Africa that retreat to south Iberia.

1.2.3 State of the art: new tomographic results

The kinematic and geodynamic evolution of the Western Mediterranean basins is still matter of much debate despite the tomographic results that have contributed to a better understanding of the deep crustal and upper mantle structure of the region. The processes that have led to the present day lithospheric configuration are not yet fully understood.

The latest works on tomography with the new data set collected within the TopoIberia project with travel time tomography (e.g. Villaseñor *et al.*, 2015) and using the full-waveform inversion (FWI) methodology (Fichtner and Villaseñor, 2015) not only confirm the presence of an arcuate east dipping slab below the Betic-Rif region, but the new FWI results show for the first time well-constrained evidence of the presence of an African slab not properly imaged in previously works. The advantage of full-waveform inversion with respect to travel time tomography is that while in travel time tomography only the first arrival of every trace is inverted, in FWI, as the name suggests, the amplitude and phase are inverted in addition to the arrival time. The FWI method increases the resolution of the final model with comparatively smaller data coverage.

The new FWI results show the separate positive anomaly that corresponds to the Alboran slab to depths of ~200 km (Figure 1.14). Deeper, at ~250 km, the image shows the presence of an E-W trending positive anomaly that is interpreted as the African slab (Figure 1.14) (Fichtner and Villaseñor, 2015).

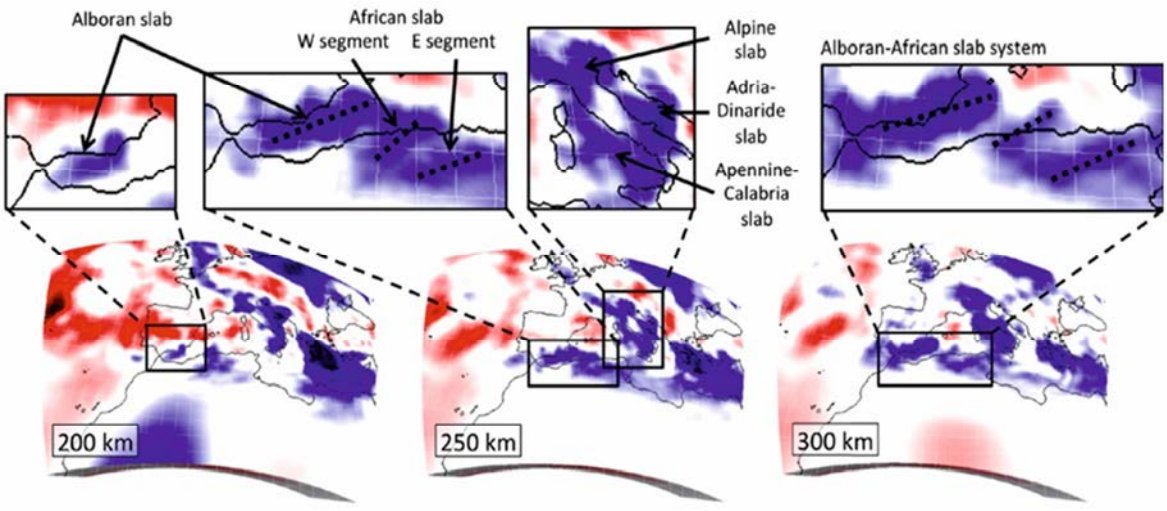

Figure 1.14. *Images of horizontal slices through the absolute variations of isotropic S velocity from 200 to 300 km depth. Dotted lines in close up figures mark possible segments of Alboran-African slabs. Note that the African slab appears possibly segmented from 250 km depth, indicating a slab detachment in the North Africa region (Fichtner and Villaseñor, 2015).*

In more detail the results show that this African slab appears to be formed by two different segments oriented slightly in a NW direction (Figure 1.14). These segments visible below 200 km depth beneath Algeria are interpreted as remnants of the slab that caused the opening of the Algero-Balearic Basin and was later detached leading to the formation of the Alboran Basin.

However, there is still no consensus about the opening of the Western Mediterranean basins, especially when we are referring to the Alboran Basin where different hypotheses have been used to explain the geometry and deep structure of the Betic-Rif region. Through different new data and techniques it seems that the scientific community is closer to achieving a consensus, but there are still many open questions. As we describe in the next chapter in more detail, this thesis work aims to discuss and update some of the old interpretations and try to answer some of those questions providing new data and interpretations. We discuss and provide constraints on the nature of the basement and the opening age and kinematics of three Western Mediterranean basins: Valencia Trough, Gulf of Lions and Algero-Balearic Basin. Moreover, our aim to discuss the kinematics of the opening of these basins should also provide constraints on the driving mechanisms that dominated the geodynamic processes.

Chapter 2: Motivation and Objectives

2.1 Interest of the study

The Western Mediterranean region has underwent a complex evolution in response to Late Mesozoic to Tertiary convergence between Africa and Iberia and the associated subduction of oceanic lithosphere (Lonergan and White, 1997; Gueguen *et al*., 1998; Rosenbaum *et al*., 2002; Faccenna *et al*., 2004; Mauffret *et al*., 2004; Jolivet *et al*., 2006, 2009). Small segmented basins were formed partially or fully as back-arc basins due to the eastward retreating of the west-directed Apenninic subduction zone (Figure 2.1). These basins are: Ligurian-Provençal Basin, Valencia Trough Basin, Algero-Balearic Basin, Alboran Basin and Tyrrhenian Basin.

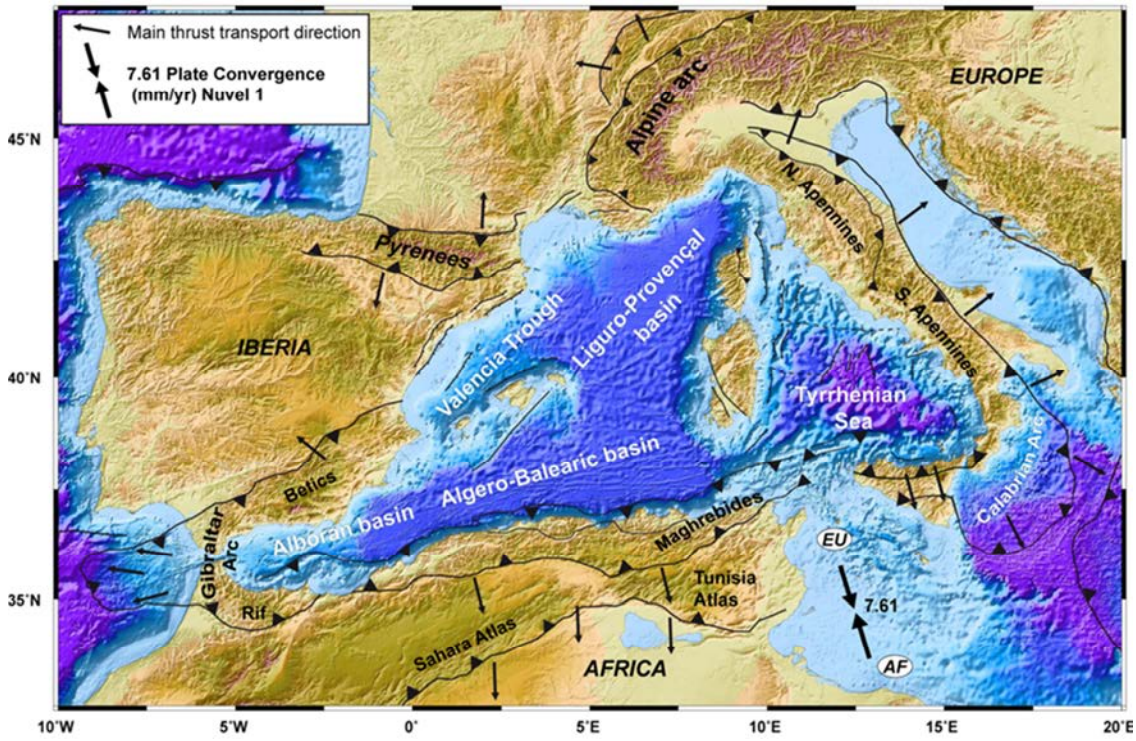

Figure 2.1. *Bathymetric and topographic map of the Western Mediterranean Sea. This image shows the main tectonic features and the location of every back-arc basin in the Western Mediterranean region. Thick black arrows indicate the direction of plate convergence. Thin black arrows indicate the transport direction of the main thrusts in the region, after Booth-Rea et al., (2007).*

The coeval occurrence of compressional and extensional processes has been the subject of numerous studies. These works have resulted into several tectonic models linking the large-scale horizontal motions with the retreat of the subduction trench (Dewey *et al*., 1973; Rehault *et al*., 1984; Platt and Vissers, 1989; Lonergan & White, 1997; Gueguen *et al*., 1998; Wortel and Spakman, 2000; Rosenbaum *et al*., 2002; Faccenna *et al*., 2004; Jolivet *et al*., 2009; Vergés and Fernández, 2012; Chertova *et al*., 2014; Dowe, *et al*., 2014).

In spite of the consensus that the rollback of the subduction slab since ~35 Ma should be the main geodynamic process driving tectonic changes, there exist a significant discrepancy between models on the spatio-temporal evolution of the subducting slab and how this evolution is explained in a particular tectonic framework. There are three main groups of models for the Western Mediterranean opening and evolution: The first one considers a rollback of an N-NW dipping subduction zone that extends from Gibraltar in the west to the north Balearic Islands in the NE (Rehault *et al*., 1984**;** Faccenna *et al*., 2004; Schettino and Turco, 2006; Carminati *et al*., 2012; Faccenna *et al*., 2014). The second one, considers a lateral segmented NW dipping slab that is confined to the Balearic margin (Mauffret *et al*., 2004; Spakman and Wortel, 2004; Frizon de Lamotte *et al*., 2009; van Hinsbergen *et al*., 2014). The third model considers a SE dipping subduction slab under the north-African margin (Vergés and Fernández, 2012). These three disparate tectonic evolution hypotheses show that there is still nowadays an open debate in the scientific community on the tectonic evolutionary model for the Western Mediterranean.

The work presented in this thesis consists on the analysis, processing and interpretation of newly collected and available geophysical data of the three main Western Mediterranean basins: The Valencia Trough Basin, The Gulf of Lions and the Algero-Balearic Basin. The main goal of this work is to advance the understanding of the geological and geophysical processes that formed the Western Mediterranean basins. After the review of major scientific studies that have defined the hypotheses of evolution of the Western Mediterranean we integrate the datasets of this thesis to discuss the timing and kinematics of the processes that controlled the opening of the Western Mediterranean basins.

The structure of this thesis is organized in three differentiated parts corresponding to the Valencia Trough, Gulf of Lions and Algero-Balearic Basins. The analysis, processing and interpretation of the dataset located in each basin have allowed us to define the nature and structure of the crust, and discuss the age and style of the tectonic processes that led to the current configuration of these basins. This work will help to further understand fundamental questions on the nature and formation of the Western Mediterranean basins.

2.2 Objectives

In order to achieve the main goal defined previously, we have defined the following scientific and technical **objectives** for every basin with their specific tasks:

1. To describe the crustal structure and geometry of the Moho of the Valencia Trough Basin:

a. To analyse (including re-processing for a better understanding of data limitations and imaging), multichannel seismic profiles ESCI-Valencia, VALSIS-819 and study SGV01, in order to define the seismic character of the basement and the geometry of the Moho.

b. To interpret the crustal and tectonic structure, and main sedimentary sequences of the basin.

c. To interpret the time and evolution of the Valencia Trough Basin formation.

2. To characterize the nature of the basement of the Gulf of Lions and deep Provençal Basin:

d. To analyse (including post-migration processing for imaging of selected segments) and interpret the grid of SPBAL01 multichannel seismic profiles in order to describe the seismic character of the basement and Moho.

e. To define different crustal domains depending on the nature of the basement and Moho.

f. To interpret the structure and the style of formation of the Gulf of Lions.

g. To study the relationship between the tectonic evolution of both Valencia Trough and Gulf of Lions.

3. Describe the nature of the basement and the tectonic structure of the Algero-Balearic Basin.

h. To analyse (including processing) and interpret TOPOMED-26 (TM26), ESCI-Valencia seismic profiles and wide-angle seismic lines P03 and P04 in order to describe the crustal and tectonic structure of the southeast Iberian margin and the deep Algerian Basin.

i. To interpret the nature of the crust by integrating the Vp velocity model of P03 wide-angle seismic profile with TOPOMED-26 (TM26) images of the tectonic.

j. To identify the nature and location of the continent-ocean transition.

k. Discuss the possible geodynamic origin of the Algero-Balearic Basin.

4. Discuss the results of the study of all basins in the framework of the Western Mediterranean basins and analyse the implications for existing evolutionary models.

Part II:

Methodology

Chapter 3: Methods

Even though all Western Mediterranean basins (WMB) formed in the same geodynamic context, each of the basins has differentiated kinematic evolution steps and timing. This thesis has been conceived as a work that reviews all existing models aiming to explain the subduction-related origin and the formation in a slab roll-back context of the WMB. To conduct this work we have integrated different geophysical methods using both industry and academic data available.

In this chapter, we describe the main fundamental concepts of the different methods that have been applied in order to obtain the different final processed data. The major part of the data used in this work is multichannel seismic data (MCS). We also integrated results from wide-angle seismic data (WAS) modelled at GEOMAR and for the sake of completeness the fundamental of the method are also included. Finally, we describe a recently developed imaging technique called “Mirror Imaging” used for the WAS and particularly useful for lines where no seismic reflection data exist.

3.1 Multichannel seismic data

Seismic reflection imaging is typically an active seismic method because it commonly uses an artificial energy source, in our case compressed air released from airguns. This technique was originally developed by oil exploration industry in 1930’s and since then it is the most commonly used in offshore and onshore geophysical exploration. It uses the principals of seismology to obtain subsurface information monitoring the travel times of elastic waves. Artificially generated by explosions, mechanic impacts or vibrations close to the surface, these elastic waves return to the surface after reflection in different subsurface interfaces and are recorded by seismometers. Multichannel seismic experiments consist on acquiring, processing and analysing the seismic record resulting from near-vertical reflections of elastic waves at different interfaces of the medium (Figure 3.1).

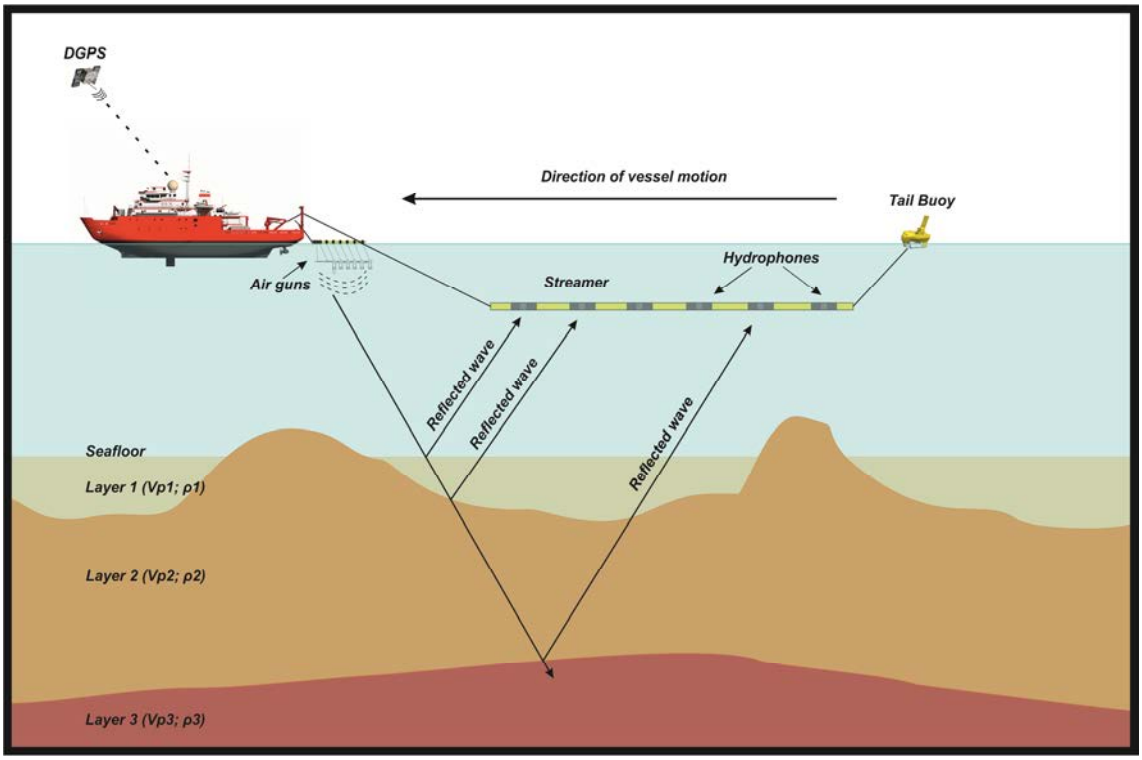

Figure 3.1 *Schematic representation of a standard marine multichannel seismic experiment. The image shows the acoustic elastic waves generated by the source (airguns) traveling down the water column and below the seafloor. Seismic waves reflected at different subsurface interfaces are recorded by the receiver system (streamer) located at certain depth (see Figure 3.2).*

The acquisition system of a marine MCS experiment consists of an array of air guns as seismic source generating an elastic pulse of energy that travels across the water layer down to the seafloor (Figure 3.2a). This elastic pulse is reflected and refracted into the different subsurface discontinuities with different acoustic impedance. The elastic wave returns to the surface where is recorded by a set of hydrophones distributed along a cable or streamer which acts as a receiver and sends all the information to the onboard computers (Figure 3.2b). The streamer which is located behind the source array also includes several devices like compasses (Figure 3.2c) that control the shape of the streamer and birds (Figure 3.2d) that control the streamer depth during the experiment. The position of the streamer is between 5 and 20 m bellow the sea surface in order to avoid signal interferences like swell noise. Finally a tail buoy (Figure 3.2e) is attached to the end of the streamer with a Global Positioning System (GPS) recording the position of every shot. The length and depth of the streamer, the number of channels (formed by hydrophones) and the source configuration depends on the objectives of the experiment.

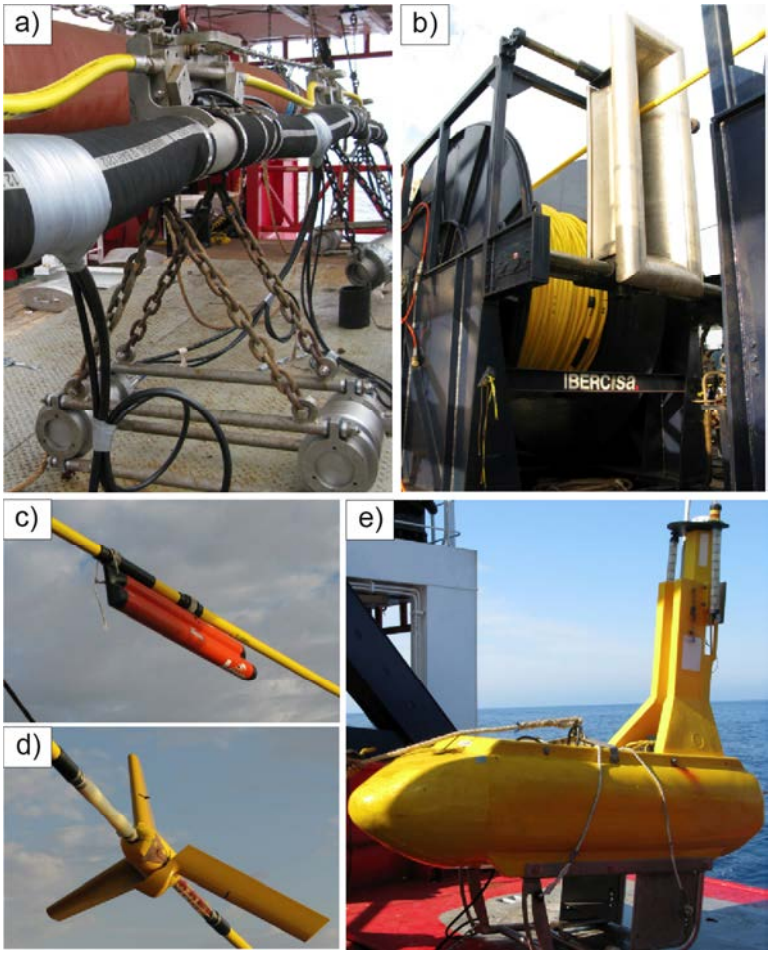

Figure 3.2 *Acquisition system during the TOPOMED (2011) MCS experiment. It includes the a) array of air guns as the seismic source, b) the 6 km-long streamer composed by the channels (hydrophones), c) the compasses, d) the birds, and e) the tail buoy.*

The returned signal is registered during a time known as “record length” and marks the maximum depth of the experiment. The data recorded is filtered and resampled in order to obtain a signal in a regular time interval (data are resampled between 2-8 ms). Data are also organized in “shot-gathers” (all the traces generated during the same shot along the profile) or “common midpoint-CMP” (all the traces recorded with same half distance between shot and receiver). For the main processing steps of the MCS data used in this thesis see chapter 5 in this section.

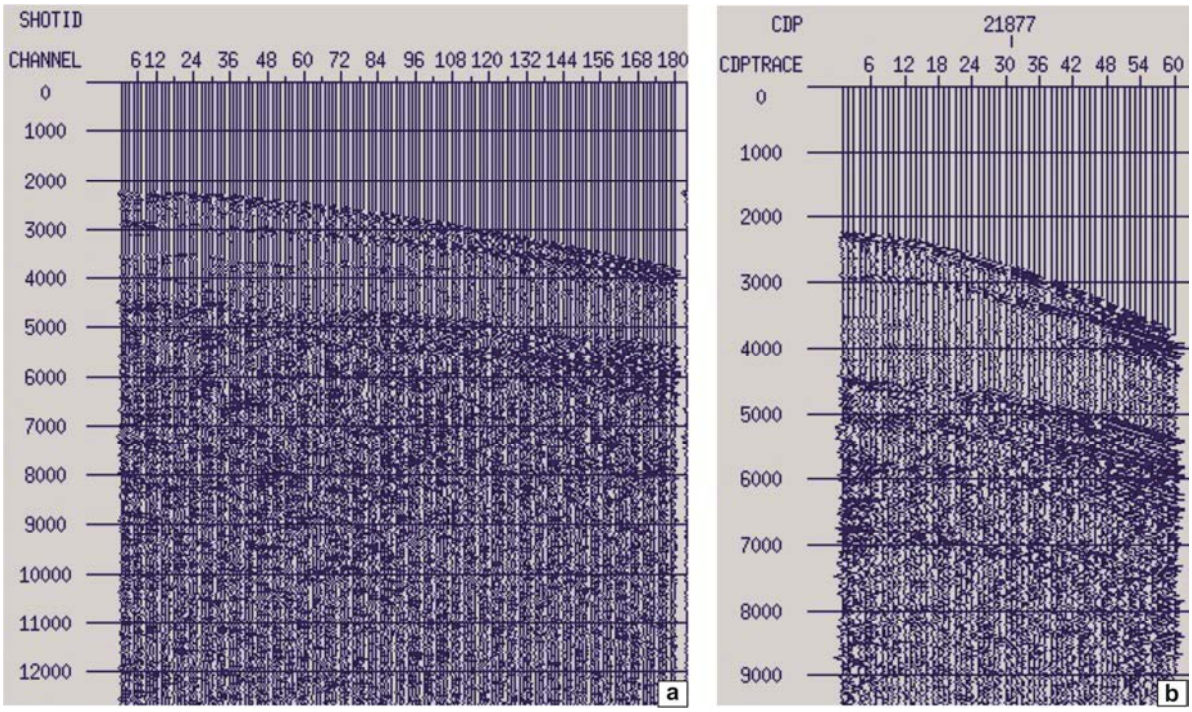

Figure 3.3 *a) Image of a shot gather of the ESCI-Valencia MCS profile with the 180 channels. b) Example of a CDP 21877 of the ESCI-Valencia profile with 60 traces per CDP.*

3.2 Wide-angle seismic data

WAS data used in this project can be classified as an active seismic method. In this case, however, consists of acquiring, processing and modelling the seismic record of both refracted and wide-angle reflected elastic waves propagated through the subsurface at a comparatively much greater distance between signal source and receiver (offset) than in a typical MCS experiment. While in MCS experiments (steep-angle seismic) only sub-critical reflexions (i.e. reflexion from a relatively small offset range) are observed, in WAS experiments normally the whole offset range where energy can be recorded is covered. Modelling these data provides information of the propagation velocity field through de subsurface and the geometry of geological discontinuities that have a contrast of impedance and produce laterally continuous reflected and refracted phases (e.g. the sediment-basement and crust-mantle boundaries) (Figure 3.4).

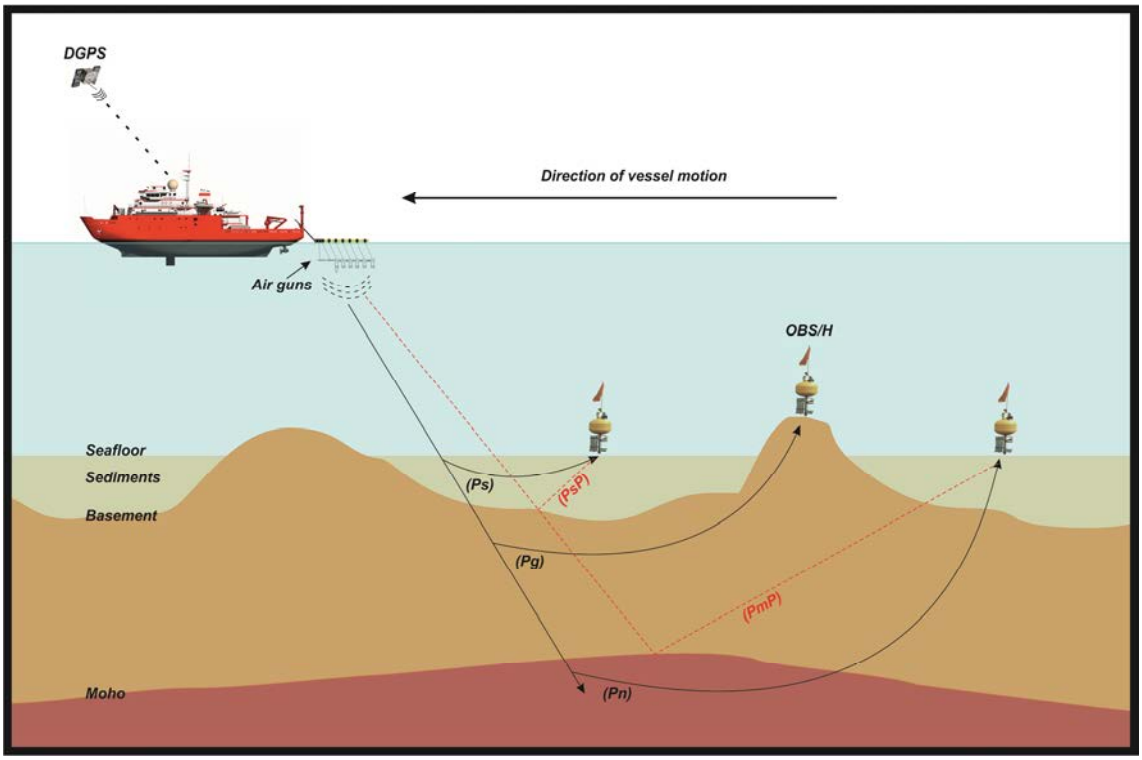

Figure 3.4 *Schematic representation of a standard marine wide-angle seismic experiment. The image shows the different P-wave seismic phases refracted through the sediments (PsP), basement (Pg) and mantle (Pn) and also the reflected waves at the sediment-basement boundary (PsP) and the crust-mantle boundary (PmP). Reflected and refracted acoustic waves are recorded by the receivers (Ocean Bottom Seismometers, OBS and Ocean Bottom Hydrophones, OBH) (see Figure 3.4).*

As in MCS experiments, the acquisition system consist of an array of air guns as seismic source (Figure 3.5a). The air gun configuration is different than in MCS experiments because lower frequencies are needed in the WAS case in order to obtain greater depths and longer offsets. The elastic wave generated by the source is recorded by a set of receivers deployed on the seabed along the track of the seismic profile called Ocean Bottom Hydrophones (OBH-Figure 3.5b) which record pressure variations in the water and Ocean Bottom Seismometers (OBS-Figure 3.5c) that measure the three components of motion (x, y, z). Source design, shot interval and the distance between receivers depends on the objective of the seismic experiment, smaller space between receiver provides more data and the final models are better constrained.

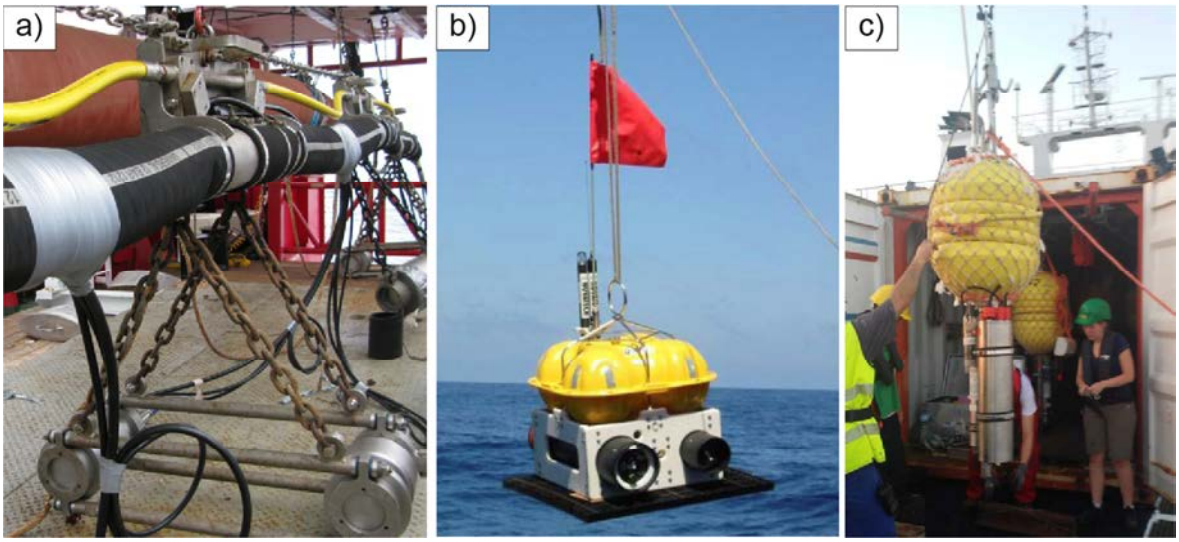

Figure 3.5 *Acquisition system of a WAS experiment. It includes the a) array of air guns as the seismic source, b) Ocean Bottom Seismometer (OBS) and c) Ocean Bottom Hydrophone (OBH).*

The recorded phases used for modelling the data are the primary P-waves and the secondary S-waves. Generally, P-waves are used for modelling WAS experiments because are more commonly visible in seismic records. These seismic waves are reflected as a result of acoustic impedance changes across the geological interfaces and refracted through them. Wide-angle reflections are normally removed during the processing steps of modelling WAS data, but they travel along large distances providing more information of boundaries like sediment-basement boundary and crust-mantle boundary (Figure 3.4). The final data recorded by the receivers consists on a continuous temporal trace that includes the seismic events produced by the arrivals of the recorded waves corresponding to the different seismic phases (Figure 3.4). The sorting by offset of these seismic traces provides the called “record section” presented in an offset-time diagram, where each trace corresponds to a shot (Figure 3.6). For the main processing steps of the WAS data used in this thesis see chapter 5 in this section.

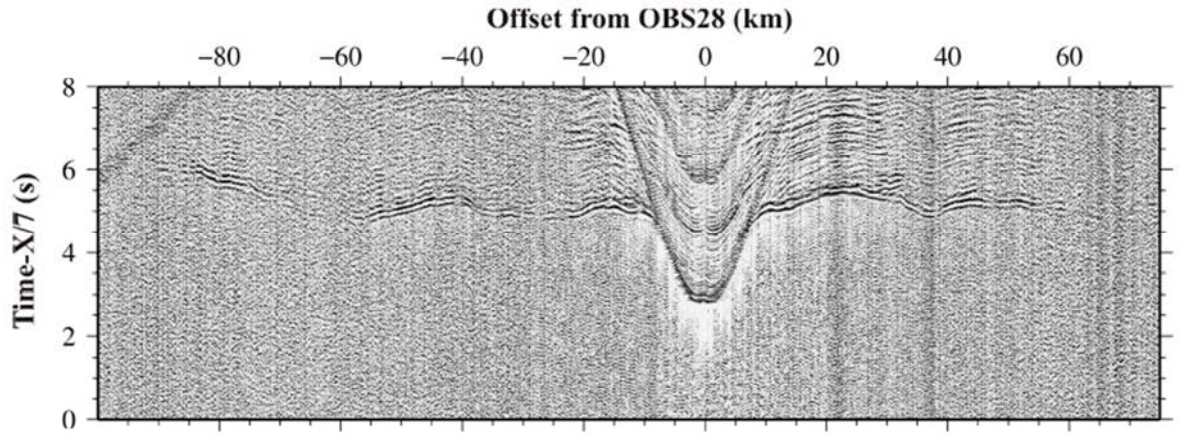

Figure 3.6 *Example of a seismic record section. The vertical axis represents a "reduced time" in seconds (reduced velocity is 7 km/s) and the horizontal axis is the offset from the OBS in km (Martínez-Loriente, 2013).*

3.3 Mirror Imaging

Mirror Imaging is a relatively new technique used during the last decade and consists in the migration of the multiple signals from wide-angle data. This process result in an image with a much broader illumination than the conventional imaging of the primaries from WAS data and it is comparable to the final migration of MCS data. Data recorded on OBS/H seismometers offer some advantages over data recorded on streamer. These are: 1) OBS/H are deployed in the seabed and therefore are less affected by noise and water layer disturbances and present higher signal to noise ratio. 2) OBS/H offer a wide-azimuth geometry which is an advantage for imaging complex structures and 3) OBS/H data also have information about shear velocities because they recorded the three components of motion (x, y, z) and converted the shear wave recorded by the horizontal component (Dash *et al.*, 2009).

Both WAS and MCS processing techniques consider the multiple signals as a noise and remove the multiples before the interpretation of the primaries. However, the multiple signals are formed by the same source signal as primaries just travelling along different paths in the subsurface interfaces. Multiple signals provide additional information because they have reflections from greater distances from receiver stations than the primaries. Figure 3.7 show and scheme about how the process works. The initial source signal travels through the water column and it is partially refracted into the seafloor and partially reflected at the water-sediment interface. The two waves (direct wave and the reflected wave) arrived at the same time at the receiver located in the seabed. Consequently, the direct wave contains the downgoing and the upgoing components above the seafloor, but only the downgoing below it and the water layer multiple wave also contains the downgoing and the upgoing components

above the seafloor and only the downgoing component below it (Figure 3.7a). On the other hand, when a reflection event run into the water-sediment interface, it gets partially transmitted into the water column and partially reflected back into the seabed. Therefore, the primary reflected signal is both upgoing and downgoing components just below the seafloor but only upgoing component just above the seafloor (Figure 3.7b) (Grion *et al.*, 2007; Dash *et al.*, 2009; Wang *et al.*, 2012). This downgoing receiver ghost of the multiple can be treated as an upgoing primary reflected downward from the sea surface. For migration process, multiple signals can be treated as primaries assuming that the data is not recorded on the seafloor but above a layer with twice the thickness of the water column.

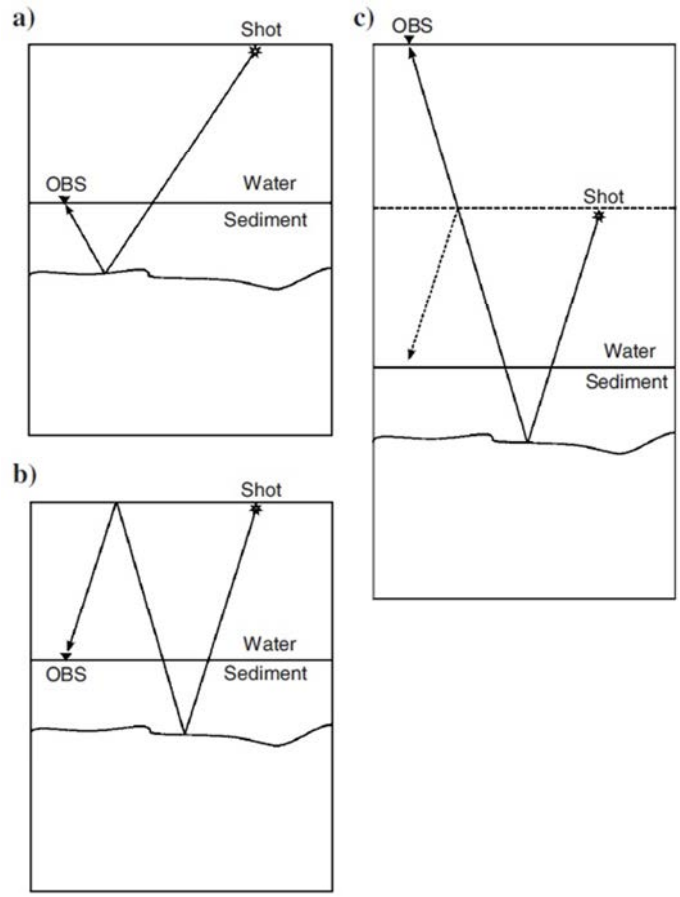

Figure 3.7 *Schematic images of the raypaths of a) upgoing primaries and b) downgoing multiples. c) for migration, multiples can be treated as primaries assuming that the data is not recorded on the seafloor but above a layer with twice the thickness of the water column (Wang et al., 2012).*

The resulting image is comparable to the image obtain from streamers. It is much better than the image resulting from the migration of the upgoing primary below the seafloor because it presents a wider illumination and a reduced exposure to shallow inhomogeneous anomalies under the seafloor. For the main processing steps of the Mirror imaging technique see chapter 5 in this section.

Chapter 4: Dataset and acquisition parameters

This chapter describes the dataset used in this thesis for each basin, Valencia Trough, Gulf of Lions and Algero-Balearic Basin (Figure 4.1). The different data set has been selected because they provide crustal-scale information, imaging the sediment section and basement structure including Moho reflections along much of the lines length. Here we describe the surveys configurations and in the next Chapter 5 we present the main processing steps either carried out by us or by other firms in the case of industry data.

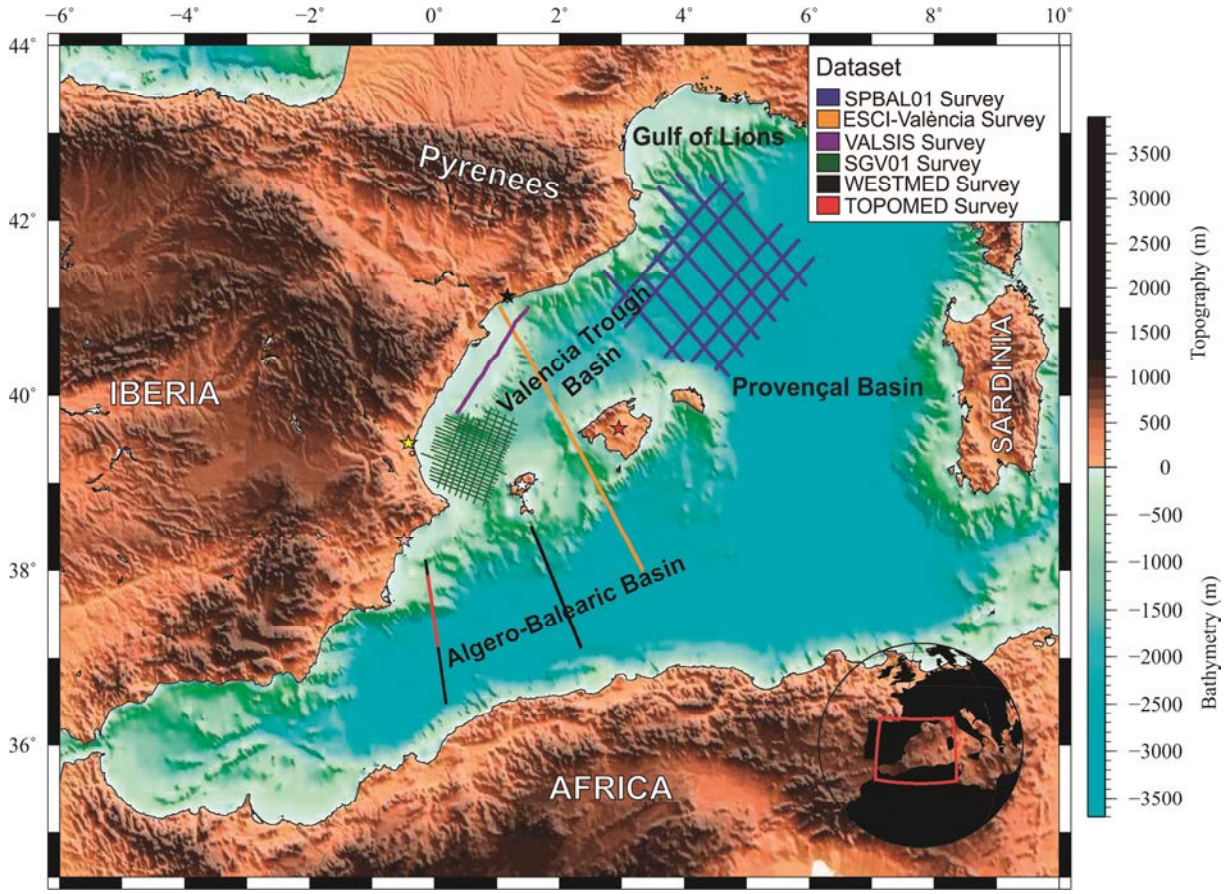

Figure 4.1 *Bathymetric and topographic map of the Western Mediterranean basins studied in this thesis: Valencia Trough Basin, Gulf of Lions and deep Provençal Basin andAlgero-Balearic Basin. The image shows the location of different datasets used in this thesis. Coloured lines correspond to MCS data and black lines correspond to WAS data. Black star is the location of the Tarragona city, yellow star the location of Valencia city and pink star the location of the Alicante city. Red star corresponds to the Mallorca Island and white star to the Eivissa Island. For the acquisition parameters of every dataset see the text in this chapter.*

4.1 Valencia Trough Basin

To study the Valencia Trough Basin we used academic and industry data. The academic data is the ESCI-Valencia MCS profile and the VALSIS-819 profile. The industry data corresponds to the SGV01 dataset (Figure 4.1). We describe below the main acquisition parameters of every experiment. The main processing steps are described in the next chapter 5.

Between February and March 1992, Geco-Prakla's survey vessel M.V.Bin Hai recorded a deep seismic line, commencing southeast of the Balearic Islands and stretching some 400 km, heading northwest between Mallorca and Eivissa to the Spanish mainland near Tarragona (Figure 4.1) The data was collected within the *"Estudios Sísmicos de la Corteza Ibérica"* ESCI project led for this line by Spanish National Research Council (Consejo Superior de Investigaciones Cientificas, CSIC) to investigate the lithosphere structure and sedimentary sequence of the Valencia Trough and the Algero-Balearic Basin. The ESCI project also collected coincident wide-angle seismic data, and thus provides reasonably well-constrained information on crustal structure (Dañobeitia *et al*., 1992; Gallart *et al*., 1994, 1995, 1997; Sábat *et al*., 1997; Vidal *et al*., 1995, 1998). The main acquisition parameters are shown in Table 4.1.

	ESCI-Valencia	SGV01	VALSIS-819
streamer (km)	4,5	6	2,4
n° channels	180	480	96
group interval (m)	25	12,5	25
source volume (in³)	7118	3530	5821
shot spacing (m)	75	25	50
fold coverage	30	120	24
trace length (s)	20	8,192	16
sample rate (ms)	4	2	4

Table 4.1 *Table with the acquisition parameters of ESCI-Valencia, SGV01 and VALSIS-819 datasets.*

The main seismic dataset used to study the Valencia Trough Basin consists on a 2D grid of MCS data from the industry survey SGV01 covering approximately 2800 km situated offshore Valencia margin (SW Valencia Trough) (Figure 4.1). The data were acquired in October 2001 by the Fugro-Geoteam's vessel R.V. Geo Baltic. The main acquisition parameters are shown in Table 4.1.

Finally, with the objective of linking the observations of crustal structure between the ESCI and SGV01 dataset, we used the academic line VALSIS-819 that runs along the offshore Ebro margin in a SW-NE direction and provides the continuity of structures that helps define the deep crustal and Moho geometry as well as the pre-tertiary top of basement across the region (Figure 4.1). During November of 1988 the Lamont-Doherty Earth Observatory's R/V Robert D. Conrad and IFREMER's R/V Jean Charcot recorded multichannel seismic reflection and wide-angle refraction profiles along the Valencia Trough within the project VALSIS (Collier *et al*., 1994; Gallart *et al*., 1990; Mauffret *et al*., 1992; Pascal *et al*., 1992; Torné *et al*., 1992; Watts *et al*., 1992). The main acquisition parameters are shown in Table 4.1.

4.2 Gulf of Lions and deep Provençal Basin

On November 2001 seismic vessel Polar Princes from Spectrum Energy conducted a survey through the northeast termination of the Valencia Trough Basin and across much of the Gulf of Lions Basin. The work involved the acquisition of the 2D seismic grid SPABL01 (Figure 4.1) with a total of ~6300 km of acquisition lines. The main acquisition parameters are show in Table 4.2 and the processing steps are described in the next chapter 5.

	SPBAL01
streamer (km)	8
nº channels	640
group interval (m)	12,5
source volume (in³)	4240
shot spacing (m)	50
fold coverage	80
trace length (s)	10
sample rate (ms)	2

Table 4.2 *Table with the acquisition parameters of SPBAL01 seismic lines.*

4.3 Algero-Balearic Basin

To study the Algero-Balearic Basin structure a 93 km-long MCS TOPOMED-26 (TM26) line was acquired during September and November 2011 onboard the Spanish R/V Sarmiento de Gamboa within the framework of *"La tectónica del arco de Gibraltar y la cordillera del Atlas: Causas litosféricas y efectos topográficos"* TOPOMED project (Figure 4.1). The main

acquisition parameters are shown in the flowing Table 4.3 and the main processing steps are described in the next chapter 5.

	TOPOMED-26
streamer (km)	6
n° channels	480
group interval (m)	12,5
source volume (in³)	4600
shot spacing (m)	50
fold coverage	60
trace length (s)	16
sample rate (ms)	2

Table 4.3 *Table with the acquisition parameters of TOPOMED-26 line.*

Additionally, we used two WAS profiles P03 and P04 acquired during August and September 2006 within the framework of WESTMED project (Figure 4.1). Data were collected with the German R/V Meteor from the Spanish mainland and from the Balearic Islands into the Algerian Basin respectively. Profile P03 is coincident with the MCS TM26 (Figure 4.1). Acquisition parameters are shown in Table 4.4 and the main processing steps of each line are described in the next chapter 5.

	P03	P04
n° receivers	20	22
receiver interval (m)	10	10
source volume (in³)	3905	3905
shot spacing (m)	150	150

Table 4.4 *Table with the acquisition parameters of P03 and P04 WAS lines.*

Chapter 5: Data processing and modelling

5.1 Multichannel seismic data

In this chapter we describe the main processing steps used in both MCS TM26 line (Chapter 4, section 4.3) and the ESCI-Valencia line (Chapter 4, section 4.1). In both lines we followed the same processing flow with different parameters. We also explain some additional post-stack processing done for VALSIS-819 MCS line (chapter 4, section 4.1) and finally, we present the main processing parameters used by Fugro and Spectrum companies in the cases of SGV01 grid lines (Chapter 4, section 4.1) and SPBAL01 grid lines (Chapter 4, section 4.2) respectively. Processing of MCS data has been done using the software package Globe Claritas.

5.1.1 MCS TOPOMED-26 and ESCI-Valencia lines

The main processing steps of MCS TM26 and ESCI-Valencia lines are described in the following processing flow (Figure 5.1).

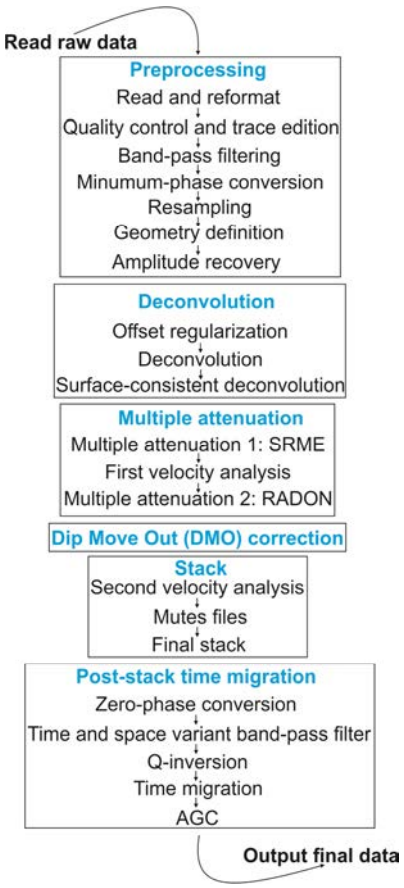

Figure 5.1 *Diagram of the processing flow followed for the TM26 and ESCI-Valencia MCS profiles. Every step is described in the following text.*

Read and Reformat

The raw data recorded in SEG-D format (shot domain) were read, and reformatted to Globe Claritas internal format. An upward bulkshift of 50 ms was applied in both TM26 and ESCI-Valencia lines in order to correct the existing lag between the shot triggering and the data recording window.

Quality control and trace edition

A quality control of the data was done, as well as edition of bad and noisy traces.

Band pass Filtering

Anti-alias, low cut butterworth filters of 1-3-100-120 Hz (TM26) and 1-3-50-60 Hz (ESCI-VAL) were applied before minimum phase conversion and resampling. This filtering partially attenuates high-amplitude, low-frequency ambient noise.

Minimum phase conversion

The minimum phase filter obtained from source wavelet modelling, estimated from the autocorrelation of data, is convolved with the data to convert the mixed phase raw data to minimum phase. Moreover, converting the data into minimum phase attenuates the signal bubble.

Resampling

Data were resampled from 2 ms to 4 ms for MCS line TM26 because the goal is to study crustal structure. ESCI-Valencia line was already sampled at 4ms (see chapter 4 section 4.1).

Geometry definition

During acquisition, shot positions were recorded with EIVA-navigation system (TM26) and NORSTAR Integrated navigation system (ESCI-Valencia). Streamer position of line TM26 was monitored with compasses and tail buoy GPS. Geometry information based on shot and streamer position for TM26 was used to calculate source-receiver offset distance and common mid-point (CMP) number. CMP coordinates were introduced in each trace header.

CMP is the point located half the distance between a shot and receiver pair (Figure 5.2). The appearance of a CMP gather is analogous to a shot gather. In one shot gather, every trace shows a different point of subsurface, while in one CMP gather every trace shows n times the same point of the subsurface in a terrain model with

plane-parallel layers. The total number traces that make a CMP are called “fold”. The reason for generating the CMPs is to add (stack) all suitable corrected traces belonging to a CMP to increase the signal/noise ratio.

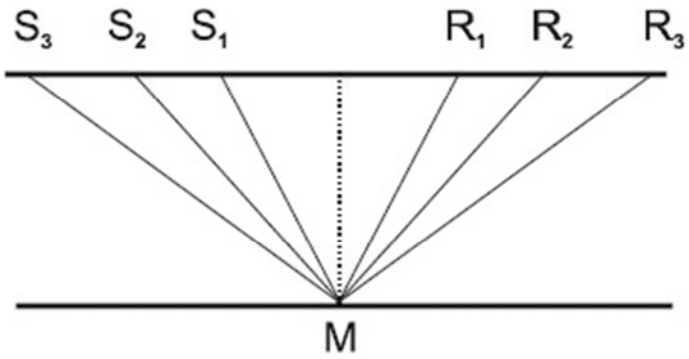

Figure 5.2 *CMP geometry. The same M point or CMP is sampled by different pair of source (S_i) and receivers (R_i).*

Amplitude Recovery

The spherical divergence correction is the compensation of the seismic wave amplitude due to geometrical spreading of the wavefront through the various velocity layers and for attenuation due to energy dissipation. It is necessary to recover the best resolution of seismic traces in time before further processing. Thus, an earth model with increasing velocity with depth is assumed. The correction of amplitude decay is done multiplying the sample of the trace by a vector of scalars that enhances the signal of the trace and is deduced semi-empirically. The scalar function **G(t)** is defined as a multiplication of four elements: a power of the two-way travel time, a power of the velocity, a power of the source-receiver offset, and an exponential term **exp (α*V*T)**.

Offset regularization

Along the processing, different steps like surface consistent deconvolution (SCD) and surface related multiple elimination (SRME) required to be performed with offset-regularized data. This is because these are 2D filters that require constant spatial sampling. In the case of line TM26 the irregular geometry arising from a crooked geometry accounting for streamer feathering requires offset regularization before Tau-p conversion. This regularization starts with the minimum offset in the profile and offset regularizes the 480 channels with a spacing of 12.5 m. In the case of the ESCI-

Valencia profile this step is not necessary because the geometry of the streamer is already regular.

Deconvolution

Earth is composed by a set of different lithology layers with different physical properties. Seismically, strata are defined by their impedance contrast (variations in density and seismic velocity), which is the reason for the reflection of the incident signal. The seismic trace (seismogram-Figure5.3) is the result of convolution of the seismic wave created by the source (source wavelet-Figure 5.3) and the Earth's impulse response with different lithology layers (Figure 5.3). The purpose of the deconvolution is to enhance the signal of the Earth's response removing the effect of the source wavelet.

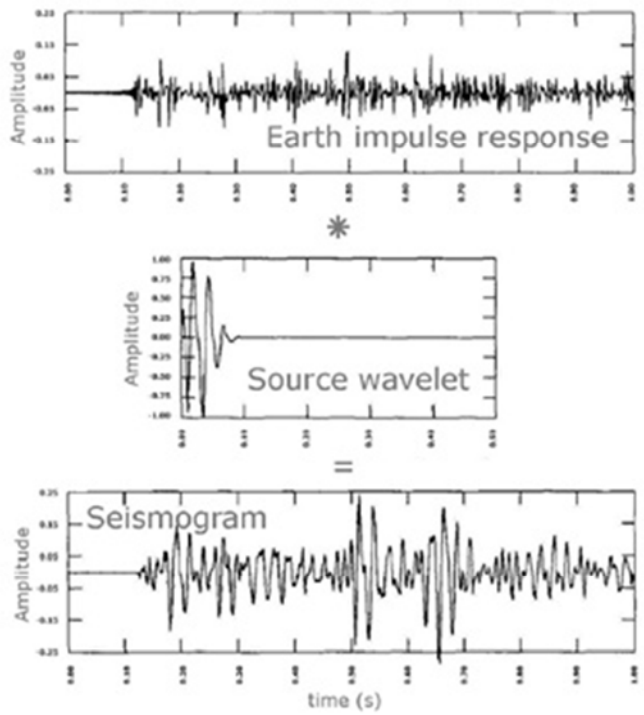

Figure 5.3 *Graphical representation of a seismic trace (seismogram) x(t) as a result of the convolution between the Earth's impulse response e(t) and the source wavelet w(t). Yilmaz, 2001.*

We can define the recorded seismogram as:

$$x(t) = w(t) * e(t)$$

Where:

x(t) = recorded seismogram

w(t) = source wavelet

e(t) = earth impulse response

$*$ = convolution

It is necessary to recover the earth impulse response e(t) from the recorded seismogram x(t). For that reason, an operator a(t) is defined as the filter that leads to e(t)

$$a(t) * x(t) = e(t)$$

So, replacing e(t) in the last equation:

$$x(t) = w(t) * a(t)\ x(t)$$

When x(t) is deleted from both sides:

$$\delta(t) = w(t) * a(t)$$

where δ(t) is the Kronecker function

$$\delta(t) = \begin{cases} 1, & t = 0 \\ 0, & t \neq 0 \end{cases}$$

Then, the operator filter is:

$$a(t) = \delta(t) * w'(t)$$

where w'(t) is the inverse of seismic wave.

Assuming that the convolution in a time domain is equivalent to the frequency domain, the last equation is converted to a frequency domain (Figure 5.4).

$$F(s(t)) = 1/F(w(t))$$

where F is the Fourier transform.

Therefore, if the initial wavelet w(t) is known, the solution to the deconvolution problem is deterministic.

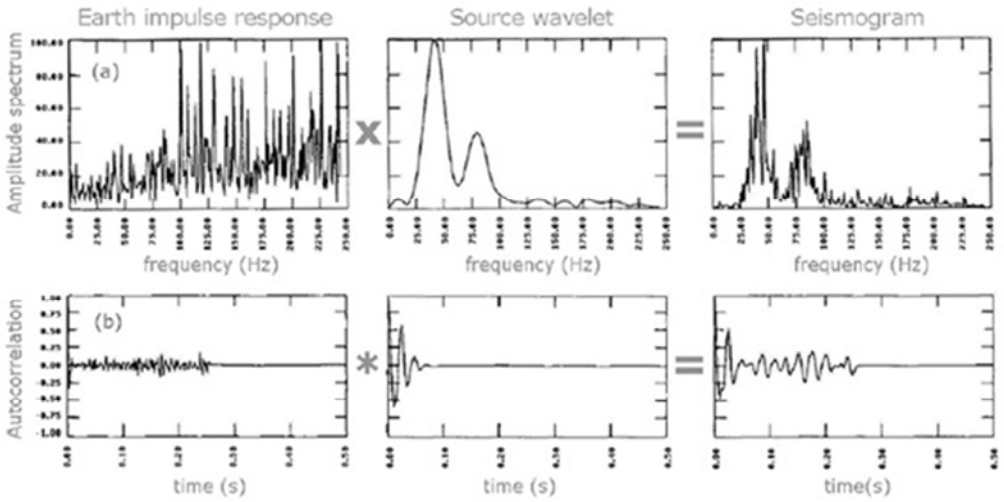

Figure 5.4 *Graphical representation of (a) Frequency spectrum of the seismogram x(t) as a result of the convolution between the source wavelet w(t) and the Earth's impulse response e(t). (b) Autocorrelation functions of the convolution. The registered seismogram (left) gets the first peak from the Earth's impulse response and the rest come from the font. Yilmaz, 2001.*

However, in the seismic experiments the initial wavelet is usually unknown, and therefore e(t) should be determined with statistical methods. The basis of the statistical deconvolution in the MCS processing is to estimate the amplitude and phase spectra of the initial wavelet w(t). The deconvolution typically uses a Wiener filter in a frequency domain. We chose to apply a Wiener deconvolution in Tau-p domain instead of time-distance domain because this process in Tau-p domain preserves better relative amplitudes and primary reflection energy. Deconvolution is used to attenuate short period multiple reverberations such as peg leg multiples and the source bubble signature. The method for deleting multiples relies on the periodicity of the multiple wavefield and the source wavelet. The best results were obtained using long operator filter and gap lengths.

Test results of the gap length indicate that the most effective value to reduce the bubble effect corresponds to a gap of 124 ms for TM26 and 32 ms for ESCI-VAL. The filter-length tests were performed considering 1) fixed filter-length values and 2) depth variable filter-length, with a constant gap of 124 ms (TM26) and 32 ms (ESCI-VAL). The most effective filter-length corresponded to the water depth at each point of the profile. 50 ms were subtracted to this value in order to avoid reaching the first multiple signal and consequently preventing undesirable partial attenuations or transformations of the multiple signal in the near-offset traces at this stage. The

deconvolution has been applied as a single window over the entire trace length in shot-sorted data. Tau-p wiener predictive deconvolution consists of inverting the time domain to Tau-p, applying a Wiener predictive deconvolution and inverting the Tau-p domain back to time domain. Parameters of the different steps are:

a. The Tau-p conversion has been performed on shot gathers with a quadratic interpolation. The minimum velocity (maximum slowness) was -1500 m/s, and the maximum velocity (minimum slowness) was 1500 m/s.

b. The Wiener deconvolution is a one-window deconvolution, performed in Tau-p domain with long filter length and gap in order to attenuate short periodicity reverberations.

c. The RHO filter is commonly used during Tau-p processing, which would otherwise have the effect of amplifying low-frequency energy. RHO applies a zero-phase filter in the frequency domain, by multiplying each value in the amplitude spectrum by the magnitude of the angular frequency. This method preserves relative trace amplitudes.

d. The Tau-p inversion allowed changing back to the time-space domain. Parameters are similar to step a.

Wiener deconvolution in the Tau-p domain helps to remove short-period multiples, to attenuate the bubble amplitude and to attenuate surface multiples (Figure 5.5).

Surface-consistent deconvolution

This technique ensures that traces from the same surface, source and receiver location (or CMP gather) have the same consistent operator applied. This deconvolution method attenuates source and receiver wavelet variation in a surface-consistent manner from the traces. Application of surface-consistent deconvolution (scdecon) shows significant improvement in data quality by reducing random noise and removing the variation of amplitudes due to near surface irregularities. This improvement of seismic data may be helpful in extracting higher structural detail during interpretation (Figure 5.5). Surface-consistent deconvolution was first performed in shot gathers and secondly in receiver gathers, with a single time-window. The parameters used are: Filter length=260 ms, Gap=24 ms (TM26) and filter length=200 ms, Gap= 24 m (ESCI-Valencia).

Multiple attenuation 1: Surface Related Multiple Elimination (SRME)

The main objective of the attenuation of the multiple in this phase of the processing flow is to have cleaner data for velocity determination. The Surface-Related Multiple Elimination (SRME) method is in addition convenient because it is not dependent on pre-existing velocity information like other attenuation methods (e.g. Radon and F/K filters). It works on a multiple prediction model on a trace by trace basis, which is adaptively subtracted from the original dataset. To obtain a maximum performance, the filter was designed on offset-regulated shot-gather sorted data. In this case, a good compromise for the offset regularization is to have the same spacing (25 m) between receiver and shot intervals. This step is achieved by doubling the number of shots by interpolation, and doubling the receiver interval. This procedure has the advantage that the final size of the data is just slightly bigger than the original and the computing time is not greatly increased. For the modelling, in order to reduce the inherent aliasing of the multiple model, the geometry needs to be regularized close to zero-offset and the data muted right above the seafloor reflection to remove any noise that may introduce artefacts. For this test, a configuration of 247 channels with a shot and channel interval of 25 m is used, where minimum offset values are close to 12.5 m, with a maximum of 6159 m for TM26 line, and a configuration of 187 channels with a maximum offset of 4655 m for ESCI-Valencia line (Figure 5.6).

Based on this dataset the multiple reflections have been modelled with the SRME module of Globe Claritas. After the creation of the model, the data has been transformed to its original geometry. In a second step, the adaptive subtraction of the model to the full data set is done in receiver domain as this gives more stability to the subtraction methods than in the shot domain (Wang, 2003). SRME is most effective in the near offset domain (first 150-200 channels or up to ~2700 m offset). The SRME is particularly effective, compared to other methods, in complex seafloor topographies. In shallow waters the SRME introduces some high-frequency noise (caused by aliasing of the model) in the deeper part of the profiles. This noise is effectively attenuated by RADON transform filtering later in the processing sequence.

First velocity analysis

A first velocity model suitable for Radon filtering and Dip Move Out (DMO) has been created. Velocity picking is performed on velocity semblance analysis each 400 CMP's or 2.5 km for TM26, and 5 km for ESCI-VAL.

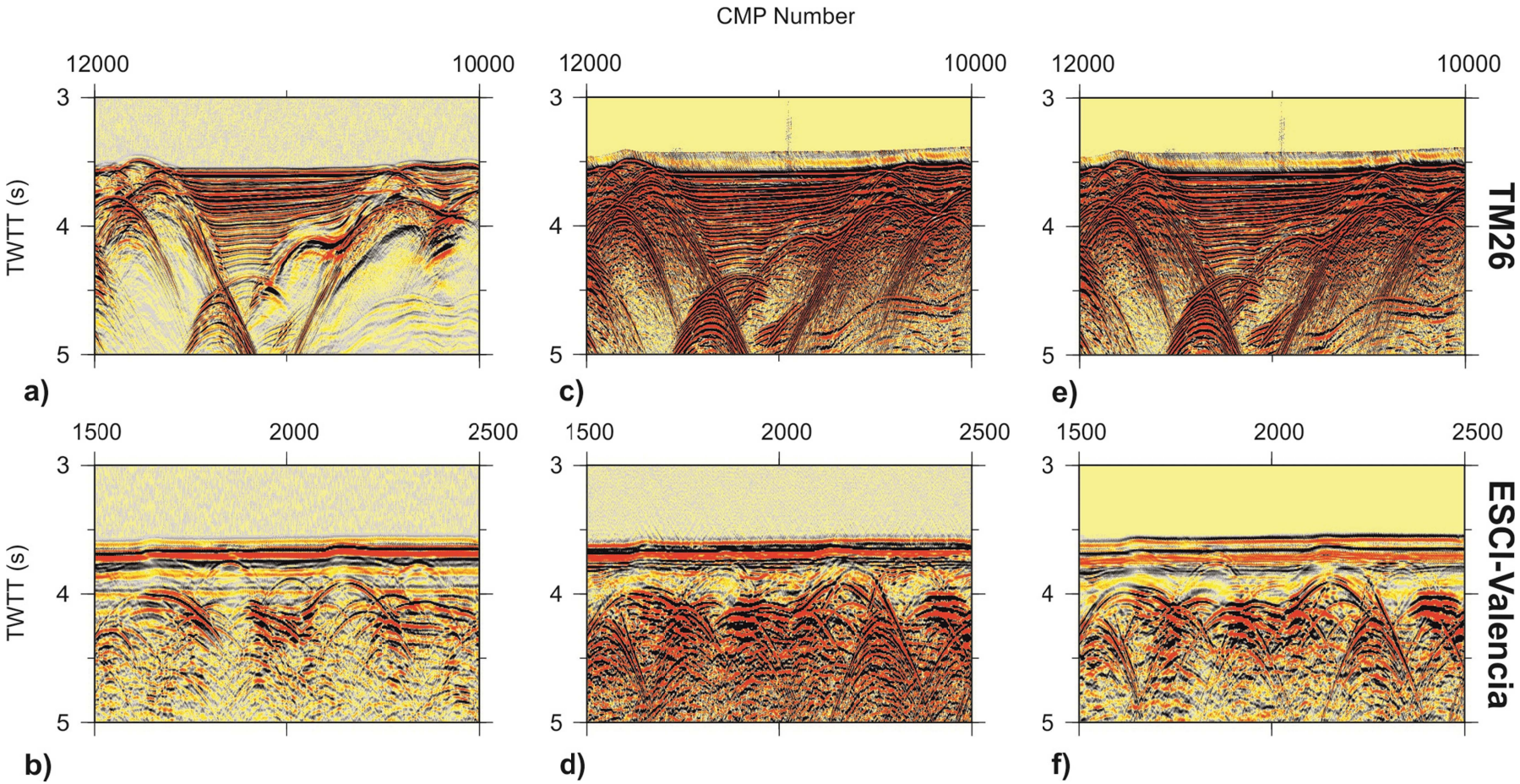

Figure 5.5 *Close ups of the deep Algerian Basin of lines TM26 and ESCI-Valencia during different processing steps. a) and b) are images of the pre-processing data, c) and d) the same image but after applying a deconvolution in a Tau-p domain and e) and f) corresponds to the same image after a surface-consistent deconvolution.*

Multiple attenuation 2: RADON filtering

Radon filtering was applied in order to further attenuate residual multiples particularly in far-offsets where the multiple was not effectively removed by the SRME process. Standard Radon methods involve transformation of CMP gathers into the parabolic Radon domain, where the multiple removal is more efficient and effective. High resolution, de-aliased multiple attenuation in the Radon domain is classed with those algorithms that rely on residual move-out to discriminate multiples from primaries. Velocities used for the Normal Move Out (NMO) must be picked with sufficient accuracy to distinguish primary energy from slightly slower multiple energy. In our case RADON filtering was applied from some 100 ms above the theoretical location of the first seafloor multiple to the end of the trace. The most important parameters for radon multiple attenuation are move-out ranges, of which there are two: Modelled and Noise. These move-out values refer to the amount of normal move-out at the far offset of the various events. The input CMP gathers were NMO corrected using a first velocity function and applied in super CMP domain (including all offset ranges). This gives a situation where there will be as many offsets in the CMP gather as there are in the shot gathers. In this case the increase in offset spatial sampling is beneficial to improve the Parabolic Radon filtering. Then the Noise parameter should be specified to model these multiples. For the selected dataset, a good move-out limits for signal and data were: Model_Ms (Moveout limits at maximum offset to be modelled): 500-4000 ms (TM26) and 400-4000 ms (ESCI-VAL) Noise_MS (Moverout limits at maximum offset of the “noise”): 504-3996 ms (TM26) and 408-3992 ms (ESCI-VAL) (Figure 5.6).

After the subtraction of the modelled multiple a Harlan signal extraction to Radon Transformation is applied. Essentially this provides a high-resolution Radon Transformation by taking the muted Parabolic Radon Transform (PRT) and the muted PRT of the input data with trace polarities randomly reversed, and inputting these two PR transforms into Harlan's signal extraction algorithm to focus the signal in the PR domain. This step ensures the preservation of relatively amplitudes and reduces the introduction of artefacts near the surface, where move-out values are large and reflections only exist on near offsets. After the application of the PRT-filtering, the CMP supergathers have been inverse-transformed to normal CMP gathers.

Dip Move Out (DMO)

CMP stacking after NMO reduces the amplitudes of both random noise and reflections with other stacking velocities. However, the signal is partially smoothed and disturbances due to aliasing noise and side diffractions are not completely removed. DMO reduces both coherent and aliasing noise even if the DMO correction is not completely accurate. NMO correction is only a time stretch, the dip move-out correction implies a time varying spatial filter, and it is often referenced as a Pre Stack Partial Migration. Claritas DMO module applies a Kirkhhoff DMO correction on pre-stack data in the time domain. This module works on NMO-corrected, common-offset sections. The NMO primary to the DMO should use a fairly smooth velocity profile. These smooth conservative velocities have been designed based on stacked datasets on which velocity zones have been digitized following the geological criteria. The assigned velocities coincide with average velocities from available information in the region. After the DMO the data have been sorted back to CMP gathers and the NMO process removed.

Second velocity analysis

Velocity picking was performed on velocity semblance analysis panel every 400 CMP on average, with the first velocity analysis being used as guide function. The aim of this second analysis is to estimate adequate root-mean-square (rms) staking velocity.

Mute files

Manual designed external or frontal mute removes the stretched far offset traces after NMO and improves the quality of the stacked datasets. Inner mute has as objective to further remove multiple energy in the near traces. Mute files were picked each 25/50 CMP for both MCS lines.

Stack

Stacking is the summation of traces within each CMP gather producing a single stacked trace. A conventional stack algorithm is used and the resulting stacked trace normalized for unity (for simple normalization **1**/**N(t)**), this function is not smoothed. Final stack is obtained using the velocity from the second velocity analysis.

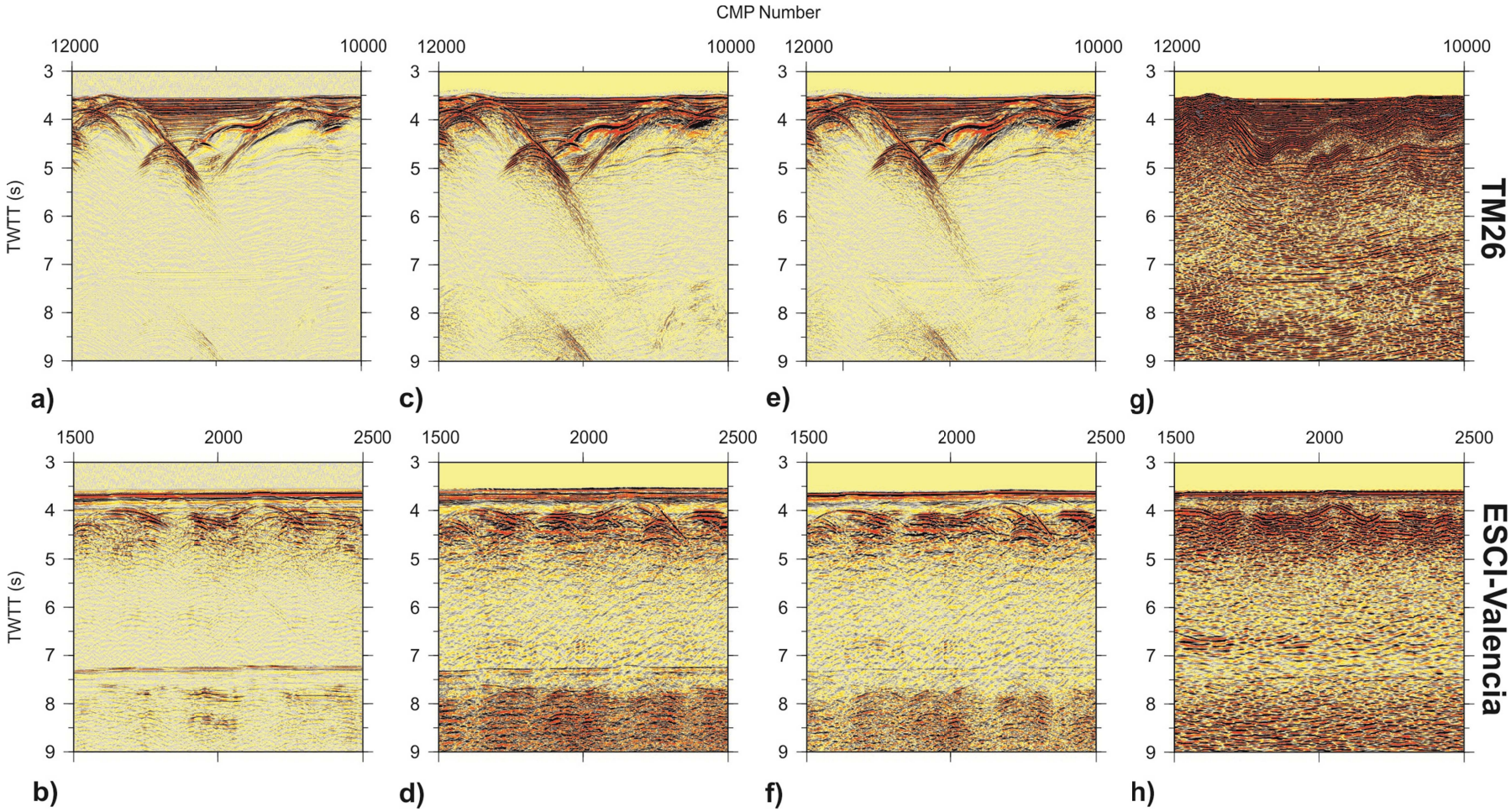

Figure 5.6 *Close ups of the deep Algerian Basin of lines TM26 and ESCI-Valencia during different processing steps. a) and b) are images of the pre-processing data, c) and d) the same image but after applying the multiple attenuation (SRME). e) and f) corresponds to the same image after the RADON filtering and g) and h) are a close ups of the final migration step.*

Zero-phase conversion

Zero-Phase operator was designed using the Globe Claritas wavelet tool. A hundred traces of a relatively flat region in the stacked profile have been autocorrelated over a length of 2500 ms with a correlation window of 500 ms. This autocorrelation signature was stacked and converted to zero-phase. A matching filter was designed to convert the data to zero-phase applied with a convolution module.

Time & space-variant band-pass filter

The objective of this band-pass frequency filter is to remove unwanted frequency components in order to improve the clarity of the imagery by increasing the signal-to-noise ratio. This is required since the higher frequencies are usually lost in the deeper sections due to various attenuation mechanisms and without filtering, the clarity of the deeper section is reduced by the presence of high-frequency noise. It is common to pass higher frequencies in the shallow part of the section and filter out high frequencies in the deeper part. In this processing sequence, the FDFILT Claritas module is used, which applies a zero-phase filter with a quasi-trapezoidal amplitude spectrum (Table 5.1). Each input trace is transformed into the frequency domain, where parts of the amplitude spectrum are zeroed and parts left unchanged, with cosine tapers to effect a smooth transition between the stop and pass bands. The phase spectrum is unchanged. Low-pass, high-pass, bandstop and bandpass filters may be applied. An inverse FFT is then performed to transform the trace back to the time domain. Filter windows were designed following the main geological domains, where frequency ranges are globally represented in Table 5.1.

TM26		**ESCI-VAL**	
Layer nº	**Filter**	**Layer nº**	**Filter**
1	10-14 / 60-70 Hz	1	9-12 / 60-80 Hz
2	8-12 / 50-65 Hz	2	8-10 / 50-70 Hz
3	5-8 / 40-55 Hz	3	7-9 / 45-60 Hz
4	3-6 / 30-45 Hz	4	6-8 / 40-50 Hz
5	1-4 / 25-30 Hz	5	4-6 / 30-40 Hz
6	1-3 / 20-25 HZ	6	1-4 / 20-30 Hz

Table 5.1 *Frequency ranges of the band-pass filter applied to the TM26 and ESCI-Valencia profiles.*

Q-inversion

The INVERSEQ module in Claritas provides a model-based post-stack gain and deconvolution, by essentially removing the dispersive absorption of the medium. It corrects the effect of seismic Q energy loss. The physical model for the mechanisms of the Q-effect assumes Q to be linear in the vicinity of the dominant frequency of the seismic signal. This frequency is identified to be 19Hz, the Q values used are 100-200 and only a gain recovery correction is applied, with no phase deconvolution.

Time migration

Migration corrects dipping reflections to their true position and collapses diffractions, resulting in a better continuity, coherence and resolution of reflections (Figure 5.6). Time migration is the last step of this processing flow. The FDMIG module of Claritas allowed performing a finite-difference time migration based on a X-T domain implicit 45 degree migration. Despite this 45-degree algorithm, experience indicates that this migration gives reasonable results for dips up to 60 degrees. The main parameters of this time migration are: 1) a smooth interval velocity model, 2) the THETA value, which corresponds to the cosine of the cut-off angle and was determined to be 0.65 for MCS line TM26 and 0.707 for MCS line ESCI-Valencia; and 3) the size of the time slices fixed to 4 ms. Time migration has been performed on a simplified velocity model created from main geologic domains.

Automatic Gain Control (AGC) scaling

Automatic Gain Control (AGC) using a 3 s running window was applied to the seismic data for display purposes after time migration.

Output

Final stack and time-migrated sections are output in standard SEGY format

Preliminary processing of the ESCI-Valencia profile was carried out by Geco-Prakla on May-November 1993. Then the line was fully re-processed by Vidal in 1995 using ITA-Landmark software. Finally, in order to improve the crustal and Moho imaging as well as the continuity and definition of pre-tertiary top of basement, we reprocessed the ESCI-Valencia seismic line using the software package Globe Claritas using algorithms that were either not available or too computer-intensive to be used in the 90's (see the MCS processing steps above). The processing main goals were to improve spatial sapling given the usually large shooting interval (75 m) and to attenuate multiple energy to improve basement structure.

In the following Figure 5.7 we compare the final time-migrated section of the ESCI-Valencia profile published by Gallart *et al*., (1997) (Figure 5.7a) and the time-migrated ESCI-Valencia profile resulting of our own processing flow (Figure 5.7b). It can be concluded that the image has been improved. In spite of the presence of salt bodies in the deep Algero-Balearic Basin, Moho reflections can be interpreted at 6.5 s TWTT. Beneath the Balearic Promontory, the Moho reflections are seen as 10-20 km-long segments located at 6.5 s TWTT at CMP 10000 and between CMP 15000-17000. Beneath the Valencia Trough Basin, Moho reflections can't be followed due to the presence of two important volcanic bodies located at CMP 20000 and 23000. Pre-tertiary top of basement is well constrained beneath the Ebro margin and along the Valencia Trough Basin. Top of basement is difficult to image in the deep Algero- Balearic Basin due to the presence of thick Messinian evaporites that mask the underlying image. Sedimentary sequence of the Valencia Trough Basin is well imaged, including the entire progradant sequence of the Ebro delta. Further interpretation of this line is presented in the next chapter 6.

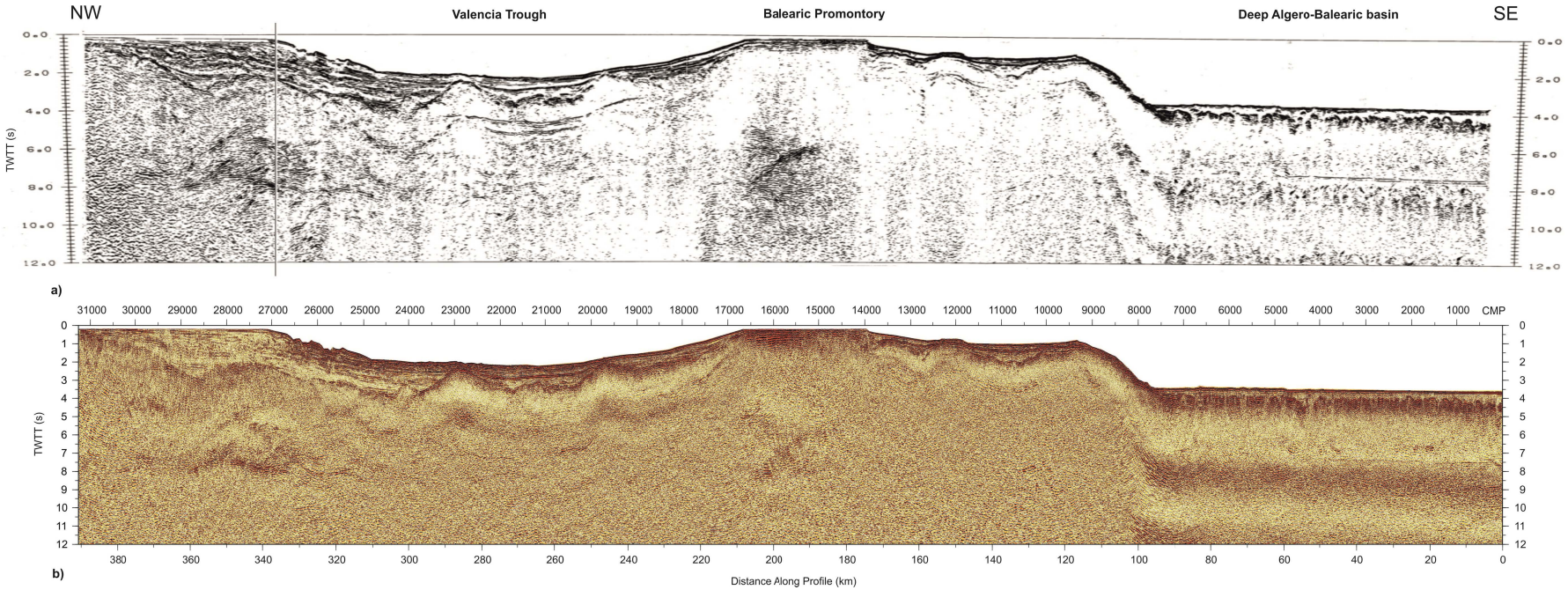

Figure 5.7 *Post-stack time migration of ESCI-Valencia profile. a) ESCI-Valencia profile published by Gallart et al., (1997). b) ESCI-Valencia profile result of the processing flow described above. The final image is quality improved as it can be seen in the Moho reflection, the top of the basement and the sedimentary sequence along the profile. For further interpretation see the next chapter 6.*

5.1.2 MCS VALSIS-819 line

A relatively simple processing of MCS VALSIS-819 (Chapter 4, section 4.1) was done at Lamont-Doherty Earth Observatory. The main processing steps included 1) a bandpass filter, 2) a noise filter, 3) a velocity-filtering applying an FK fan filter to the raw data, 4) a normal moveout correction (NMO) and 5) migration.

To improve the image quality, we further processed the stack through a post-stack deconvolution with a gap length of 124 ms and a filter length of 360 ms and a post-stack finite differences time migration with a velocity model created from available information of velocities of the main geological units in the area. In the following Figure 5.8 we compare the results from the time-migrated section of the VALSIS-819 published by Collier *et al*. (1994) (Figure 5.8a) and the final time-migrated section obtained after a deconvolution and post-stack migration (Figure 5.8b). VALSIS-819 MCS line extends from the Alicante shelf (SW) to offshore Tarragona (NE) along the Ebro platform (Figure 4.1). The image presented by Collier *et al*. (1994) is shorter, as they only show the Ebro platform section.

The image obtained by the deconvolution and migration of the stack displays a continuous high reflective band of reflections between 7 -8 s TWTT interpreted as the Moho reflections from the correpondance with ESP results (Maillard *et al*., 1999). An overlying 2 s TWTT thick band of reflections are identified between km 50 and km 150, which are interpreted as lower crust reflections. These lower crust reflections disappear towards both ends of the profile beneath the Alicante shelf and offshore Tarragona. Pre-tertiary top of basement and overlying Mesozoic to recent sedimentary sequence is well imaged along the profile. Further interpretation of this line is discussed in the next chapter 6.

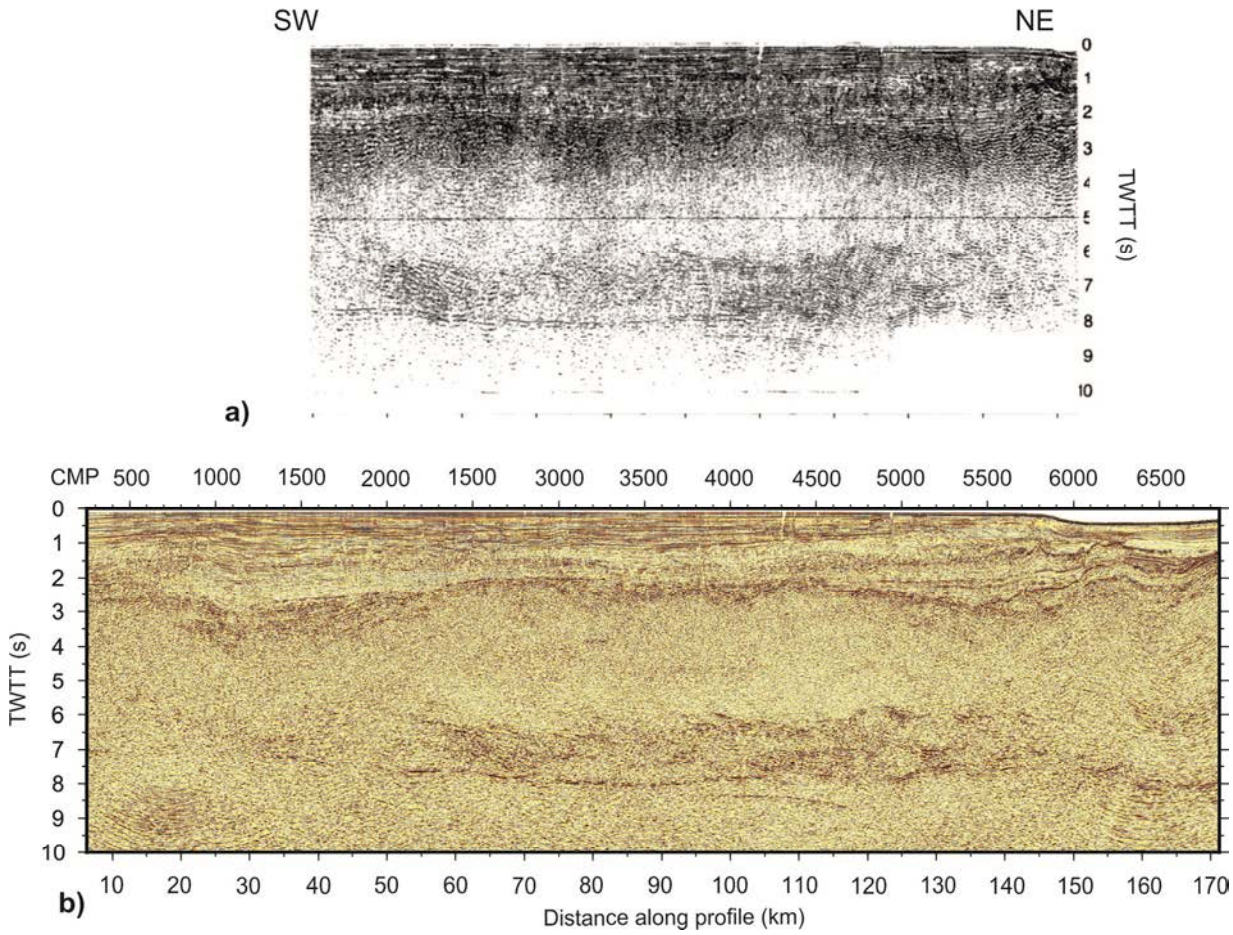

Figure 5.8 a) Migration section of VALSIS-819 MCS profile *published by Collier et al., (1994). b) Post-stack time migrated VASLIS-819 MCS line. The final image is quality improved as it can be seen in the Moho reflection, the top of the basement and the sedimentary sequence along the profile. For further interpretation see the next chapter 6.*

5.1.3 MCS SGV01 grid

Processing of 2D MCS grid SGV01 (Chapter 4, section 4.1) was performed by Robertson Research International Ltd including a 1) pre-stack predictive deconvolution with a gap of 32 ms and a filter length of 300 ms, 2) data resampling at 4 ms, 3) amplitude compensation to give a good balance of amplitudes down the record, 4) frequency-wavenumber (F-K) dip filter to remove noise on shot gathers (1250 m/s), 5) velocity analysis, 6) radon filtering, 7) dip moveout correction, 8) a prestack time migration using a constant velocity of 1500 m/s and 9) a post-stack Kirchhoff migration using a smoothed 2D velocity model from stacking velocities and a maximum half-aperture of 9000 m. Further post-stack processing included 10) a time variant band-pass filter and 11) two windows AGC.

5.1.4 MCS SPBAL grid

Processing of 2D MCS grid SPBAL (Chapter 4, section 4.2) was performed by Spectrum Energy Ltd including 1) a trace edition, 2) gain recovery, 3) resampling to 4 ms, 4) parabolic radon filtering, 5) dip move out, 6) deconvolution with a gap of 32 ms and a filter length of 240 ms, 7) normal move out correction, 8) spatially variant FK filter and 9) a Omega-X algorithm migration that is a frequency domain algorithm widely used by industry.

5.2 Wide-angle seismic data

5.2.1 WAS P03 line

Wide-angle seismic data (WAS) are processed to improve the signal-to-noise ratio and visually recognize the lateral correlation of the seismic phases in the record section. Although other processing steps may be applied, typically processing flow includes: 1) a relocation of the instruments in the seafloor due to the effect of oceanic currents, 2) a predictive deconvolution, 3) a time and offset variant bandpass filter and 4) an amplitude balancing. After WAS data are processed, they are modelled in terms of phases identifiable and laterally coherent over many traces. A conventional nomenclature is used for the following P-wave phases: Pg (upper crust), Pc (lower crust), Pn (upper mantle), PcP (reflected waves of mid-crust) and PmP (reflected waves of Moho boundary) (Zelt *et al*., 1994). Manual or automatic picking of the arrival times of every phase is the initial data set for the modelling.

Modelling of WAS data can be carried out using two different methods: forward modelling or inversion. The forward modelling implies a velocity model manually build that is improved by trail-and-error until an acceptable match between the observed and simulated data occurs. This method entails to much subjective analysis although it was a widely used method until 90's. The second method is the inverse or tomographic method. This method determines the velocity model in a more automated process (Korenaga *et al*., 2000). The tomographic method is divided in two main parts. The first part, known as forward problem, consists on tracing the ray paths and calculating travel-times of these rays. The second part, known as the inverse problem, consists on modifying, in an iterative way, the initial model inverting travel time residuals which is the difference between the real data and the synthetic data. WAS data in this work were processed and modelled at GEOMAR using a joint refraction and reflection travel time inversion method, implemented in the Tomo2d code (Korenaga *et al*., 2000; Grevemeyer, 2014 personal communication). This method allows obtaining a two-dimensional velocity model and also the geometry of a single floating reflector (Figure 5.9 a).

The initial model is modified successively until the standard deviation value equals approximately the uncertainty of the observed data (Figure 5.9b). The linear sensitivity of the inversion is provided by the Derivative Weight Sum (DWS) which is also a measure of the ray coverage (Figure 5.9c).

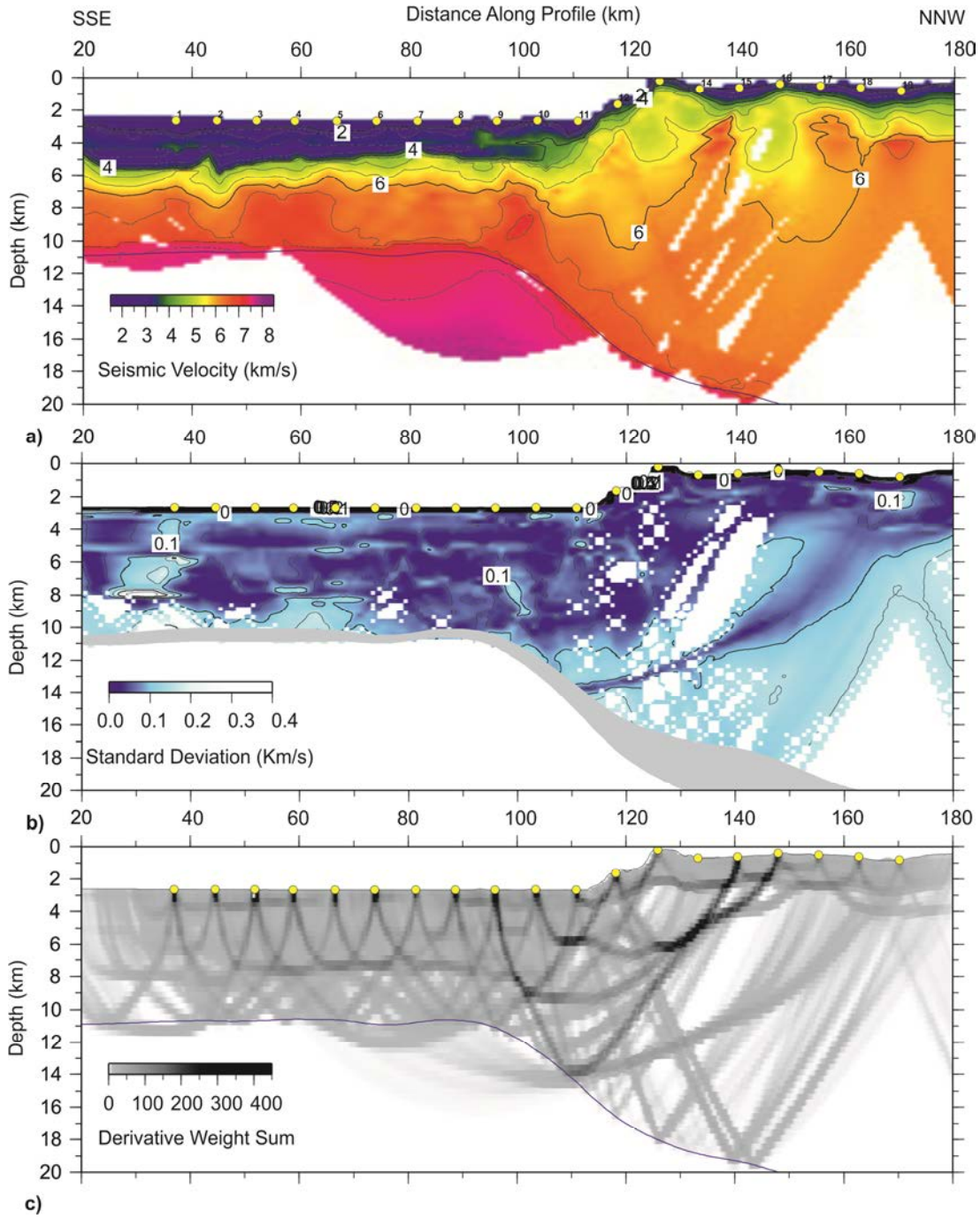

Figure 5.9 *a) Final velocity model of WAS line P03 obtained by the Tomo2d inversion method (Korenaga et al., 2000; Grevemeyer, 2014 personal communication). b) Standard deviation model of the WAS line P03. c) Derivative Weight Sum of the WAS profile P03. a) and b) are used to calculate a) during the inverse problem.*

5.3 Mirror Imaging

5.3.1 WAS P04 line

On WAS profile P04 we first applied a conventional imaging for the upgoing wavefield just below the seafloor (primary) and after that, we applied mirror imaging to the downgoing wavefield just above the seafloor (multiple) (see chapter 3, section 3.3). The software used was Omega from Schlumberger Limited and the main processing steps are shown in the following work flow (Figure 5.10).

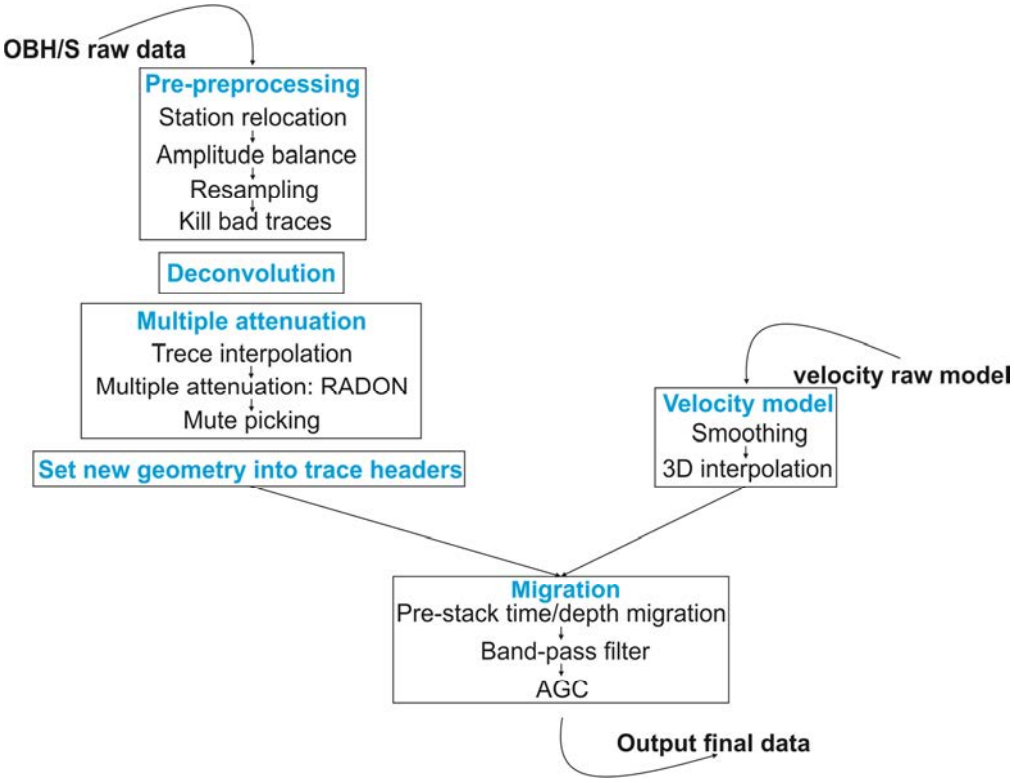

Figure 5.10 *Diagram of the processing flow followed for the P04 WAS line.*

Foremost steps in processing the data are: 1) quality control and trace edition. Due to a certain uncertainty in the OBS seafloor position because the ocean currents, we corrected for both source and receivers coordinates. Several OBS had to be relocated. After that, 2) we balanced the amplitude of every OBS, 3) resampled the data in order to obtain more coverage (4 ms in time and 5 m sampling in depth) and 4) killed bad traces (Figure 5.11a). Further processing included 5) a deconvolution with the aim to attenuate the signal bubble (Figure 5.11b), (6) a radon filter with a trace interpolation (Figure 5.11c), and 7) mute picking.

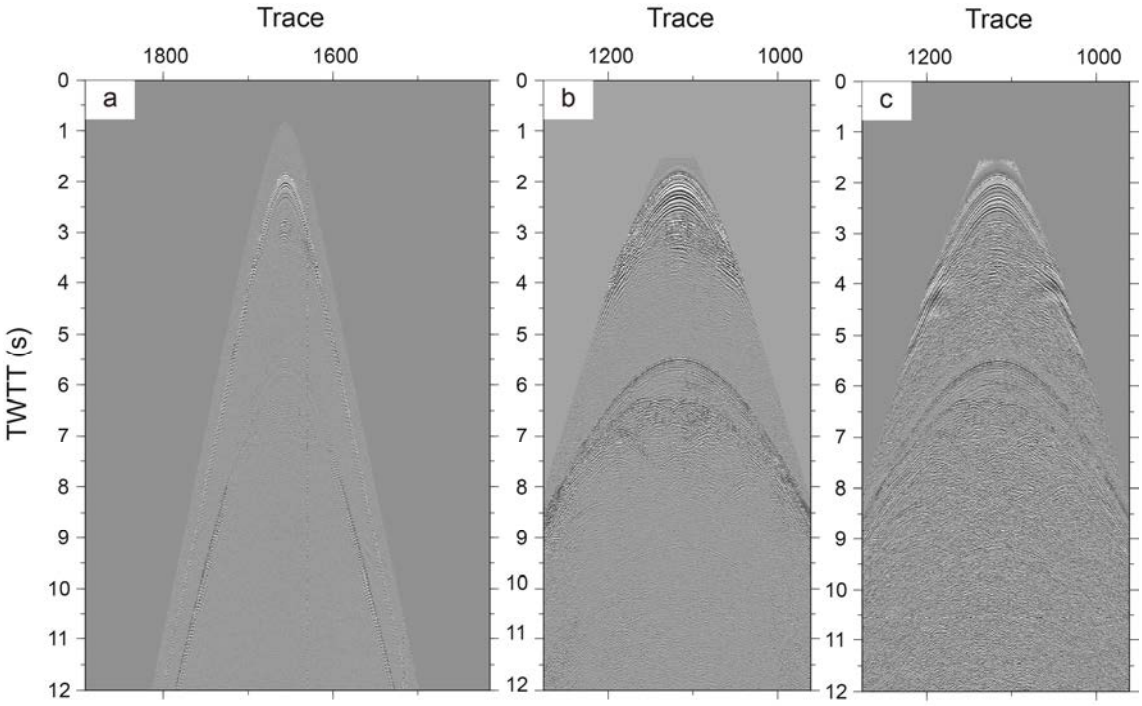

Figure 5.11 *Image of one OBS of WAS line P04. a) OBS after the pre-processing quality control. b) OBS after the deconvolution step. c) OBS after the radon filtering.*

Once the processing of all the OBS was finished, the following step was 8) to set the geometry information into the trace headers. For this it was necessary to build a crooked line between shots and receivers. Shots and receivers are rarely in line so we calculated a crooked line with the best fitting between shots and receivers and then introduced this new geometry into the trace headers. At the same time, and before the migration of the upgoing wavefield just below the seafloor (primary), it was necessary to do an interpolation of the velocity model in order to obtain a velocity value in every point between the crooked line (previously calculated) and the line defined by the coordinates of the velocity model. The input velocity model was obtained from the 2D traveltime tomography modelled by GEOMAR described in the previous section 5.2 (Figure 5.12).

The last step of the processing was migration. For that, we applied 9) a Kirchoff pre-stack time and depth migrations to the upgoing primary wavefield with an aperture angle of 60º. Finally, we applied a 10) Band-pass filter and (11) a time-variant automatic gain control (AGC). The processing flow for the downgoing wavefield just above the seafloor (multiple) have the same steps, the only difference is the change of geometry of the crooked line and the velocity model. New geometry was designed such that the receivers were placed effectively at the sea surface (not on the seafloor) of a water column twice as thick as the original water layer (see section 5.2).

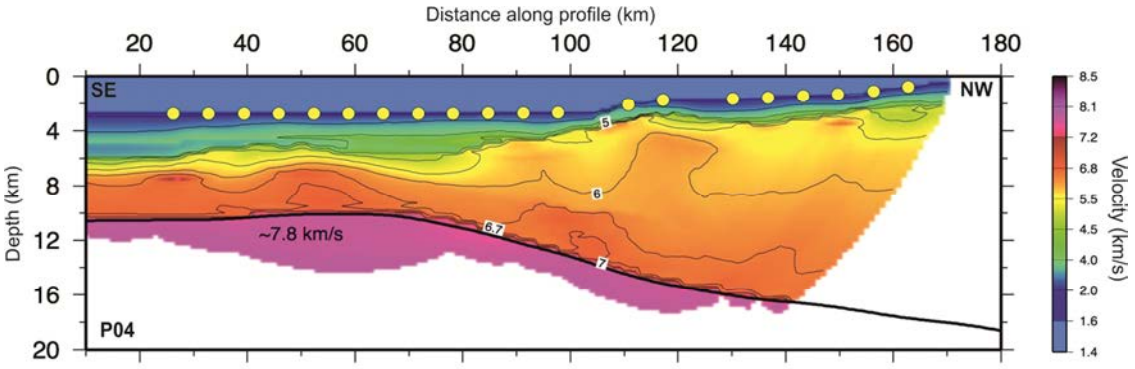

Figure 5.12 *Final velocity model of WAS line P04 obtained by the Tomo2d inversion method (Korenaga et al., 2000) and modelled by GEOMAR. This velocity model is the input model for the migration of the WAS line P04.*

The seismic record resulting from mirror imaging is comparable to a conventional MCS image. Figure 5.13 shows the migrated section of the WAS P04 in TWTT (Figure 5.13a) and depth (Figure 5.13b) after mirror imaging processing flow. Despite the fact that WAS data of the WESTMED project (Chapter 4, section 4.3) was not conceived with the intention to apply mirror imaging, the results show reasonable quality. It has been possible to obtain a seismic section where no deep-penetrating streamer data exists. P04 profile goes from the deep Algero-Balearic Basin to the south Eivissa margin in a SE-NW direction (Figure 4.1). For further interpretation see chapter 8.

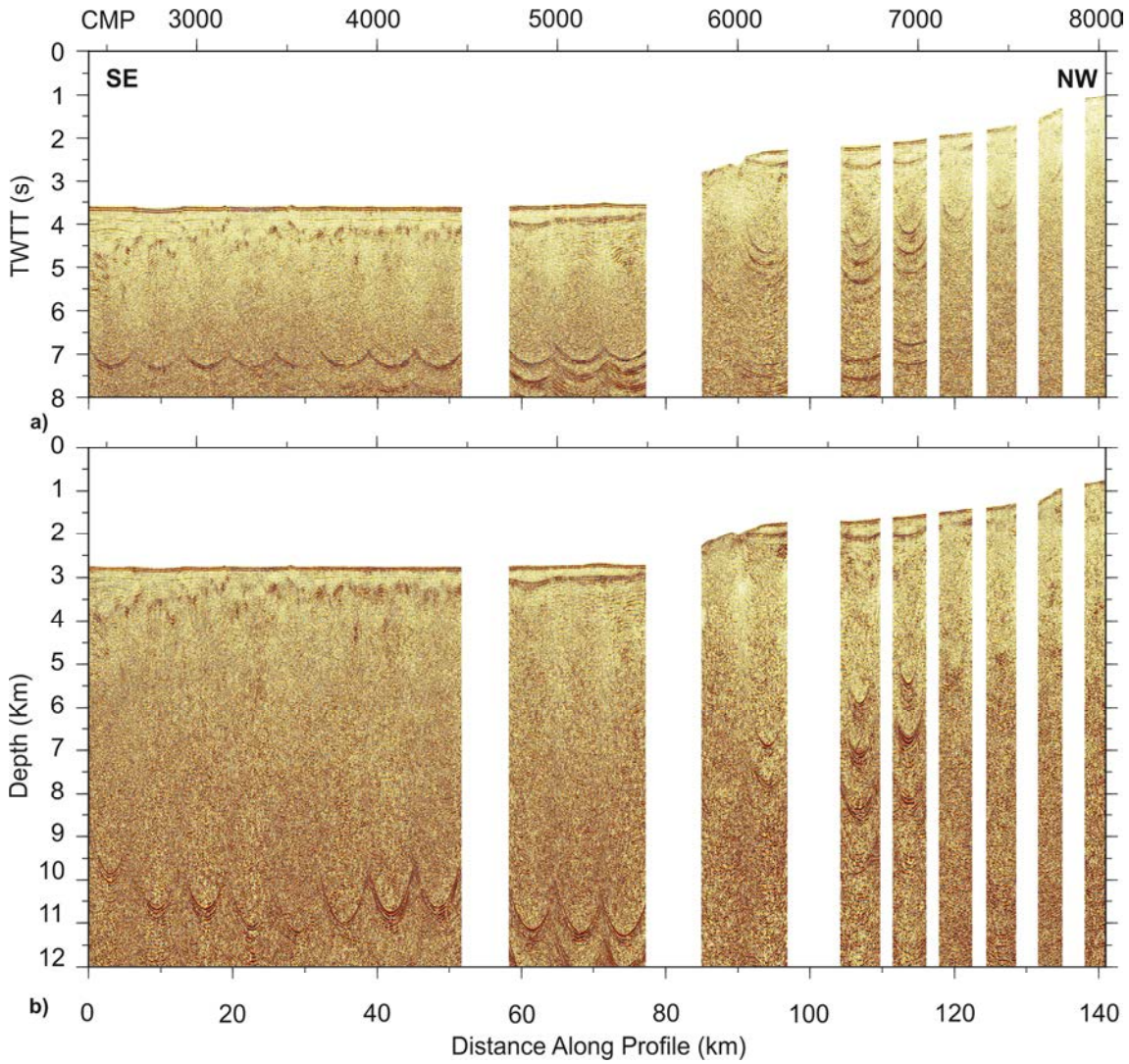

Figure 5.13 *Migrated sections from the WAS P04 profile using the mirror imaging technique. a) Final time-migrated section of multiple signal from the WAS P04 profile. b) Final depth-migrated section of multiple signal from the WAS P04 profile.*

5.4 Aeromagnetic data

As supplementary information useful to discuss the results of this thesis, we used the aeromagnetic data from the western Mediterranean region published by Galdeano and Rossignol (1977). The magnetic map allows a visualization of the upper crust in the subsurface, particularly the spatial geometry of bodies of rock and the presence of faults and folds. This is particularly useful where bedrock is obscured by surface sand, soil or like in this case, water. Aeromagnetic data were once presented as contour plots like in the case of the Galdeano and Rossignol (1977) map (Figure 5.14). In order to improve the visualization of this data, we digitized all contours using the Didger mapping software. After that, using the

ArcGis software we built a grid interpolating the data with the Topo to Raster tool that uses an iterative finite difference interpolation technique. The final image was plotted using the GMT-Generic mapping Tools software (Wessel *et al.*, 1991, 1995, 1998, 2013) (Figure 5.15).

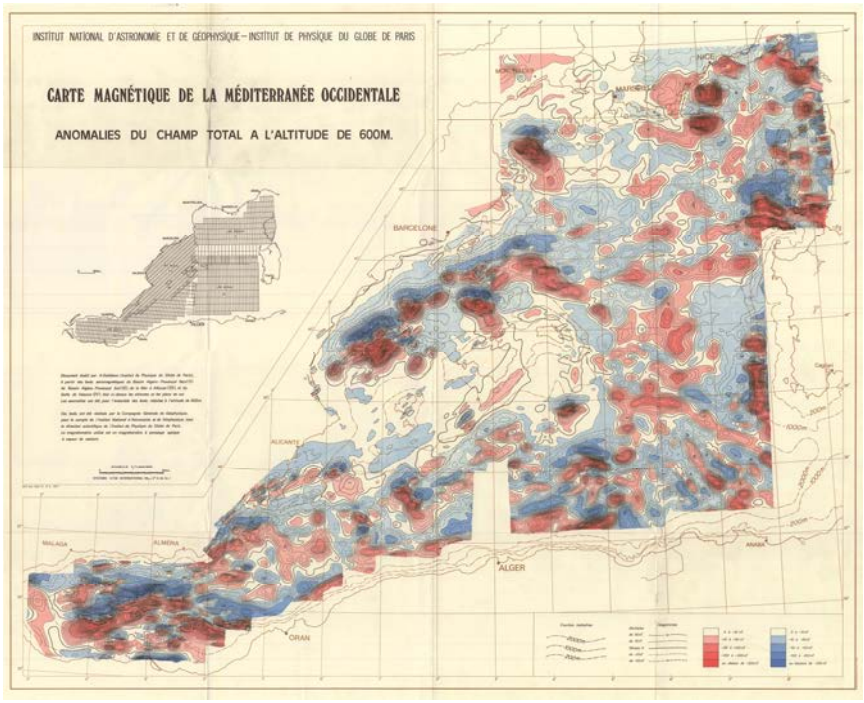

Figure 5.14 Original *aeromagnetic map of the western Mediterranean region as published by Galdeano and Rossignol (1977).*

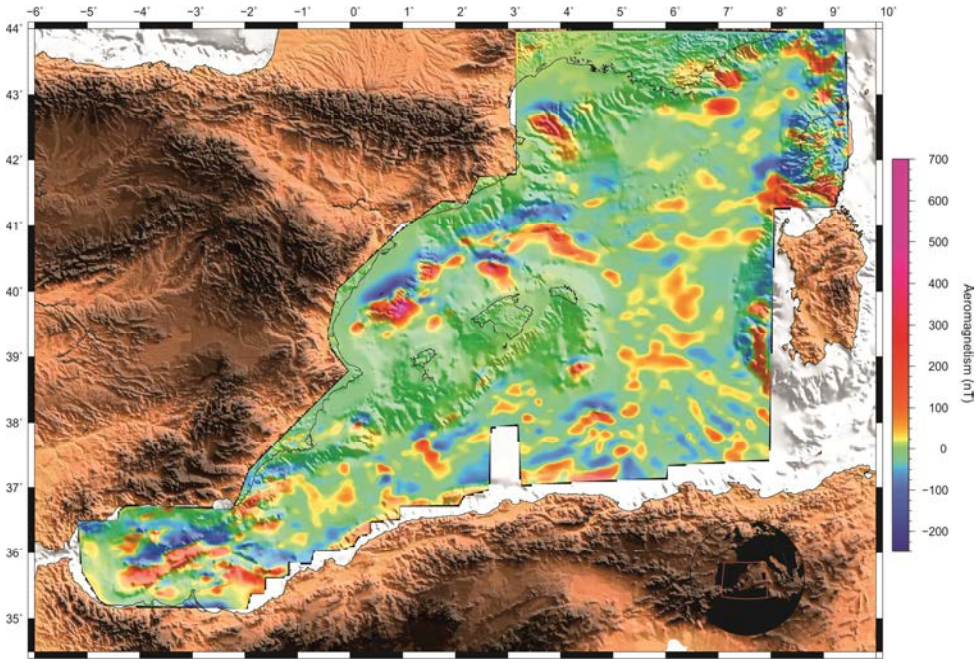

Figure 5.15 *Aeromagnetic map of the western Mediterranean region digitized from the Aeromagnetic map published by Galdeano and Rossignol (1977) (Figure 5.14).*

Part III:

Results

Chapter 6: Valencia Trough Basin

6.1 Introduction

The Valencia Trough Basin (VTB) is located between the north-eastern coastal region of the Iberian Peninsula and the Balearic Islands (Figure 6.1). It is one of a number of small basins in the Western Mediterranean interpreted to have been formed during the Neogene convergence between Africa and Europe. The VTB extends onshore into the Catalan Coastal Ranges. To the SW, it is bounded by the south-eastern end of the Iberian Chain. The eastern margin of VTB is formed by the Balearic Promontory, which is part of the external zones of the Betic thrust and fold system.

The origin and evolution of the VTB is debated, while some authors have considered the Valencia Trough as a back-arc extensional basin formed during the Neogene subduction of the Africa beneath Europe (Dewey *et al*., 1973; Rehault *et al*., 1984; Lonergan & White, 1997; Rosenbaum *et al*., 2002; Faccenna *et al*., 2004; Jolivet *et al*., 2006; Dowe, *et al*., 2014), other works have emphasized Mesozoic extensional features (Roca *et al*., 1992; Roca, 1996; Salas *et al*., 2001). Studies done by Roca *et al*. (1992) and Salas *et al*. (2001) conclude that the crustal thinning of the Valencia Trough Basin cannot result only from Neogene extension and proposed a model that includes the Mesozoic and Paleogene evolution of the Valencia Trough Basin. These authors consider the Mesozoic and Neogene extensional events equaly important to explain the crustal thinning of the VTB.

The main geology of the VTB is well known due to numerous studies since the ‘70s. Together with refraction and reflection marine experiments there are several petrological studies along the entire Iberian margin that have contributed a considerable volume of data on the geology of the Valencia Trough Basin (Dañobeitia *et al*., 1992; Pascal *et al*., 1992; Torné *et al*., 1992; Gallart *et al*., 1994, 1995; Vidal *et al*., 1997, 1998; Maillard *et al*., 1999)

Here, we first describe the seismic character of the basement and identify Moho reflections that we also use to define the variations in the thickness of the interpreted crystalline basement along the basin. Moreover, we interpret the main sedimentary units present in the whole trough in order to discuss the existing evolutionary models. Finally, we present some considerations for a new formation model for the rift phase of the Valencia Trough Basin. To conduct this work, we reprocessed available academic data and integrated them with more modern industry multichannel seismic data that allow us to define the main features of the basin.

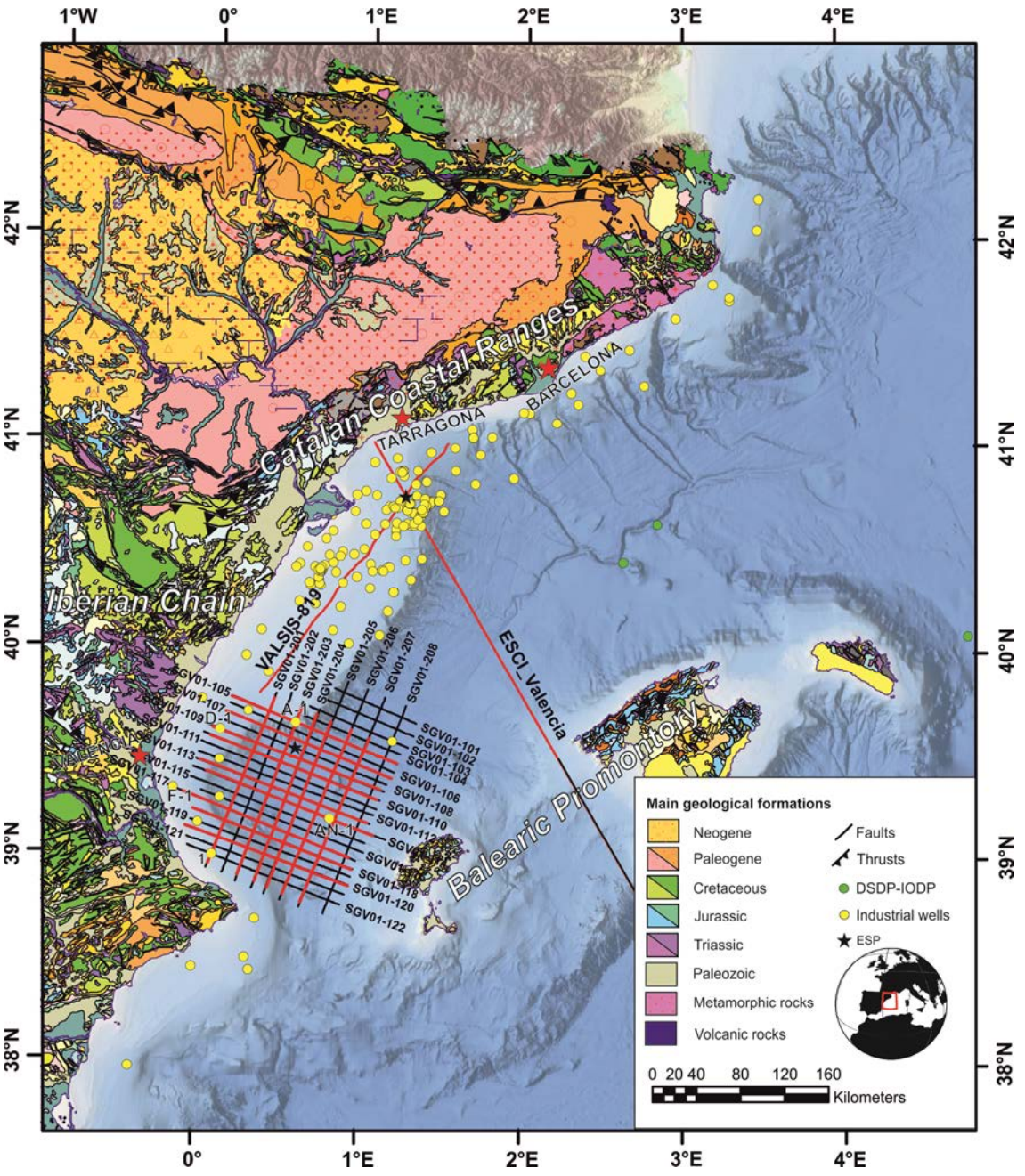

Figure 6.1: *Bathymetric and geologic map of the Valencia Trough Basin (NE of Iberian Peninsula). It is formed by two main geologic and geographical domains. The Catalan-Valencia domain; includes the southeastern end of the NW-SE Iberian Chain, the NE-SW Catalan Coastal Ranges and the western and northern offshore areas of the Valencia Trough. The Betic-Balearic domain; includes the Balearic Promontory that corresponds to the northeast prolongation of the Betic thrust and fold belt and the adjacent offshore areas of the Valencia Trough. The Valencia Trough is a basin with a NW-SE direction. ESCI-Valencia red line corresponds to multichannel seismic profiles acquired between February and March 1992 by Geco-Prakla's survey vessel M.V.Bin Hai and reprocessed and interpreted for this work (Figure 6.2a). VALSIS-819 red line correspond to the multichannel seismic profile acquired in November of 1988 by Lamont-Doherty's vessel Robert D. Conrad and the*

IFREMER operated vessel Jean Charcot also reprocessed and interpreted for this work (Figure 6.2b). SGV01 2D grid corresponds to multichannel seismic lines acquired in October 2001 by the Furgo-Geoteam's vessel R.V. Geo Baltic. Red segments correspond to the segments of the SGV01 profiles interpreted and discussed in the text (Figures 6.4, 6.5). Green dots mark locations of DSDP and ODP holes. Yellow dots marked the locations of different industrial wells used in the interpretation of the seismic lines SGV01 (Lanaja, J.M., 1987). Black star marked the location of an Expanded Spread Profile (ESP). From NE to SW, red stars mark the location of Barcelona, Tarragona and Valencia cities.

6.2 Geological Setting

Relative motion between European and African plates with respect to North America is known since the first analysis of magnetic anomalies and fracture zones in the Atlantic Ocean (Pitman and Talwani, 1972). Each magnetic anomaly lineation delineates a former ridge axis and it is thus an isochron for a former accreting plate margin. The fracture zones are approximately vector traces, indicating the direction of relative motion of the accreting margins. The patterns of magnetic lineations and of the fracture zones along which these lineations are offset define the geometry of which plates have separated (Dewey *et al*., 1973).

Africa and South America started to separate from North America in Triassic times; South America began to break apart from Africa in Jurassic times and the primary movement of Europe away from North America began in the Cretaceous period (Smith, A., 1971; Phillips *et al*., 1972; Dewey *et al*., 1973). The structural and magmatic complexity of the Valencia Trough Basin responds to different kinds of motion that African and European plates have had since the Mesozoic. This complexity is evident in the whole region, where replacement between tectonic and magmatic processes related to every phase of motion has been progressive and has not occurred synchronously throughout the region (Roca, 1996). For this reason two domains with different structural features (the Catalan-Valencian and the Betic-Balearic) have been differentiated (Fontboté *et al*., 1990).

6.2.1 Catalan-Valencian domain

This domain includes the southeastern end of the NW-SE striking Iberian Chain, the NE-SW trending Catalan Coastal Ranges and the western and northern offshore areas of the Valencia Trough (Figure 6.1). Pre-Neogene structure of the southeastern Iberian Chain is characterized by E-W to NW-SE oriented Mesozoic basins shortened during Paleogene

compression phase caused by the collision between Iberia and Europe during the Pyrenean orogeny (Fontboté *et al*., 1990; Salas *et al*., 2001). During Paleogene basin inversion, pre-existing faults were reactivated and a system of thrust sheet developed, employing Muschelkalk and Keuper evaporites as detachment surfaces (Salas *et al*., 2001). In the Catalan Coastal Range the contractive Paleogene structure is characterized by a set of sinistral ENE-WSW to NE-SW trending faults. These faults had normal slip during the Mesozoic times. During the Neogene extensional phase new normal fault oriented NNE-SSW and NNW-SSE were generated, cutting through the Paleogene structures in the southeastern Iberian Chain (Parés *et al*., 1992). Extension in the Catalan Coastal Range caused the formation of a host and graben system orientated ENE-WSW to N-S. These normal faults resulted from the re-work of major Paleogene strike-slip faults.

6.2.2 Betic-Balearic domain

The Betic-Balearic domain includes the Balearic Promontory that corresponds to the northeast prolongation of the Betic thrust and fold belt and the adjacent offshore areas of the Valencia Trough (Figure 6.1). It consists of northwest trending thrust sheets stacked in a piggy-back sequence and affected by ENE-WSW trending normal faults, resulted from the reactivation of pre-existing thrusts (Fontboté *et al*., 1990). Two different tectonic processes developed in the Western Mediterranean affected the Betic-Balearic domain during the Neogene: 1) A compressional event during the Late Oligocene-Middle Miocene that build up the thrust system and 2) An extensional event during the Middle-Late Miocene related to the opening of the Algerian Basin due to subduction of African Lithosphere beneath Iberia (Fontboté at al., 1990; Roca *et al*., 1992).

6.3 Seismic character of the basement and Moho

We used in this work three different datasets: ESCI-Valencia profile (400 km-long) shot perpendicular to the strike of the trough across the middle segment of the basin, VALSIS-819 profile (170 km-long) shot along the shelf of the NW Iberian margin and the SGV01 grid of 2D lines (2800 km) in the SW Valencia Trough Basin (Figure 6.1) The images provide information of the seismic character of the basement and Moho in the whole area.

6.3.1 Deep Valencia Trough Basin

The ESCI-Valencia reflection seismic line crosses the VTB in a NW-SE direction (Figure 6.1). ESCI-Valencia extends from offshore Tarragona (Figure 6.1), crossing the Valencia Trough and the Balearic Promontory into the Algero-Balearic Basin. Previous reflection and wide-

angle seismic academic studies date mainly from the 80's or early 90's (Dañobeitia *et al*., 1992; Gallart *et al*., 1994, 1995; Vidal *et al*., 1997, 1998; Maillard *et al*., 1999) and modern deep penetrating data has only been collected by industry. The depth of the Moho discontinuity, determined where velocity changes from crustal velocities (here typically < 7.5 km/s) to mantle velocities (here typically > 7.8 km/s), has been locally mapped with 1D Expanded Spread Profiles (ESP) along the continental shelf and trough (Pascal *et al*., 1992; Torné *et al*., 1992) and low-resolution 2D profiles with marine shots, a few OBS and land stations (Dañobeitia *et al*., 1992; Gallart *et al*., 1994, 1995; Vidal *et al*., 1997, 1998) coincident with ESCI-Valencia reflection line.

Figure 6.2a shows 198 km of re-processed ESCI-Valencia profile from NW Iberian margin to SE Balearic Promontory. In this time-migrated section, we interpret a strong and laterally fairly continuous reflections situated from 7.5 to 8.5 s TWTT as the Moho discontinuity, also described by Vidal *et al*. (1998). The Moho reflection is strong beneath both Iberian and Balearic margins and weaker in the centre of the trough. Our processing has enhanced Moho imaging across the VTB, where it remains at fairly constant TWTT throughout the profile.

The top of the basement (black dots in Figure 6.2a) is well imaged beneath the Iberian margin. We interpret the basement top as a surface situated at ~4.5 s TWTT marking the change between an upper section formed by well-stratified reflections (interpreted as Mesozoic strata) and a lower part with weaker reflectivity interpreted as the upper crystalline crust. Top of the basement is deeper at the centre of the trough, and is more difficult to follow because of the presence of volcanic edifices and multiple energy not fully eliminated. Interestingly, a basement thickness of ~3.5 s TWTT (~10-11 km with velocities from Vidal *et al*., 1998) remains almost constant under the trough, increasing beneath the Balearic margin to ~18 km thick.

Intra-basement reflectivity is generally weak, but 30 km offshore under the Iberian margin, lower crust reflectivity forms locally a 1-2 s TWTT thick band (km 340-380, Figure 6.2a). Some authors interpret that this lower crust reflectivity was created prior to the Late Oligocene/Early Miocene stretching event (Watts *et al*., 1990; Torné *et al*., 1992; Collier *et al*., 1994), and interpreted that the lower crust reflectivity is absent in the trough because it was destroyed during extension (Collier *et al*., 1994). Beneath the Balearic margin a band of 2 s TWTT thick lower crust reflectivity is observed (from km 200 to km 220 in the profile). In this case, two trends of reflections can be identified: one is flat, and the other dips in NW direction. Differences in crustal structure between the Iberian and Balearic domains are suggested by the difference in structural styles. Whereas the Iberian margin has been under

various extensional and compressional pulses since Mesozoic times with a last extensional event in the Neogene times, the Balearic margin was under compression during Neogene times. The position of the boundary between these two domains is debated. Roca *et al*. (1992) suggested that the boundary is located near the Valencia Trough axis while Maillard *et al*. (1992) moves the position between these two domains closer to the Balearic Promontory. We note that the presence of different volcanic structures located in the centre of the trough may indicate that the boundary between the extensional Iberian domain and the compressional Balearic domain might not be located in the trough axis but possibly closer to the Balearic margin.

6.3.2 North-West Iberian margin

Profile VALSIS-819 located in the Iberian margin with a SW-NE direction displays distinctive lower crust reflectivity along much of its length. Figure 6.2b shows well-developed reflectivity consisting in a 50 km-long band of 2-5 km long horizontal reflections between 6-8 s TWTT. This trend of reflections terminates at the base of the band marked by a laterally more coherent event interpreted as the Moho discontinuity (white dots in Figure 6.2b). Lower crust reflectivity is best developed from CMP ~2000-6000 (km 25-70), roughly under the Ebro platform. A change in the lower crust behaviour occurs at km ~70 where reflectivity becomes weaker to the NE and disappears offshore Tarragona (Figures 6.1, 6.2b). A similar change in lower crustal reflectivity occurs towards the SW, from km 25 to the SW end of the profile reflectivity becomes weaker until it disappears.

Lower continental crust reflectivity observed in different margins elsewhere might be related to ductile shearing or magmatic intrusions. The origin of lower crust reflectivity has been discussed in other deep seismic lines in Western Europe. Bois *et al*. (1988) interpreted that lower crust reflectivity under France may be the result of metamorphism and magmatism in the lower crust as a consequence of a regional thermal event associated with extension, which occurred during the rifting of the Alpine Tethys ocean and the initiation of the Mesozoic cratonic basins during the Late Triassic-Middle Jurassic. The absence of lower crust reflections in the axis of the Valencia Trough (Figure 6.2a) does not favor that reflections were created by Neogene extension because it should have a clear expression where the extension is maximal (Peddy *et al*., 1989). Moreover, Watts *et al*. (1990) subsidence study supports that the layered lower crust existed before the Neogene event. Thus, the formation of the layered crust must then be pre-Tertiary in age (Maillard *et al*., 1999).

The basement thickness decreases from the NE to the SW. Beneath the Ebro margin the basement thickness is ~3.5 s TWTT (~10.5 km), and thins towards SW with a minimum

thickness of ~2.5 s TWTT (~7.5 km) at the SW end of the profile, under the Valencia shelf (Figures 6.1, 6.2b).

6.3.3 South-West Valencia Trough Basin

The grid of industry data in the southwestern end of the Valencia Trough Basin allows mapping the Moho reflection from offshore Tarragona city to offshore Valencia city under much of the continental platform and slope. Multichannel seismic line SGV01-201 runs with similar SW-strike and ends to the NE about 2-3 km from the southwestern end of VALSIS-819 line (Figure 6.2c). VALSIS-819 shows clear and continuous reflections situated at 7-8 s TWTT interpreted as the Moho. The interpretation of Moho is supported by the wide-angle results from ESCI-Valencia Project (Dañobeitia *et al*., 1992; Gallart *et al*., 1994, 1995; Vidal *et al*., 1997, 1998; Maillard *et al*., 1999) that crosses VALSIS-819 on km 140. Moho reflection becomes gradually shallower from the NE at ~8 s TWTT towards the SW shoaling to 6.7-7.0 s TWTT at the SW end of the VALSIS-819 profile.

Figure 6.2: *(a) Poststack time migration of ESCI-Valencia line reprocessed and interpreted for this work. (b) Poststack time migration of VASLSIS-819 line also reprocessed and interpreted for this work. (c) Poststack time migration of line SGV01-201 interpreted and discussed for this work. (d) Poststack time migration of line SGV01-110 interpreted and discussed for this work. For the location of every line see Figure 6.2e. White dots mark the reflections interpreted as Moho discontinuity. Black dots mark the boundary between an upper section formed by multiple reflections that appear well stratified (interpreted as Mesozoic strata), and a lower part with weaker reflectivity interpreted as the upper crystalline crust as top of the basement. Green dots mark the high reflective horizon interpreted as the Oligocene unconformity marking the top of Mesozoic sequence. Blue dots mark an also high reflective horizon interpreted as the Messinian top sequence (MTS). Vertical black lines mark the intersection between profiles. e) Reference map with the profiles location.*

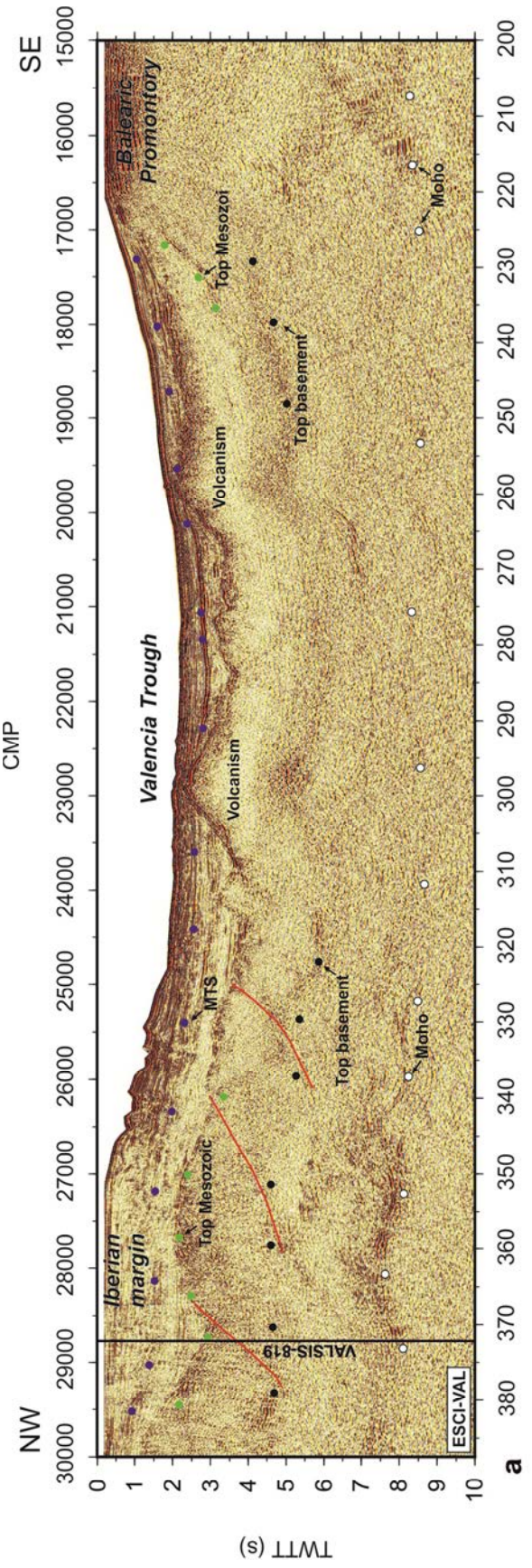
NW
SE
CMP
TWTT (s)
Iberian margin
Valencia Trough
Balearic Promontory
Top Mesozoic
MTS
Volcanism
Top basement
Moho
VAL-SIS-819
ESCI-VAL
a

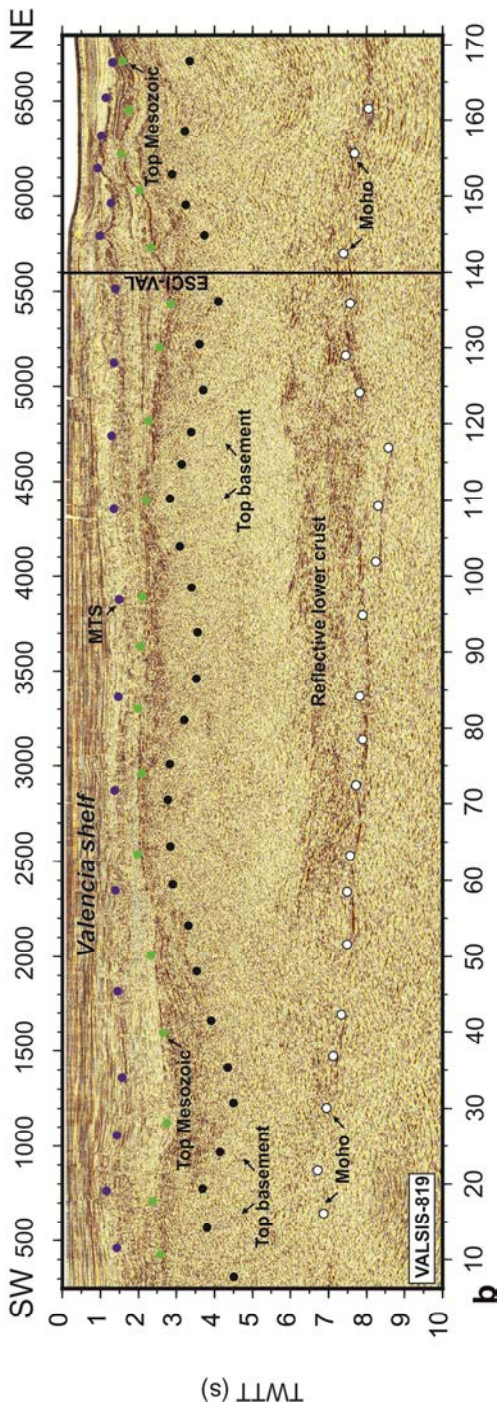
SW
NE
TWTT (s)
Valencia shelf
MTS
Top Mesozoic
Top basement
Reflective lower crust
Moho
ESCI-VAL
VALSIS-819
b

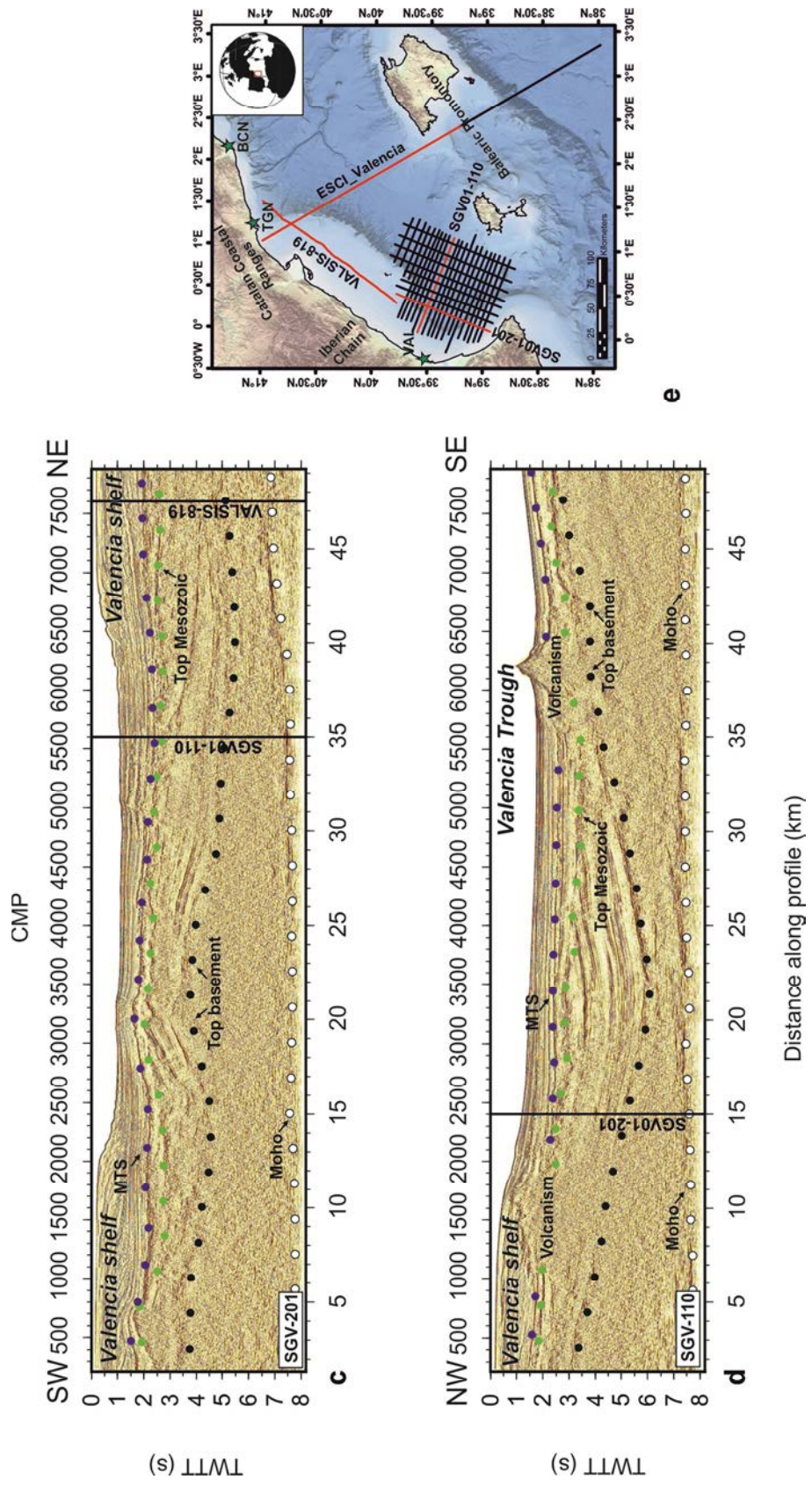
e
BCN
TGN
VAL
ESCI_Valencia
VALSIS-819
SGV01-110
SGV01-201
Balearic Promontory
Catalan Coastal Ranges
Iberian Chain
c
SW
NE
CMP
Valencia shelf
MTS
Top Mesozoic
Top basement
Moho
SGV-201
TWTT (s)
d
NW
SE
Valencia Trough
Volcanism
SGV-110
Distance along profile (km)

Line SGV-01 displays high amplitude, fairly continuous reflections at ~7 s TWTT beneath the NE Valencia shelf, interpreted as Moho reflections, as a continuation of similar reflections in profile VALSIS-819 (white dots in Figures 6.2b and 6.2c). Moho discontinuity becomes deeper to the SW reaching 8 s TWTT at the end of the profile. Top of the basement (black dots in Figure 6.2c) and Moho reflections indicate that a minimum basement thickness of only 1.5 s TWTT (~4.5 km assuming velocities from ESCI-Valencia under the shelf) occurs at km ~45. From km 45, basement thickness increases towards SW, with a maximum thickness of ~4 s TWTT (~12 km) at the SW end of the profile. The lower crust reflectivity imaged on profile VALSIS-819 that disappears towards the southwestern end of the line does not occur on SGV01-201 (Figure 6.2c).

Line SGV01-110, perpendicular to the margin, shows a crustal structure that bears resemblance to line ESCI-Valencia but with no reflective lower crust (Figure 6.2d). Line SGV01-110 shows a strong and continuous reflection at ~7.5 s TWTT interpreted as Moho (white dots in Figure 6.2d) because it has been continuously traced from ESCI-Valencia where it is well constrained. The top of the basement is generally well defined often by a group of bright reflections (e.g. CMPs 3500-5500 Figure 6.2d) away from where the structure is obscured by recent volcanism (Figure 6.2d). Basement thickness at the centre of SGV01-110 is 1.5 s TWTT (~4.5 km), which does not match the morphological centre of the trough, and thickens towards both ends. A 3.5 s TWTT thick (~7-8 km thick), well-stratified sedimentary sequence that occurs at the centre of the profile is made of Mesozoic strata drilled in several wells (Figure 6.1) situated in the link region between Iberian and Catalan Coastal Ranges structures.

It seems that the layered lower crust is related to the formation of Mesozoic basins. This is well imaged in both Iberian and Balearic margin (Figures 6.2a, b) but, beneath the Columbretes Basin where a 7-8 km thick Mesozoic stratum is present, no layered lower crust is detected. Even though, some lower crust reflections are imaged at the centre of the basin (Figure 6.2d).

6.4 Variation in crustal thickness

As described in the previous section, the basement does not thin from under the shelf towards the Valencia Trough centre, although its thickness changes along and across the basin. In the southwestern region of the VTB, basement thickness decreases from ~3 s TWTT or ~9 km to ~1.5 s TWTT or ~4.5 km (Figure 6.2d). In contrast, along the ESCI-

Valencia profile, basement thickness remains rather constant from the centre of the trough where is ~3 s TWTT (~9 km) towards both margins (Figure 6.2a).

To understand the basin formation we have mapped the Moho reflection, the top of the basement, the top of Mesozoic sediment unit and the Messinian top sequence (MTS) across the lines of the SGV01 grid. A total of 15 representative interpreted lines are shown in Figures 6.4 and 6.5. We constrained the interpretation using industry wells (Lanaja, J.M., 1987), located on several lines from the grid (Figure 6.1) and that calibrate the top of the Mesozoic unit (Figure 6.6). We point out that well Columbretes A-1 present in lines SGV01-105 and SGV01-203 (Figures 6.4a, 6.5b) may have a poor description of the drilled sequence, because it is interpreted to present more than 3 km of Miocene sediments whereas the seismic profiles (Figures 6.4a and 6.5b) clearly show that it penetrates the top Mesozoic unconformity much shallower than in the description provided by Shell International in 1974 (Lanaja, J.M. 1987).

We used the Moho and top of the basement reflections to map basement thickness in TWTT. After the horizon picking we built a surface grid using a near-neighbor algorithm with a cell size of 3 km, and later converted time to depth using velocity information from published wide-angle seismic experiments (Pascal *et al*., 1992; Torne *et al*., 1992, Vidal *et al*., 1998). To avoid creating artefacts from lateral velocity changes we assumed a constant basement velocity of 6.5 km/s that represents well the average basement velocity (Figure 6.3). Velocities ranging from 5.5 to 6.5 would change little the main features of the basement thickness map, which will be later discussed.

Figure 6.3: *Basement thickness map centred on the SW end of the Valencia Trough Basin. Black lines (SGV01-101 to SGV01-208) correspond to multichannel seismic lines interpreted and discussed in this work (Figures 6.1, 6.4, 6.5). Basement thickness is represented in different colours from white colours (thicker values) to light blue colours (thinner values). This map shows the Columbretes Basin as square-shape geometry typical of pull-apart basins bounded by vertical faults with a strike-slip movement. The map also shows two small sub-basins with thicker crustal values than Columbretes Basin. For more information see the text (Chapter 6, section 6.4).*

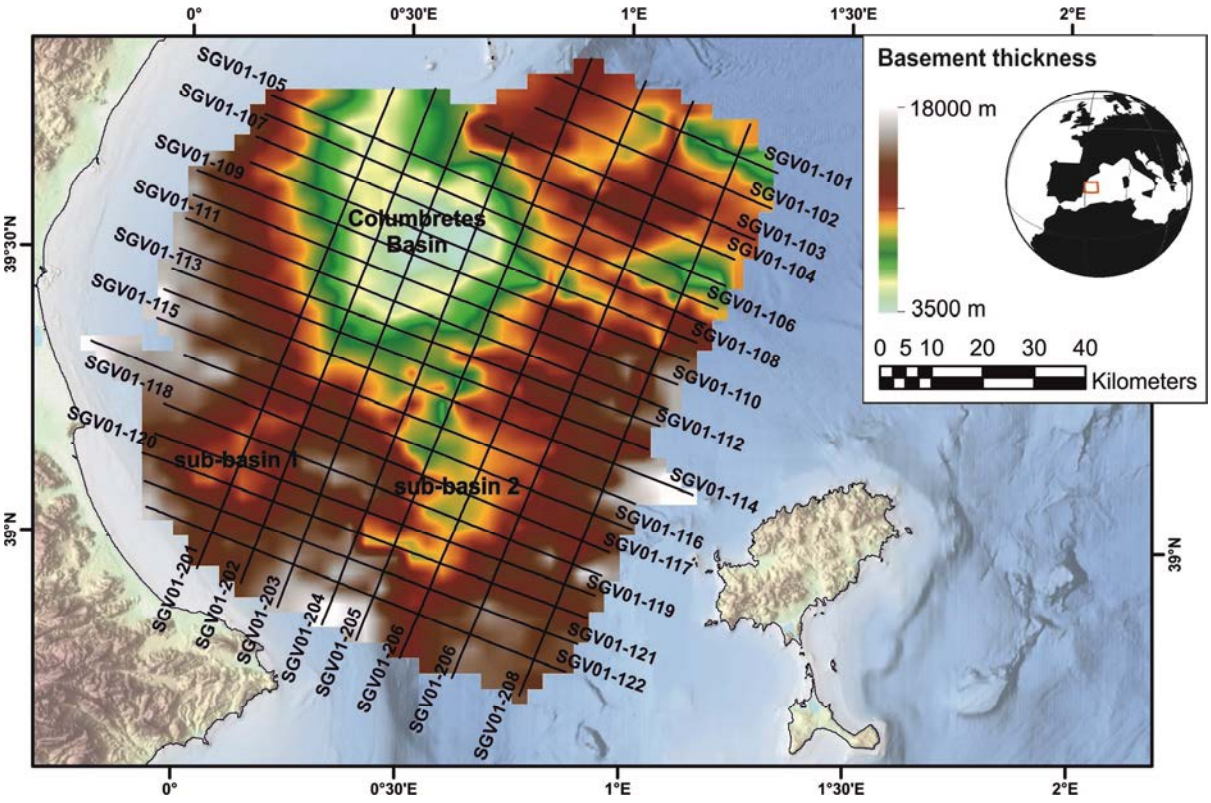

The uncertainty in horizon mapping to create the map is difficult to assess, but in most segments the Moho is a well-defined reflection, with a negligible picking uncertainty of a ~0.1 s TWTT or ~300 m assuming 6.5 km/s (Figures 6.4, 6.5). There are a few segments with complex structure or Neogene volcanic constructions where the Moho is not a distinct event and it is difficult to map with uncertainties of ~0.5 s TWTT or ~1.5 km (e.g. Figure 6.5d CMPs 7000-8700), in such cases we chose to connect two well-defined picks by a gentle morphology horizons that would not create unwanted artifacts. The top of the basement, understood as the upper limit of the crystalline (igneous or metamorphic rocks) basement, is difficult to unambiguously discern, as oldest sediment units might be comparatively more intensively deformed –thus not easily imaged- and have high velocity (close to crystalline rocks) due to compaction and induration.

In spite of that, a well-layered Jurassic-Cretaceous unit is usually bounded at its base by clear and laterally continuous reflections that we have taken as the top of the basement. However, a poorly visible lower Jurassic–Triassic unit is locally present in the form of discontinuous packages of reflections that define local graben structures difficult to map. Some reflections interpreted as intra-basement might be part of a highly consolidated sediment unit, perhaps even older than Triassic. Neogene volcanism also locally masks the top of the basement reflection at the same locations where Moho is obscured. However, the

uncertainty on whether an old sediment unit is present is typically limited to packages few-hundreds-milliseconds thick and restricted to few segments of the entire grid. This uncertainty could change some aspect of the basement thickness map, but it would not notably change either the trends of variations or the location of the main basins. In this work we have only interpreted the major features that seem consistent over a number of lines of the grid.

The basement thickness map shows important variations in crustal structure in the southwestern end of the Valencia Trough Basin with several well-defined local deep basins. The main basin, referred as the Columbretes Basin (e.g. Roca et a., 1992; 1996; Maillard *et al*., 1993; 1999; Salas *et al*., 2001), is located offshore the linking zone between the NW-SE Iberian system and NE-SW Catalan Coastal Ranges, and has been described by some authors to have developed mainly during the Late Jurassic-Early Cretaceous times (Salas, *et al*., 2001).

The variations in basement thickness show several abrupt changes that delineate several basins of rectangular-shape in map view (Figure 6.3), with abrupt lateral changes in thickness possibly indicating that they are bounded by steep faults. The deepest and largest basin is the Columbretes Basin, whose centre is located roughly at 39.5ºN-0.5ºE (Figure 6.3), with a minimum basement thickness about 1.5 s TWTT (~4.5 km) (e.g. Figures 6.4c, d and 6.5b, c) thickening towards the shelf to ~17.5 km (Figure 6.3). We selected 15 profiles from the SGV01 grid to explain basement morphology and sedimentary units distribution. Figures 6.4a-i displays 9 lines striking NW-SE and Figures 6.5a-f 6 lines striking NE-SW (Figure 6.1).

Columbretes Basin structure is well displayed on profiles SGV01-105 (Figure 6.4a) and SGV01-113 (Figures 6.3, 6.4e). Basement thickness at the centre of the Columbretes Basin decreases from ~6 km at SGV01-105 (Figure 6.4a) to ~4.5 km at SGV01-109 (Figure 6.4c). Basement thickness increases from the basin centre (from ~4.5 km in SGV01-110 (Figure 6.4d) to ~13.5 km in SGV01-118 and SGV01-120 (Figures 6.4h-i respectively)) to the SW trough margin. The rectangular-shaped basin does not extend south of SGV01-113 (Figure 6.4e), where the basement configuration changes from very thin crust beneath the deep Columbretes Basin to ~7.5 km thick basement in SGV01-113 and SGV01-114 (Figures 6.4e, f). Further SW the thickness map shows a change in the basement configuration displaying two Mesozoic sub-basins imaged on profile SGV01-117 (Figure 6.4g). These Mesozoic sub-basins are well displayed in the thickness map (Figure 6.3), sub-basin-1 has a thinned ~7.5 km basement and sub-basin-2 has a basement thinned to ~7 km, both sub-basins separated by a basement high ~10.5 km thick.

The geometry of the Mesozoic Columbretes Basin is well displayed on perpendicular profiles SGV01-201 to SGV01-205 striking SW-NE (Figures 6.3, 6.5a-d). The thinnest basement, 4.5 km thick, is imaged on SGV01-203 and SGV01-204 (Figure 6.5b, c respectively). There is a change in the basement configuration to the SW from SGV01-205 (Figure 6.5d) to the SW in the map (Figure 6.3) where the basement thickens from ~6 km at the centre of profile SGV01-205 (Figure 6.5d) to ~10 km on SGV01-206 and SGV01-207 lines (Figures 6.5e, f respectively).

Figure 6.4: *Poststack time migration of SGV01 survey lines (see Figure 6.1 for location). From NE to SW, (a) Multichannel seismic line (MCS) SGV01-105. (b) MCS line SGV01-107. (c) MCS line SGV01-109. (d) MCS line SGV01-110. (e) MCS line SGV01-113. (f) MCS line SGV01-114. (g) MCS line SGV01-117. (h) MCS line SGV01-118. (i) MCS line SGV01-120. White dots mark the reflections interpreted as the Moho discontinuity located in all profiles at 7.5-8 s TWTT. Black dots mark the boundary between an upper section formed by multiple reflections that appear well stratified (interpreted as Mesozoic strata), and a lower part with weaker reflectivity interpreted as the upper crystalline crust as top of the basement. Green dots mark the high reflective horizon interpreted as the Oligocene unconformity marking the top of the Mesozoic sequence. Blue dots mark another high reflective horizon interpreted as the Messinian top sequence (MTS). Red stars mark the location of the different industrial wells used to interpret the sedimentary sequence (Figures 6.1, 6.6). Dashed vertical lines mark the location of every well in depth. Short black lines mark profile intersection.*

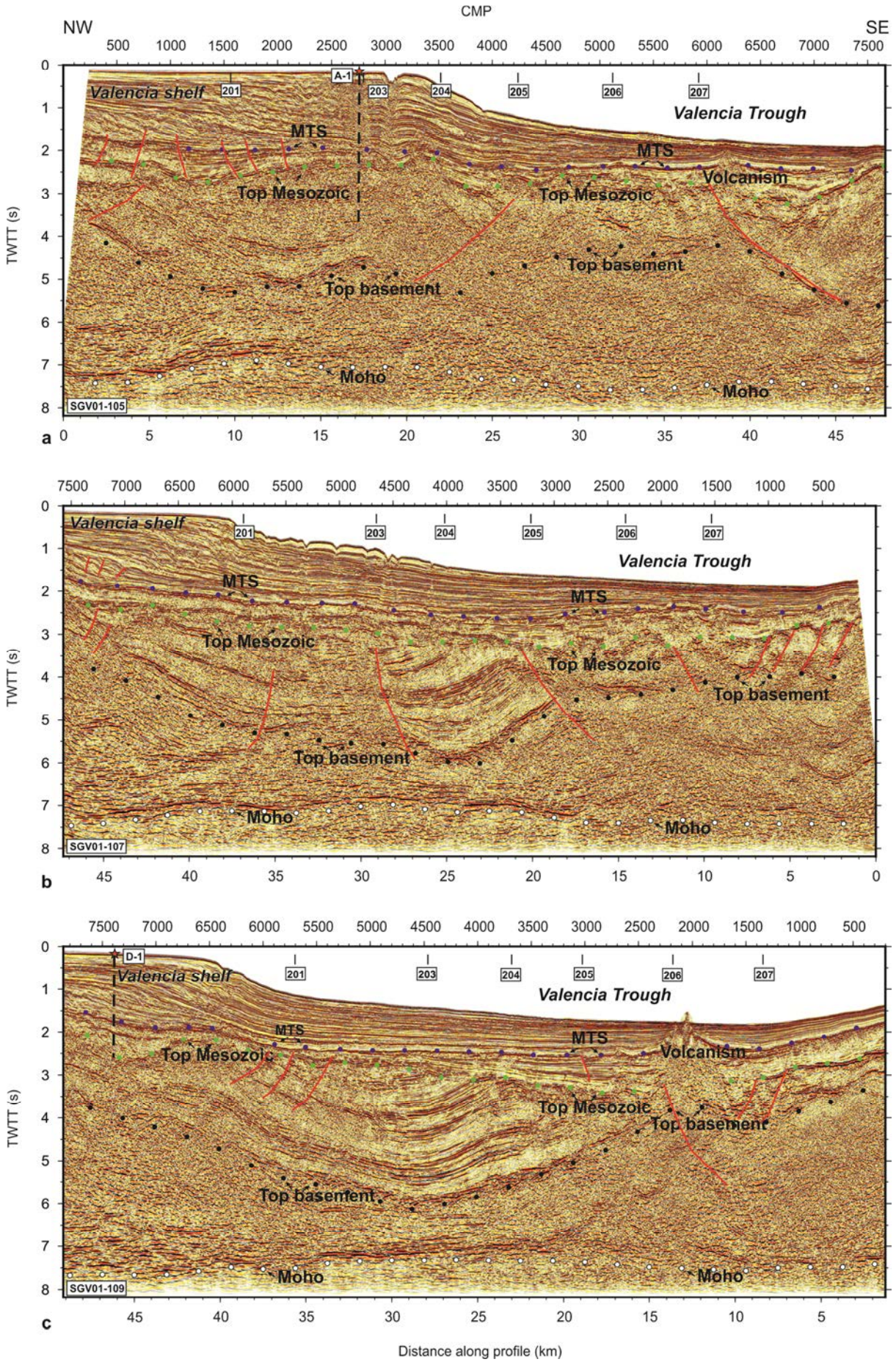
CMP
NW
SE
Valencia shelf
Valencia Trough
MTS
Top Mesozoic
Top basement
Volcanism
Moho
A-1
D-1
SGV01-105
SGV01-107
SGV01-109
TWTT (s)
a
b
c
Distance along profile (km)

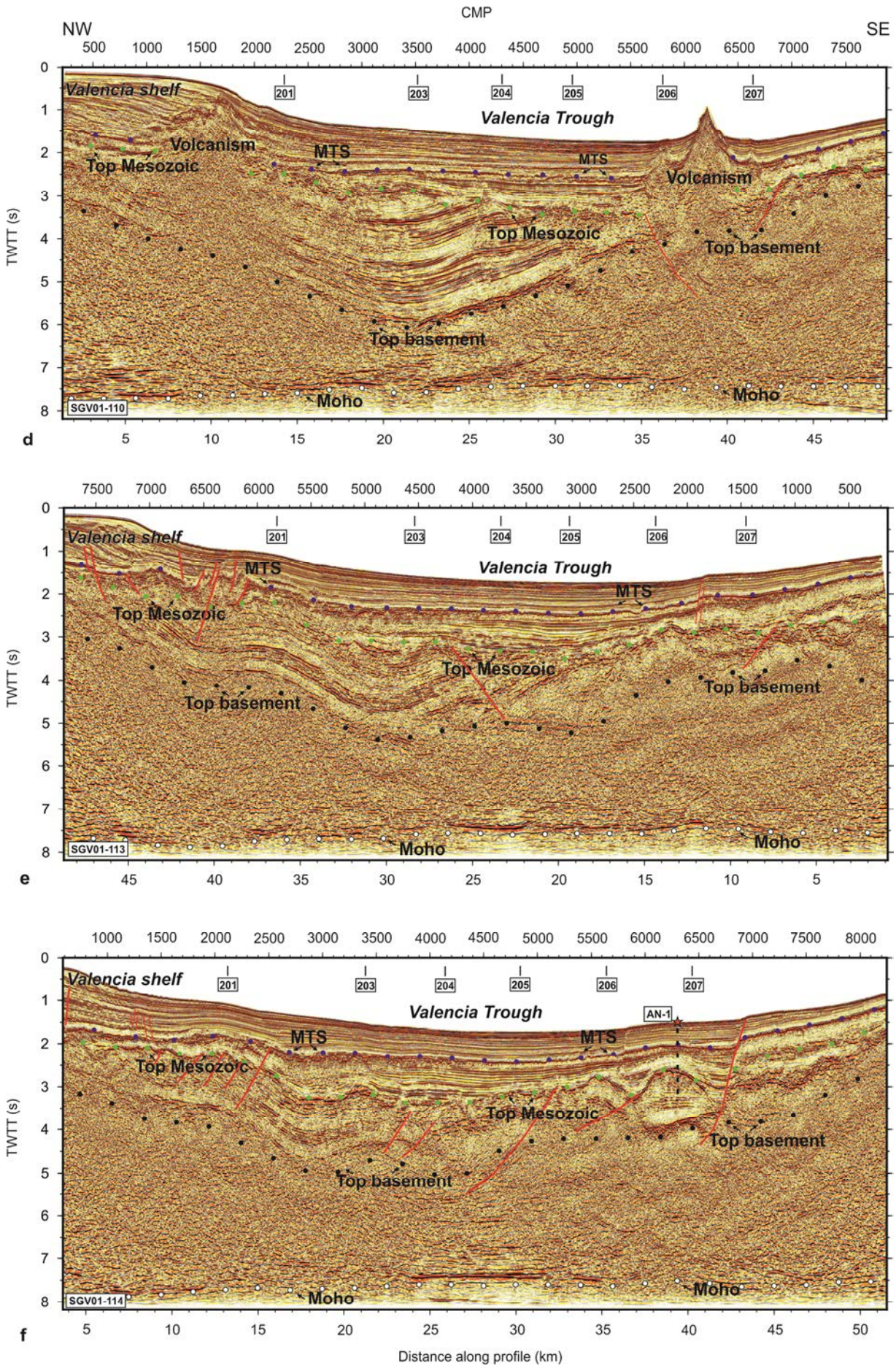
CMP
NW
SE
Valencia shelf
Valencia Trough
Volcanism
Top Mesozoic
MTS
Top basement
Moho
SGV01-110
SGV01-113
SGV01-114
AN-1
TWTT (s)
d
e
f
Distance along profile (km)

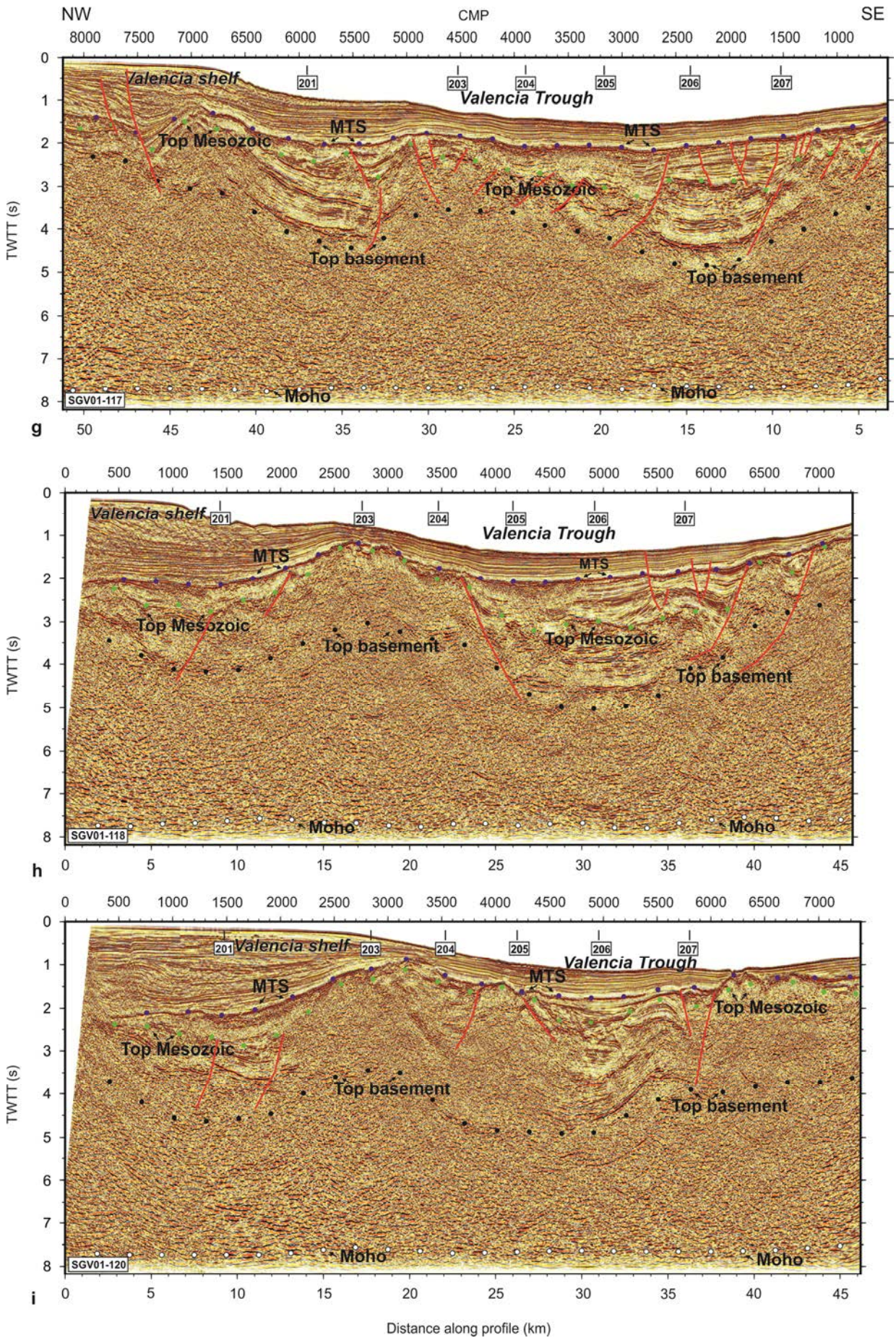
NW
CMP
SE
8000 7500 7000 6500 6000 5500 5000 4500 4000 3500 3000 2500 2000 1500 1000
Valencia shelf
201
203
204
205
206
207
Valencia Trough
MTS
MTS
Top Mesozoic
Top Mesozoic
Top basement
Top basement
Moho
Moho
SGV01-117
TWTT (s)
g
50 45 40 35 30 25 20 15 10 5
0 500 1000 1500 2000 2500 3000 3500 4000 4500 5000 5500 6000 6500 7000
Valencia shelf
201
203
204
205
206
207
Valencia Trough
MTS
MTS
Top Mesozoic
Top basement
Top Mesozoic
Top basement
Moho
Moho
SGV01-118
TWTT (s)
h
0 5 10 15 20 25 30 35 40 45
0 500 1000 1500 2000 2500 3000 3500 4000 4500 5000 5500 6000 6500 7000
201
Valencia shelf
203
204
205
206
207
Valencia Trough
MTS
MTS
Top Mesozoic
Top Mesozoic
Top basement
Top basement
Moho
Moho
SGV01-120
TWTT (s)
i
0 5 10 15 20 25 30 35 40 45
Distance along profile (km)

6.5. Sedimentary Sequence

Even though no detailed study has been previously done, the extensional event leading to the formation of the Columbretes Basin is probably related to the postulated sinistral motion between Africa and Euroasia during Mesozoic times, when the basin was the locus of deposition of thick Mesozoic carbonate series (Roca *et al*., 1992). The geometry of the sediment infill of this basin is poorly known from low penetration and low resolution reflection seismic data (Roca *et al*., 1996). Modern industry seismic data presented in this work reveals in greater detail the structure of the Columbretes Basin and its 7-8 km Mesozoic and Tertiary strata infill (Figures 6.4 and 6.5). The sedimentary cover of the Valencia Trough contains several Mesozoic and Tertiary sedimentary units, but for the purpose of this study we have differentiated only two major units delimited by an important erosional surface: A Mesozoic unit mainly developed during the Tethys rifting, and a fundamentally Neogene-Quaternary sedimentary sequence characterized by the presence of Miocene strata with a clear Messinian unit and a well-developed fundamentally Plio-quaternary Ebro-river progradant unit forming much of the Iberian continental platform (Cameselle, A., 2015). In contrast, Paleogene sediment units are thin and scarce in industry wells offshore.

Figure 6.5: *Poststack time migration of SGV01 survey lines (see Figure 6.1 for location). From NW to SE, (a) Multichannel seismic line (MCS) SGV01-201. (b) MCS line SGV01-203. (c) MCS line SGV01-204. (d) MCS line SGV01-205. (e) MCS line SGV01-206. (f) MCS line SGV01-207. White dots mark the reflections interpreted as the Moho discontinuity located in all profiles at 7.5-8 s TWTT. Black dots mark the boundary between an upper section formed by multiple reflections that appear well stratified (interpreted as Mesozoic strata), and a lower part with weaker reflectivity interpreted as the upper crystalline crust as top of the basement. Green dots mark the high reflective horizon interpreted as the Oligocene unconformity marking the top of the Mesozoic sequence. Blue dots mark an also high reflective horizon interpreted as the Messinian top sequence (MTS). Red stars mark the location of the different industrial wells used to interpret the sedimentary sequence (Figures 6.1, 6.6). Dashed vertical lines mark the location of every well in depth. Short black lines mark profile intersection.*

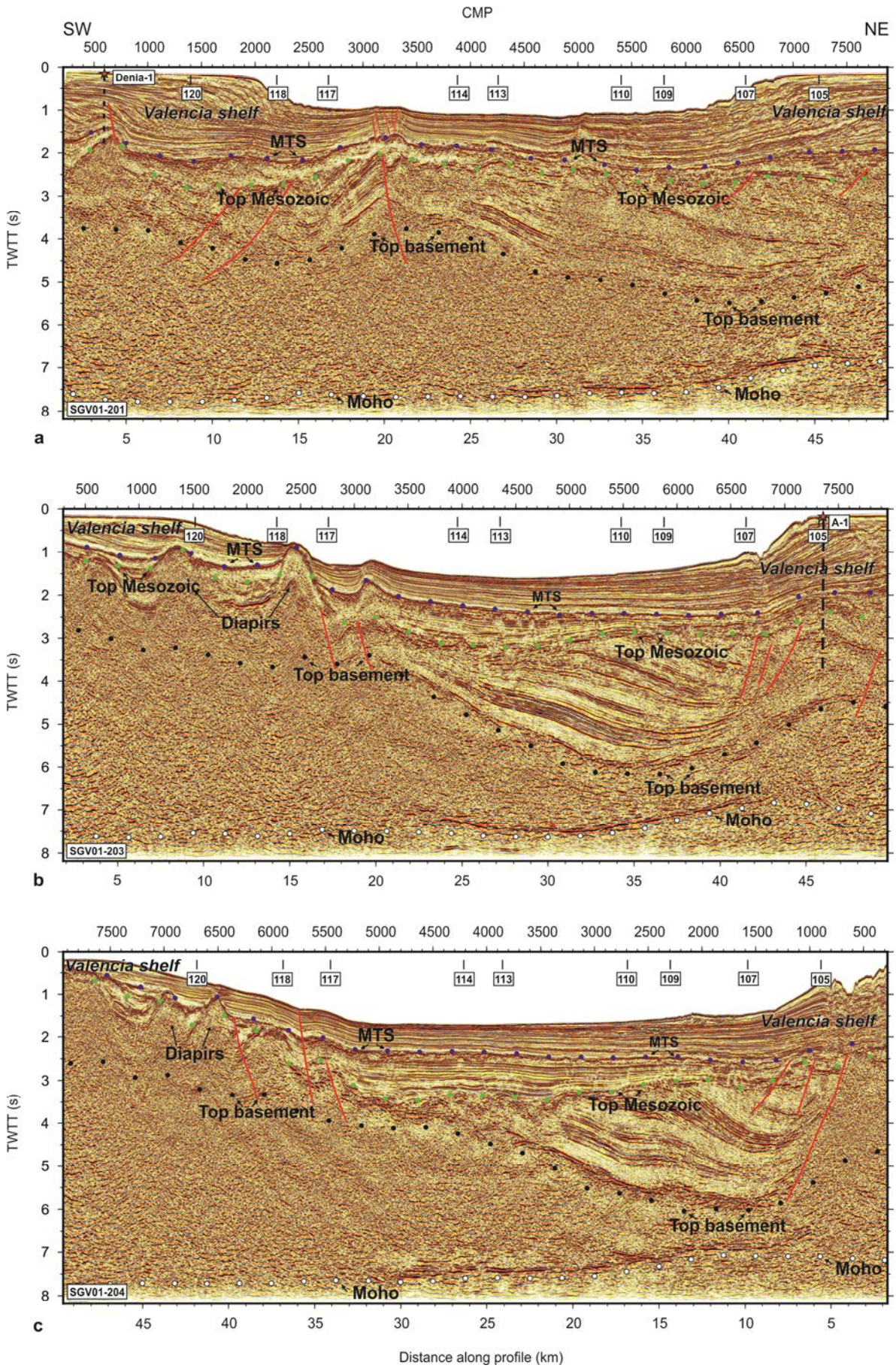
CMP
SW
NE
Denia-1
Valencia shelf
MTS
Top Mesozoic
Top basement
Moho
SGV01-201
a
TWTT (s)
A-1
Diapirs
SGV01-203
b
SGV01-204
c
Distance along profile (km)

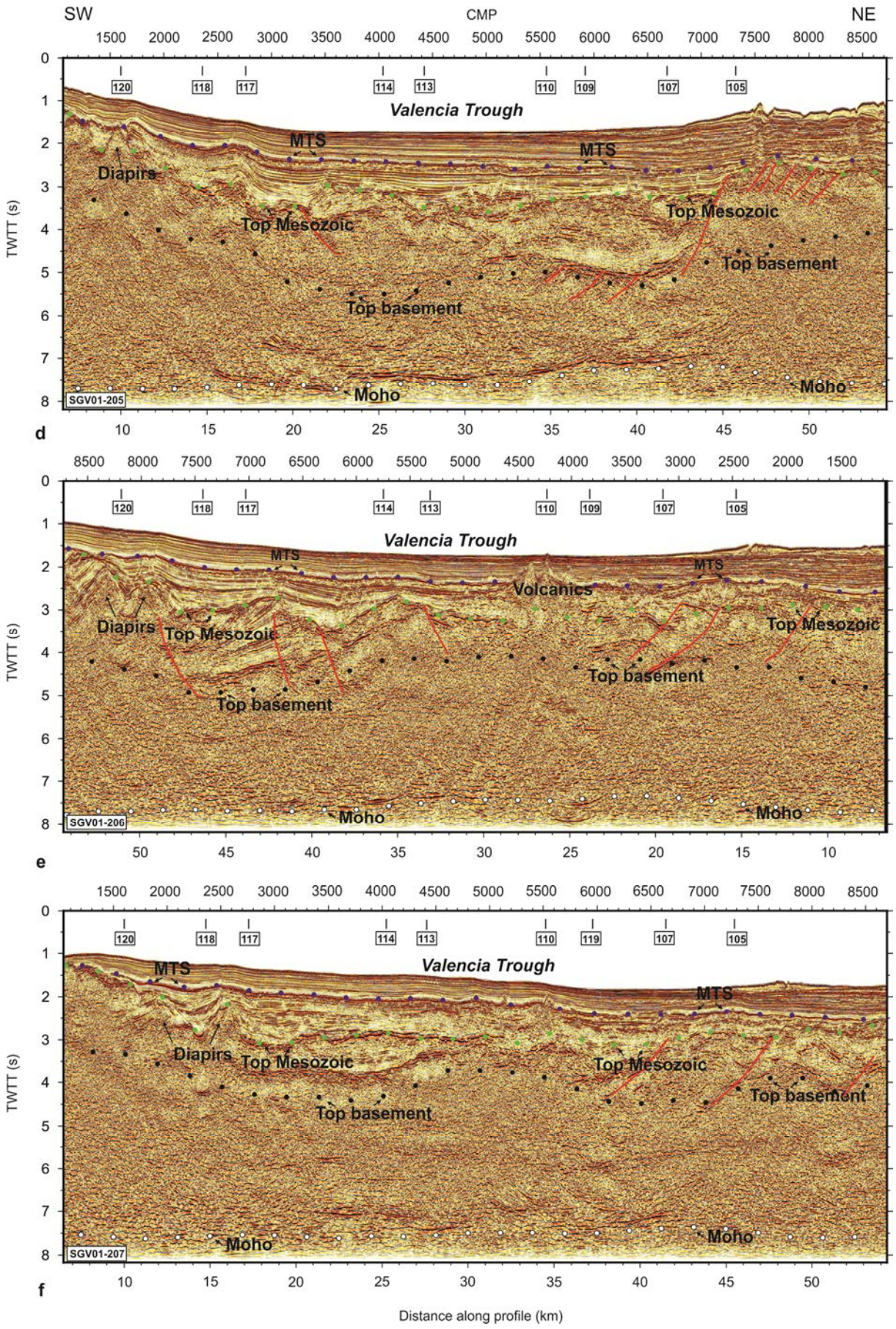
SW
CMP
NE
Valencia Trough
MTS
Diapirs
Top Mesozoic
Top basement
Moho
Volcanics
SGV01-205
SGV01-206
SGV01-207
TWTT (s)
Distance along profile (km)
d
e
f

6.5.1 Mesozoic stratigraphy

Basement in this region is known to be low-grade metamorphic rocks intensely deformed during the Variscan orogeny with associated granitic rocks of Late Paleozoic age (Roca *et al*., 1992). This Paleozoic basement was thinned during Mesozoic times as shown in Figures 6.4 and 6.5. Overlying the stretched Paleozoic basement, a Mesozoic cover, drilled at several locations, fills the depressions (Figures 6.4, 6.5 and 6.6). While in the central VTB the maximum Mesozoic thickness is ~3 km thick (Figure 6.2a) in the Columbretes Basin (SW VTB) the Mesozoic infill reaches 8 km of thickness (Figures 6.4b-d, 6.5b, c).

Previous studies (e.g. Roca *et al*., 1992; Roca, 1996; Salas *et al*., 2001) divided the Mesozoic sequence into four main units from bottom to the top: 1) a first Triassic unit deposited in continental and transitional environments, 2) a second Jurassic unit deposited in shallow and deep marine environments 3) a third Early Cretaceous unit deposited also in shallow and deep marine environments and, 4) a fourth Upper Cretaceous unit generally eroded, deposited in shallow marine environments.

Data presented in this work shows a variable thickness of the Mesozoic sequence. It is interpreted as a sedimentary sequence limited at its base by the top of crystalline basement (black dots in seismic profiles) and at its top by high amplitude reflections marking and irregular horizon, interpreted as a possibly Oligocene erosive unconformity (green dots in seismic profiles). Mesozoic thickness increases from the northern segment of the Valencia Trough (Figure 6.2a) towards its southwestern end (Figure 6.2d). In ESCI-Valencia line (Figure 6.2a), the Mesozoic cover is visible in both Iberian and Balearic margins, being thicker in the Iberia margin, reaching ~2 s TWTT. To the south, the Mesozoic sequence extends along the Iberian margin (Figure 6.2b) reaching a maximum thickness of ~3.5 s TWTT in the centre of Columbretes Basin (Figure 6.2d). In the area of the Columbretes Basin, the thickness of the Mesozoic sequence is extremely variable. Figures 6.4 and 6.5 show that the maximum Mesozoic thickness is located at the centre of the Columbretes Basin (Figures 6.4b-d, 6.5b, c). Here, the sedimentary sequence is characterized by different layers corresponding to Triassic, Jurassic and Cretaceous facies, reaching 3.5 s TWTT (7-8 km). It is important to remark the presence of large-offset basement faults bounding the Columbretes Basin (Figures 6.4a-d, h, 6.5c, d). The fault planes are not clearly visible in the seismic images, but their location can be inferred from the sediment thickness variations and the basement thickness map. These large-offset faults are responsible of basin formation. The Columbretes Basin evolved into a series of tilted blocks towards the edges of the basin bounded by medium and large offset normal faults (Figures 6.4f, g, i, 6.5a, e, f). These

blocks present a more chaotic sediment distribution, in some cases obscured by the presence of volcanic edifices and Triassic diapirs (e.g. profile SGV01-206, Figure 6.5e).

The top of the Mesozoic sequence is clearly visible in all lines, and in most places it is marked by an important erosive surface, often with hundreds of meters of relief that is clearly visible in all profiles and interpreted as an Oligocene unconformity possibly marking the end of the Paleogene contractive period (Figures 6.2, 6.4, 6.5). This Oligocene erosional unconformity clearly separates Tertiary sediments from Mesozoic sediments.

6.5.2 Neogene-Quaternary stratigraphy

The Neogene-Quaternary infill of the Valencia Trough Basin has been subdivided into four depositional sequences, separated by boundaries corresponding in part to major unconformities (Bartrina *et al*., 1992; Maillard *et al*., 1992, Roca *et al*., 1992; Maillard *et al*, 2006; Urgeles *et al*., 2011; Cameselle *et al*., 2015). From bottom to top: 1) Lower Neogene Unit: deposited in continental to marine transition environments. 2) Middle Neogene Unit: characterized by progradant sequences. 3) Messinian Unit: with a deposition of evaporitic sequences in the deep central and north-east parts of the Valencia Trough (Driussi *et al*., 2014; Maillard *et al*., 2014; Cameselle, A., 2015) and 4) Upper Plio-Quaternary Unit: with a reactivation of the progradant deltaic systems from the Spanish coast into the Valencia Trough (Nelson and Maldonado, 1990) and carbonate shelf sedimentation in the Betic-Balearic domain (Alonso *et al*., 1988).

The Neogene to Quaternary sedimentary sequence is limited to the base by the Oligocene unconformity (green dots) (Figures 6.2, 6.4, 6.5). A strong and reflective horizon with an erosive character marks the top of Messinian Unit (blue dots) dividing Neogene-Quaternary sequence in three main units: 1) Pre-Messinian Unit is formed by the Lower and Middle Neogene units and presents variable thickness along the trough. It has been commonly interpreted as the syn-rift sediments of the Neogene extensional event separating the Balearic Promontory from Iberia. In our data, the Neogene extensional event is not as important as the Mesozoic extensional event. It is characterized by the presence of small offset normal faults and few large normal faults probably reactivating Mesozoic structures (e.g. SGV01-117 and SGV01-118, Figures 6.4g, h respectively). 2) The top of the Messinian Unit is characterized by a continuous highly reflective horizon with an erosive character present in all profiles, marking the sea level dropdown associated to the salinity crisis in the Western Mediterranean (Figures 6.2, 6.4 and 6.5). 3) The post-Messinian Unit is formed essentially by the progradation of the Ebro deltaic system along the Iberian margin (Camesselle *et al*., 2015) (Figures 6.4 and 6.5). Tectonic activity is minor, with few small

offset normal faults cutting the sedimentary sequence, but generally with minor displacement (Figures 6.4e-g), and it is affected by the Neogene volcanism (Figures 6.4c, d, 6.5e).

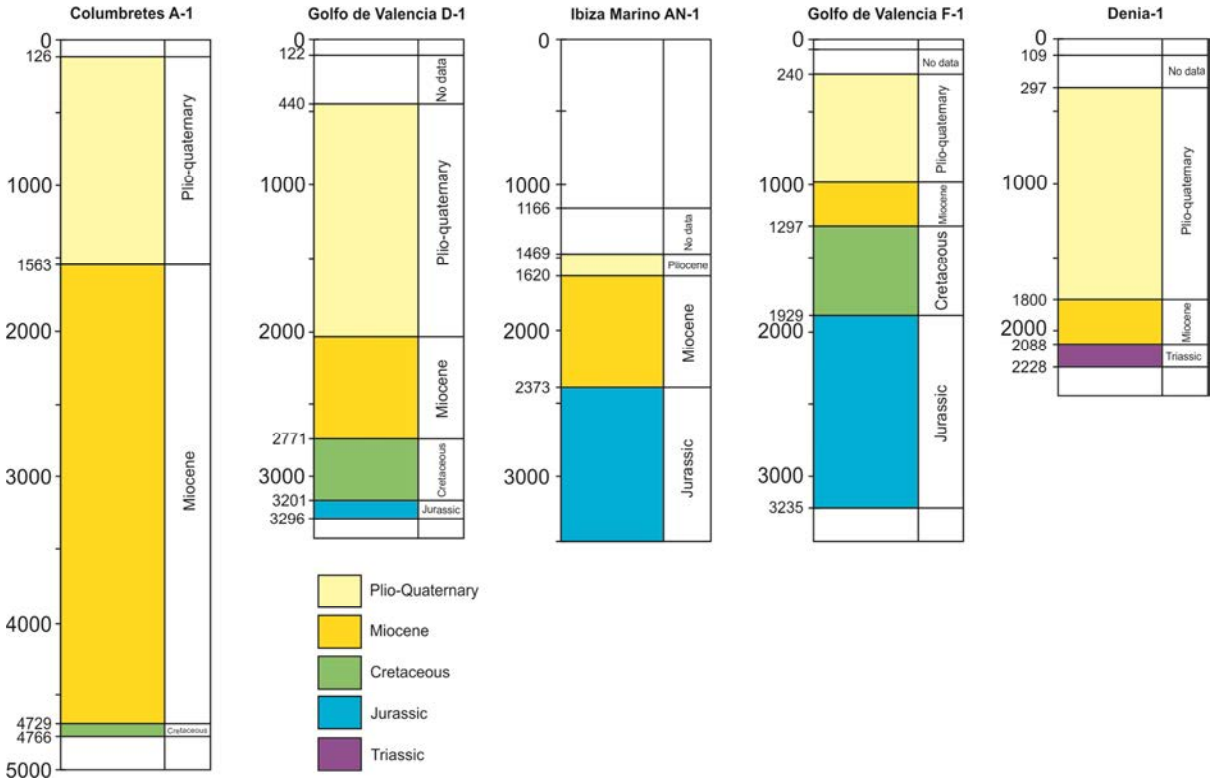

Figure 6.6: *Correlation of stratigraphic wells located SW of Valencia Trough used to interpret and discuss the sedimentary sequence of this region. We used the Golfo de Valencia D-1, the Ibiza Marino AN-1, the Golfo de Valencia F-1 and Denia-1. See location in Figures 6.1, 6.4 and 6.5. (Lanaja, J.M., 1987).*

6.6 Neogene Volcanism

Although many studies of the Valencia Trough indicate that the formation of the basin was associated to important extrusive volcanic activity, few studies have focused on the magmatic evolution of this basin (Martí *et al*., 1990; Martí *et al*., 1992; Martínez *et al*., 1996).

According to Salas *et al*. (2001), the Mesozoic evolution of the Iberian Peninsula Rift system can be divided into four rift and post-rift stages: A Triassic rift cycle and a subsequent Early Jurassic post-rift stage have basaltic volcanic activity associated along the northern and southern margins of the Iberian system. During the subsequent Latest Jurassic-Early Cretaceous rifting stage there is little evidence of magmatic activity despite the considerable

crustal stretching controlling the subsidence of the Mesozoic basins. Some studies describe the magmatic activity during the Mesozoic times in the Valencia Trough Basin region (Gómez *et al*., 1976; Ortí *et al*., 1980; Salas *et al*., 2001). However, the most distinct volcanic activity is a complex system of volcanic edifices that range in age from the Early Miocene to recent times and are distributed onshore and offshore along the trough.

The Cenozoic evolution of the Valencia Trough Basin is characterized by two volcanic phases: An Early Miocene, and a Late Miocene to recent volcanic cycles. The first volcanic cycle at 24-18.6 Ma (Martí *et al*., 1992) produced calc-alkaline rocks studied along the thrusts of the Betic-Balearic domain and offshore the Catalan-Valencia domain. The second volcanic cycle produced alkaline volcanic rocks distributed along the main extensional faults at the margin of the Valencia Trough Basin: ENE-WSW to N-S faults in the Iberian margin, and NW-SE oriented faults along the North Balearic fault zone postulated to run from the eastern Pyrenees to the north of Menorca. The alkaline volcanism ranges in age from 10 Ma to recent. According to Martí *et al*. (1992), three different zones can be distinguished within this area of volcanism: Valencia (2-1.3 Ma), Columbretes (1-0.3 Ma) and the Catalan zone made of three sub-zones: L'Empordà (10-8 Ma), La Selva (7.9-1.7 Ma) and La Garrotxa (0.1-0.01 Ma).

6.6.1 Volcanic edifices

Offshore the Iberian margin, volcanic edifices occur mainly along the trough. Figure 6.2a shows that in the central segment of the ESCI-Valencia profile there are two buried volcanic edifices, approximately 15-20 km wide and 3 km high, corresponding to distinct magnetic anomalies in the aeromagnetic map of Galdeano and Rossignol (1977) that has no associated superficial expression in the bathymetry map (Figure 6.1). The presence of these volcanic constructions causes strong attenuation of seismic energy obscuring the underlying structure in the seismic images. The broadest and highest magnetic anomaly in the Valencia Trough Basin is located under the Columbretes Islands at the SW end of the trough, spanning about 10.000 km^2 (Galdeano and Rossignol 1977). The flank of the subaerial volcanic manifestation that forms the Columbretes volcanic system is imaged on profiles SGV01-105, 109 and 110 (Figures 6.4a, c, d respectively) The deep seismic profiles allow identifying several submerged volcanic seamounts (e.g. Figures 6.4c, d) and volcanic bodies without superficial expression (e.g. Figures 6.4a, d). The age of the volcanic constructions along the Valencia Trough has been estimated as Early Miocene to Late Miocene-recent, but the edifices imaged on the seismic data probably do not span such a long period of time and a modern detail study is needed to assess the main construction period that in a first approximation based on our seismic interpretations we interpret as Miocene, fundamentally

Pre-Messinian in age (e.g profile SGV01-109, 110, Figures 6.4c, d respectively). The Jurassic volcanism was described in some areas of Iberian Chain (Ortí *et al*., 1980) and has not been geophysically detected in the Valencia Trough.

6.7 Discussion

6.7.1 Style and age of crustal thinning

Valencia Trough Basin constitutes the oldest Western Mediterranean basin. Wide angle seismic data indicates that is floored by continental crust, possibly amalgamated during the Variscan orogeny. The evolution of the basin, with several main episodes, has been analyzed in different studies (e.g. Roca, 1996; Cavazza *et al*., 2004). The region was extended during a Mesozoic rifting phases preceding the middle Jurassic opening of the oceanic Atlantic-Tethys basin and the early-Cretaceous opening of the Bay of Biscay-Pyrenean basin. Mesozoic rift basins in the area of VTB were inverted and uplifted during the Paleogene and interpreted to have caused a major regional unconformity. During Miocene times, the Variscan basement and the Mesozoic sedimentary cover underwent an extensional phase that led to the current Valencia Trough Basin structure (Roca *et al*., 1992, Roca, E., 1996; Salas *et al*., 2001).

Mesozoic evolution of the Valencia Trough Basin is characterized by a significant lithospheric thinning. Subsidence studies (Salas *et al*., 1993) applying a pure shear extensional model give a thinning factor about 1.5. A similar value of 1.58 is estimated for the Neogene extension (Roca *et al*., 1992). Our results provide more information about the thinning during the Mesozoic. As the seismic profiles in Figures 6.4 and 6.5 shows, the thinnest crust is detected in the SW end of the Valencia Trough, in the confluence zone between the Iberian Chain and the Catalan Coastal Ranges. Here, the basement thins down to only 4.5 km thick. This is the area where the Mesozoic sedimentary cover presents the maximum thickness of ~7-8 km. The Columbretes Basin is a small basin with an important thinning; this together with its rectangular-shape geometry indicates a pull-apart basin type of formation, dominated by strike-slip tectonics. The sub-vertical faults bounding the basin may be the offshore continuation of NW-SE striking major fault systems of the Iberian Chain and NW-SW faults of the Catalan Coastal Ranges.

During the Late Cretaceous-Paleogene stage, the Iberian Peninsula was under compression caused by convergence between the Eurasia and Africa plates. This situation resulted in the formation of sinistral NE-SW strike-slip faults in the Catalan Coastal Ranges and a complex system of NW-SE to E-W striking thrusts and dextral strike-slip faults in the Iberian Chain

onshore. However, we observe no evidence of major tectonic activity in the basin, let alone crustal thickening in the Valencia Trough for this phase. It seems that shortening and crustal thickening occur in the Pyrenees and Iberian Chain, although in the SW sector of the Valencia Trough, some compression may have been accommodated through offshore NW-SE and NE-SW strike-slip faults bounding the Columbretes Basin, producing strata folding (Figure 6.2c) with possible reactivation of preexisting faults. The Paleogene compressive event may be associated to a variable deep erosion of the Mesozoic sediments in the area of Valencia Trough displayed as a deep-incised erosive surface, clearly visible in all seismic profiles as an erosion unconformity (Figures 6.4 and 6.5).

During the Early-Middle Miocene, synchronously with the Corsica-Sardinia block rotation and the opening of the Liguro-Provencal Basin, the Valencia Trough Basin underwent two types of processes: First, the formation of a horst and graben system oriented ENE-WSW to N-S along the Catalan Coastal Ranges and the SE end of the Iberian Chain as a consequence of WNW-ESE to E-W extension phase (Roca *et al*., 1992, Roca, E., 1996). This extensional event was accomodated through re-working of faults that delimited the Mesozoic basins and had been inverted during the Paleogene (Roca *et al*., 1992, Roca, 1996). Second, the Betic-Balearic domain underwent the progressive stacking of thrust sheets with the development of a piggy-back system in a WNW direction (Fontboté *et al*., 1990).

Finally, from Middle Miocene to recent times, while in the Catalan-Valencia domain extension stopped, the Betic-Baleric domain underwent a new phase of extension. This tectonic change from compression to extension has been related to opening of the Algerian Basin (Fontboté *et al*., 1990) and extrusion of alkaline volcanic rocks (Roca, E., 1996).

6.7.2 Implications for the Neogene evolution of the Valencia Trough Basin

Extension is not the only mechanism that has governed the formation of the Valencia Trough Basin. The opening of this basin situated at the NW of the Mediterranean Sea has involved different processes. While first studies carried out by Rehault at al. (1984), Burrus, J. (1984) and Malinverno & Ryan (1986) have interpreted the formation of the Valencia Trough Basin as a result of a back-arc extension of the “eastward” retreating Neogene Apennine subduction hinge zone, it now seems evident that the geodynamic evolution of this basin underwent different stress configurations since the end of the Variscan orogeny.

Data presented in this work allows us to distinguish three main stages that contributed to the present day configuration of the Valencia Trough Basin:

1) A first Mesozoic stage in which the region was subjected to extensional stresses that forms wide basins in the Iberian Chain, Catalan Coastal Ranges and in particularly in the linking zone between both domains (Salas *et al*., 1993 and 2001) and generated alkaline volcanism in the region. Offshore, we can identify a deep and well-defined Mesozoic basin, the Columbretes Basin, with a maximum crustal thickness of 1.5 s TWTT and a Mesozoic sedimentary sequence reaching more than 3 s TWTT (Figures 6.4 and 6.5) and several minor sub-basins with similar rectangular geometry.

2) A Paleogene stage dominated by compressive processes that affected the entire Iberian Peninsula and originated different structures like thrusts, folds and strike faults depending on the orientation of every structure with respect to the stress field. Our data supports that crustal thickening during this period was minor in the Valencia Trough Basin. Apparently, compressional stress was accommodated by previous extensional Mesozoic faults, which were inversely reactivated during the Paleogene. This compressional stage may be denoted by a regional unconformity carved into the Mesozoic sediments and is visible in all our profiles (Figures 6.2, 6.4 and 6.5).

3) Finally, a last Neogene-Quaternary stage characterized by a complex geodynamic context of slab retreat to the SE of the Balearic Promontory, including extensional processes affecting the Catalan-Valencia domain and compressional processes affecting the Betic-Balearic domain. Reflecting this complexity, an important volcanism was developed with a first calc-alkaline composition and a second alkaline pulse.

We infer from our data that the present day configuration of the VTB is strongly dominated by the Mesozoic structure. Some structures active during the Cenozoic were reactivated former primary Mesozoic structures, as inferred from profile SGV01-114, where faults generated during the Mesozoic were reactivated later during the Neogene to recent times (Figure 6.4f). In this way, depending on the orientation of any structure with respect to the N-S stress field, during the Paleogene compressional event, transpressional systems (e.g. Iberian Chain and the Catalan Coastal Ranges) or thrusts faults systems (e.g. Pyrenees) were formed. Later, during the NW-SE Neogene extensional event, E-W and NW-SE margins were inactive while NE-SW margins were reactivated. (Roca, 1996).

We observe few important extensional structures in our data that might indicate the opening of the Valencia Trough Basin in Neogene times. There exist some minor Neogene faults in our profiles, but they have not enough displacement to form the basin. This observation and lack of apparent thickening of the crust related to the Paleogene compressional event support that the Valencia Trough Basin was largely formed during a Mesozoic phase. We

interpret that the Valencia Trough is not a Neogene basin formed by the SW prolongation of the NW-SE opening of the Gulf of Lions. We interpret that the Neogene extensional event that occurred in the Valencia Trough Basin, especially in the formation of different horsts and grabens in the Catalan-Valencia domain, are structures causing minor crustal thinning. The detailed age of the different volcanic expressions throughout the trough remains unclear. Thus, we support that during the Mesozoic occurred the first and more important extensional event that produced the main crustal extension in the basement of the trough as supported by the interpretation presented in our seismic data (Figures 6.2, 6.4 and 6.5).

Chapter 7: Gulf of Lions and deep Provençal Basin

7.1 Introduction

The Gulf of Lions is the north-westernmost deep Mediterranean continental margin that forms part of the Ligurian-Provençal Basin (Figure 7.1). Situated offshore south-east France and NE Spain, the Gulf of Lions is limited to the north-east by the Ligurian Sea, to the south-west by the Valencia Trough Basin, and to the east by the conjugate margin of Corsica-Sardinia continental block.

The opening of the Ligurian-Provençal Basin took place during Oligocene-Miocene times. While some authors relate the opening of the Gulf of Lions with the southward propagation of the Saône Graben (Ziegler,1992), most authors interpret the formation of the Gulf of Lions as a back-arc basin system, the opening of which is related to the eastward roll-back of the west-directed Apenninic subduction zone (Cohen, C.R., 1980; Le Douran *et al*., 1984; Rehault *et al*., 1984; Gueguen *et al*., 1998; Jolivet *et al*., 2000, 2006, 2015).

The main geological features of the Gulf of Lions are well known since the first deep penetration wide-angle seismic marine experiments (Expanded Spread Profiles (ESP) were shot in the region (Le Douaran *et al*., 1984; Pascal *et al*., 1993), when the nature of the crust and the style of thinning of the continental margins were first described. After these first studies, modern refraction and reflection seismic data were acquired in the basin including the Gulf of Lions and conjugate Sardinia margins (Contrucci *et al*., 2001; Gailler *et al*., 2009, Moulin *et al*. 2015, Afilhado *et al*., 20015), which allowed knowing in more detail the crustal P-wave velocity structure and style of basin formation. These latter studies defined three regions with different crustal characteristics extending into the deep basin from both margins (Gulf of Lions and Sardinian): 1) Continental crust thinning from ~20 km under the shelf edge to 6-8 km under the foot of slope, 2) a transition zone between continental and oceanic crust characterized by a shallow high-velocity layer crust at both margins of the basin, which nature has been proposed to be: a) serpentinized upper mantle (Pascal *et al*., 1993; Contrucci *et al*., 2001; Gailler *et al*., 2009), b) magmatic intrusions (Gailler *et al*., 2009), or c) exhumed lower crust (Jolivet *et al*., 2015) and 3) a thin oceanic crust showing a vertical velocity gradient characteristic of oceanic layers 2 and 3, situated at the centre of the basin.

Throughout this chapter we present the interpretation of a grid of modern industry multichannel seismic profiles that clearly display the seismic character of every domain. We discuss the possible nature of every domain and frame the results within the context of the Western Mediterranean back-arc basins.

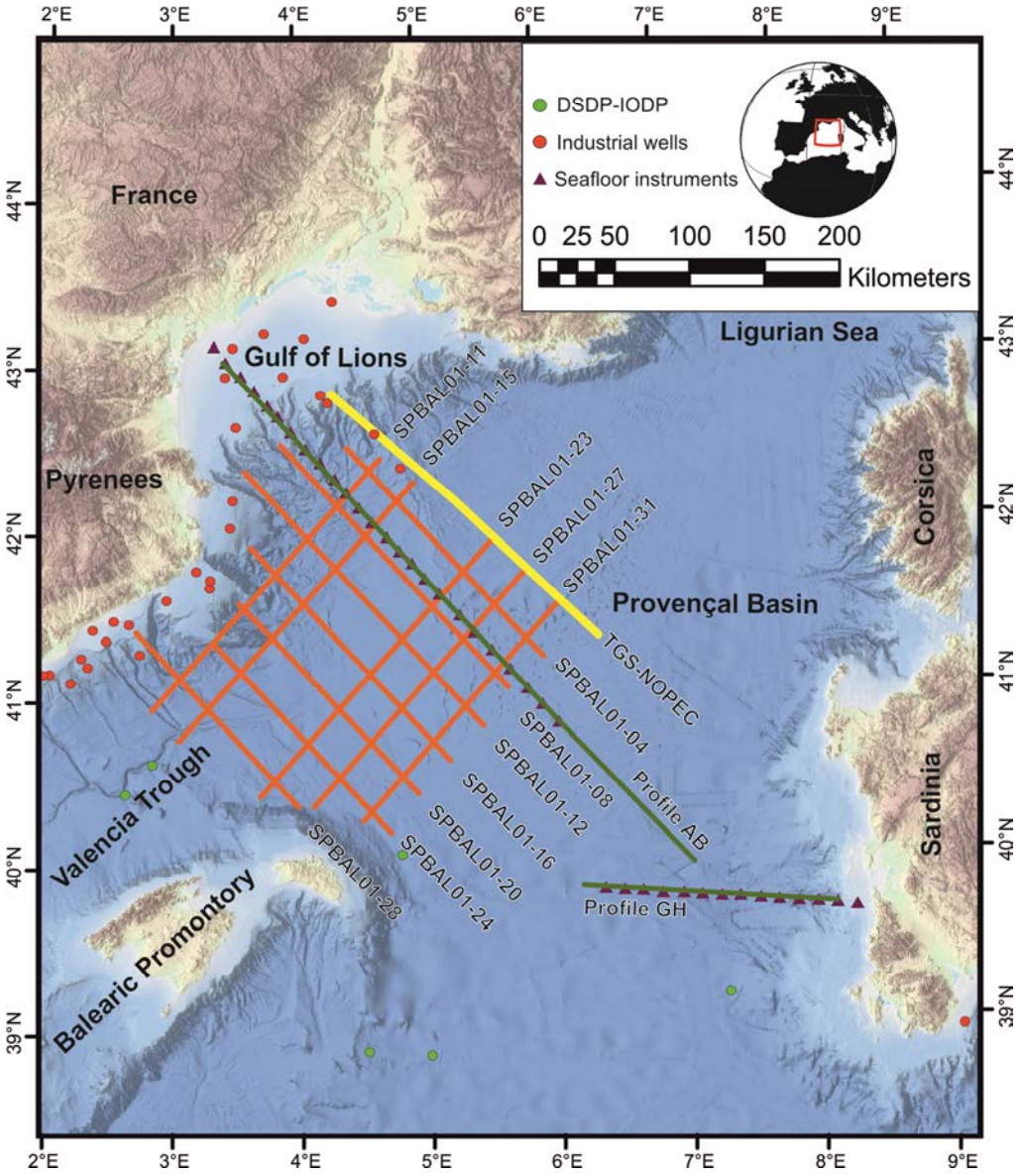

Figure 7.1: *Bathymetric and topographic map of the Gulf of Lions (SE France). It is bounded by the Ligurian Sea (NE), the Provençal Basin and Corsica-Sardinia continental margin (E), the Algero-Balearic Basin (S) and the Valencia Trough and the Balearic Promontory (SW). Lines in orange correspond to multichannel seismic profiles SPBAL01 acquired by Spectrum Energy's vessel Polar Princes on November 2001. Green lines correspond to two wide-angle seismic profiles acquired on the N/O Atlante during the Sardinia cruise (2006), purple triangles correspond to the position of every seafloor instrument (Gailler et al., 2009). Yellow line corresponds to a multichannel seismic line acquired by TGS-NOPEC M/V Zephir 1 in 2001 (Jolivet et al., 2015). These lines have been useful to complement our study and helped us delineate the limits of the different crustal domains. Light green dots mark the location of DSDP and IODP sites in the area and red dots mark the location of different industrial wells.*

7.2 Geological Setting

The geological evolution of the Western Mediterranean results from the interaction between subduction processes and extensional tectonics. This region consists of different marine basins (Ligurian-Provençal Basin, Valencia Trough Basin, Algero-Balearic Basin, Alboran Basin and Tyrrhenian Basin), which were formed partially or fully as back-arc basins due to the retreat of mainly west-directed subduction zones since Oligocene times (Auzende *et al*., 1973; Dewey *et al*., 1973; Cohen *et al*., 1980; Rehault *et al*., 1984; Roca and Desegaulx, 1992; Vegas, 1992; Watts *et al*., 1993; Gueguen *et al*., 1998; Jolivet *et al*., 2000; Rosenbaum *et al*., 2002).

The Ligurian-Provençal Basin is located in the northwestern Mediterranean Sea and includes the Ligurian Sea in its northeastern part and Provençal Basin and Gulf of Lions in its southwestern part (Figure 7.1). In the Gulf of Lions, rifting started probably during the middle Oligocene (~30 Ma, e.g. Burrus, 1984). From Rupelian time the Variscan blocks of Corsica, Sardinia and Calabria where subjected to ~30º counterclockwise rotations (Burrus, 1984). Tectonic activity ceased in the Aquitanian/Early Burdigalian (20-19 Ma) possibly due to the collision of Corsica, Sardinia and Calabria with the Apennines and the cessation of back-arc extension in the Ligurian-Provençal Basin (Burrus, 1984; Rehault *et al*., 1984; Chamot-Rooke *et al*., 1999; Rosenbaum *et al*., 2002; Bache *et al*., 2010) or by re-adjustments of the slab geometry in the upper mantle, which caused the flocus of extension to shift further east to the Tyrrhenian Basin (Faccena *et al*., 2001).

A right lateral strike-slip fault (North-Balearic Fracture Zone) separating the Valencia Trough Basin from the Gulf of Lions was interpreted based on a lineation defined by strong magnetic anomalies (Galdeano and Rossignol, 1977). During the Oligocene-Early Miocene extensional event, the North-Balearic Fracture Zone (NBFZ) is interpreted to act as a boundary separating the clockwise opening of the Valencia Trough Basin, where the top of the acoustic basement is 4000 m deep, from the counterclockwise opening of the Liguto-Provencal Basin, where the basement is located at 5000-6000 m depth (Maillard *et al*., 1992, 2003), in an overall geometry that resembles a “swinging door” (Martin, 2006). The North-Balearic Fracture Zone roughly delineates the flowline of the movement of Sardinia during its Miocene rotation (Maillard and Mauffret, 1999). Northeastward, a second strike-slip fault, the Catalan Fracture Zone (CFZ), is postulated to separate the Gulf of Lions from the Pyrenean belt (Mauffret *et al*., 2001; Maillard *et al*., 2003) and is proposed to be located along the Cap de Creus canyon. These two fracture zones guided the opening of the basin and are interpreted as a transfer zone between the Gulf of Lions and the Valencia Trough Basin (Mauffret *et al*., 2001; Maillard *et al*., 2003).

7.3 Crustal and tectonic domains

Twelve MCS profiles extend across the Gulf of Lions continental shelf and slope into the deep basin (Figure 7.1). Similarly to previous results from wide-angle seismic data (Gailler *et al*., 2009), we have interpreted three different domains based on changes in the crustal thickness, the style of thinning and fault geometry. We have also noticed differences in basement reflectivity and in the geometry and distribution of the overlying sediment (Figures 7.2 to 7.13). Our interpretation integrates results of wide-angle seismic profiles AB and GH of Gailler *et al*. (2009) and reflection seismic profile TGS-NOPEC (Jolivet *et al*., 2015) (Figure 7.1).

According to previous studies, the continental domain (CD) extends from the upper continental slope of the Gulf of Lions, where it is characterized by a crustal thickness of ~20 km that abruptly thins seaward as indicated by a shoaling Moho depth from 20 km to <10 km. This domain shows NE-SW fault-bounded tilted blocks forming semi-grabens inferred from the grid data appear with a direction roughly parallel to the continental margin strike. Available wide-angle data results show low vertical velocity gradients in the upper crust and general velocity values in agreement with thinned continental crust (Christensen and Mooney, 1995). The difference in the continental domain between both Gulf of Lions and Sardinia margin is that the velocities of the lower crust are higher along the Gulf of Lions (Pascal *et al*., 1993; Gailler *et al*., 2009; Bache *et al*., 2010).

A second domain interpreted as a transition zone between continental crust and oceanic crust (COT) is characterized by a broad zone (100 km) of about ~5 km crustal thickness, based on our seismic reflection images and nearby wide-angle data. Refraction data indicate a lower crustal velocity in this domain, ranging from 7.9 to 7.5 km/s in the Sardinia margin, which is neither typical of continental crust nor oceanic crust (Pascal *et al*., 1993; Gailler *et al*., 2009). The nature of this COT is discussed later in this chapter.

Finally, a third interpreted domain is an oceanic domain (OD) characterized by typically layered oceanic vertical velocity gradients, with an upper layer showing a high-velocity vertical gradient (layer 2) and a second layer with a lower velocity gradient (layer 3) (White *et al*., 1992). Nonetheless, oceanic crustal thickness across the basin is ~5 km thinner than a typical oceanic crust (Le Douaran *et al*., 1984; Pascal *et al*., 1993; Contrucci *et al*., 2001; Gailler *et al*., 2009; Moulin *et al*., 2015). This oceanic domain has only been interpreted in a few seismic profiles because salt bodies obscure the image of the basement structure due to strong lateral velocity changes.

7.3.1 Continental domain

Continental domain structure

Continental crust has been imaged in every seismic profile shot across the Gulf of Lions continental shelf and slope. Here we describe the basement structures that characterize the continental domain integrating the results from lines SPBAL01-04, 8, 12, 16, 20, 24 and 28 (Figures 7.2-7.8) that extend from the continental shelf into the deep basin, lines SPBAL01-11 and 15 that cover only through the continental slope of Gulf of Lions (Figures 7.9-7.10) and lines SPBAL01-23, 27 and 31 that run from the continental slope NE Minorca island into the deep Gulf of Lions Basin (Figures 7.11-7.13).

Under the continental shelf and slope all profiles display a basement tectonic structure characterized by large-offset normal faults. These faults are cutting the basement and bounding 1-10 km wide rotated blocks generally forming half-grabens and locally hosts and grabens (Figures 7.2-7.5 and 7.8). Rotated sediment units are syn-tectonic infill accommodating in space between blocks. These syn-tectonic sediments do no present significant internal structure and are overlain by parallel to sub-parallel post-tectonic sedimentary units. Lines SPBAL01-20 and 24 display different basement geometry (Figures 7.6-7.7) with comparatively fewer faults cutting the basement on line SPBAL01-24 (Figure 7.7) and no evidence of large-offset faults cutting the basement on line SPBAL01-20 (Figure 7.6). This difference between the former lines could represent a real variation of tectonic structure or an imaging problem due to a change in orientation of the tectonic fabric.

The top of the basement appears as a relatively low to medium amplitude reflective surface that is clearly visible in most lines (e.g., line SPBAL01-16, Figure 7.5). The top of the basement deepens towards the deep basin, where it is cut by numerous smaller normal faults. On line SPBAL01-24 the top of the basement is imaged as low amplitude reflections overlain by syn-tectonic sediments (Figure 7.7).

Figure 7.2: *Poststack time migration of line SPBAL01-04 (see Figure 7.1 for location). Reflections situated at 8 s TWTT are interpreted as the Moho with different nature through the profile (see text). Three interpreted domains are delimited with a line above in different colours: continental domain (green line), transitional domain (blue line) and oceanic domain (pink line). White dots at the base of the crust highlight an internal crust reflection or a possible detachment fault linking both continental and transition domains.*

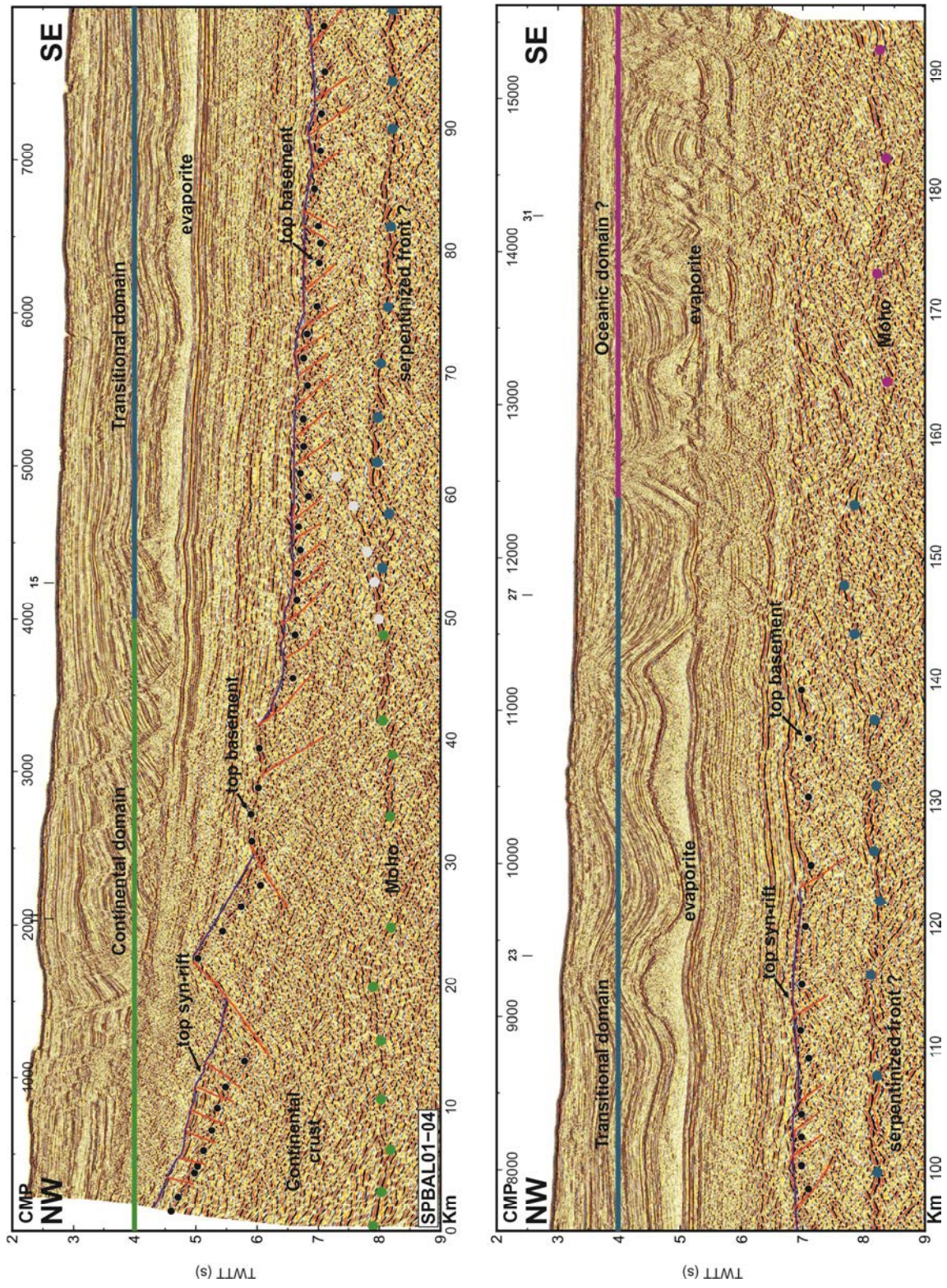
SE
NW
CMP
Transitional domain
Continental domain
evaporite
top basement
top syn-rift
Continental crust
Moho
serpentinized front ?
SPBAL01-04
Km
TWTT (s)
Oceanic domain ?

The base of the crust is interpreted as horizontal to subhorizontal comparatively high-amplitude reflections from the Moho boundary situated at 7-8 s TWTT. We have used an average velocity of 6 km s^{-1} to calculate crustal thickness. Beneath the slope of the Gulf of Lions, basement thickness ranges from ~10.5 to ~7.5 km on line SPBAL01-04 (Figure 7.2); ~12 to ~7.5 km on line SPBAL01-08 (Figure 7.3); ~16.5 to ~7.5 km on line SPBAL01-12 (Figure 7.4), and ~18 to ~7.5 km on lines SPBAL01-16 and SPBAL01-28 (Figures 7.5 and 7.8). Basement thickness decreases rapidly from under the slope to the deep basin, and increases from the Gulf of Lions to the Valencia Trough Basin as seen on lines SPBAL01-16 and 28 (Figures 7.5 and 7.8). On lines SPBAL01-20 and 24 it is difficult to determine crustal thickness due to the low continuity of reflections from the top of the basement as the presence of large volcanic edifices mask reflections underneath and does not permit a clear interpretation (Figure 7.6, CMP 12000 and CMP 9000; Figure 7.7, CMP 6000).

Profiles SPBAL01-11 and 15 run in SW-NE direction through the Iberian slope at the NE end of the Valencia Trough Basin to the middle of Gulf of Lions (Figures 7.1, 7.9 and 7.10). Unlike the other lines, there are few basement faults imaged in these profiles, possibly because they are oriented roughly in the same direction as fault plane strike. Two basement highs imaged on these lines (CMP 5000-6000 in Figure 7.9 and CMP 7500-8000 in Figure 7.10) are of undetermined nature, although on line SPBAL01-15 a ridge displays folded strata instead of crystalline rock. A similar structure is found on lines SPBAL01-23, 27 and 31 (Figures 7.11-7.13) where only few faults are imaged and syn-tectonic sediments show little internal structure (e.g., line SPBAL01-23, Figure 7.11 or line SPBAL01-31 Figure 7.13)

Figure 7.3: *Poststack time migration of line SPBAL01-08 (see Figure 7.1 for location). Reflections situated at 8 s TWTT are interpreted as the Moho with different nature through the profile (see text). Three interpreted domains are delimited with a line above in different colours: continental domain (green line), transitional domain (blue line) and oceanic domain (pink line). White dots at the base of the crust highlight an internal crust reflection or a possible detachment fault linking both continental and transition domains.*

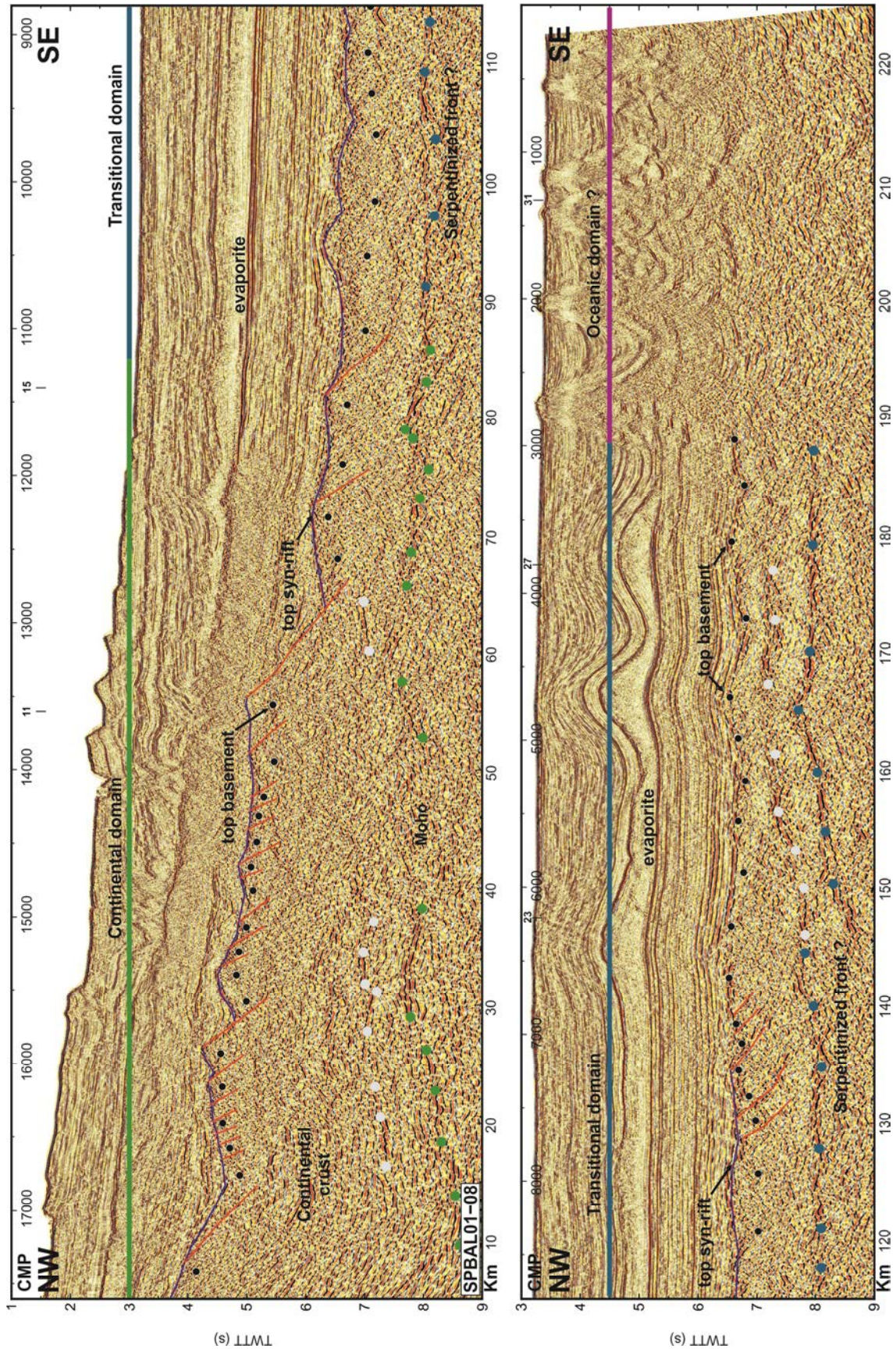
NW
SE
CMP
Km
TWTT (s)
Continental domain
Transitional domain
Oceanic domain ?
top basement
top syn-rift
evaporite
Moho
Continental crust
Serpentinized front ?
SPBAL01-08

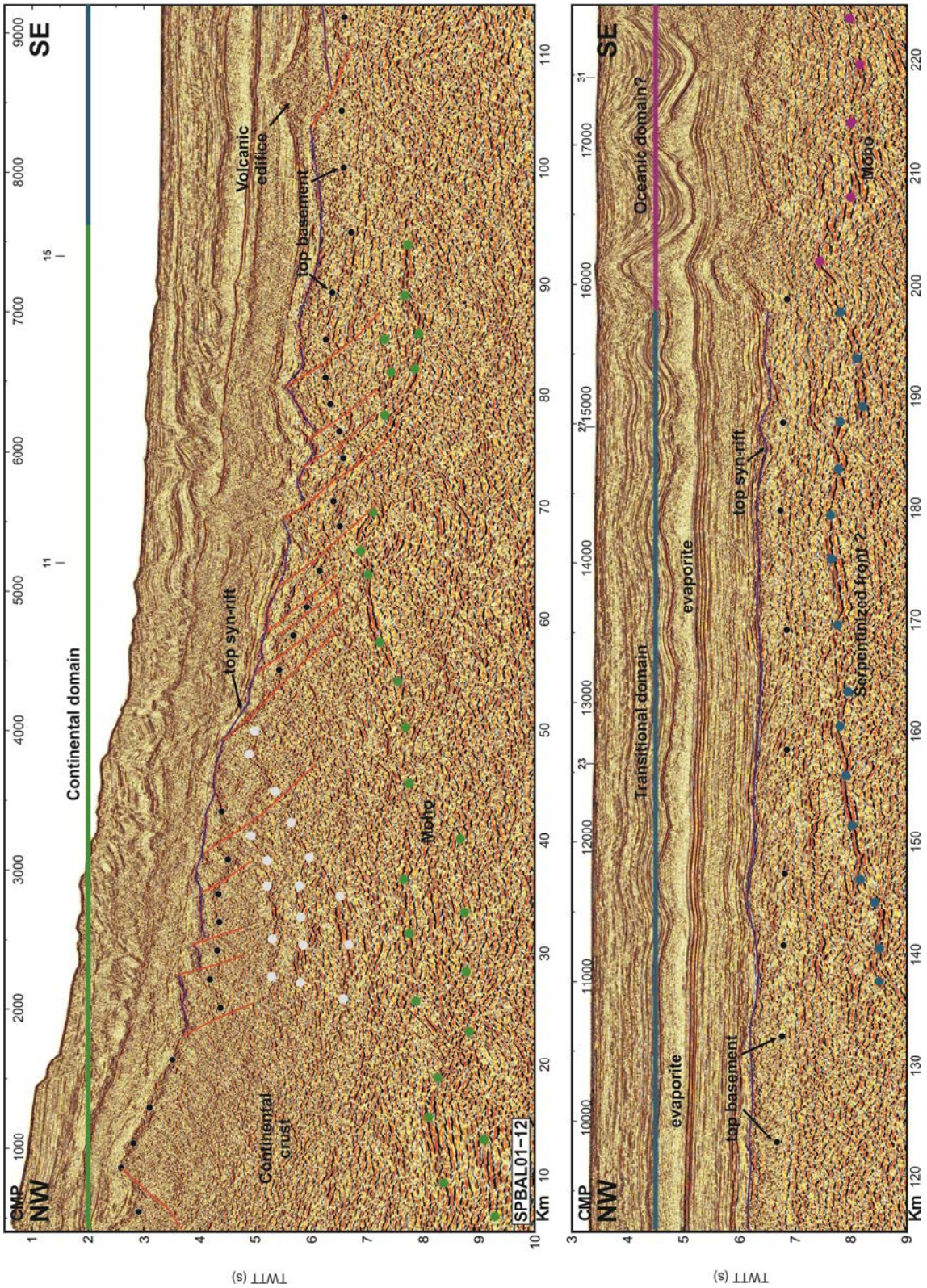

Figure 7.4: *Poststack time migration of line SPBAL01-12 (see Figure 7.1 for location). Reflections situated at 7-9 s TWTT are interpreted as the Moho with different nature through the profile (see text). Three interpreted domains are delimited with a line above in different colours: continental domain (green line), transitional domain (blue line) and oceanic domain (pink line). White dots highlight internal crustal reflections.*

The top of the basement appears as low amplitude reflections, sometimes difficult to identify, and overlain by thin syn-tectonic sediments (e.g., line SPBAL01-27, Figure 7.12). The two highs shown on Figure 7.12 crop out at the seafloor and are visible in the low-resolution bathymetry map with a WNW-ESE orientation (Figure 7.1). The base of the crust, as in previously shown profiles, is characterized by high amplitude reflections at 7-8 s TWTT and interpreted as the Moho boundary. Basement thickness ranges from ~18 to ~9 km on line SPBAL01-11 (Figure 7.9) with a maximum crustal thickness of ~21 km beneath the basement high and from ~9 to ~7.5 km on line SPBAL01-15 (Figure 7.10) with a maximum crustal thickness of 15 km beneath the ridge. Basement thickness ranges from ~8 km to ~7 km on lines SPBAL01-23, 27 and 31 (Figures 7.11-7.13).

Continental domain interpretation

Below the slope, tilted blocks are interpreted as continental crust. Previous studies done by Pascal *et al*. (1993) indicate a velocity of ~6.2 km s^{-1} for this layer in agreement with velocity of thinned continental crust (Christensen and Mooney, 1995). Crustal thinning occurs abruptly under the slope of the Gulf of Lions margin where basement thickness decreases from ~18 km to ~7.5 km in less than 50 km. This thinning is associated to intense faulting on the region and the formation of NE-SW oriented half grabens. According to several authors, the continental domain in the Gulf of Lions is wider than in the Sardinia conjugate domain (Rollet *et al*., 2002; Gailler *et al*., 2009; Moulin *et al*., 2015).

This tectonic structure and the apparent asymmetry between both margins of the basin is typical of many conjugate continental margin systems described in numerous magma-poor margin pairs including the Galicia Bank (Boillot & Froitzheim, 2001; Ranero & Gussinyé, 2010), the Iberian abyssal plain (Dean & Minshull, 2000; Whitmarsh *et al*., 2001) the South China Sea (Cameselle *et al*., 2015) and the Tyrrhenian Basin (Moeller *et al*., 2013).

Figure 7.5: *Poststack time migration of line SPBAL01-16 (see Figure 7.1 for location). Reflections situated at 8-9 s TWTT are interpreted as the Moho with different nature through the profile (see text). Two interpreted domains are delimited with a line above in different colours: continental domain (green line) and a transfer zone (purple line). This domain is interpreted as a transfer zone between two main right-lateral strike-slip faults; the North-Balearic fracture zone and the Catalan fracture zone that separates the evolution of Valencia Trough Basin from the Gulf of Lions.*

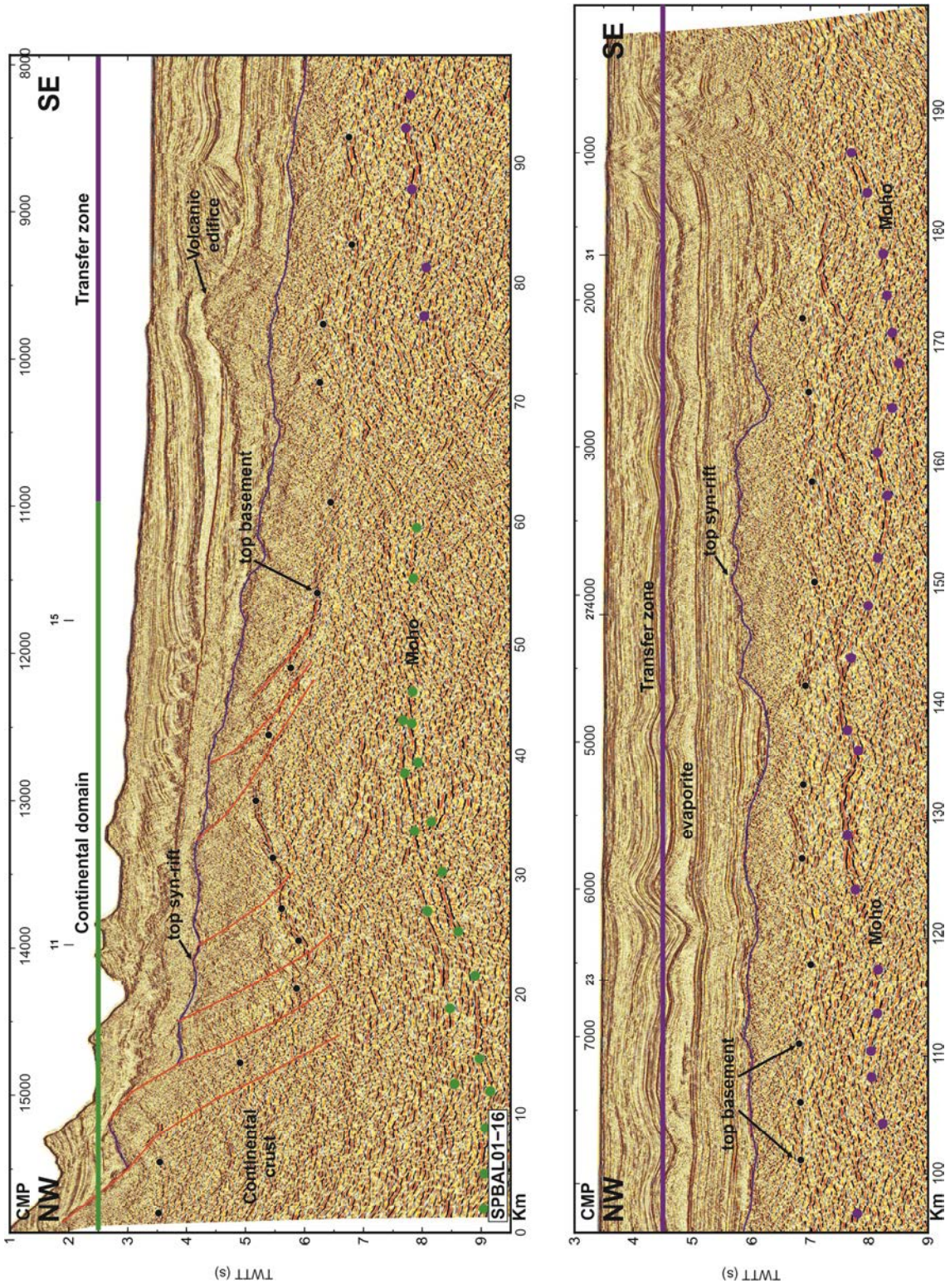
NW
SE
CMP
Km
TWTT (s)
Continental domain
Transfer zone
Volcanic edifice
top basement
top syn-rift
Moho
Continental crust
SPBAL01-16
evaporite

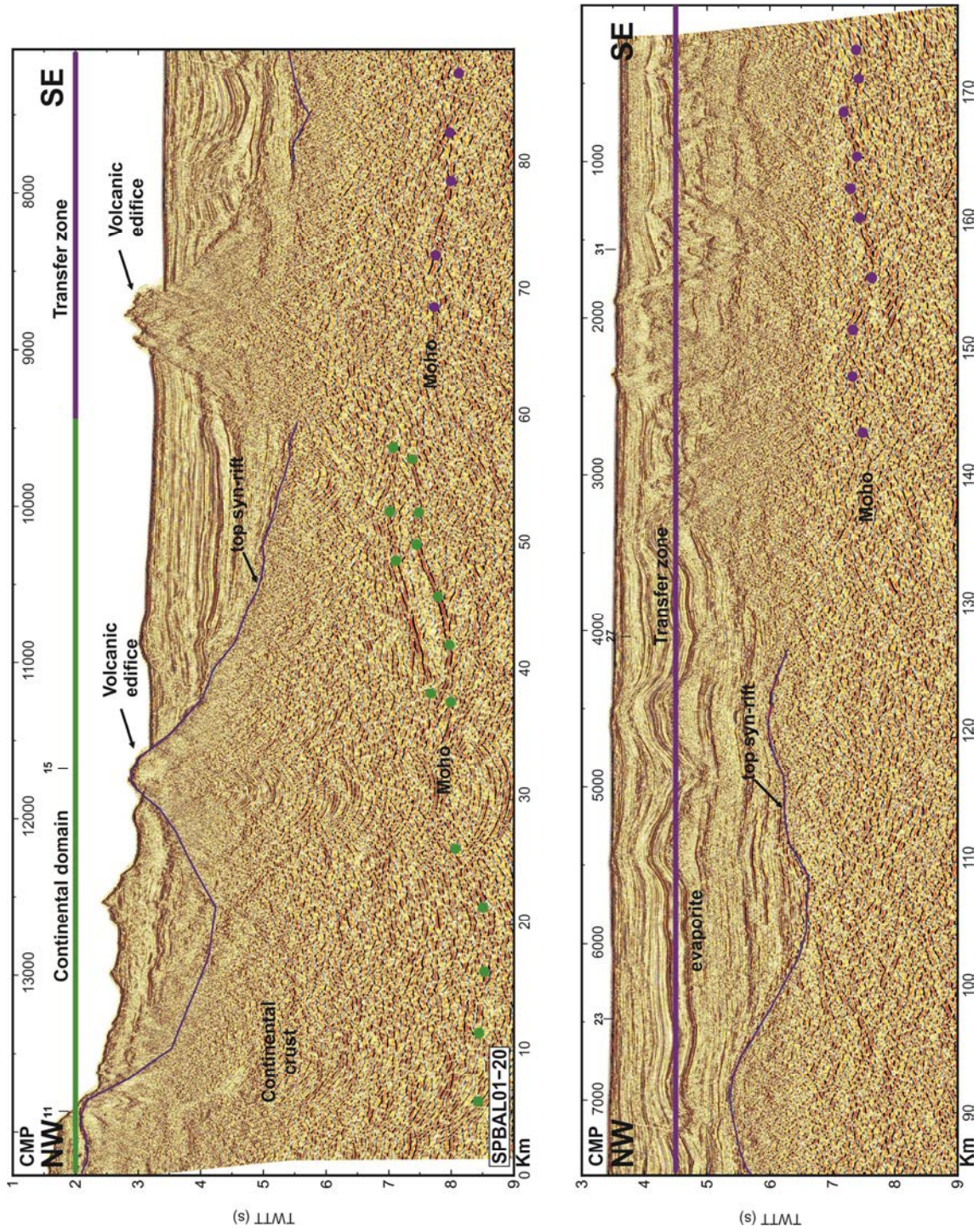

Figure 7.6: *Poststack time migration of line SPBAL01-20 (see Figure 7.1 for location). Reflections situated at 7-8 s TWTT are interpreted as the Moho with different nature throughout the profile (see text). Two interpreted domains are delimited with a line above in different colours: continental domain (green line) and a transfer zone (purple line). This domain is interpreted as a transfer zone between two main right-lateral strike-slip faults; the North-Balearic fracture zone and the Catalan fracture zone that separates the evolution of Valencia Trough Basin from the Gulf of Lions.*

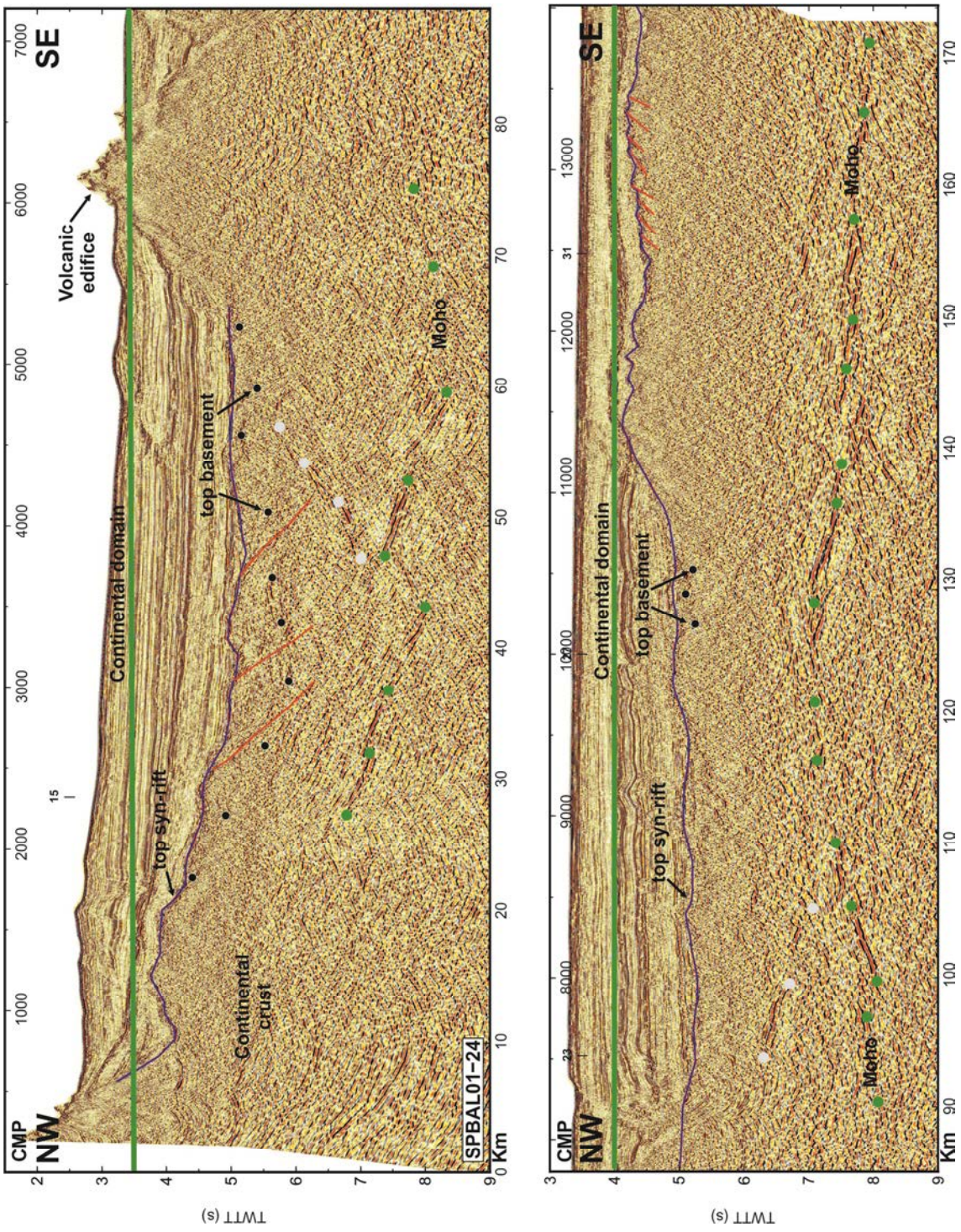

Figure 7.7: *Poststack time migration of line SPBAL01-24 (see Figure 7.1 for location). The image displays a band of reflections situated between 7-8 s TWTT interpreted as the Moho. Only the continental domain is interpreted (green line above the profile). The top of the basement (black dots) is not clearly imaged because the presence of a huge volcanic edifice located between CMP 5000 and CMP 7000 masks the seismic energy. This profile is interpreted to be entirely located on the continental crust of the Valencia Trough Basin.*

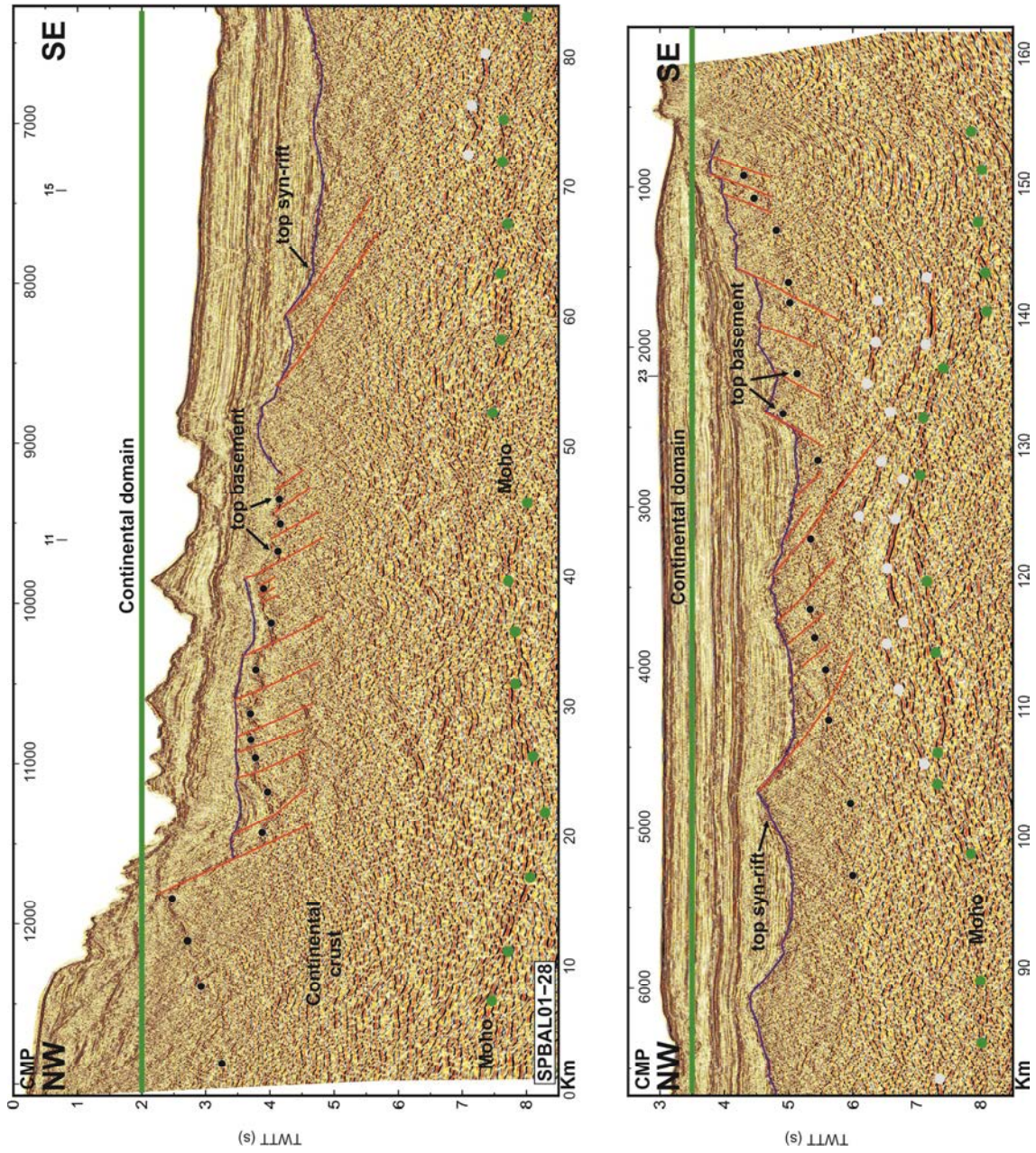

Figure 7.8: *Poststack time migration of line SPBAL01-28 (see Figure 7.1 for location). The image display a continuous band of reflections situated between 7.5 and 8 s TWTT interpreted as the Moho. Only the continental domain is interpreted (green line above the profile). White dots represent internal crust reflections possibly marking the limit between upper crust and lower crust.*

While it is clear that lines SPBAL01-11, 15 and 28 (Figures 7.9, 7.10 and 7.8) display a continental domain along the whole line, the rest of lines exhibit changes in crustal configuration. On lines SPBAL01-04, 8, 12 and 16 (Figures 7.2-7.5) the continental domain present faults that cut and tilt the basement blocks. Under the deep basin, however, the nature of the basement changes when large-offset faults cutting the basement disappear and

the crust thins to less than 8 km thick. Lines SPBAL01-20 and 24 display an overall different crustal geometry because there is no evidence of faults cutting through and rotating the basement that, given its thickness and location, it is most likely continental crust. A right lateral strike-slip fault system (North Balearic Fracture Zone) mapped by the associated strong magnetic anomalies may have separated the Valencia Trough Basin from the Gulf of Lions (Galdeano & Rossignol, 1977). Northward, the Catalan Fracture Zone (CFZ) bounds the Gulf of Lions from the Pyrenean belt (Mauffret *et al*., 2001; Maillard *et al*., 2003). These two fracture zones are inferred to have formed during the opening of the basin and are interpreted as a transfer zone between the Gulf of Lions and the Valencia Trough Basin (Mauffret *et al*., 2001; Maillard *et al*., 2003).

A thick chaotic sedimentary unit overlaying thinned continental crust may represent syn-tectonic sediments, that summed to the lack of clear extensional faults leads us to interpret that lines SPBAL01-16, 20 and 24 (Figures 7.5-7.7) image the fault structure in this region in an oblique way, which otherwise is typically interpreted as a transfer zone, or an area of oblique extension during the formation of the Gulf of Lions.

7.3.2 Continent-ocean transition domain

Transition domain description

We describe here the main structures that characterize the continent-ocean transition domain imaged on NW-SE oriented lines SPBAL01-04, 8, 12, (Figures 7.1,7.2-7.4) and on the SW-NE oriented lines SPBAL01-23, 27 and 31 (Figures 7.1,7.11-7.13).

Several characteristic features permit us to distinguish the faulted continental domain from this transitional domain. From the abrupt thinning of the continental crust (~18 km to ~7.5 km thick) towards the centre of the basin, the top of the basement is characterized by a sub-horizontal medium-high reflective horizon dissected by small-offset normal faults (Figures 7.2-7.4). The base of the basement layer is imaged as horizontal to subhorizontal high amplitude reflections at 8 s TWTT. The thickness of this layer bound at its base by strong reflections ranges from 1.0-1.3 s TWTT (e.g., profile SPBAL01-04, Figure 7.2). Based on previous studies done by Le Douran *et al*. (1984) and Pascal *et al*. (1993) we use 6 km s^{-1} to estimate thickness.

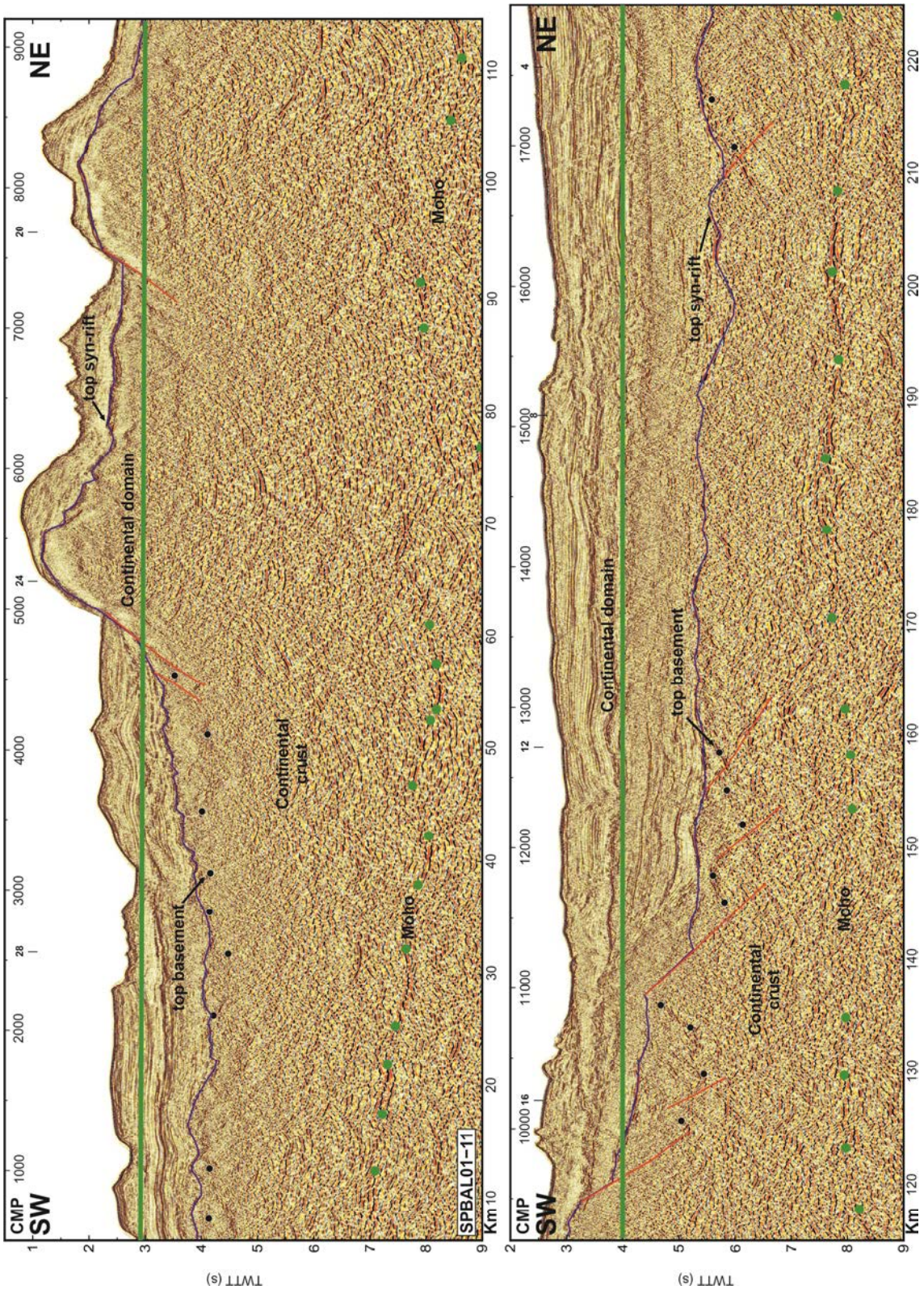

Figure 7.9: *Poststack time migration of line SPBAL01-11 (see Figure 7.1 for location). The image displays a continuous band of reflections situated between 7-8 s TWTT interpreted as the Moho. Only the continental domain is interpreted (green line above the profile). The apparent lack of fractured and tilted blocks in this profile is explained by the coincident orientation of the profile and main fault plains that originate the opening of the Gulf of Lions.*

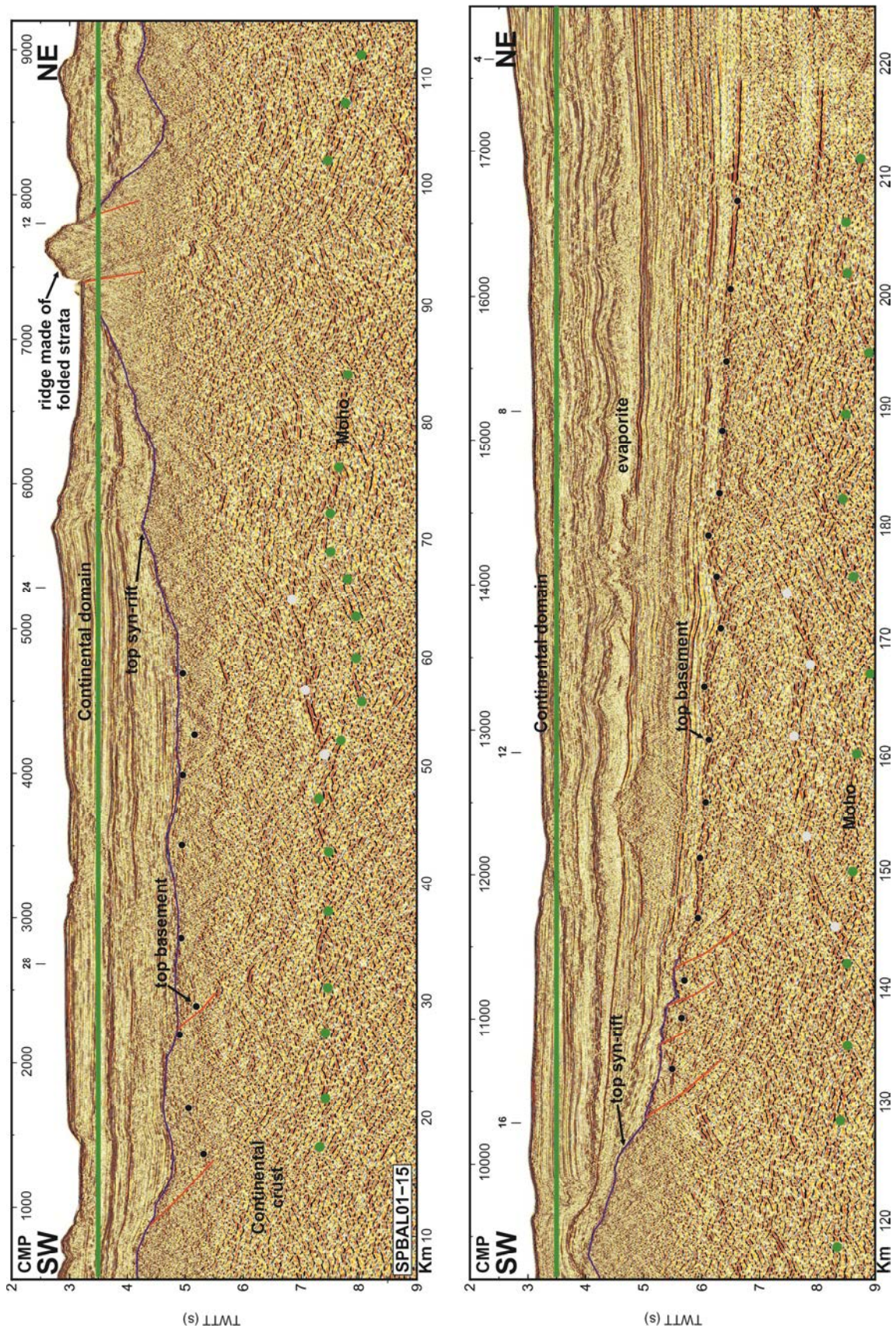
SW
NE
CMP
Km
TWTT (s)
Continental domain
top syn-rift
top basement
Moho
Continental crust
ridge made of folded strata
SPBAL01-15
evaporite

Figure 7.10: *Poststack time migration of line SPBAL01-15 (see Figure 7.1 for location). The image displays a continuous band of reflections situated between 7.5-8 s TWTT interpreted as the Moho. Only the continental domain is interpreted (green line above the profile). White dots highlight internal crust reflections possibly marking the limit between upper crust and lower crust.*

Thickness of the transition crust in profiles SPBAL01-04, 8 and 12 ranges from 1.0-1.3 s TWTT (~3 to 4 km) and generally remains constant for distances of tens of kilometres (Figures 7.2-7.4). A thin overlaying sediment strata, sometimes with no clear internal structure, presents a syn-tectonic geometry that smoothens the gentle half graben structure at the top of the basement (e.g., profile SPBAL01-08 Figure 7.3 between CMP 9000 and CMP 10000).

Lines SPBAL01-23, 27 and 31 exhibit some different characteristics in crustal structure. As described above, there is no clear evidence of faulted and tilted blocks in the continental domain, perhaps due to a profile orientation roughly parallel to the fault planes of the main grabens of the Gulf of Lions. The transitional domain in these profiles is also quite different: the images do not display the top of basement dissected by small-offset normal faults -as in profile SPBAL01-04 (Figure 7.2)-. In profiles SPBAL01-23 and 27 the basement is characterized by tilted faulted blocks, bounded by small-offset faults and overlain by syn-tectonic sediment (Figures 7.11 and 7.12). Profile SPBAL01-31 shows a more complex image, difficult to interpret even the top of the basement geometry because halokinetic movements of evaporites have created a complex velocity field that disturbs seismic imaging (Figure 7.13). The base of the crust is imaged as horizontal to subhorizontal high amplitude Moho reflections at ~8 s TWTT.

Transition domain interpretation

This transition domain is interpreted to represent a region of neither continent nor ocean typical character. The basement layer of this domain is about 3-4 km thick and previous studies (Pascal *et al*., 1993; Gailler *et al*., 2009) suggest that the velocity structure of this layer is neither typical of continental crust nor of oceanic crust. According to ESP's experiments, this region has upper crustal velocities ranging from 6-6.2 km s^{-1} and lower crustal velocity anomalously high, that reaches 7.9 km s^{-1} in the Gulf of Lions deep margin, while in the Sardinia deep margin velocity reaches 7.5 km s^{-1}. This domain is ~100 km wide in the Gulf of Lions and ~40 km wide offshore Sardinia (Gailler *et al*., 2009).

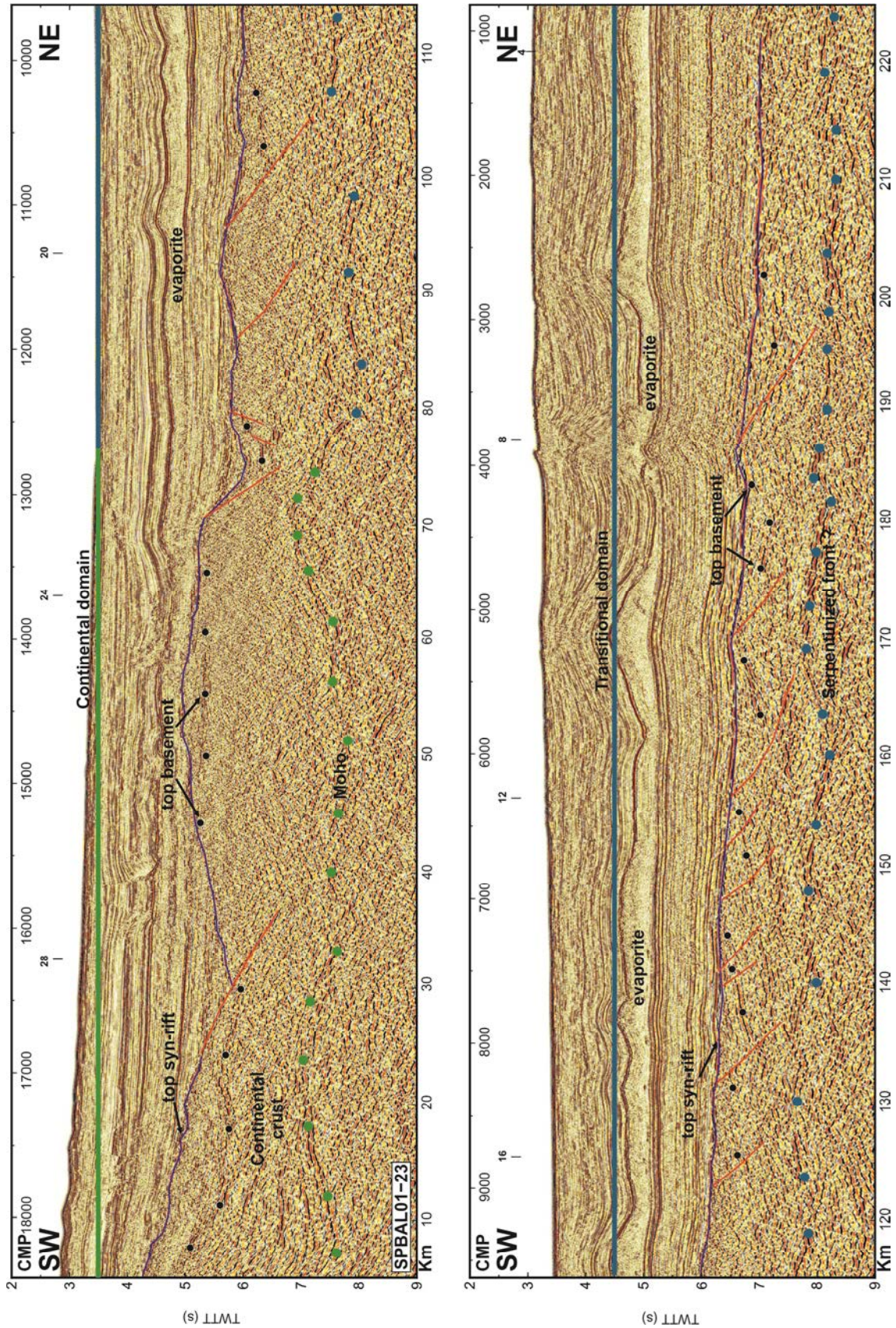
SW
NE
CMP
Km
TWTT (s)
Continental domain
evaporite
top basement
top syn-rift
Continental crust
Moho
SPBAL01-23
Transitional domain
Serpentinized front ?

Figure 7.11: *Poststack time migration of line SPBAL01-23 (see Figure 7.1 for location). The image displays a continuous band of reflections situated between 7.5-8 s TWTT interpreted as the Moho. Two interpreted domains are delimited with a line above in different colours: continental domain (green line) and transitional domain (blue line).*

The high velocities at the base of the layer of this domain are higher than velocities of either typical continental or lower oceanic crust (White *et al*., 1992; Christensen & Mooney, 1995) questioning its nature. Similar high-velocity bodies have been imaged at other transition zones in magma-poor margins as the Iberia Abyssal Plain (Dean *et al*., 2000), the Tagus Abyssal plain (Sallarès *et al*., 2013), the Nova Scotia margin (Funck *et al*., 2004), and some Mediterranean basins like the Tyrrhenian Basin (Prada *et al*., 2014) where they have been interpreted as exhumed and partially serpentinized mantle rocks, supported by drilling results. Nevertheless, these high velocities might be also explained by several other hypotheses that have previously been proposed for the Gulf of Lions: a) magmatic additions, b) upper mantle material, exhumed during the initial opening of the basin and c) thin continental crust overlying serpentinized mantle material.

Magmatic additions or intrusions are interpreted to be associated to the extrusive volcanism commonly found on volcanic margins, for example in the Davis Strait where magmatic underplating is observed and interpreted to be related to the Greenland-Iceland plume (Funck *et al*., 2007). This hypothesis would require a high asthenospheric temperature and usually is associated to a thick magmatic crust. The absence of associated subaereal or shallow submarine volcanic productions related to the opening of NW Mediterranean basins do not favour this hypothesis.

Second and third hypotheses involve upper mantle material. These hypotheses might be consistent with the presence of high velocities found in the lower crust along the margin of the Gulf of Lions. Exhumed mantle material is proposed at magma-poor margins (Chamot-Rooke, 1999; Dean *et al*., 2000; Funck *et al*., 2004; Sallarès *et al*., 2013; Prada *et al*., 2014) where no clear waves reflected from the Moho discontinuity (PmP reflections) are found in wide-angle data. The seismic images presented in this work display a clear band of highly reflective material across the whole domain. This boundary horizon is roughly at the expected TWTT for clear wide-angle reflections in the wide-angle data of Gailler *et al*. (2009), but these arrivals have not been integrated in the tomographic modelling during velocity inversion, so their significance in the velocity structure is still unclear. Therefore, the nature of this transition domain remains debatable, it might be related to thin continental crust

overlying serpentinized mantle material, but it is unlikely that 3-4 km thin lower continental crust has extended at constant thickness for about 140 km (Gulf of Lions + Sardinia domains) without breakup. Rather, we interpret that the presence of this highly reflective horizon might represent a serpentinization front. The velocities of 7.2-7.9 km/s for this 3-4 km thick shallow layer agree well with those expected for partially serpentinized mantle rocks exhumed after continental break up before the formation of an oceanic spreading centre. In summary, even though some allochthonous klipples of dismembered continental material may be present as observed in the Iberia abyssal plain, we propose that the transition zone is made of exhumed mantle that is possibly being serpentinized. The significance of the abrupt Vp transition at its based producing wide-angle reflections awaits to be explored.

7.3.3 Oceanic domain

Oceanic domain description

Oceanic crust has been identified from images on a few profiles in the deeper part of the basin. In the MCS profiles SPBAL01-04, 8, 12 and 31 it is difficult to image basement structures due to the presence of salt domes (Figures 7.2-7.4 and 7.13). Structure below the salt domes cannot be clearly interpreted as the seismic images are highly disturbed by the scattering and lateral velocity changes.

There is some previous (inconclusive) evidence that the steep salt domes region is underlain by oceanic crust. Pascal *et al*. (1993) and Contrucci *et al*. (2001) analysed wide-angle data and concluded that the high basement velocity detected in the transitional domain disappears in the deep basin and is replaced by a lower velocity (6.9 km s^{-1}) characteristic of oceanic crust (White *et al*., 1992). Further, vertical velocity gradients in this domain are characteristic of oceanic layers 2 and 3 (Gailler *et al*., 2009), although the oceanic crust is about ~5 km thick, somewhat less than typical oceanic crust (~6-7 km).

Figure 7.12: *Poststack time migration of line SPBAL01-27 (see Figure 7.1 for location). The image displays a continuous band of reflections situated between 7-8 s TWTT interpreted as the Moho with different nature through the profile (see text). Two interpreted domains are delimited with a line above in different colours: continental domain (green line) and transitional domain (blue line). White dots at the base of the crust between both continental and the transitional domain highlight internal crustal reflections marking possibly the limit between upper crust and lower crust.*

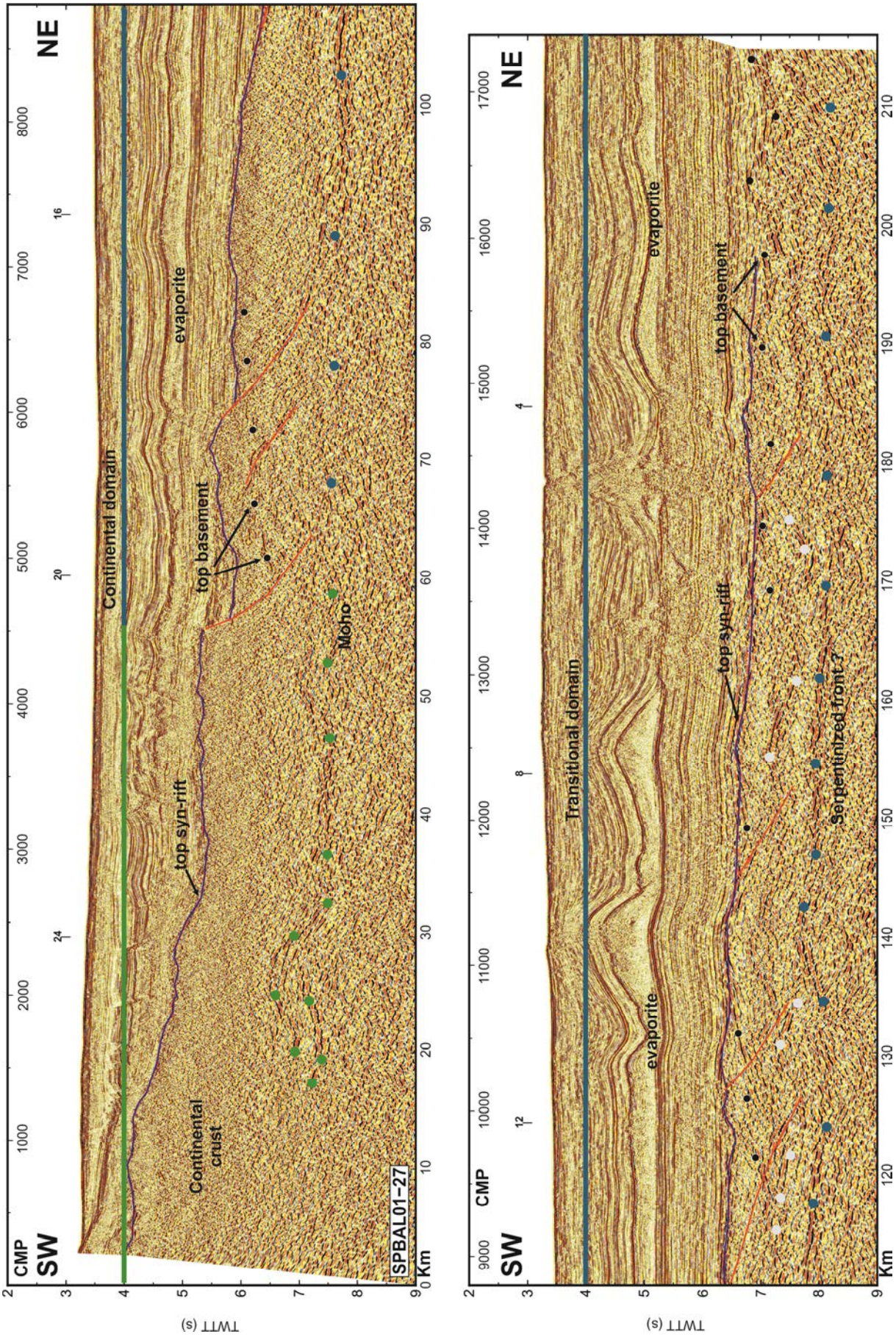
NE
SW
CMP
Km
TWTT (s)
Continental domain
evaporite
top basement
top syn-rift
Moho
Continental crust
SPBAL01-27
Transitional domain
Serpentinized front ?

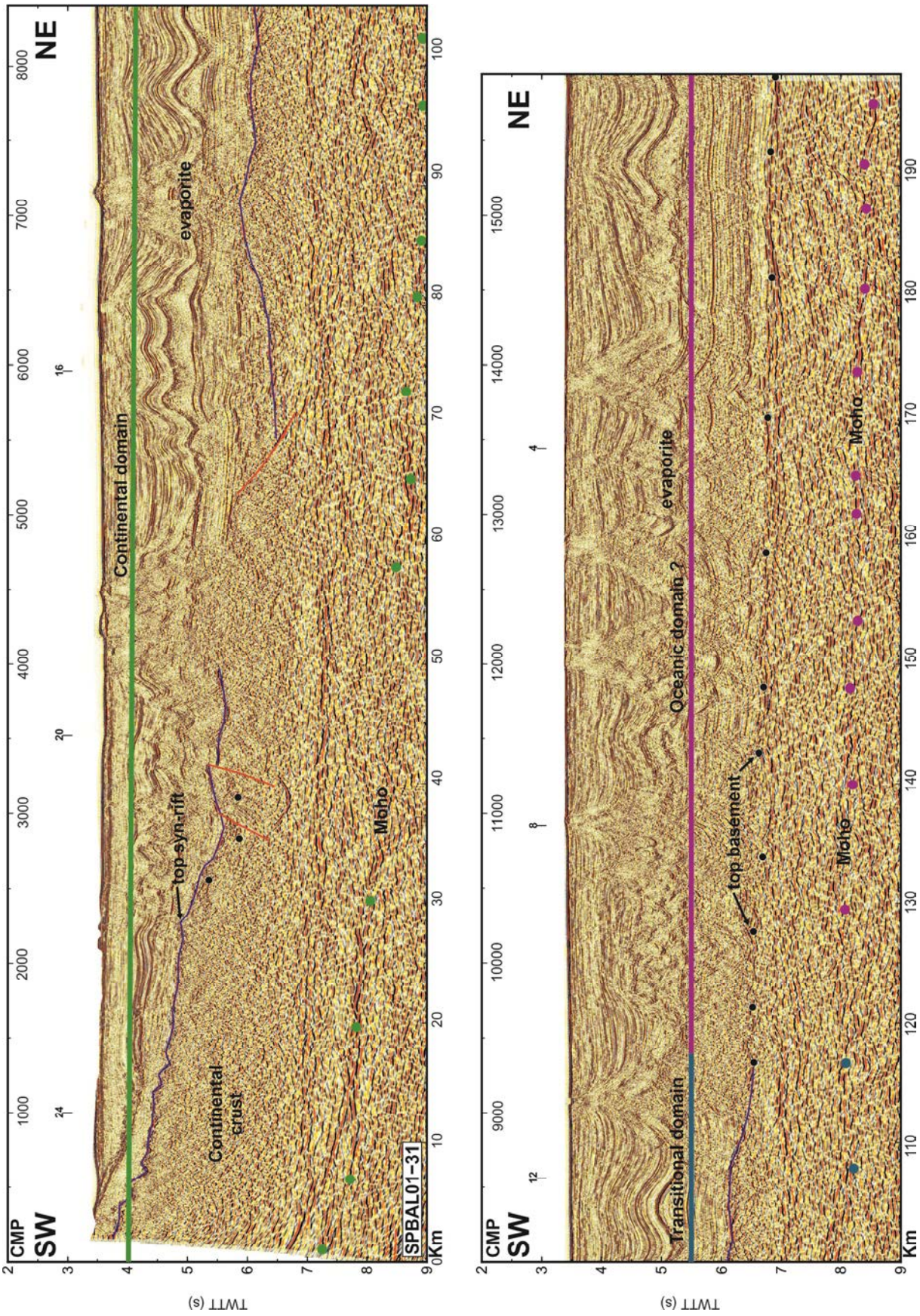
SW
NE
CMP
Km
TWTT (s)
Continental domain
evaporite
top syn-rift
Continental crust
Moho
SPBAL01-31
Transitional domain
Oceanic domain ?
top basement

Figure 7.13: *Poststack time migration of line SPBAL01-31 (see Figure 7.1 for location). The image displays a continuous band of reflections situated between 7.5-8 s TWTT interpreted as the Moho with different nature through the profile (see text). Three interpreted domains are delimited with a line above in different colours: continental domain (green line), transitional domain (blue line) and oceanic domain (pink line).*

The top of the basement appears as low to medium amplitude reflections overlain directly by a sub-horizontal post-tectonic sedimentary sequence (e.g. line SPBAL01-04, Figure 7.2 and line SPBAL01-31, Figure 7.13). The base of the crust is imaged as horizontal to subhorizontal high amplitude reflections interpreted as the Moho, situated at 7-8 s TWTT (e.g. lines SPBAL01-04, Figure 7.2; line SPBAL01-12, Figure 7.4 and line SPBAL01-31, Figure 7.13).

Oceanic domain interpretation

Thin oceanic crust is often found next to magma-poor margins (e.g. Funk *et al*., 2004) were it is attributed to oceanic spreading at slow rates at the onset of oceanic accretion. In this case, the decrease of crustal thickness might be related to the loss of conductive heat from the mantle welling up beneath the rift in oceanic basins. Gailler *et al*. (2009) conclude that this unusually thin oceanic crust has been emplaced under the influence of a cool slab in a back-arc basin, with the final lithospheric breakup occurring close to the Sardinia side.

7.4 Discussion

7.4.1 Breakup and formation of the continent-ocean transition in magma-poor margins.

A high-velocity zone in the lower crust has been described in several Atlantic-type rifted margins. Its presence is interpreted as magmatic underplating on magma-dominated margins resulting from the partial melting of the upper mantle during rifting (White and McKenzie, 1989; Reston, 2009) or partially serpentinized upper mantle peridotites exhumed in the continental breakup zone on magma-poor margins (Dean *et al*., 2000; Boillot *et al*., 2001; Sallarès *et al*., 2013).

Reston (2009) reviews the common features of magma-poor margins from North and Central Atlantic. These common features are: 1) Extreme crustal thinning from ~30 km to few km over a distance of 100-200 km. 2) A transition zone between continental crust and oceanic crust characterized by a moderate velocity gradient (~0.2 km s^{-1}) passing down from

velocities of 5 km s^{-1} to close to 8 km s^{-1} and weak magnetic anomalies. This anomalous crust has been interpreted as partially serpentinized exhumed mantle. 3) Beneath extreme thinned continental crust (less than 8 km), the presence of intermediate velocity zones between crust and mantle (7-7.8 km s^{-1}) and a velocity gradient close to 0.1 s^{-1}. These zones are interpreted as "undercrusting" of unroofed mantle peridotites partially serpentinized. 4) At some margins, the unroofed mantle is covered with low velocity, and local mounds up to 3 km high, interpreted as serpentine breccias and sedimentary serpentine mounds formed by lateral transport due to collapse of serpentinite highs. Finally, 5) the presence of a sharp reflection between the highly thinned continental crust, and the underlying serpentinized mantle. This reflection has been described and named in different margins such west of Galicia, named as S reflection, in the Iberia Abyssal Plain, named as H reflection (Reston, 2007) and beneath the Porcupine Basin, named as P reflection (Reston *et al*., 2001, 2004). This reflection not only appears to separate the crustal rocks from the underlying serpentinized mantle, but might have also act as a detachment surface on which overlying faulted blocks slipped.

As previously mentioned, a main characteristic of magma-poor margins is the presence of anomalous transition zones between clear continental and oceanic crust domains. These transition domains are characterized by the lack of magmatism and the presence of exhumed and serpentinized mantle material. Serpentinized mantle occurs through faults that link the mantle peridotites with the surface and allow the reaction between water and mantle peridotites (Bayrakci *et al*., 2016). This process requires a completely brittle crust, which can only occur through changes in rheology during the lithospheric extension. As a result, initial extension in the upper crust is produced by brittle faulting and by ductile creep at the middle and lowermost crust. However, these zones do not remain fixed. While the crust thins, reduction in temperature and pressure produce that rocks which originally deformed by plastic creep gradually become brittle and fracture. The result is that the entire crust becomes brittle over time (Perez-Gussinye & Reston 2001). Finally, depending on how the different lithospheric levels are coupled, the initial deformation approximately symmetric between margins becomes strongly asymmetric during the last stages of margin breakup (Ranero & Perez-Gussinye, 2010).

The Gulf of Lions is interpreted as a back-arc basin that opened due to the eastward roll-back of the west-directed Apenninic subduction zone (Cohen, C.R., 1980; Le Douran *et al*., 1984; Rehault *et al*., 1984; Gueguen *et al*., 1998; Jolivet *et al*., 2000, 2006, 2015). It is interpreted as a magma-poor margin and the asymmetry between the Gulf of Lions and the Sardinia margin is clear according to several authors (Burrus, 1984; Rollet *et al*., 2002; Gailler *et al*., 2009). Our results support a continental domain formed by fault that tilted

basement blocks, preceding a thin anomalous transition domain over a distance of ~100 km, with weak magnetic anomalies (Galdeano and Rossignol, 1977) and high lower crust velocities (7.5 km s^{-1}) interpreted as exhumed and serpentinized mantle material (Figure 7.14). In the seismic images we identify a strong reflective layer situated at 8 s TWTT that is interpreted as a possible serpentinized front, similar to the reflections described in magma-poor margins such as west Galicia, Iberia Abyssal Plain and Porcupine Basin (Reston *et al*., 2001, 2004 and Reston, 2007). Finally, a third region is made of thin oceanic crust (< 5 km) showing vertical velocity gradients characteristic of layers 2 and 3 (Pascal *et al*., 1993; Contrucci *et al*., 2001; Gailler *et al*., 2009). This crust might have been emplaced under the influence of a cool slab in back-arc basin, with the final breakup occurring close to the Sardinia side (Gailler *et al*., 2009) (Figure 7.14).

7.4.2 Opening of the Gulf of Lions; Role of the transfer zone between Valencia Trough Basin and the Gulf of Lions.

The eastward roll-back of the west-directed Apenninic subduction zone is the most accepted mechanism to produce the opening of the Gulf of Lions (Cohen, C.R., 1980; Le Douran *et al*., 1984; Rehault *et al*., 1984; Gueguen *et al*., 1998; Jolivet *et al*., 2000, 2006, 2015). Roll-back of the subduction zone during Rupelian time (30 Ma) produced tensile stress in the overriding continental lithosphere. This extension was expressed by rifting and the generation of NE-SW oriented grabens in the Gulf of Lions continental domain. According to some studies (Ziegler *et al*., 1992; Séranne, 1999) back-arc extension possibly overlaps to the north of Gulf of Lions margin with the West European Rift system (Ziegler *et al*., 1992), and reactivates some grabens initiated during Priabonian time (35 Ma) under E-W extensional stresses (Sérenne, 1999).

The crustal structure is in agreement with a magma-poor nature in the Gulf of Lions margin and the formation of a ~100-km-wide thin anomalous transitional crust. Continental breakup occurred at Early Miocene times decentred toward the Corsica-Sardinia margin. This asymmetry is typical of back-arc margins where a narrow margin forms on the side of the volcanic arc, close to the subduction zone, whereas the conjugate margin widens by tectonic extension (Rollet *et al*., 2002).

Figure 7.14 shows the crustal limits interpreted integrating the two wide-angle seismic profiles from Gailler *et al*. (2009) (Figure 7.1) and the multichannel seismic profile from Jolivet *et al*. (2015) (Figure 7.1). The analysis of the 2D grid of multichannel seismic SPBAL01 lines allows us to extend and refine the crustal limits in the Gulf of Lions area. We infer that the limit between the continental domain and the continent-ocean transition domain

is located near the position suggested by previous authors, in between SPBAL01-11 and 15 (Figures 7.9, 7.10 and 7.14). The continental edge extends to near line SPBAL01-24 which images continental crust all along (Figures 7.7 and 7.14). The limit between the continental domain and the continent-ocean transition domain runs to the SE crossing lines SPBAL01-23, 27 and 31 (Figures 7.11-7.13 and 7.14). The second crustal limit marks the boundary between the continent-ocean transition domain and the ocean domain. This limit differs from the interpretation by Gailler *et al*. (2009) and Jolivet *et al*. (2015). Although the presence of evaporite domes complicates seismic imaging, in profiles SPBAL01-04, 08, 12 and 31, we could attribute the 5 km thick basement to oceanic crust (Figures 7.2-7.4 and 7.13). As a consequence, the limit between continent-ocean transition domain and ocean domain is located between SPBAL01-27 and SPBAL01-31 lines, and thus closer to SPBAL01-27 (Figure 7.14).

A NW-SE trend of magnetic anomalies may represent the deformation zone between the North-Balearic and the Catalan strike-slip fault zones (Figure 7.14). The area between both structures has been previously described as a transfer zone between the deformation of the Gulf of Lions and Valencia Trough Basin with two pulses of activity separated by a Middle Miocene tectonic quiescence (Maillard and Mauffret, 1999; Mauffret *et al*., 2001). These two main fault systems have right-lateral movement related to the southeastward drift of the Corsica-Sardinia block. It is difficult to define the trace of any of these main faults in the seismic images presented in this work. There are some structures that could be related to these faults, but no large-scale sub-vertical faults have been detected. Notwithstanding this, the presence of thick syn-tectonic sediments with poor internal structure points us to think that the seismic profiles are probably oriented roughly parallel to the strike of the faults in the region. In this view, the entire area could represent a region of more distributed oblique rifting deformation with neither well-defined major strike-slip faults nor well-formed fault planes of the shear zones.

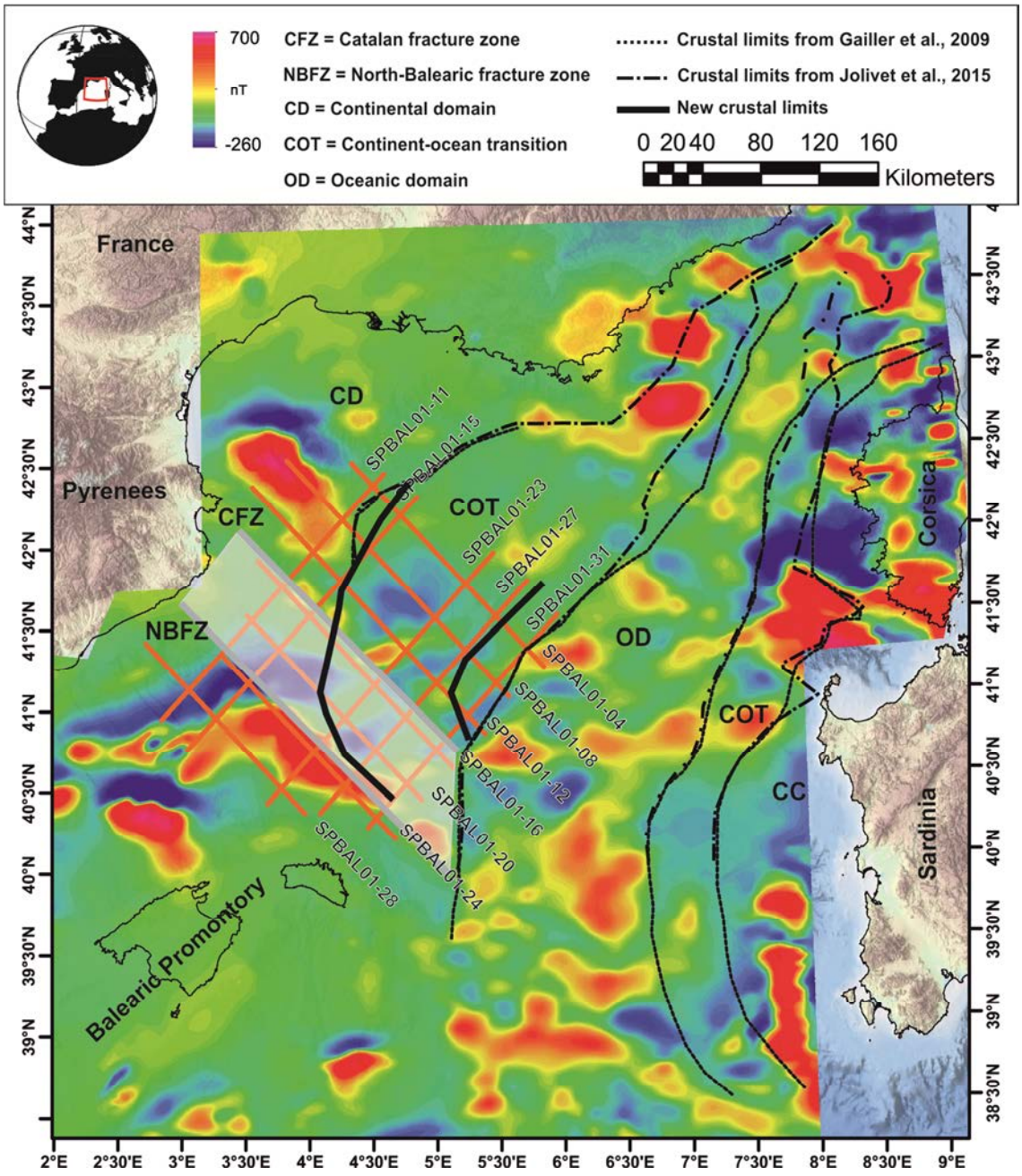

Figure 7.14: *Aeromagnetic map centred on the Gulf of Lions and Ligurian Sea area (after Galdeano and Rossignol, 1977). Orange lines correspond to MCS SPBAL01 interpreted and discussed in this work. Black lines mark the limits between the different crustal domains (CD = Continental domain; COT = Continent-ocean transition domain; OD = Oceanic domain). Crustal domain identification was carried out through interpretation of the presented profiles and modification of previous interpretations done by Gailler et al. (2009) Gueguen, (1995) and Jolivet et al. (2015). Grey lines mark linear magnetic anomalies interpreted as fracture zones (NBFZ = North-Balearic Fracture Zone; CFZ = Catalan Fracture Zone. The light-grey area between both lines has been interpreted as a transfer zone between Gulf of Lions and the Valencia Trough Basin (Maillard and Mauffret, 1999; Mauffret et al., 2001).*

Chapter 8: Algero-Balearic Basin

8.1 Introduction

The Algero-Balearic Basin, located between the Balearic Islands and North Africa, is limited to the north by the Balearic Promontory, to the south by the coast of North Africa, to the west by the Alboran Basin and to the east by the Liguro-Provençal Basin (Figure 8.1).

Since the first studies of the Western Mediterranean region, the Algero-Balearic Basin has been interpreted by most authors as a back-arc basin formed due to slab rollback (Rehault *et al*., 1984; Dewey *et al*., 1989; Lonergan and White, 1997; Gueguen *et al*., 1998; Frizon de Lamotte *et al*., 2000; Jolivet and Faccenna, 2000; Gelabert *et al*., 2002; Rosenbaum *et al*., 2002; Schettino and Turco, 2006). The opening of the Algero-Balearic Basin started during the Late Oligocene (25-23 Ma) when the kabylies block drifted away from an initial position south of the Balearic Promontory and finished around 15-18 Ma when the Kabylies block was accreted to the African margin. The kinematics of the opening of the Algero-Balearic Basin is still a matter of debate. While some authors consider that the Algero-Balearic Basin opened in a N-S direction due to the roll-back of a NW directed subducting slab (Rehault *et al*., 1984**;** Vergés and Sàbat, 1999; Faccenna *et al*., 2004; Schettino and Turco, 2006; Jolivet *et al*., 2009; Carminati *et al*., 2012; Faccenna *et al*., 2014), others consider the opening of the Algero-Balearic Basin in a E-W direction during the westward migration of the Alboran block (Lonergan and White, 1977; Mauffret *et al*., 2004; Spakman and Wortel, 2004; Camerlenghi *et al*., 2009; Gutscher *et al*., 2012; Acosta *et al*., 2013; Chertova *et al*., 2014; van Hinsbergen *et al*., 2014).

The different existing models predict a variety of continental margin structures (extensional or transcurrent) and transitions to oceanic crust (rifted type –again magma poor or classical- or abrupt in a transcurrent setting), but the original crustal configuration is inadequately known because it is obscured by post-Messinian deformation in North Africa (Leprêtre *et al*., 2013; Badji *et al*., 2014; Medaouri *et al*., 2014; Bouyahiaoui *et al*., 2015) and little studied in the Balearic promontory with only one crustal-scale published profile of the structure (e.g. Vidal *et al*., 1998) imaged on ESCI-Valencia multichannel line (Figure 8.1).

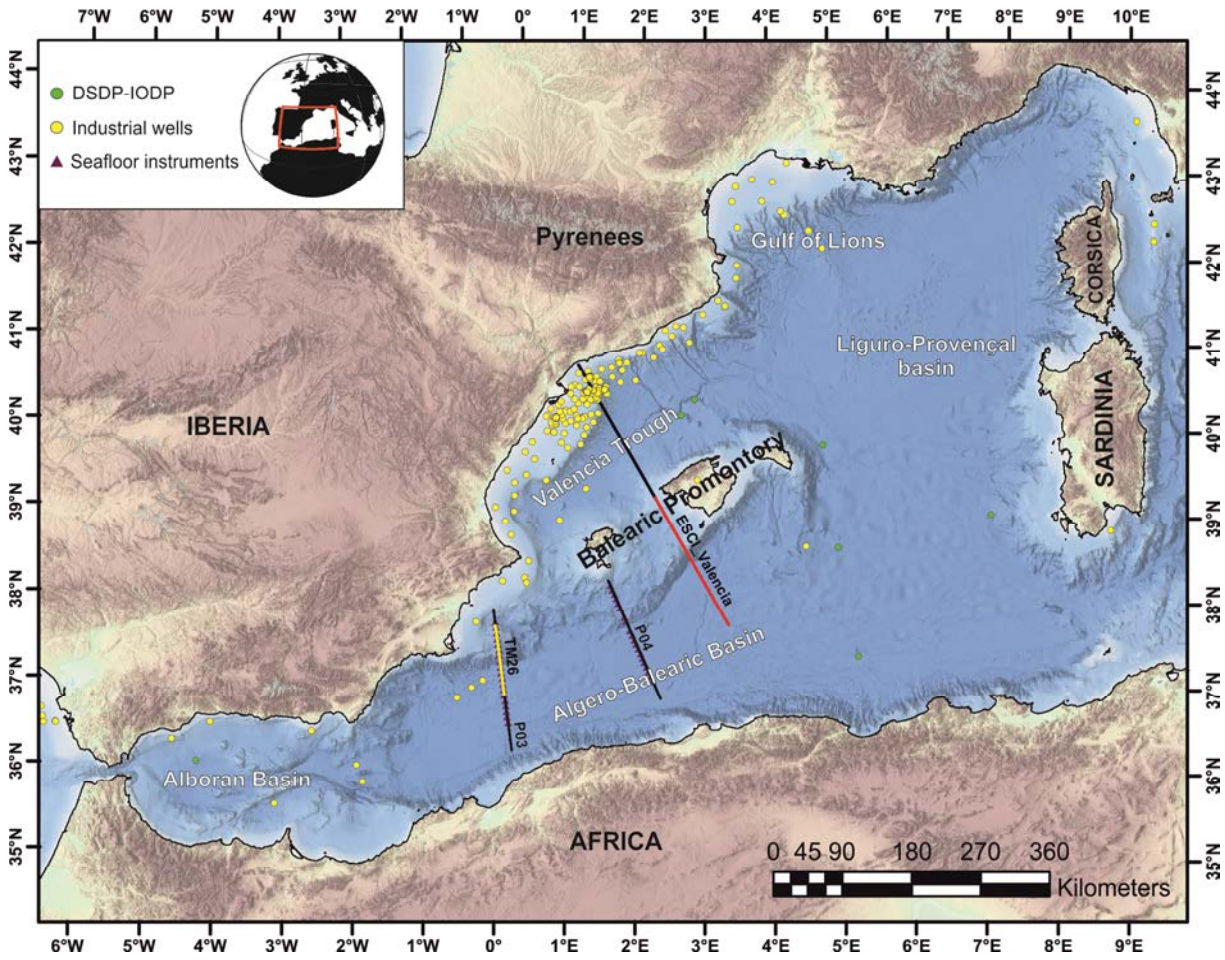

Figure 8.1: *Bathymetric and topographic map of the Western Mediterranean basins. The Algero-Balearic Basin is bounded by the Balearic Promontory to the north, the North Africa margin to the south, the south Liguro-Provençal Basin to the east and the Alboran Basin to the west. Lines in black correspond to the wide-angle seismic profiles WESTMED P03 and P04 acquired by the German R/V Meteor on August 2006. Red line corresponds to southern half of the multichannel seismic profile ESCI-Valencia acquired on February 1992 by Geco-Prakla's survey vessel M.V.Bin Hai and used in this section. Yellow line corresponds to the multichannel seismic profile TM26 acquired on September 2011 by the Spanish R/V Sarmiento de Gamboa. Light green dots mark the location of DSDP and IODP sites. Yellow dots mark the location of different industrial wells in the area. Purple triangles mark the position of the seafloor instruments used to acquired wide-angle seismic profiles P03 and P04.*

This work presents the results from a ~180 km long wide-angle seismic profile (P03) acquired across southeastern Iberian margin and into the Algerian Basin in a NNW-SSE direction and a ~90 Km long multichannel seismic profile (TM26) coincident with the former across the continental margin (Figure 8.1). In addition, along strike changes in margin structure have been studied by reprocessing the ESCI-Valencia line that crosses the south Balearic margin and extends into the deep Algerian Basin. Seismic images from the wide-

angle seismic profile P04 have also been obtained using the multiple arrival (not the primary) of the wavefield recorded in Ocean Bottom Seismometers with the modern technique of mirror imaging (Figure 8.1). The main goal of this work is to estimate the thickness, nature and tectonic structure of the crust beneath the southeastern Iberian margin and Algerian Basin, as well as to identify the type of continent-ocean transition and discuss the possible geodynamic origin of the region. To shed some light on these issues, we discuss the 2D Vp model obtained from wide-angle seismic modelling with a joint refraction and reflection travel-time inversion together with the multichannel seismic profile images, integrating velocity and tectonic structure of the southeastern Iberian margin. The comparison of the Vp model with available velocity compilations of different crustal types has interpreting the nature of geological domains and understand the transition between continental crust underneath Iberian margin and oceanic crust in the deep Algero-Balearic Basin.

8.2 Geological Setting

The study area is located in the central and westernmost sector of the Algero-Balearic Basin. It is limited to the north by the easternmost sector of the Internal Betic Zone (southeast Iberian margin) and the Balearic Promontory (Figure 8.1). The Balearic Promontory is a 348 km long, 105 km wide and 1-2 km high structural elevation oriented NE-SW which contains the Balearic Islands: Eivissa, Formentera, Mallorca and Menorca (Acosta *et al*., 2013). The Promontory separates the Valencia Trough to the northwest from the Algero-Balearic Basin to the southeast (Figure 8.1). The northeastern end of the Promontory is separated from the Liguro-Provençal Basin by a steep continental slope that may be related to the postulated North-Balearic Fracture Zone (NBFZ), which has being inferred from the presence of a strong magnetic anomaly trending NW-SE from offshore Pyrenees to the deep Liguro-Provençal Basin (Galdeano and Rossignol, 1977- Figure 8.2). To the south, the study area is limited by the deep Algerian Basin, assumed to be oceanic in nature and covered by a thick layer of Messinian evaporites and older terrigenous sediments (Mauffret *et al*., 1992; Vidal *et al*., 1998; Leprêtre *et al*., 2013; Maillard and Mauffret, 2013; Medaouri *et al*., 2014; Badji *et al*., 2015; Driussi *et al*., 2015). The western end of the study area is marked by another strong magnetic anomaly trending N-S that marks the boundary between the westernmost Algero-Balearic Basin and the eastern Alboran Basin (Galdeano and Rossignol, 1977; Figure 8.2).

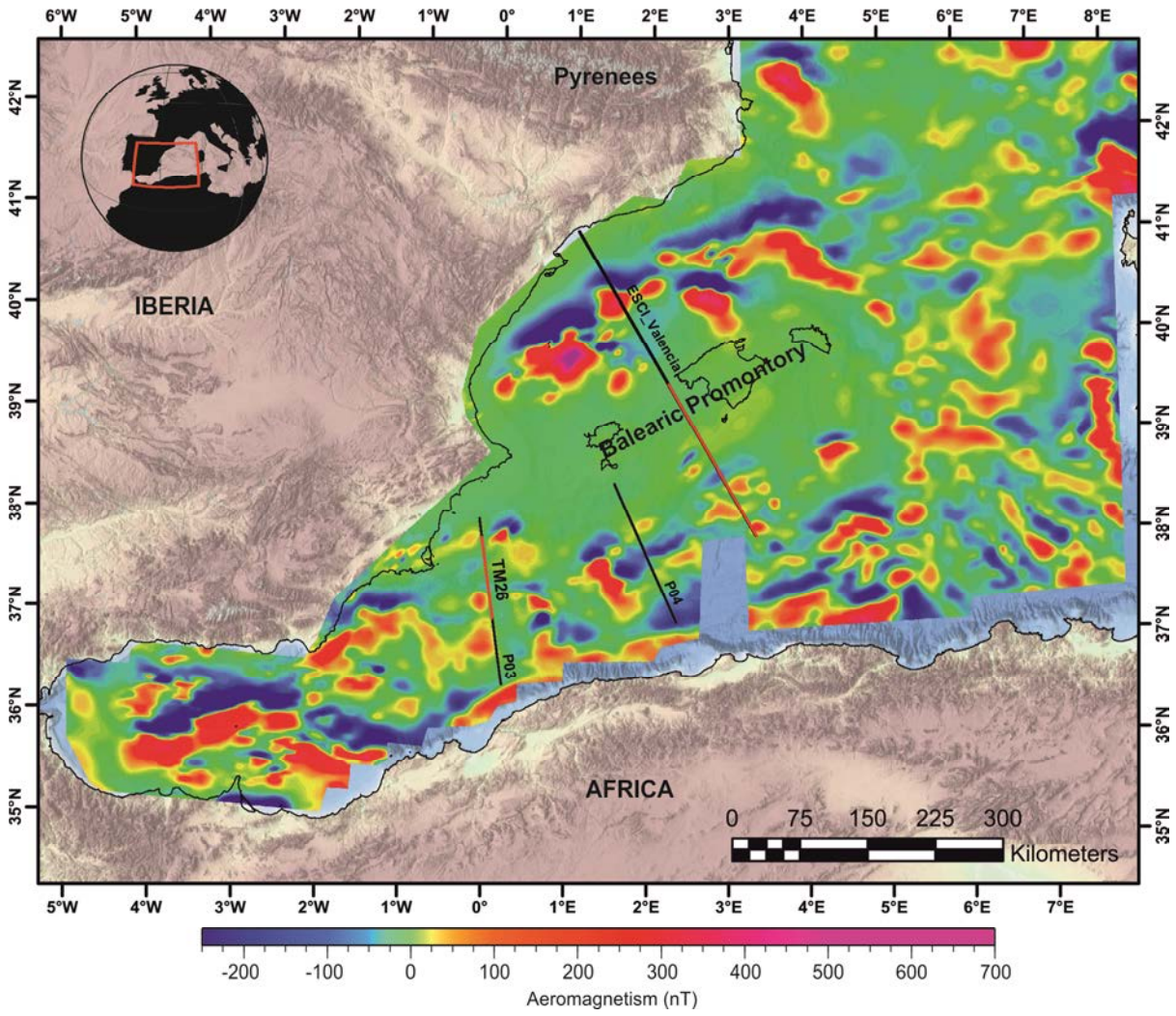

Figure 8.2: *Aeromagnetic map digitized from Galdeano and Rossignol (1977) centered on the Algero-Balearic Basin. Straight lines correspond to the seismic lines processed, interpreted and discussed in this work (see Figure 8.1). This map shows the complex distribution of magnetic anomalies in the whole area and the interaction between volcanic anomalies and seafloor spreading anomalies.*

The southeastern Iberian margin and the Balearic Promontory are interpreted to undergo a complex geological evolution unlike the deep Algerian Basin. Two different tectonic processes affected the Betic-Balearic domain during the Neogene: first a compressional event during the Late Oligocene that built up the piggy-back thrust system of the Balearic Promontory and secondly an extensional event during the Miocene related to the opening of the Algero-Balearic Basin due to the roll-back of the northwest dipping subduction of the African lithosphere beneath Europe (Fontboté *et al.*, 1990). This extensional episode gave birth to two steep scarps: the Emile Baudot escarpment south of the Balearic Islands, and the Mazarron escarpment southeast of the Iberian margin. The nature of these two scarps is

not clear and while some authors interpreted them as normal faults (Vergés and Sábat, 1999), other authors interpreted them as right-lateral transform faults (Mauffret *et al.*, 1992; Acosta *et al.*, 2013; Driussi *et al.*, 2015).

8.3 Velocity structure

Tomographic modelling of the wide-angle seismic data resulted in the crustal velocity structure shown in Figure 8.3. The Vp model displays the velocity of the crust and uppermost mantle as well as the geometry obtained for the Moho discontinuity. The main characteristic of the velocity model is the lateral variations in sedimentary layer thickness, the complex velocity structure showing abrupt lateral changes in basement velocity and the abrupt crustal thinning towards the deep basin. The velocity structure defines three main domains along profile P03 (Figure 8.3).

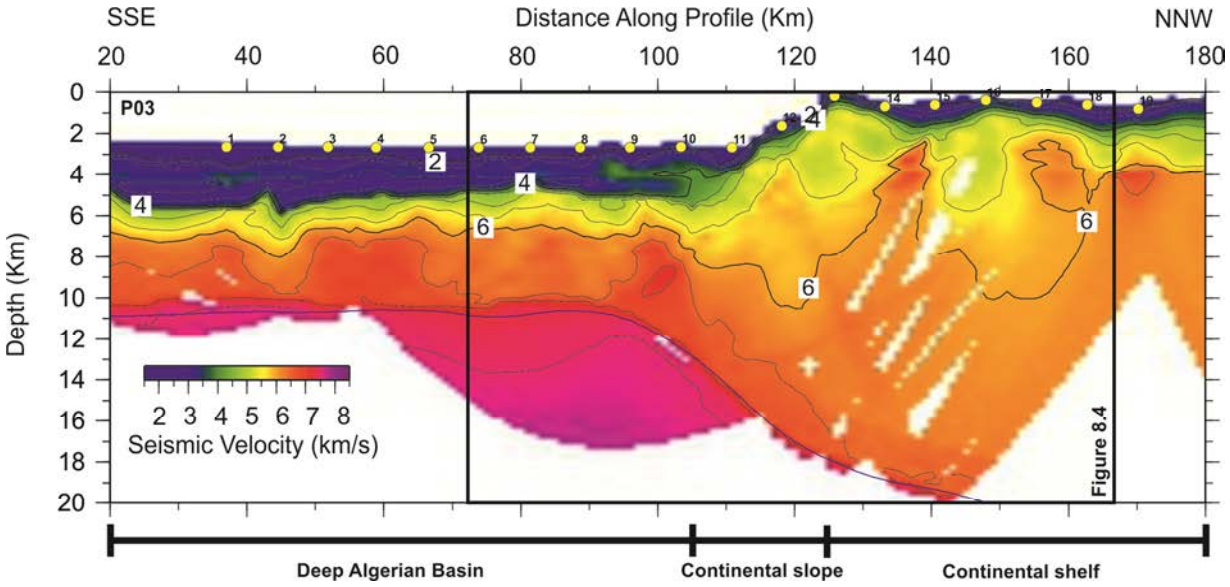

Figure 8.3: *Final P-wave velocity model of the crust, uppermost mantle and the Moho (blue line) geometry along the wide-angle seismic profile P03 from the southeastern Iberian margin to the deep Algerian Basin. The image is divided in three sections from west to east: continental shelf, continental slope and deep Algerian Basin (see the text for more information). Yellow circles show the position of seafloor instrumentation (OBHs and OBSs) used during the data acquisition. Note that in deep Algerian Basin the tomographic model presents an inversion of seismic velocities from 4.5 km/s to 3 km/s. This inversion could be related to the existing salt deposits in the Algerian Basin (CMP12000-10000). The black box corresponds to the part of the WAS profile coincident with the MCS profile TM26 (see Figure 8.4).*

8.3.1 Continental shelf

This domain extends from profile km 180 up to km 125 corresponding to the Alicante shelf on the southeastern Iberian margin. The main feature of this domain is the presence of a basement high (Seco de Palos Seamount) with underlying velocities ranging 5-5.5 km/s in the upper crust, and between 6-6.5 km/s in the lower crust (Figures 8.3 and 8.4). The basement velocity structure displays abrupt lateral changes in velocity at 4 km depth. Two subvertical high velocity zones 10-20 km wide are detected below the continental shelf, with velocities ranging from 6 to 6.8 km/s. The Moho reflector in this first domain shallows from ~20 km depth to 18 km towards the southeast.

8.3.2 Continental slope

The second domain goes from profile km 125 at the end of the continental margin to km 105 at the foot of the continental slope (Figure 8.3). It is marked by an abrupt thinning of the continental crust from 18 to 13 km in 20 km distance. The vertical velocity gradient is almost constant with depth around ~0.3 $^{s-1}$, but it changes at the foot of the continental slope, where a velocity inversion is found in the upper crust and a high velocity zone is observed in the lower crust (Figure 8.3).

8.3.3 Deep basin

The third domain extends from profile km 115 up to km 20 (Figure 8.3). The model displays 2-3 km thick sediment cover with a Vp of 1.5-2 km/s at the top and 4 km/s at the base. A velocity inversion at a depth of ~4 km is observed across much of the basement. Sediment velocitiy increases from ~2 km/s to 3.5-4 km/s at ~4 km depth and decreases to ~3 km/s just below. This velocity inversion occurs underneath the Messinian salt layers in the deep basin (Figure 8.4). Underneath the sedimentary cover the basement has an average thickness of ~6 km, characterized by a two-layer velocity structure ranging from ~5 to ~6 km/s in the upper crust and from ~6 to ~7 km/s in the lower crust. Although the thickness of the crust is rather constant, there are local lateral variations in the velocity of the lower crust ranging from ~6 km/s up to ~7.4 km/s. The Moho discontinuity in this domain is well-constrained between km 20 and 115 at a depth of 11 km.

8.4 Tectonic image

Three seismic images are used to study the tectonic structure of the continental shelf and slope of the Betic-Balearic margin and the adjacent deep Algerian Basin. From west to east we describe the basin structure: first the continental shelf and slope of the southeast Iberian margin and the Mazarron escarpment using the multichannel seismic profile TM26 (Figure 8.1, 8.2 and 8.4 a). Additionally, we also compare the Vp model converted to two-way travel time from wide-angle seismic profile P03 with the coincident MCS-TM26 to contrast the tectonic structure with the velocity model (Figure 8.4b). Further to the northeast, we study the tectonic structure of the continental shelf and slope south of the Eivissa margin (Figure 8.1, 8.2 and 8.5 a) using records of the ocean bottom seismometers of profile WAS-P04 obtained applying the mirror imaging technique to the multiple of the primary wavefield (Grion *et al*., 2007; Dash *et al*., 2009; Wang *et al*., 2012). Finally, the reprocessed multichannel seismic profile ESCI-Valencia is used to study the tectonic structure of the continental shelf and slope south of the Mallorca Island and Emile Baudot escarpment (Figures 8.1, 8.2 and 8.5 b).

8.4.1 Continental shelf

The MCS-TM26 profile shows the Alicante continental shelf from km 166 up to km 125 (Figure 8.4). The main feature is the presence of the Seco the Palos basement high at CMP ~6000 interpreted as volcanic in nature (Comas *et al*., 2000; Acosta *et al*., 2013) and the absence of clear faults and related tilted blocks, with the exception of one minor fault bounding a small basin between CMP 3000-3500. This small basin is filled by different channel systems (Figure 8.4a), that could be related to the abrupt sea-fall that took place during the Messinian (Hsü *et al*., 1977; Duggen *et al*., 2003; Garcia-Castellanos *et al*., 2009; Cameselle and Urgeles, 2016). The drastic sea-level fall caused that subaerial areas were affected by erosion and continental drainage systems. An overlying strong and continuous reflector identified at 1 s TWTT displays substantial lateral continuity interpreted as the result of the reflooding that took place at the end of the Messinian. The top of the basement is a non-clear reflection at the base of the well stratified reflectors at the easternmost sector of the Internal Betic Zone (Paleozoic-Mesozoic in age) (Alfaro *et al*., 2002; Acosta *et al*., 2013; Maillard and Mauffret, 2013). The position of the basement top is supported by the WAS-P03 profile in which we can see how the isovelocity contour of 4 km/s (interpreted as the basement top velocity) fits well with the base of the stratified reflectors (Figure 8.4b). Clear Moho reflections can be seen at depths of 6.5-7s TWTT fitting well with the modelled Moho obtained through the tomography inversion of the wide-angle profile P03 (Figure 8.4).

Although the mirror image of the migrated P04 profile is not as good as profile TM26, partially due to the large spacing between OBS stations, it allows identifying the main tectonic features. The continental shelf south of Eivissa is relatively flat, gently deepening southeast from profile km 92 to 140 (Figure 8.5a). Unlike the TM26 profile, this profile does not contain neither basement highs nor faults and associated tilted block structure. Moho reflections are identified at depths of 6.5 s TWTT, with a total basement thickness around ~6 s TWTT or ~18 km (Figure 8.5a). Further northwest, the ESCI-Valencia profile images the southern Mallorca continental shelf from profile km 117 to 140 (Figure 8.5b). It presents a series of features similar to the other profiles, with a flat continental platform without normal faults and tilted structures. It also shows a basin of 1 s TWTT thick, whose base is interpreted as Mesozoic basement (Figure 8.5b). This interpretation is assumed from onshore studies in the Balearic Promontory (Rodríguez-Perea *et al*., 1987; Sàbat *et al*., 2011). At 1.5 s TWTT a strong and continuous reflection is interpreted as the top of the Messinian unit formed during the salinity crisis. Moho reflections are visible between 7-8 s TWTT yielding a total basement thickness of around ~5.5-6 s TWTT or ~18 km thick.

8.4.2 Continental slope

The Continental slope in the southeastern Iberian margin extends from profile km 125 to km 105 and is characterized by the presence of the steep Mazarron escarpment (Figure 8.1). The Mazarron escarpment is a ~145 km long E-W scarp with a maximum relief of 2300 m that gradually decreases towards both ends. The slope of the scarp ranges from 14-31º and is cut by many canyons and gullies (Acosta *et al*., 2013; Driussi *et al*., 2015). The presence of these hundred meters deep canyons masks possible fault and tilted structures in the continental slope. At the foot of the escarpment there is a sedimentary wedge with layer fanning reaching 2.5 s TWTT of thickness, while at the top of Seco de Palos basement high the sedimentary cover is only ~0.2 s TWTT thick (Figure 8.4). Although Moho reflections are masked by poorly attenuated high amplitude multiple reflections and thus not observed under the slope (Figure 8.4a), they are imaged by the tomographic velocity model at ~7-8 s TWTT (Figure 8.4b). Crustal thickness in the continental slope ranges from 6 s TWTT (~18 km) to 3.5 s TWTT at the foot of the slope (~11 km).

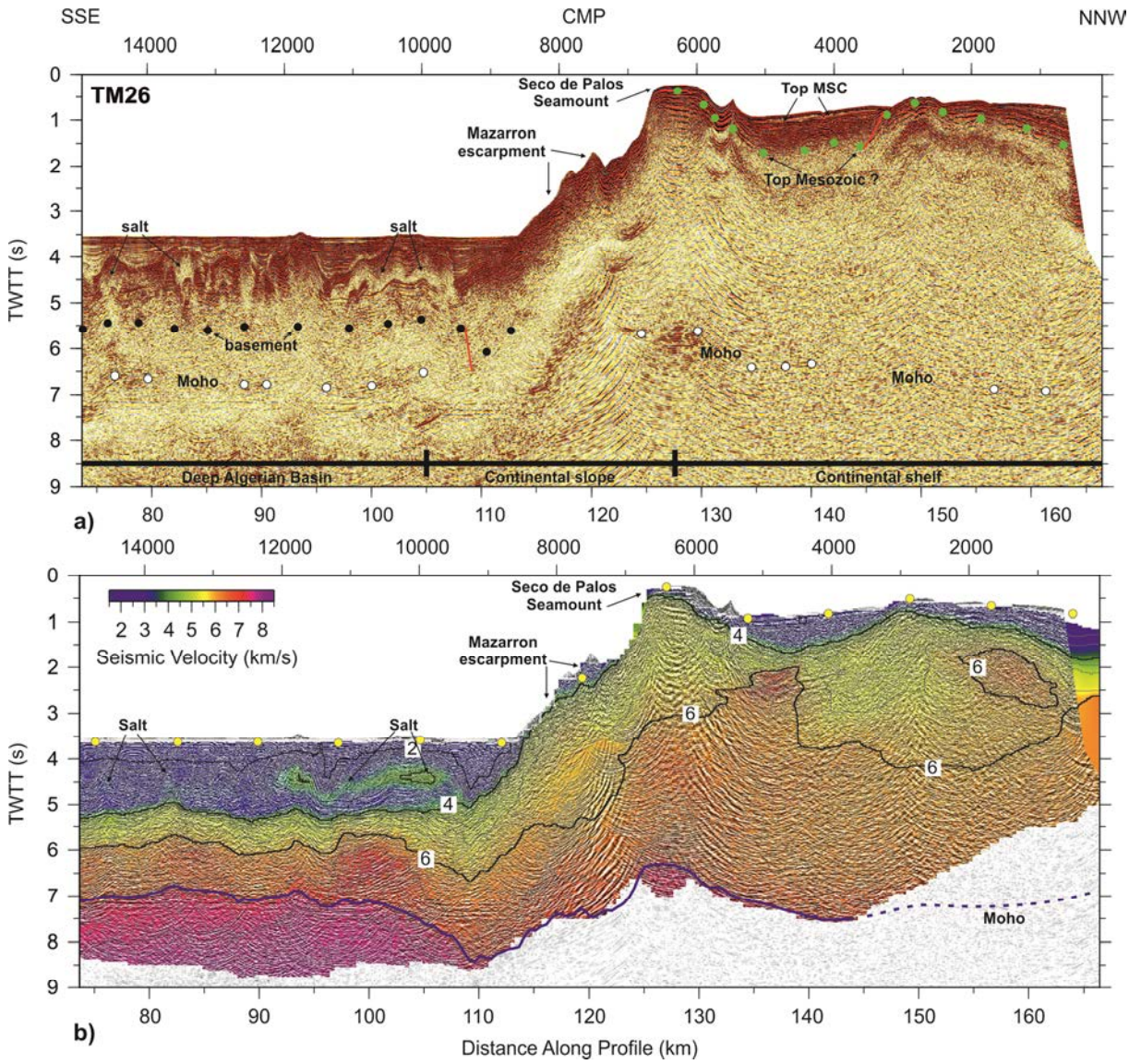

Figure 8.4: *a) Post-stack time migration of the profile TM26. This profile is divided in three sections from west to east: Continental shelf, continental slope and deep Algerian Basin (see text for details). White dots display the location of reflections interpreted as the crustal-mantle boundary (Moho). Black dots display the base of the well stratified sediments interpreted as the basement in deep Algerian Basin. Green dots also display the base of the well stratified reflectors in the continental shelf interpreted as Mesozoic basement in this region. b) Post-stack time migration profile TM26 overlaid with the TWTT converted version of the P-wave seismic velocity model of line P03 (Figure 8.3). Yellow dots display the location of OBS stations along the profile. Dashed blue line corresponds to the continuation of Moho reflection in accordance with the MCS TM26 interpretation (a).*

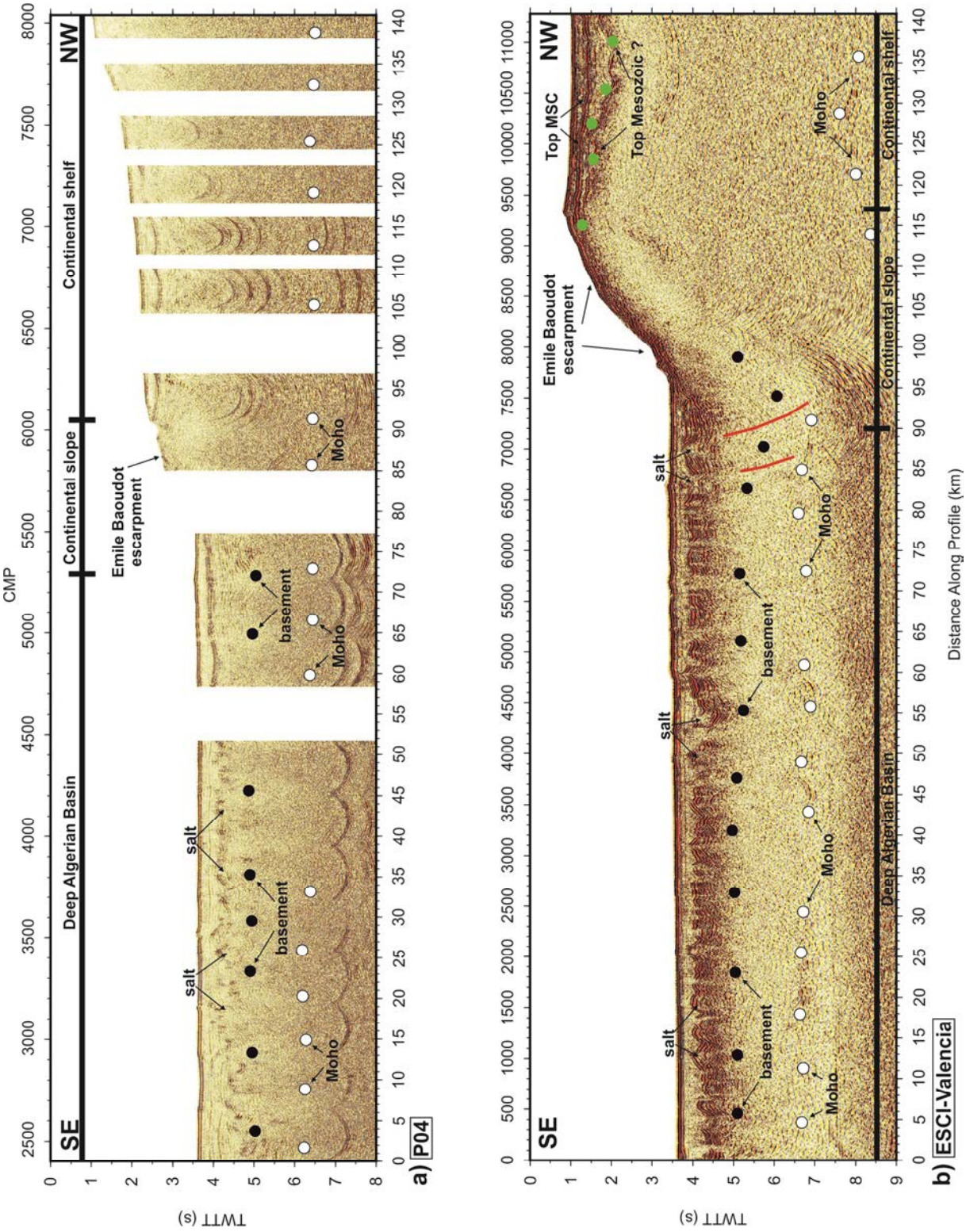

Figure 8.5: *a) Post-stack time migration of profile P04. This profile is obtained by mirror imaging the WAS-P04 profile acquired during the WESTMED survey (Figure 8.1). b) Post-stack time migration of profile ESCI-Valencia. These profiles are divided in three sections from west to east: Continental shelf, continental slope and deep Algerian Basin (see the text for more information). White dots display the location of reflections interpreted as the crustal-mantle boundary (Moho). Black dots display the base of the well stratified reflectors interpreted as the basement in deep Algerian Basin. Green dots also*

display the base of the well stratified reflectors in the continental shelf interpreted as Mesozoic basement in this region.

Further northeast, the continental slope south of the Eivissa margin is not clearly imaged in our data. Bathymetry and the MCS profile P04 show a gentler slope than the Mazarron escarpment (Figure 8.5a). Moho reflections are imaged at 6.5 s TWTT under the slope, defining a crustal thickness of around 3.5 s TWTT (~11 km). The continental slope of the southern Eivissa margin is the southwest end of the Emile Baoudot escarpment. The Emile Baudot escarpment is a 180 km long NW-SE scarp with a maximum relief ranging from 1600 to 1400 m and a steep slope that ranges between 3º to 12º. As the Mazarron escarpment, the Emile Baudot escarpment is incised by a complex canyon system and no recent faults have been clearly identified (Acosta *et al*., 2001, 2004; Camerlenghi *et al*., 2009; Driussi *et al*., 2015). South of Mallorca margin, the Emile Baudot scarp is imaged in profile ESCI-Valencia (Figure 8.4b), although as in profile TM26, no Moho reflections are imaged below the continental scarp.

8.4.3 Deep basin

Deep Algerian Basin south of the Betic-Balearic margin is characterized by the presence of a 2-2.5 s TWTT sedimentary cover which can be divided in two main units. 1) Plio-Quaternary sediments showing lateral variations in thickness ranging between 0.5 to 1.5 s TWTT (Figures 8.4 and 8.5) and 2) Miocene sediments characterized by the presence of salt layers with a variable thickness ranging from 0.5 to 1 s TWTT deposited during the Messinian salinity crisis between 7.2-5.3 Ma (Hsü *et al*., 1977) and characterized by high internal reflectivity. These salt layers produce a pronounced velocity inversion clearly seen in tomographic velocity models (Figures 8.3 and 8.4). Due to their plastic behaviour they produce diapiric structures that can be clearly seen along the three profiles (Figures 8.4 and 8.5). The top of the basement is interpreted as the base of the well stratified reflectors at 5-5.5 s TWTT, and can be locally identified as a reflection that roughly coincides with the isovelocity contour of 4 km/s in the tomographic velocity model (Figure 8.4b). Moho reflections are identified as segmented high amplitude reflections situated in all three profiles at 6.5 s TWTT. However, the Moho location obtained by velocity modelling and converted to TWTT is slightly deeper, located at 7-7.5s TWTT (Figure 8.4b). This observation may be explained due to the seismic anisotropy caused by the different propagation wave velocity of the wide-angle seismic data and multichannel seismic data (Sallarès *et al*., 2013). Basement thickness is fairly constant along the basin about 1.5 s TWTT or ~6 km.

8.5 Discussion

8.5.1 Nature of the crust

In order to discuss the nature of the crust in the south Betic-Balearic domain, we compared 1-D velocity/depth profiles sampled every 2 km through the tomographic velocity model of P03 and velocity compilations of extended continental crust (Christiansen and Mooney, 1995) and of Atlantic oceanic crust (White *et al.*, 1992). The tomographic velocity model displays three different domains; Continental domain, continent-ocean transition and oceanic domain (Figure 8.6).

Continental domain

This domain extends under the continental shelf of the southeastern Iberian margin (Figure 8.6a). As described previously in section 8.4.1, there is no evidence of important faulting or tilted blocks in the continental shelf that explains the basin formation. The 1-D velocity profiles of this domain present a vertical velocity structure that fits well with the compilation of extended continental crust velocities (Christiansen and Mooney, 1995). Lower crust velocities range between 6 to 6.5 km/s while upper crust velocities present lateral variations (Figure 8.6b). The Tomographic velocity model displays two high velocity anomalies with an upper crust velocity between 6.5-6.8 km/s between 136-140 km and 152-180 km (Figure 8.6a). 1-D velocity profiles show how these anomalies represent higher upper crust velocities (reaching ~7 km/s) than typical continental crust. The presence of this anomalous velocity structure with abrupt lateral variations in the upper crust together with the absence of extensional structures led to interpret this first domain as a continental domain with possible magmatic intrusions that mask extensional structures related to basin opening in this region.

The Aromagnetic map (Figure 8.2) shows dipolar magnetic anomalies located southeast of the Iberian margin and along the south Balearic margin that support the idea that the high velocity anomalies beneath the continental shelf of southern Iberia have a magmatic nature (Figures 8.3, 8.4 and 8.6). This is also supported by different studies that described the presence of different seamounts, volcanic in nature, located in the southeastern Iberian margin and the Balearic Promontory (Acosta *et al.*, 2004, 2013; Vázques, J.T. *et al.*, 2015).

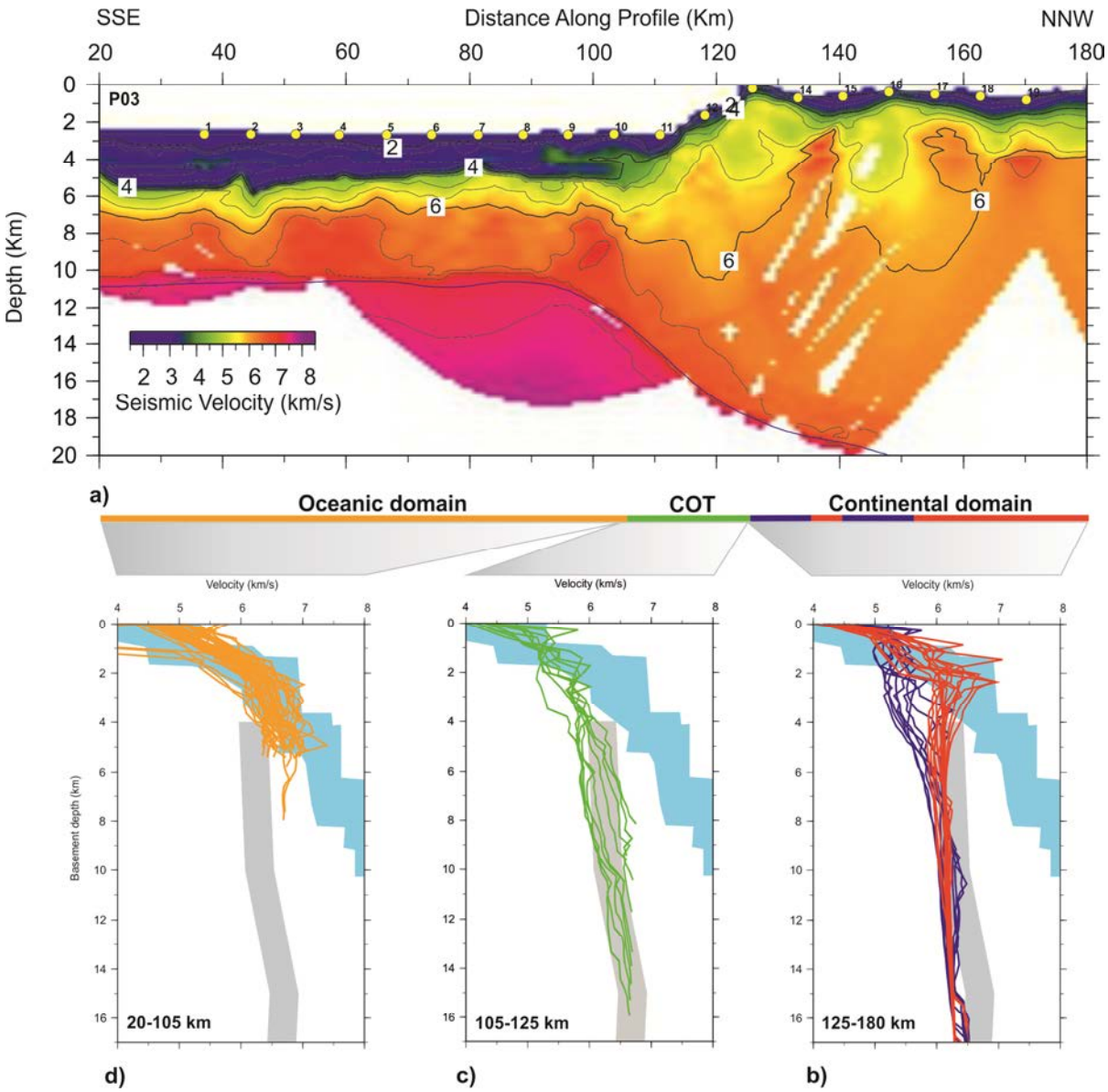

Figure 8.6: *a) Final P-wave velocity model of the crust, uppermost mantle and the Moho (blue line) geometry along the wide-angle seismic profile P03 extending from the southeastern Iberian margin to the deep Algerian Basin (Figure 8.3). This profile is divided into 3 domains: Continental domain, continent-ocean transition domain, oceanic domain (see text for more information). b) 1-D velocity profiles extracted from the tomographic model (2 km laterally-averaged) of the continental domain from 125 to 180 km. 1D velocity-depth profiles of reference include a 20 km thick continental crust (gray band) (Christensen and Mooney, 1995) and 0-7 Ma Atlantic oceanic crust (light blue band) (White et al., 1992). These profiles are divided in two colours; the blue ones correspond to those profiles that present low upper crust velocities and the red ones, correspond to those profiles that present high upper crust velocities interpreted as magmatic intrusions (see text for more information). c) 1-D velocity profiles of the continent-ocean transition domain from 105 to 125 km (light green lines). These profiles present vertical velocities close to the continental ones but slightly higher than in the previous continental domain, especially lower crust velocities are higher than the previous and*

slightly higher than the continental compilation (gray band). d) 1-D velocity profiles of the oceanic domain from 20 to 105 km (orange lines). These profiles present vertical velocities close to the ocean-Atlantic type (light blue band) and show a crustal thickness around ~6 km (see text for more information).

Continent-ocean transition domain

A second domain located southeast of domain 1 is characterized by an abrupt thinning of the crust from under the continental shelf edge towards the deep Algerian Basin (Figure 8.6a). The transition between the continental and oceanic crust is a ~20 km wide zone where velocities are neither clearly continental nor oceanic (Figure 8.6c). This continent-ocean transition is narrower than most of the other Western Mediterranean margins: ~100 km in the Gulf of Lions (Gailler *et al*., 2009), 35-40 km along the northern Ligurian margin (Rollet *et al*., 2002) 40 km along the western Sardinia margin (Gailler *et al*., 2009) and 100 km in the Tyrrhenian Basin (Prada *et al*., 2015). 1-D velocity profiles show intermediate velocities to be faster than typical continental crust, but slightly slower than typical oceanic crust (Figure 8.6c). The nature of the continent-ocean transition is a matter of debate due to the lack of geophysical data in this region. The presence of high velocities in the lower crust is against the hypothesis of pre-existing crustal extension, because fracturation and fluid alteration during crustal stretching would be expected to decrease lower crustal velocities.

The tectonic structure of the continental slope shows little fault structures despite the prominent thinning of the basement towards the deep basin. Crustal thickness under the continental shelf edge is 18 km, thinning to 6 km at the foot of the slope implying a stretching factor of β=3 in 20 km. The abrupt crustal thinning and narrow steep slope may be indicative of a strike-slip deformation (Leprêtre *et al*., 2013; Badji *et al*., 2015; Driussi *et al*., 2015). However, no sediment infill or kinematic indicator has been observed in the data indicating transtensional or transpressional movements. Another possibility is that the SE Iberian and Balearic margin are part of a high asymmetric conjugate margin system. This hypothesis, however, cannot be easily tested because the conjugate margin of Algeria has a thick salt infill that prevents a detailed imaging of the deep structure, and the margin is currently being tectonically deformed under compressional stresses. Nevertheless, velocity models obtained from wide-angle seismic data in the Algerian margin indicate that the continental crust structure is fairly similar to the SE Iberian and Balearic margin (Leprêtre *et al*., 2013; Maillard and Mauffret, 2013; Medaouri *et al*., 2014; Badji *et al*., 2015).

Oceanic domain

A third domain occurs in the deep Algerian Basin. The nature of this crust appears not related to extension of continental crust for several reasons: First, the fairly constant thickness of the crust along distance appears to support that this crust has no origin in a pre-existing continental crust extension. Second, there is no evidence of faulted structures indicative of important extension (Figures 8.4 and 8.5). Third, 1-D velocity profiles displays a two-layer velocity structure resembling the velocity structure from oceanic crust (Figure 8.6d). Wide-angle seismic data crossing the south Iberian margin towards the Algerian Basin show deep basin velocities ranging from ~6 to 7 km/s (Figure 8.6a). 1-D velocity profiles match well with the compilations of Atlantic oceanic crust (White *et al*., 1992) with a typical layer 2 and 3. Figure 8.6d displays a layer 2 with a rapid increase in velocities from 4.5 to 6.5 km/s in the uppermost 2.5-3 km of the basement and a gentler gradient in layer 3, with velocities ranging from 6.5 to 7 km/s, locally reaching 7.4 km/s. Although layer 2 and layer 3 appear characteristic of oceanic crust, the lower crust displays somewhat low velocities in the lowermost 2 km of the crust where oceanic crust typical velocities are above 7 km/s. It is interpreted that the oceanic crust was formed by back-arc magmatic processes which may not be similar to mid-ocean spreading centres. Similar velocity models and lower crust velocities have been described in back-arc magmatic crust of the Tyrrhenian Basin (Prada *et al*., 2014; 2015).

8.5.2 Implications for kinematic models

The morphology and crustal structure of the south Iberian and south Balearic margin exhibit an abrupt transition between continental and oceanic domain. A similar kind of sharp transition between domains has been described in several transform margins such as the Côte d'Ivoire-Ghana margin (Sage *et al*., 1997; Basile *et al*., 1993, 1998, 2013), French Guiana margin (Greenroyd *et al*., 2007, 2008) or the Grand Bank margin (Keen *et al*., 1990). Moreover the morphology of the Mazarron and the Emile Baudot escarpments could be interpreted as transform margins formed by strike-slip motion as it was speculated in previous works (Lonergan and White, 1997, Acosta *et al*., 2001, 2013; Mauffret *et al*., 2004). Although the morphology of these two scarps is abrupt, the presence of Miocene volcanic edifices along the south Betic-Balearic margin complicates crustal structure as indicated in the complex Vp model and makes difficult to describe the tectonic structure in more detail (Acosta *et al*., 2002).

Although kinematic reconstructions of the region are highly disputed, the most likely conjugate margin to the south Betic-Balearic is the north Tipaza-Algiers margin (Leprêtre *et al*., 2013). This margin is characterized by an oceanic type basement 5-6 km thick in the deep north Algerian Basin and a narrow or even absent transition between continent and oceanic crust (10 km) with a steep margin slope interpreted as a transform margin (Leprêtre *et al*., 2013). The most recent tomographic and seismic studies of the mantle support an E-W opening of the Algerian Basin and a lithosphere tearing along the Algerian margin as a result of a westwards rollback of the Alboran block (Chertova *et al*., 2013; van Hinsbergen *et al*., 2014). This E-W opening of the Algerian Basin is conducted through STEP (Subduction-Transform Edge Propagator) faults proposed by different authors (Govers *et al*., 2005; Chertova *et al*., 2014; van Hisnbergen *et al*., 2014; Badji *et al*., 2015). This geodynamic progression has been interpreted to produce a magnetic expression as E-W trending anomalies located north of Algerian margin (Figure 8.2). Moreover, recent studies by Fichtner *et al*. (2015) have revealed the presence of a segmented slab beneath the Algerian margin. In contrast, along the south Betic-Balearic margin this kind of magnetic pattern is not observed.

Data presented here do not provide enough information to re-define the kinematics of the opening of the Algero-Balearic Basin. However, the observations point to a multiphase evolution of the south Betic-Balearic and Algerian margin including: 1) a NW-SE opening of the Algero-Balearic Basin due to the roll-back of the subduction slab. This would led to a transtensional movement along the south Betic-Balearic margin with a component of a right lateral strike-slip motion and a left-lateral strike slip motion north of the Algerian Basin. 2) the collision of the Kabylies block to the north Africa margin and 3) a segmentation and possible slab detachment in the western Algerian margin due to the rotation of the Alboran block and the retreat of the Gilbraltar arc. All these processes agree to the Vp model of the crustal structure and tectonic structure observed in our seismic data along the South-Balearic margin.

Part IV:

Discussion

Chapter 9: Implications of this thesis in the geodynamic evolution of the Western Mediterranean basins

The main purpose of this thesis work is to define the tectonic structure, the nature of the basement, and to estimate the age and geodynamic setting during the formation of the three main Western Mediterranean basins: Valencia Trough Basin, Gulf of Lions and Algero-Balearic Basin. The results derived from this study allow us to discuss the timing and the main tectonic processes that led to the current configuration of these basins.

Different reconstructions of the tectonic evolution of the Western Mediterranean basins have been published during the last three decades (Rehault *et al*., 1984; Dewey *et al*., 1989; Lonergan and White, 1997; Gueguen *et al*., 1998; Frizon de Lamotte *et al*., 2000; Jolivet and Faccenna, 2000; Gelabert *et al*., 2002; Rosenbaum *et al*., 2002; Spakman and Wortel, 2004; Jolivet *et al*., 2009; Gutscher *et al*., 2012; Vergés *et al*., 2012; Chertova *et al*., 2014; Faccenna *et al*., 2014; van Hinsbergen *et al*., 2014), some of which were briefly reviewed in the introductory chapter. All these kinematic and geodynamic models differ in a number details as they are mainly based on land data and mantle tomography models that can be integrated into different interpretations. Notwithstanding this, they all share the concept that slab rollback is the main process that triggered the opening of the Western Mediterranean basins.

Here, we divided the geodynamic models in two kind of models: 1) Continuous slab models (Figure 9.1) and 2) Segmented slab models (Figure 9.2). The first ones consider the subduction rollback of a unique and continuous slab from the north Apennines to the Betic-Rif region (Rehault *et al*., 1984**;** Faccenna *et al*., 2004; Schettino and Turco, 2006; Jolivet *et al*., 2009; Carminati *et al*., 2012; Faccenna *et al*., 2014). The second ones consider the subduction rollback of a segmented slab that evolves in a different way depending on the regional stresses acting on each time (Wortel and Spakman, 2000; Spakman and Wortel, 2004; Vergés *et al*., 2012; Chertova *et al*., 2014; van Hinsbergen *et al*., 2014). Although the differences between these evolutionary models are evident, both models consider that the opening of the Western Mediterranean basins starts in the NE of the Liguro-Provençal Basin at Oligocene times followed by the opening of the Valencia Trough Basin, the Algero-Baleric Basin and finally the Alboran and Tyrrhenian Basin.

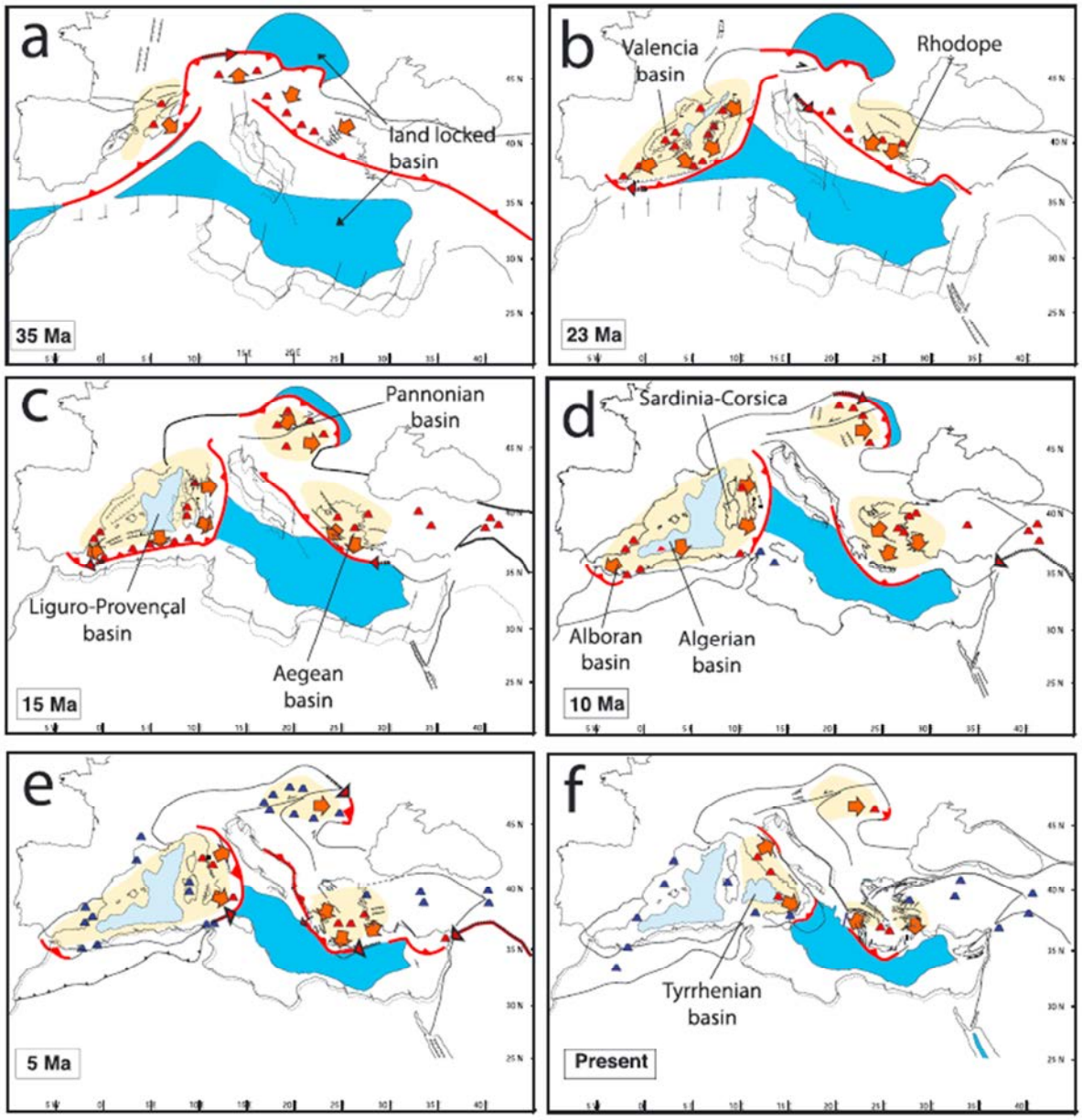

Figure 9.1 *Reconstruction of the Mediterranean region since 35 Ma until present. Note that this geodynamic model considers the opening of the Western Mediterranean basins as a subduction rollback of a continuous slab from the Apennines to the Betic-Rif region. Red lines indicate active subduction in each time. Red and blue volcanoes indicate calcalkaline and anorogenic volcanism respectively. Yellow regions correspond to extended areas and red arrows mark the stretching direction (Faccenna et al., 2014).*

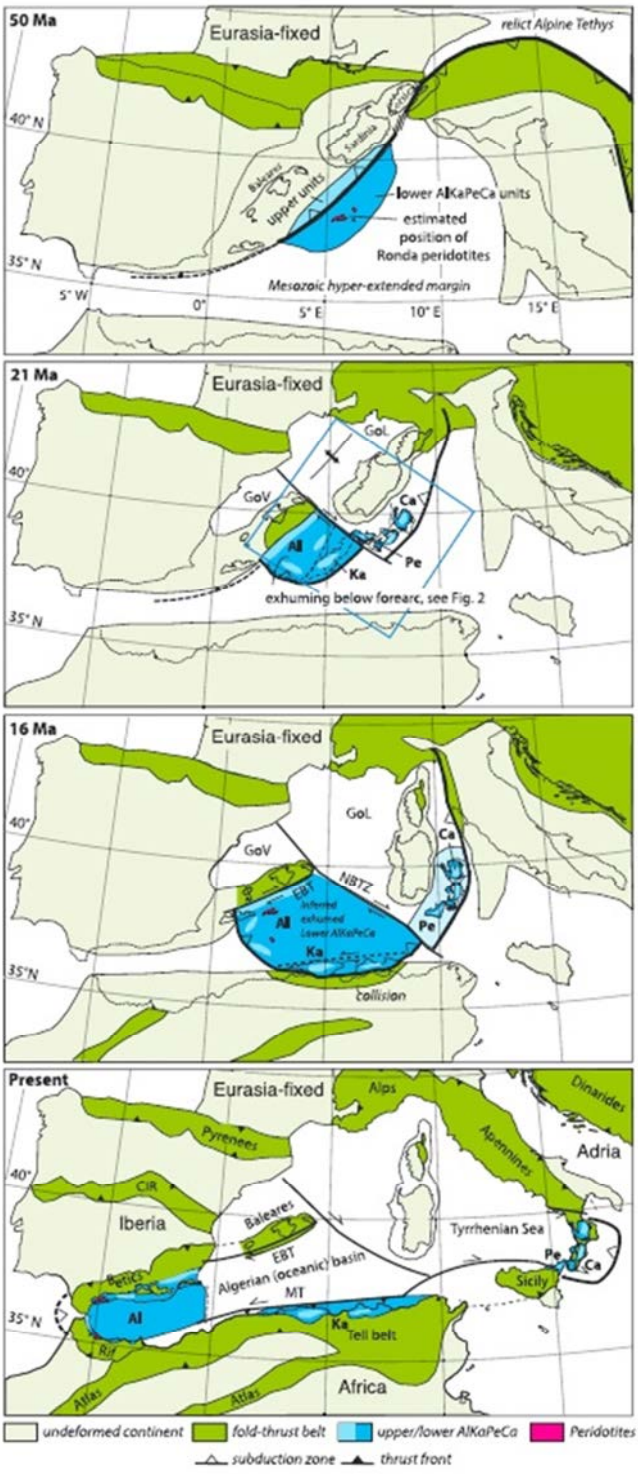

Figure 9.2 *Reconstruction of the Western Mediterranean region since 50 Ma until present. Note that this geodynamic model considers the opening of the Western Mediterranean basins as a consequence of a differential evolution of a segmented slab. Al = Alboran; Ca = Calabria; CIR = Central Iberian Ranges; EBD = Emile Baudot Transform; GoL = Gulf of Lions; GoV = Gulf of Valencia; Ka = Kabylides; NAT = North African Transform; NBTZ = North Balearic Transform Zone; Pe = Peloritani Mountains (van Hinsbergen et al., 2014).*

From our study we conclude that the Valencia Trough Basin constitutes the oldest Western Mediterranean basin. It is floored by continental crust, which was amalgamated during the Variscan orogeny. The region was extended mainly during a Mesozoic rifting phase characterized by a strong lithospheric thinning that produced the maximum crustal thinning in the region (4.5 km thick) preceding the middle Jurassic opening of the oceanic Atlantic-Tethys Basin and the mid-Cretaceous opening of the Bay of Biscay-Pyrenean Basin. The Mesozoic rift basins in the area of VTB were inverted and uplifted during the Paleogene time inducing the development of a major unconformity. During Miocene time, the Variscan basement and the Mesozoic sedimentary cover underwent a minor extensional phase that did not modify fundamentally the basement structure of the Valencia Trough Basin. We do not observe important extensional structures in our data that could explain the opening of the Valencia Trough Basin in the Neogene times. There exist some minor faults in our profiles, but they have not enough displacement with associated syn-rift sediment that may have formed the current basin configuration. This observations and the lack of apparent thickening of the crust related to the Paleogene compressional event support that the Valencia Trough Basin was largely formed during a Mesozoic phase. We interpret that the Valencia Trough Basin crustal configuration is not Neogene in age, thus not formed by the SW prolongation of the NE-SW opening of the Gulf of Lions. We interpret that the Neogene extensional event that occurred in the Valencia Trough Basin, especially in the formation of different horsts and grabens in the Catalan-Valencia domain, are structures causing minor crustal thinning. Most of the volcanic expressions through the trough are Tertiary in age, but their exact age remains un-clear because they have not been calibrated with the seismic images. Thus, we support that the first and more important extensional event that produced the main crustal extension in the basement of the trough occurred during the Mesozoic as supported by the interpretation presented in our seismic data in Chapter 6 (Figures 6.2, 6.4 and 6.5).

This is a major point of difference with basically all Western Mediterranean reconstructions that consider that most of the >50 km opening of the Valencia Trough Basin and crustal thinning occurred as rifting prolonged from NE to SW during the opening of the Gulf of Lions (Rehault *et al*., 1984; Dewey *et al*., 1989; Lonergan and White, 1997; Gueguen *et al*., 1998; Frizon de Lamotte *et al*., 2000; Jolivet and Faccenna, 2000; Gelabert *et al*., 2002; Rosenbaum *et al*., 2002; Spakman and Wortel, 2004; Jolivet *et al*., 2009; Gutscher *et al*., 2012; Vergés *et al*., 2012; Chertova *et al*., 2014; Faccenna *et al*., 2014; van Hinsbergen *et al*., 2014) .

Our interpretation agrees with an eastward rifting of the Gulf of Lions related to roll-back of the west-directed Apenninic subduction zone (see Chapter 7 and Figures 9.1 and 9.2 from this chapter) (Cohen, C.R., 1980; Le Douran *et al*., 1984; Rehault *et al*., 1984; Gueguen *et*

al., 1998; Jolivet *et al*., 2000, 2006, 2015; Granados *et al*., 2016). Extension driven by the retreat of the subduction slab causing the eastward rotation of the Corsica-Sardinia block produced a magma-poor Gulf of Lions margin and the formation of a ~100 km wide thin anomalous transitional basement unit that we interpret as serpentinized exhumed mantle bounded at its base by a clear reflection that might represent a serpentinization front. Continental breakup occurred at Early Miocene times decentred toward the Corsica-Sardinia margin. (Rollet *et al*., 2002).

Figure 7.14 (see Chapter7), shows a NW-SE trend of magnetic anomalies located NE of the Balearic Promontory. This anomaly group has a trend and an associated tectonic structure that we infer that represents the region of strike-slip and/or oblique slip often referred in literature as The North-Balearic and the Catalan strike slip fault zones (Figure 7.14, Chapter 7). The area between both structures has been previously described as a transfer zone between Gulf of Lions and Valencia Trough Basin with two pulses of activity separated by a middle Miocene tectonic quiescence (Maillard and Mauffret, 1999; Mauffret *et al*., 2001). Kinematically, this fault system has a right-lateral movement related to the southeastward drift of the Corsica-Sardinia block. In the data presented in this work it is difficult to define the trace of any of these main faults because clear large-scale strike-slip typical structures have not been imaged either in the basement or the sediment. There are some structures that could be related to these faults, but the presence of thick syn-tectonic sediments lead us to think that probably the orientation of seismic profiles cut the main faults in the transfer domain in an oblique direction. Alternatively, the entire area could represent a zone of oblique rifting without well-defined strike slip major faults containing well-formed fault planes and major shear zones, but a region of more distributed oblique rifting deformation.

Alternative interpretations of the basement nature in the Gulf of Lions are proposed by other authors (e.g. Jolivet *et al*., 2015; Moulin *et al*., 2015; Granados *et al*., 2016). They interpret the transition zone between the thinned continental crust and the oceanic crust as an exhumed lower crust. For the lower crust exhumation to take place, the formation of large structures known as detachments is required. Figures 9.3 and 9.4 show two profiles from the Gulf of Lions oriented NW-SE and SW-NE respectively, Granados *et al*. (2016) interpret a 100 km of lower crust exhumation with a fairly constant thickness of 5 km (Figures 9.3 and 9.4). If this interpretation is correct, the top of basement in these profiles should act as the detachment continuation. The idea of a lower crust exhumation is based on the study done by Moulin *et al*. (2015) who remodeled the wide-angle seismic profile presented by Gailler *et al*. (2009) using forward modelling. They interpret this domain as a “thin exhumed lower continental crust overlying a heterogeneous, intruded lower layer”.

Our interpretation is based on a spatiotemporal evolution of the crust. This evolution is framed in a back-arc setting where a 30 km of continental crust is thinned through faulted and tilted blocks until it breaks up giving way to the exhumed mantle. This exhumed mantle is then serpentinized due to mantle hydration. This interpretation was presented by Gailler *et al*. (2009) who present several hypotheses to explain the presence of a high velocity zone in the transition zone between the continental and the oceanic crust. One of these hypotheses is that this high velocity zone could be related to an upper mantle material exhumed and serpentinized during the initial opening of the basin. Exhumed mantel is present in other Western Mediterranean basins (e.g. Tyrrhenian Basin). Prada *et al*. (2014) interpret the basement at Magnaghi and Vavilov Basins as exhumed mantle material. This interpretation is based on other regions with similar vertical velocity gradients as the Iberia Abyssal Plain where basement is made of serpentinized mantle material (Dean *et al*., 2000; Sallarès *et al*., 2013).

Another open discussion point is the opening of the Algero-Balearic Basin. In contrast to a N-S opening of the Algero-Balearic Basin (as shown in Figure 9.1), recent tomographic and seismic studies of the mantle support an E-W opening of the Algerian Basin (as in Figure 9.2), and a lithosphere tearing along the Algerian margin as a result of a westwards rollback of the Alboran block (Chertova *et al*., 2013; van Hinsbergen *et al*., 2014). This E-W opening of the Algerian Basin is conducted through STEP (Subduction-Transform Edge Propagator) faults proposed by different authors (Govers *et al*., 2005; Chertova *et al*., 2014; van Hisnbergen *et al*., 2014; Badji *et al*., 2015). This geodynamic progression has been interpreted to produce a magnetic expression as an E-W trending anomalies located north of Algerian margin (Figure 8.2, Chapter 8). Moreover, recent studies by Fichtner and Villaseñor. (2015) have revealed the presence of a segmented slab beneath the Algerian margin. Along the south Betic-Balearic margin, in contrast, this kind of magnetic pattern is not observed (Figure 8.2, Chapter 8).

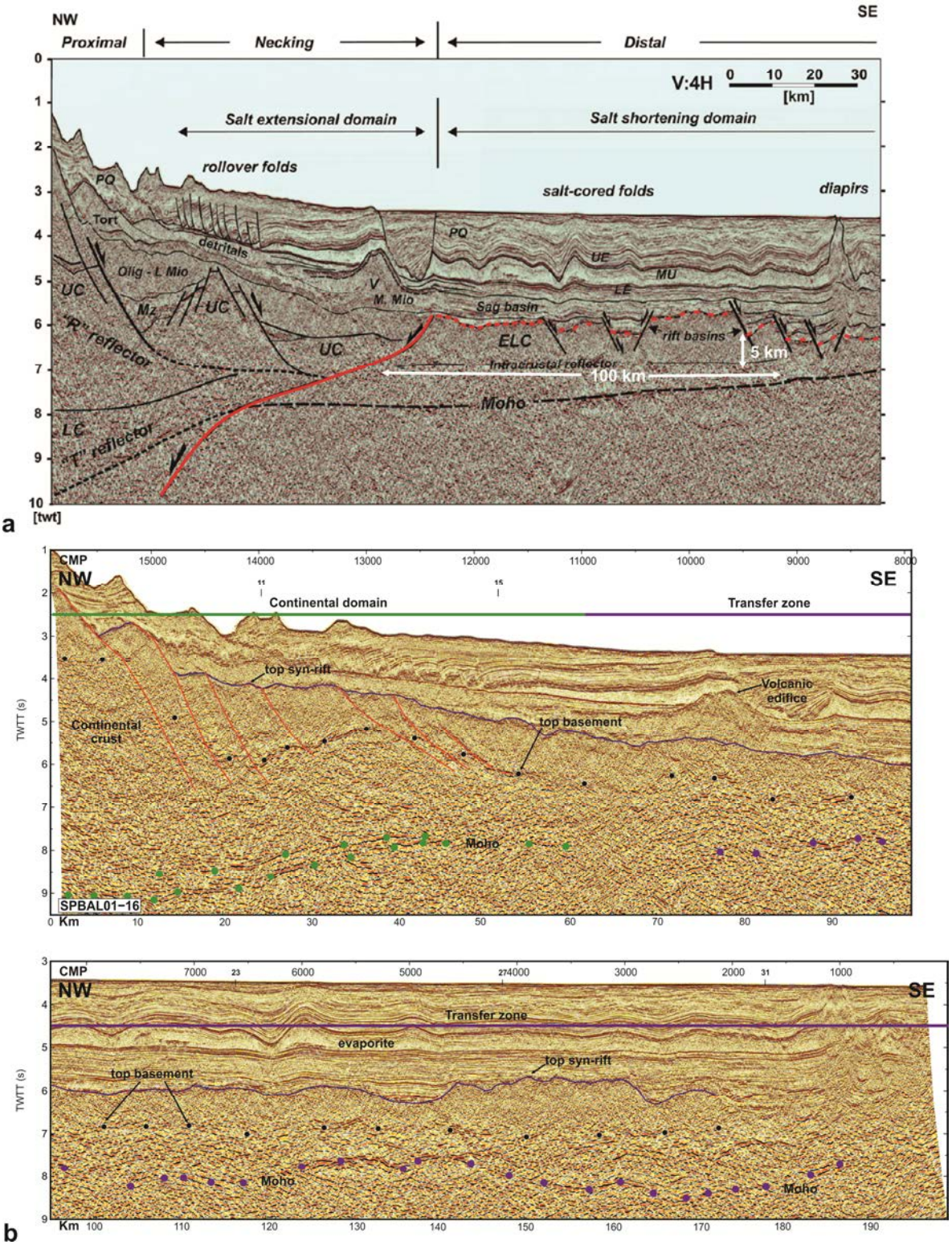

Figure 9.3 *a) Seismic section SPBAL01-16 modified from Granados et al. (2016). PQ, Pliocene–Quaternary; UE, Upper Evaporites; MU, Mobile Unit (megahalite body); LE, Lower Evaporites; Tort, Tortonian; M Mio, middle Miocene; Olig - L Mio, Oligocene–lower Miocene; Mz, Mesozoic basin. UC, upper crust; LC; lower crust. Red line marks the geometry of the detachment. b) Poststack time migration of line SPBAL01-16 interpreted for this thesis (see Chapter 7).*

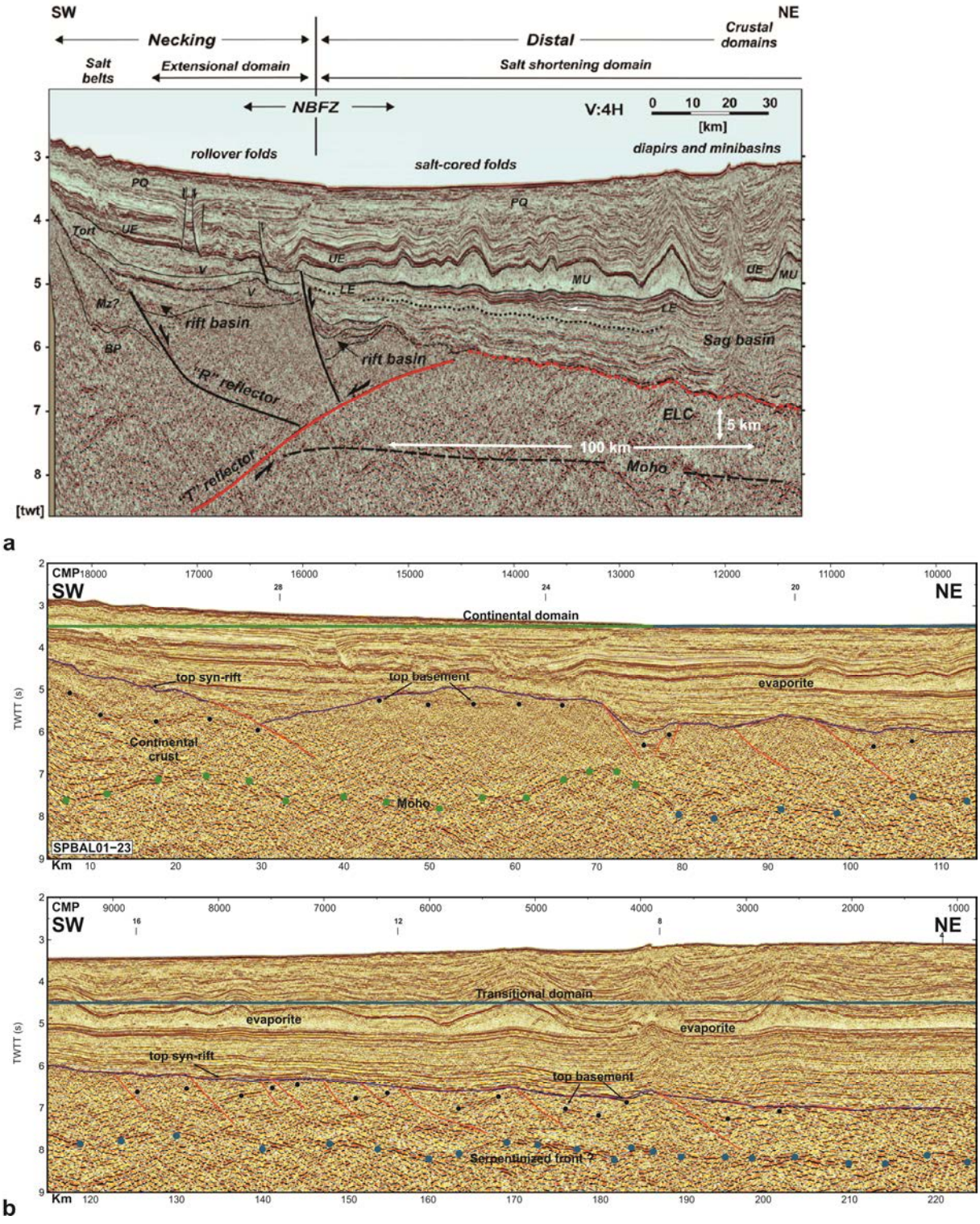

Figure 9.4 *a) Seismic section SPBAL01-23 modified from Granados et al. (2016). PQ, Pliocene–Quaternary; UE, Upper Evaporites; MU, Mobile Unit; LE, Lower Evaporites; Tort, Tortonian; Mz, Mesozoic basin; ELC, exhumed lower cruts; V, volcanics; NBFZ, North Balearic Fracture Zone; BP, Balearic Promontory. Red line marks the geometry of the detachment. b) Poststack time migration of line SPBAL01-23 interpreted for this thesis (see Chapter 7).*

Data presented in this thesis do not provide enough information to re-define the kinematics of the opening of the Algero-Balearic Basin. However, the observations point to a multiphase evolution of the south Betic-Balearic and Algerian margin including: 1) a NW-SE opening of the Algero-Balearic Basin due to the roll-back of the subduction slab. This would lead to a transtensional movement along the south Betic-Balearic margin with a component of a right lateral strike-slip motion and a left-lateral strike slip motion north of the Algerian Basin. 2) the collision of the Kabylies block to the north Africa margin and 3) a segmentation and possible slab detachment in the western Algerian margin due to the rotation of the Alboran block and the retreat of the Gilbraltar arc. All these processes agree with the Vp model of the crustal structure and tectonic structure observed in our seismic data along the South-Balearic margin (Figures 8.3, 8.4 and 8.5 in Chapter 8).

A new kinematic model for the whole opening history of the Western Mediterranean basins is beyond the scope of our work, and would require integration with other datasets from Tyrrhenian and Alboran Basins, and an extended study of the West Sardinia and Corsica margins. Moreover, to advance in the model, a more detailed reconstruction of submarine volcanic activity, imaged in the seismic data in all three basins but inadequately studied in the literature is required. Notwithstanding this, the findings of our work should be integrated in new reconstructions, while existing ones need to be reviewed.

Part V: Conclusions & Outlook

Chapter 10: Conclusions

The results obtained from the processing and analysis of the different datasets present in this work along with the integration of previous works of the Western Mediterranean basins has permitted discussion on the nature of the basement and the time and formation mechanisms of the main three Western Mediterranean basins. This section presents the main conclusions derived from the geophysical study done in the Valencia Trough Basin, Gulf of Lions Basin and Algero-Balearic Basin.

10.1 Valencia Trough Basin

- MCS data analysis reveals the Moho position throughout the Valencia Trough, located between 7.5-8.5 s TWTT.

- Basement thickness increase from the centre of the trough (10-11 km, ESCI-Valencia line) to both Iberian and Balearic margins (18 km), but decreases from the centre of the trough to the SW end of the basin where the thinnest basement of only 4.5 km is found.

- A crustal thickness map reveals rectangular-shape geometry for the Columbretes Basin.

- The Columbretes Basin is bounded by large-offset steep faults of Mesozoic age and filled by 7-8 km of Mesozoic sediments.

- Seismic sections show that the main tectonic structures that controlled the formation of the trough are Mesozoic. The reactivation of these tectonic structures during the Paleogene as contractive structures is minor, and some of them were reactivated during the Neogene extensional event.

- The Neogene extensional event in the Valencia Trough Basin was principally accommodated in the Catalan-Valencia margin where different NE-SW oriented horst and grabens were generated. However, no significant tectonic structures related to this extensional event are seen in our seismic interpretations. A few tectonic structures are identified causing minor displacement and horizontal extension.

- The Valencia Trough Basin is the oldest Western Mediterranean basin floored by continental crust and characterized by a major crustal thinning occurred during Mesozoic times.

10.2 Gulf of Lions and deep Provençal Basin

- Below the Gulf of Lions continental slope, tilted blocks bounded by large-offset normal faults are interpreted as continental crust.

- Crustal thinning occurs laterally abrupt under the slope of the Gulf of Lions margin where basement thickness decreases from 18 to 7.5 km in less than 50 km.

- This thinning of the continental crust is associated to intense faulting on the region and the formation of half grabens oriented NE-SW.

- After an abrupt thinning of the continental crust a change in basement configuration is identified in profiles SPBAL01-04, 08, 12, 23, 27 and 31. Top of the basement is characterized by a medium-high reflective horizon dissected by small-offset normal faults and is interpreted as the continent-ocean transition domain.

- This transition zone is imaged as a layer bounded at its bottom by a fairly constant reflector and with a fairly constant thickness of 3-4 km across a ~100 km wide zone where velocities are neither typically continental nor oceanic.

- We interpreted that the presence of this reflective horizon at the base of the layer may represent a serpentinization front. Velocities of 7.2-7.9 km/s for the 3-4 km thick thin layer agree well with those expected for partially serpentinized mantle rocks exhumed after continental break up before the formation of an oceanic spreading centre.

- Oceanic crust has been identified in the deeper part of the basin imaged by few profiles (e.g. SPBAL01-04, 08, 12 and 31). This is supported by available seismic velocity information. It is difficult to see any crustal structure due to the presence of salt domes. Oceanic crust is ~4-5 km thick, somewhat less than typical oceanic crust (6-7 km).
- We observe a NW-SE trend of magnetic anomalies that may represent a set of tectonic structures: In literature, the North-Balearic and the Catalan strike slip fault

zones are interpreted in this region. In the data presented in this work it is difficult to define the trace of any of these main fault zones, but the presence of thick syn-tectonic sediments lead us to think that probably the seismic profiles cut in an oblique direction the orientation of existing faults.

- The area between both faults could represent a zone of oblique rifting without well-defined strike slip major faults nor well-formed fault planes and major shear zones, but a region of more distributed oblique rifting deformation.

10.3 Algero-Balearic Basin

- Tomographic modelling of the wide-angle seismic profile P03 together with the coincident WAS profile TM26 located southeast of the Iberian margin define three main domains along the profile with different geological and geophysical characteristics.

- The Continental domain extends from profile km 180 to km 125 under the continental shelf of the southeastern Iberian margin. The tectonic structure is characterized by the presence of a basement high (Seco de Palos Seamount) interpreted as volcanic in nature and the absence of clear faults and related tilted blocks. The 1-D velocity profiles of this domain present a vertical velocity structure that fits well with the compilation of extended continental crust velocities (Christiansen and Mooney, 1995). Basement velocity structure in the continental shelf displays abrupt lateral changes in velocity with the presence of two subvertical 10-20 km wide high velocity zones (ranging from 6 to 6.8 km/s) interpreted as magmatic intrusions. Both MCS-TM26 and WAS-P03 profiles display clear Moho reflections at 6.5-7 s TWTT depth, shallowing from 20 km to 18 km towards the southeast.

- Continent-ocean transition domain extends from km 125 to km 105 along line TM26. The tectonic structure is characterized by the presence of the steep Mazarron escarpment. A sedimentary wedge with layer fanning reaching a thickness of 2.5 s TWTT is present at the foot of the escarpment. The 1-D velocity profiles of this domain display a narrow transition between continental and oceanic crust of 20 km where velocities are neither clearly continental nor oceanic. Although in MCS-TM26 profile Moho reflections are not observed, they can be imaged by the WAS-P03 profile located at 7-8 s TWTT. The crust thins from 18 km under the continental shelf to 6 km at the foot of the slope.

- An oceanic domain extends from profile km 105 under the deep basin. The tectonic structure is characterized by the presence of 2-2.5 s TWTT of sedimentary cover with important diapiric structures and the presence of Moho reflections located at 6.5 s TWTT (11 km). 1-D velocity profiles of this domain match well with the compilations of Atlantic oceanic crust velocities (White ***et al***., 1992), as they show a typical layer 2 with a rapid increase in velocities from 4.5 to 6.5 km/s in the uppermost 2.5-3 km of the basement and a gentler gradient in layer 3, with velocities ranging from 6.5 to 7 km/s, locally reaching 7.4 km/s.

- Interpretations of multichannel seismic profiles and tomographic velocity models of the south Iberian margin and south Balearic margin allow us to conclude that these margins present an abrupt transition between continental and oceanic domain with the presence of two steep Mazarron and Emile Baoudot escarpments. Although some authors interpreted the south Betic-Balearic margin as a transform margin formed by strike slip motion, the presence of volcanic edifices along the south Betic-Balearic margin obscures the details of the tectonic.

Chapter 11: Outlook

The results of this thesis provide new information concerning the basement structure and the age of formation of the Valencia Trough. Further, a detailed study of the MCS dataset present in the Gulf of Lion has led us to define three geophysical domains. The spatial distribution of these domains has allowed us to discuss the conceptual model that attempts to explain how the extension leads the formation of the Gulf of Lions. Finally, the tectonic structure of the Algero-Balearic Basin interpreted from the MCS data together with the integration of new WAS data in the region also allowed to define three different geophysical domains and discuss the age and style of the opening and formation of the central and western Algero-Balearic Basin. Still number of questions remains unresolved. In this section, we present a proposal for the acquisition of new seismic data and the location of several drilling sites in an attempt to resolve some of the open questions.

11.1 Geophysical transects

Figure 11.1 show the location of the seismic sections proposed in order to shed some light on the open questions arised in this study. We propose to acquire both refraction and reflection seismic data.

- **Val-1, Val-2**: Wide-angle seismic profiles located in the transition zone between the Valencia Trough and the Gulf of Lions (Figure 11.1). We propose an NE-SW orientation for these two profiles in order to perpendicularly cut the main structures. The acquisition of new wide-angle seismic data in this region should provide a velocity model to study the crustal structure and transition of the basement between the Valencia Trough and the Gulf of Lions.

- **Val-3**: This wide-angle seismic profile located SW of the Valencia Trough Basin, that includes land stations in the Iberian margin and the Eivissa island, will provide information about the basement structure of the area and together with the existing WAS profile P04 south of the Eivissa island provide an entire image of the Valencia Trough Basin and the Algero-Balearic Basin.

- **Gol-1, Gol-2**: These two wide-angle seismic profiles were already acquired on 2006 and modelled using travel time tomography by Gailler ***et al***. (2009) (Figure 11.1). Later on 2015 Moulin ***et al***. (2015) and Afilhado ***et al***.(2015) remodelled the data using forward modelling. We propose to remodel these two profiles using the joint

refraction and reflection travel time tomography. This new modelling should provide a better constrain of the velocity anomalies as well as the geometry of the Moho reflector.

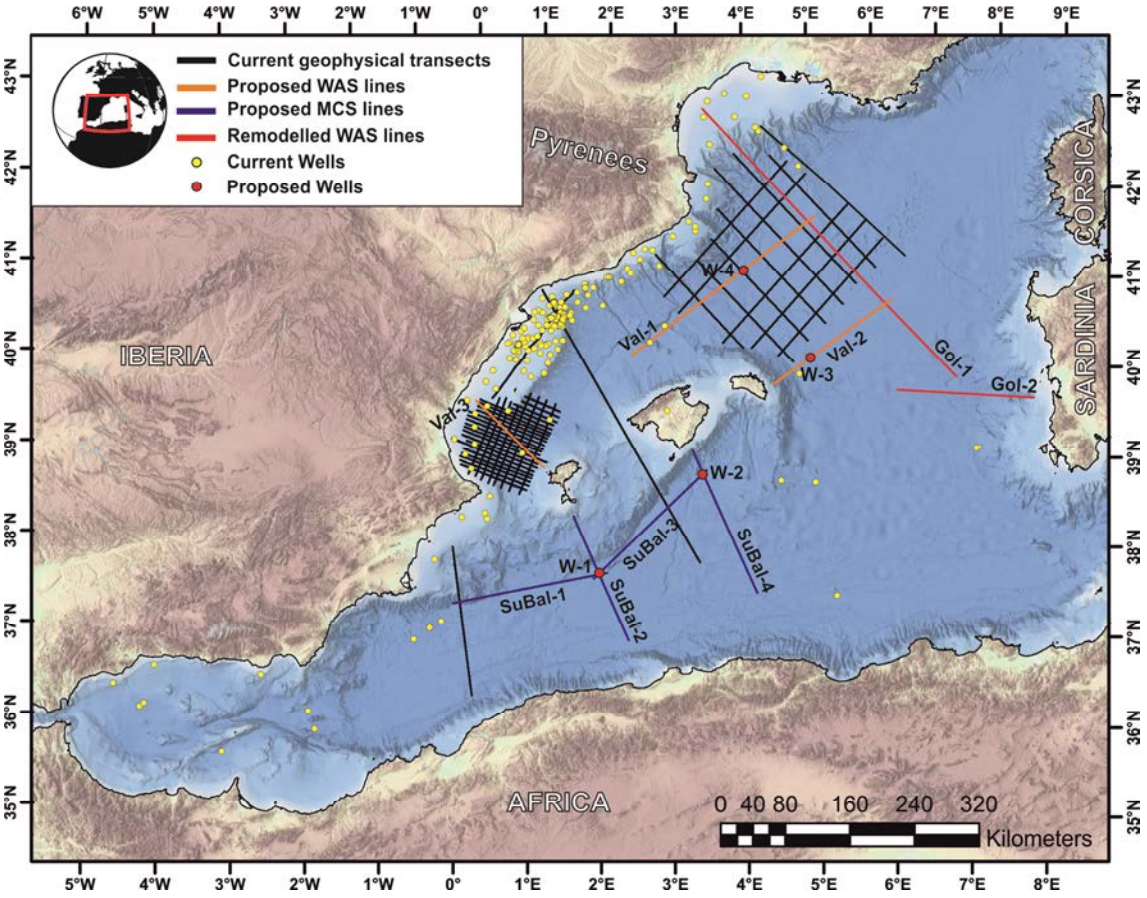

Figure 11 .1 ***Geophysical and drilling survey proposal.***

- **SuBal-2, SuBal-4**: We propose the acquisition of new multichannel seismic data orientated NW-SE coincident with the WESTMED wide-angle seismic profiles P04 and P05 respectively (Figure 11.1). The acquisition of this new data will allow to obtain an image of the tectonic structure along the south Balearic margin and the deep Algerian Basin and help constraining the velocity models of this region and define the opening of the Algero-Balearic Basin.

- **SusBal-1, SudBal-3**: We propose the acquisition of two MCS lines oriented E-W and NE-SW respectively to connect the SudBal-2 and SudBal-4 MCS lines. These two lines located in the south Betic-Balearic margin will allow us to define the tectonic structure of the margin and the transition to the deep Algerian Basin.

11.2 Drilling

Figure 11.1 shows the location of several DSDP-IODP project (International Ocean Drilling Program) and industry (Lanaja ***et al***., 1987) drilling sites in the Western Mediterranean area carried out during the last decades. We propose the location of some wells aiming to gather new information about the rifting processes.

- **W-1, W-2**: These two wells are located in the intersections between Sudbal-1/SudBal-2 and SudBal-3/SudBAl-4 respectively to study the age of the syn-rift sediments and in consequence to know the age of the opening of the Algero-Balearic Basin.

- **W-3, W-4**: These two wells are located on the WAS profiles Val-1 and Val-2 respectively in the transition area between the Valencia Trough and the Gulf of Lions. This area could represent an area of more oblique rifting deformation. These two wells would allow us to know the age of the syn-rift sediments and in consequence to constrain the timing of the opening of the Gulf of Lions and the role of this transition zone between basins.

Part VI:

References

References

Acosta, J., Muñoz, A., Herranz, P., Palomo, C., Ballesteros, M., Vaquero, M., Uchupi, E., 2001. Geodynamics of the Emile Baudot Escarpment and the Balearic Promontory, western Mediterranean. Mar. Pet. Geol. 18, 349–369. doi:10.1016/S0264-8172(01)00003-4

Acosta, J., Canals, M., López-Martínez, J., Muñoz, A., Herranz, P., Urgeles, R., Palomo, C., Casamor, J.L., 2002. The Balearic Promontory geomorphology (western Mediterranean): morphostructure and active processes. Geomorphology 49, 177–204.

Acosta, J., Ancochea, E., Canals, M., Huertas, M., Uchupi, E., 2004. Early Pleistocene volcanism in the Emile Baudot Seamount, Balearic Promontory (western Mediterranean Sea). Mar. Geol. 207, 247–257. doi:10.1016/j.margeo.2004.04.003

Acosta, J., Fontán, A., Muñoz, A., Muñoz-Martín, A., Rivera, J., Uchupi, E., 2013. The morpho-tectonic setting of the Southeast margin of Iberia and the adjacent oceanic Algero-Balearic Basin. Mar. Pet. Geol. 45, 17–41. doi:10.1016/j.marpetgeo.2013.04.005

Alfaro, P., Delgado, J., Estévez, A., Soria, J.M., Yébenes, A., 2002. Onshore and offshore compressional tectonics in the eastern Betic Cordillera (SE Spain). Mar. Geol. 186, 337–349. doi:10.1016/S0025-3227(02)00336-5

Afilhado, A., Moulin, M., Aslanian, D., Schnuerle, P., Klingelhoefer, F., Nouze, H., Rabineau, M., Leroux, E., Beslier, M.-O., 2015. Deep crustal structure across a young passive margin from wide-angle and reflection seismic data (The SARDINIA Experiment) - II. Sardinia's margin. Bull. LA Soc. Geol. Fr. 186, 331–351. DOI: 10.2113/gssgfbull.186.4-5.331

Allaby, M. (2008), Oxford Dictionary of Earth Science, Oxford University Press Inc., New York, pp. 654.

Alonso, B., Guillén, J., Canals, M., Serra, J., Acosta, J., Herranz, P., Sanz, J.L., Calafat, A., Catafau, E., 1988. Los sedimentos de la plataforma continental balear. Acta Geològica Hispànica 23, 185–196.

Auzende, Jean-Marie, Bonnin, Jean, Olivet, Jean-Louis, 1973. The origin of the western Mediterranean basin. Geol. Soc. London 129, 607–620. doi:10.1144/gsjgs.129.6.0607

Bache, F., Olivet, J.L., Gorini, C., Aslanian, D., Labails, C., Rabineau, M., 2010. Evolution of rifted continental margins: The case of the Gulf of Lions (Western Mediterranean Basin). Earth Planet. Sci. Lett. 292, 345–356. doi:10.1016/j.epsl.2010.02.001

Badji, R., Charvis, P., Bracene, R., Galve, A., Badsi, M., Ribodetti, A., Benaissa, Z., Klingelhoefer, F., Medaouri, M., Beslier, M.-O., 2015. Geophysical evidence for a transform margin offshore Western Algeria: a witness of a subduction-transform edge propagator? Geophys. J. Int. 200, 1027–1043. doi:10.1093/gji/ggu454

Bartrina, M.T., Cabrera, L., Jurado, M.J., Guimerà, J., Roca, E., 1992. Evolution of the central Catalan margin of the Valencia trough (western Mediterranean). Tectonophysics 203, 219–247. doi:10.1016/0040-1951(92)90225-U

Basile, C., Mascle, J., Popoff, M., Bouillin, J.P., Mascle, G., 1993. The Ivory Coast-Ghana transform margin : a marginal ridge structure deduced from seismic data. Tectonophysics 222.

Basile, C., Mascle, J., Benkhelil, J., Bouillin, J.-P., 1998. Geodynamic evolution of the Cote d'Ivoire-Ghana transform margin: an overview of Leg 159 results. Proc. Ocean Drill. Program, Sci. Results 159, 101–110.

Basile, C., Maillard, A., Patriat, M., Gaullier, V., Loncke, L., Roest, W., Mercier de Lépinay, M., Pattier, F., 2013. Structure and evolution of the demerara plateau, offshore french guiana: Rifting, tectonic inversion and post-rift tilting at transform-divergent margins intersection. Tectonophysics 591, 16–29. doi:10.1016/j.tecto.2012.01.010

Bayrakci, G., Minshull, T.A., Sawyer, D.S., Reston, T.J., Klaeschen, D., Papenberg, C., Ranero, C., Bull, J.M., Davy, R.G., Shillington, D.J., Perez-Gussinye, M., Morgan, J.K., 2016. Fault-controlled hydration of the upper mantle during continental rifting. Nat. Geosci. 9, 1–6. doi:10.1038/ngeo2671

Bezada, M.J., Humphreys, E.D., Toomey, D.R., Harnafi, M., Dávila, J.M., Gallart, J., 2013. Evidence for slab rollback in westernmost Mediterranean from improved upper mantle imaging. Earth Planet. Sci. Lett. 368, 51–60. doi:10.1016/j.epsl.2013.02.024

Blanco, M.J., Spakman, W., 1993. The P-wave velocity structure of the mantle below the Iberian Peninsula: evidence for subducted lithosphere below southern Spain. Tectonophysics 221, 13–34. doi:10.1016/0040-1951(93)90025-F

Boillot, G., Grimaud, S., Mauffret, A., Mougenot, D., Kornprobst, J., Mergoil-Daniel, J., Torrent, G., 1980. Ocean-continent boundary off the Iberian margin: a serpentinite diapir west pf the Galicia bank. Earth Planet. Sci. Lett. 48, 23–34.

Boillot, G., Froitzheim, N., 2001. Non-volcanic rifted margins, continental break-up and the onset of sea-floor spreading: some outstanding questions. Geol. Soc. London, Spec. Publ. 187, 9–30. doi:10.1144/GSL.SP.2001.187.01.02

Bois, C., Cazes, M., Hirn, A., Mascle, A., Matte, P., Montadert, L., Pinet, B., 1988. Contribution of deep seismic profiling to the knowledge of the lower crust in France and neighbouring areas. Tectonophysics 145, 253–275. doi:10.1016/0040-1951(88)90199-0

Booth-Rea, G., Ranero, C.R., Grevemeyer, I., Martínez-Martínez, J.M., 2007. Crustal types and tertiary tectonic evolution of the Alborán sea, western Mediterranean. Geochemistry, Geophys. Geosystems 8, 1–25. doi:10.1029/2007GC001639

Bouyahiaoui, B., Sage, F., Abtout, A., Klingelhoefer, F., Yelles-Chaouche, K., Schnurle, P., Marok, A., Deverchere, J., Arab, M., Galve, A., Collot, J.Y., 2015. Crustal structure of the eastern Algerian continental margin and adjacent deep basin: implications for late Cenozoic geodynamic evolution of the western Mediterranean. Geophys. J. Int. 201, 1912–1938. doi:10.1093/gji/ggv102

Burrus, J., 1984. Contribution to a geodynamic synthesis of the Provençal Basin (North-Western Mediterranean). Mar. Geol. 55, 247–269. doi:10.1016/0025-3227(84)90071-9

Burrus, J., 1989. Review of geodynamic models for extensional basins; The paradox of stretching in the gulf of Lions (Northwest Mediterranean). Bull. Soc. Geol. Fr. 2, 337–393.

Calvert, A., Sandvol, E., Seber, D., Barazangi, M., Roecker, S., Mourabit, T., Vidal, F., Alguacil, G., Jabour, N., 2000. Geodynamic evolution of the lithosphere and upper mantle beneath the Alboran region of the western Mediterranean: Constraints from travel time tomography. J. Geophys. Res. 105, 10871–10898.

Camerlenghi, A., Accettella, D., Costa, S., Lastras, G., Acosta, J., Canals, M., Wardell, N., 2009. Morphogenesis of the SW Balearic continental slope and adjacent abyssal plain, Western Mediterranean Sea. Int. J. Earth Sci. 98, 735–750. doi:10.1007/s00531-008-0354-8

Cameselle, A.L., Urgeles, R., De Mol, B., Camerlenghi, A., Canning, J.C., 2015. Late Miocene sedimentary architecture of the Ebro Continental Margin (Western Mediterranean): Implications to the Messinian Salinity Crisis. Int. J. Earth Sci. 103, 423–440. doi:10.1007/s00531-013-0966-5

Cameselle, A.L. (2015) Sedimentary processes and resulting continental margin configuration during large-sclae sea-level drawdown: The Messinian Salinity Crisis in the Western Mediterranean Sea. Doctoral dissertation, Tesis Doctoral, Univ. Barcelona).

Cameselle, A.L., R.Ranero, C., Franke, D., Barckhausen, U., 2015. The continent-ocean transition on the northwestern South China Sea. Basin Res. n/a–n/a. doi:10.1111/bre.12137

Cameselle, A.L., Urgeles, R., 2016. Large-scale margin collapse during Messinian early sea-level drawdown: The SW Valencia trough, NW Mediterranean. Basin Res. 1–20. doi:10.1111/bre.12170

Carlson, R.L., Herrick, C.N., 1990. Densities and porosities in the oceanic crust and their variations with depth and age. J. Geophys. Res. 95, 9153–9170. doi:10.1029/JB095iB06p09153

Carminati, E., Wortel, M.J.R., Spakman, W., Sabadini, R., 1998. The role of slab detachment processes in the opening of the western-central Mediterranean basins: Some geological and geophysical evidence. Earth Planet. Sci. Lett. 160, 651–665. doi:10.1016/S0012-821X(98)00118-6

Carminati, E., Lustrino, M., Doglioni, C., 2012. Geodynamic evolution of the central and western Mediterranean: Tectonics vs. igneous petrology constraints. Tectonophysics 579, 173–192. doi:10.1016/j.tecto.2012.01.026

Cavazza, W., Roure, F., Spakman, W., Stampfli, G.M., Ziegler, P. a., (Eds), 2004. The TRANSMED Atlas. The Mediterranean Region from Crust to Mantle, Springer, Berlin Heidelberg. doi:10.1007/978-3-642-18919-7

Chamot-Rooke, N., Gaulier, J.M., Jestin, F., 1999. Constraints on Moho depth and crustal thickness in the Liguro-Provençal basin from a 3D gravity inversion: geodynamic implications. Geol. Soc. London, Spec. Publ. 156, 37–61. doi:10.1144/GSL.SP.1999.156.01.04

Chertova, M. V., Spakman, W., Geenen, T., Van Den Berg, A. P., Van Hinsbergen, D.J.J., 2014. Underpinning tectonic reconstructions of the western Mediterranean region with dynamic slab evolution from 3-D numerical modeling. J. Geophys. Res. Solid Earth 119, 5876–5902. doi:10.1002/2014JB011150

Christensen, M.I., Mooney, W.D., 1995. Seismic velocity structure and composition of the continental crust - a global view. J. Geophys. Res. Earth 100, 9761–9788.

Cohen, C.R., 1980. Plate tectonic model for the Oligo-Miocene evolution of the Western Mediterranean. Tectonophysics 68, 283–311.

Collier, J.S., Buhl, P., Torne, M., Watts, A. B., 1994. Moho and lower crustal reflectivity beneath a young rift basin: results from a two-ship, wide-aperture seismic-reflection experiment in the Valencia Trough (western Mediterranean). Geophys. J. Int. 118, 159–180. doi:10.1111/j.1365-246X.1994.tb04681.x

Comas, M., Talukder, A., Woodside, J., Volkonskaya, A., 2000. V. 3. South Balearic Basin: The Palomares and Mazarrón margin. V.3.1. Seismic data. Multidisciplinary Study of Geological Processes on the North East Atlantic and Western Mediterranean Margin ICO Technical Series No. 56, UNESCO 2000, 91-95.

Contrucci, I., Nercessian, A., Béthoux, N., Mauffret, A., Pascal, G., 2001. A Ligurian (Western Mediterranean Sea) geophysical transect revisited. Geophys. J. Int. 146, 74–97. doi:10.1046/j.0956-540x.2001.01418.x

Dañobeitia, J.J., Arguedas, M., Gallart, J., Banda, E., Makris, J., 1992. Deep crustal configuration of the Valencia trough and its Iberian and Balearic borders from extensive refraction and wide-angle reflection seismic profiling. Tectonophysics 302, 37–55.

Dash, R., Spence, G., Hyndman, R., Grion, S., Wang, Y., Ronen, S., 2009. Wide-area imaging from OBS multiples. Geophysics 74, Q41–Q47. doi:10.1190/1.3223623

De Lis Mancilla, F., Stich, D., Berrocoso, M., Martín, R., Morales, J., Fernandez-Ros, A., Páez, R., Pérez-Peña, A., 2013. Delamination in the Betic Range: Deep structure, seismicity, and GPS motion. Geology 41, 307–310. doi:10.1130/G33733.1

Dean, S.M., Minshull, T.A., Whitmarsh, R.B., Louden, K.E., 2000. Deep structure of the ocean-continent transition in the southern Iberia Abyssal Plain from seismic refraction profiles : The IAM-9 transect at 40o20'N. J. Geophys. Res., 105(B3), 5859–5885, doi:10.1029/1999JB900301.

Dewey, J.F., Pitman III, W.C., Ryan, W.B.F., Bonnin, J., 1973. Plate Tectonics and the Evolution of the Alpine System Plate Tectonics and the Evolution of the Alpine System. Geol. Soc. Am. Bull. 84, 3137–3180. doi:10.1130/0016-7606(1973)84<3137

Dewey, J.F., Helman, M.L., Knott, S.D., Turco, E., Hutton, D.H.W., 1989. Kinematics of the western Mediterranean. Geol. Soc. London, Spec. Publ. 45, 265–283. doi:10.1144/GSL.SP.1989.045.01.15

Docherty, C., Banda, E., 1995. Evidence for the eastward migration of the Alboran Sea based on regional subsidence analysis: A case for basin formation by delamination of the subcrustal lithosphere? Tectonics 14, 804–818.

Doré, T., Lundin, E., 2015. Hyperextended continental margins — Knowns and unknowns. Geol. 43, 95–96. doi:10.1016/0040

Douwe J. J. van Hinsbergen, Reinoud L. M. Vissers, and W.S., 2014. Origin and consequences of western Mediterranean subduction, rollback, and slab segmentation. Tectonics 33, 393–419. doi:10.1002/tect.20125.Received

Driussi, O., Maillard, A., Ochoa, D., Lofi, J., Chanier, F., Gaullier, V., Briais, A., Sage, F., Sierro, F., Garcia, M., 2014. Messinian Salinity Crisis deposits widespread over the Balearic Promontory: Insights from new high-resolution seismic data. Mar. Pet. Geol. 1–14. doi:10.1016/j.marpetgeo.2014.09.008

Driussi, O., Briais, A., Maillard, A., 2015. Evidence for transform motion along the South Balearic margin and implications for the kinematics of the opening of the Algerian basin. Bull. Soc. géol. Fr. 186, 353–370. doi:10.2113/gssgfbull.186.4-5.353

Duggen, S., Hoernle, K., van den Bogaard, P., Rüpke, L., Phipps Morgan, J., 2003. Deep roots of the Messinian salinity crisis. Nature 422, 602–606. doi:10.1038/nature01553

Faccenna, C., Piromallo, C., Crespo-Blanc, A., Jolivet, L., Rossetti, F., 2004. Lateral slab deformation and the origin of the western Mediterranean arcs. Tectonics 23, n/a-n/a. doi:10.1029/2002TC001488

Faccenna, C., Becker, T.W., Auer, L., Billi, A., Boschi, L., Brun, J.P., Capitanio, F.A., Funiciello, F., Horvàth, F., Jolivet, L., Piromallo, C., Royden, L., Rossetti, F., Serpelloni, E., 2014. Mantle dynamics in the Mediterranean. Rev. Geophys. 52, 283–332. doi:10.1002/2013RG000444.

Fichtner, A., Villaseñor, A., 2015. Crust and upper mantle of the western Mediterranean – Constraints from full-waveform inversion. Earth Planet. Sci. Lett. 428, 52–62. doi:10.1016/j.epsl.2015.07.038

Fontboté, J.M., Guimerà, J., Roca, E., Sàbat, F., Santanach, F., Fernández-Ortigosa, F., 1990. The Cenozoic Geodynamic Evolution of the València Trough (Western Mediterranean). Rev. la Soc. Geológica España 3, 249–259.

Fowler, C. M. R. (1990), The Solid Earth: An Introduction to Global Geophysics, Cambridge University Press, Cambridge, United Kingdom, 685 pp.

Franke, D., 2013. Rifting, lithosphere breakup and volcanism: Comparison of magma-poor and volcanic rifted margins. Mar. Pet. Geol. 43, 63–87. doi:10.1016/j.marpetgeo.2012.11.003

Frizon de Lamotte, D., Saint Bezar, B., Bracène, R., Mercier, E., 2000. The two main steps of the Atlas building and geodynamics of the western Mediterranean. Tectonics 19, 740–761.

Funck, T., 2004. Crustal structure of the northern Nova Scotia rifted continental margin (eastern Canada). J. Geophys. Res. 109, B09102. doi:10.1029/2004JB003008

Funck, T., Jackson, H.R., Louden, K.E., Klingelhöfer, F., 2007. Seismic study of the transform-rifted margin in Davis Strait between Baffin Island (Canada) and Greenland: What happens when a plume meets a transform. J. Geophys. Res. Solid Earth 112, 1–22. doi:10.1029/2006JB004308

Gailler, A., Klingelhoefer, F., Olivet, J.L.J.-L., Aslanian, D., 2009. Crustal structure of a young margin pair: New results across the Liguro–Provencal Basin from wide-angle seismic tomography. Earth Planet. Sci. Lett. 286, 333–345. doi:10.1016/j.epsl.2009.07.001

Galdeano, A., Rossignol, J.C., 1977. Contribution de l'Aeromagnetisme a l'etude du Golfe de Valence (Mediterranee Occidentale). Earth Planet. Sci. Lett. 34, 85–99.

Gallart, J., Vidal, N., Dañobeitia, J.J., 1994. Lateral variations in the deep crustal structure at the Iberian margin of the Valencia trough imaged from seismic reflection methods Trough Working Group . Tectonophysics 232, 59–75.

Gallart, J., Vidal, N., Dañobeitia, J.J.J., 1995. Multichannel seismic image of the crustal thinning at the NE Iberian margin combining normal and wide angle reflection data. Geophys. Res. Lett. 22, 489. doi:10.1029/94GL03272

Gallart, J., Vidal, N., Estévez, A., Pous, J., Sàbat, F., Santisteban, C., Suriñach, E., 1997. The ESCI València Trough vertical reflection experiment: a seismic image of the crust from the NE Iberian Peninsula to the Western Mediterranean. Soc. Geol. España 8 (4), 1995: 431-448

Garcia-Castellanos D., Estrada F., Jiménez-Munt I., Gorini C., Fernàndez M., Vergés J., De Vicente R., 2009. Catastrophic flood of the Mediterranean after the Messinian Salinity Crisis. Nature 462, 778–781. doi:DOI:\t10.1038/nature08555

Gelabert, B., Sàbat, F., Rodríguez-Perea, A., 2002. A new proposal for the late Cenozoic geodynamic evolution of the western Mediterranean. Terra Nov. 14, 93–100.

Gomez, J.J., Trell, A., Pérez, P., 1976. Presencia y edad de vulcanitas en el Jurásico del Norte de Valencia (Cordillera Ibérica, España). Acta geológica hispánica 11, 1–7.

Govers, R., Wortel, M.J.R., 2005. Lithosphere tearing at STEP faults: Response to edges of subduction zones. Earth Planet. Sci. Lett. 236, 505–523. doi:10.1016/j.epsl.2005.03.022

Granado, P., Urgeles, R., Sàbat, F., Albert-Villanueva, E., Roca, E., Muñoz, J.A., Mazzuca, N., Gambini, R., 2016. Geodynamical framework and hydrocarbon plays of a salt giant: the NW Mediterranean Basin. Pet. Geosci. petgeo2015-084. doi:10.1144/petgeo2015-084

Greenroyd, C.J., Peirce, C., Rodger, M., Watts, A.B., Hobbs, R.W., 2007. Crustal structure of the French Guiana margin, West Equatorial Atlantic. Geophys. J. Int. 169, 964–987. doi:10.1111/j.1365-246X.2007.03372.x

Greenroyd, C.J., Peirce, C., Rodger, M., Watts, A.B., Hobbs, R.W., 2008. Do fracture zones define continental margin segmentation? — Evidence from the French Guiana margin. Earth Planet. Sci. Lett. 272, 553–566. doi:10.1016/j.epsl.2008.05.022

Gribble, R.F., Stern, R.J., Newman, S., Bloomer, S.H., O'Hearn, T., 1998. Chemical and Isotopic Composition of Lavas from the Northern Mariana Trough: Implications for Magmagenesis in Back-arc Basins. J. Petrol. 39, 125–154. doi:10.1093/petrology/39.1.125

Grion, S., Exley, R., Manin, M., Miao, X.G., Pica, A., Wang, Y., Granger, P.Y., Ronen, S., 2007. Mirror imaging of OBS data. First Break 25, 37–42. doi:10.3997/1365-2397.2007028

Gueguen, E., 1995. Le bassin Liguro-Provencal: un veritable ocean. Thèse de Doctorat, Université de Bretagne Occidentale, Brest, France, Example de segmentation des marges et de hiatus cinématique. Implications sur les processus d'amincissement crustal.

Gueguen, E., Doglioni, C., Fernandez, M., 1998. On the post-25 Ma geodynamic evolution of the western Mediterranean. Tectonophysics 298, 259–269. doi:http://dx.doi.org/10.1016/S0040-1951(98)00189-9

Gutscher, M.A., Dominguez, S., Westbrook, G.K., Le Roy, P., Rosas, F., Duarte, J.C., Terrinha, P., Miranda, J.M., Graindorge, D., Gailler, A., Sallares, V., Bartolome, R., 2012. The Gibraltar subduction: A decade of new geophysical data. Tectonophysics 574–575, 72–91. doi:10.1016/j.tecto.2012.08.038

Hsü, K.J., Montadert, L., Bernoulli, D., Bianca Cita, M., Erickson, A., Garrison, R.E., Kidd, R.B., Mèlieres, F., Múller, C., Wright, R., 1977. History of the Mediterranean slinity crisis. Nature 267, 495–500.

Jolivet, L., Faccenna, C., 2000. Meditterranean extension and the Africa-Eurasia collision. Tectonics 19, 1095–1106. doi:10.1029/2000TC900018

Jolivet, L., Augier, R., Robin, C., Suc, J.P., Rouchy, J.M., 2006. Lithospheric-scale geodynamic context of the Messinian salinity crisis. Sediment. Geol. 188–189, 9–33. doi:10.1016/j.sedgeo.2006.02.004

Jolivet, L., Faccenna, C., Piromallo, C., 2009. From mantle to crust: Stretching the Mediterranean. Earth Planet. Sci. Lett. 285, 198–209. doi:10.1016/j.epsl.2009.06.017

Jolivet, L., Gorini, C., Smit, J., Leroy, S., 2015. Continental Break-up and the dynamics of rifting in back-arc basins : the Gulf of Lion margin. Tectonics 34, 662–679. doi:10.1002/2014TC003570

Keen, C.E., Kay, W.A., Roest, W.R., 1990. Crustal anatomy of a transform continental margin. Tectonophysics 173. doi:10.1016/0040-1951(90)90244-3

Kennett, B.L.N., Engdah, E.R., Buland, R., 1995. Constraints on seismic velocities in the Earth from traveltimes. Geophys. J. Int 122, 108–124. doi:10.1111/j.1365-246X.1995.tb03540.x

King, S.D., Anderson, D.L., 1995. An alternative mechanism of flood basalt formation. Earth Planet. Sci. Lett. 136, 269–279. doi:10.1016/0012-821X(95)00205-Q

Korenaga, J., Kelemen, P.B., 2000. Major element heterogeneity in the mantle source of the North Atlantic igneous province. Earth Planet. Sci. Lett. 184, 251–268. doi:10.1016/S0012-821X(00)00308-3

Korenaga, J., 2004. Mantle mixing and continental breakup magmatism. Earth Planet. Sci. Lett. 218, 463–473. doi:10.1016/S0012-821X(03)00674-5

Lanaja, J.M., Querol, R., Navarro, A., 1987. Contribución de la exploración petrolífera al conocimiento de la geología de España. Inst. Geológico y Min. España 1–465.

Le Douran, S., Burrus, J., Avedik, F., 1984. Deep structure of the North-Western Mediterranean Basin: results of a two-ship seismic survey. Mar. Geol. 55, 325–345.

Leprêtre, A., Klingelhoefer, F., Graindorge, D., Schnurle, P., Beslier, M.O., Yelles, K., Déverchère, J., Bracene, R., 2013. Multiphased tectonic evolution of the Central Algerian margin from combined wide-angle and reflection seismic data off Tipaza, Algeria. J. Geophys. Res. Solid Earth 118, n/a-n/a. doi:10.1002/jgrb.50318

Levander, A., Bezada, M.J., Niu, F., Humphreys, E.D., Palomeras, I., Thurner, S.M., Masy, J., Schmitz, M., Gallart, J., Carbonell, R., Miller, M.S., 2014. Subduction-driven recycling of continental margin lithosphere. Nature 515, 253–256. doi:10.1038/nature13878

Lonergan, L., White, N., 1997. Origin of the Betic-Rif mountain belt. Tectonics 16, 504–522.

Maillard, A., Mauffret, A., Watts, A. B., Torné, M., Pascal, G., Buhl, P., Pinet, B., 1992. Tertiary sedimentary history and structure of the Valencia trough (western Mediterranean). Tectonophysics 203, 57–75. doi:10.1016/0040-1951(92)90215-R

Maillard, A., Mauffret, A., Watts, A. B., Torné, M., Pascal, G., Buhl, P., Pinet, B., 1992. Long-listening multichannel seismic profiles in the Valencia trough (Valsis 2) and the Gulf of Lions (ECORS): A comparison. Tectonophysics 203, 285–304. doi:10.1016/0040-1951(92)90215-R

Maillard, A., Mauffret, A., 1993. Structure et volcanisme de la fosse de Valence (Méditerranée nord-occidentale). Bull. la Société Géologique Fr.

Maillard, A., Mauffret, A., 1999. Crustal structure and riftogenesis of the Valencia Trough (north-western Mediterranean Sea). Basin Res. 11, 357–379. doi:10.1046/j.1365-2117.1999.00105.x

Maillard, A., Gaullier, V., Vendeville, B.C., Odonne, F., 2003. Influence of differential compaction above basement steps on salt tectonics in the Ligurian-Provençal Basin, northwest Mediterranean. Mar. Pet. Geol. 20, 13–27. doi:10.1016/S0264-8172(03)00022-9

Maillard, A., Gorini, C., Mauffret, A., Sage, F., Lofi, J., Gaullier, V., 2006. Offshore evidence of polyphase erosion in the Valencia Basin (Northwestern Mediterranean): Scenario for the Messinian Salinity Crisis. Sediment. Geol. 188–189, 69–91. doi:10.1016/j.sedgeo.2006.02.006

Maillard, A., Mauffret, A., 2013. Structure and present-day compression in the offshore area between Alicante and Ibiza Island (Eastern Iberian Margin). Tectonophysics 591, 116–130. doi:10.1016/j.tecto.2011.07.007

Maillard, A., Driussi, O., Lofi, J., Briais, A., Chanier, F., Hübscher, C., Gaullier, V., 2014. Record of the Messinian Salinity Crisis in the SW Mallorca area (Balearic Promontory, Spain). Mar. Geol. 357, 304–320. doi:10.1016/j.margeo.2014.10.001

Malinverno, A., Ryan, W.B.F., 1986. Extension in the Tyrrhenian sea and shortening in the Apennines as a result of arc migration driven by sinking of the lithosphere. Tectonics 5, 227–245.

Martí, J., Mitjavila, J., Roca, E., Aparicio, A., 1992. Cenozoic magmatism of the Valencia trough (western Mediterranean) : relationship between structural evolution and volcanism . Tectonophysics 203, 145–165.

Martin, A.K., 2006. Oppositely directed pairs of propagating rifts in back-arc basins: Double saloon door seafloor spreading during subduction rollback. Tectonics 25, 1–21. doi:10.1029/2005TC001885

Martinez Gonzalez, R.M., Lago San José, M., Valenzuela Ríos, J.I., Vaquer Navarro, R., Salas, R., 1996. El magmatismo alcalino jurásico del sector SE de la Cadena Ibérica: composición y estructura. Geogaceta.

Martinez, F., Okino, K., Ohara, Y., Reysenbach, A.L., Goffredi, S.K., 2007. Back-arc basins. Oceanography 20, 116–127.

Martínez-Loriente, S. (2013) Geophysical and geological characterization of the active structures and of the nature of the basement in the Eurasia-Africa plate boundary (SW Iberian Margin): Implications for regional geodynamics and seismic hazard assessment Doctoral dissertation, Tesis Doctoral, Univ. Barcelona).

Mauffret, A., Maillard, A., Pascal, G., Torné, M., Buhl, P., Pinet, B., 1992. Long-listening multichannel seismic profiles in the Valencia trough (Valsis 2) and the Gulf of Lions (ECORS): A comparison. Tectonophysics 203, 285–304. doi:10.1016/0040-1951(92)90215-R

Mauffret, A., Maldonado, A., Campillo, A.C., 1992. Tectonic Framework of the Eastern Alboran and Western Algerian Basins , Western Mediterranean 104–110.

Mauffret, A., Durand De Grossouvre, B., Tadeu Dos Reis, A., Gorini, C., Nercessian, A., 2001. Structural geometry in the Eastern Pyrenees and Western Gulf of Lion (Western Mediterranean). J. Struct. Geol. 23, 1701–1726. doi:10.1016/S0191-8141(01)00025-6

Mauffret, A., Frizon de Lamotte, D., Lallemant, S., Gorini, C., Maillard, A., 2004. E-W opening of the Algerian Basin (Western Mediterranean). Terra Nov. 16, 257–264. doi:10.1111/j.1365-3121.2004.00559.x

Medaouri, M., Déverchère, J., Graindorge, D., Bracene, R., Badji, R., Ouabadi, A., Yelles-Chaouche, K., Bendiab, F., 2014. The transition from Alboran to Algerian basins (Western Mediterranean Sea): Chronostratigraphy, deep crustal structure and tectonic evolution at the rear of a narrow slab rollback system. J. Geodyn. 77, 186–205. doi:10.1016/j.jog.2014.01.003

Moeller, S., Grevemeyer, I., Ranero, C.R., Berndt, C., Klaeschen, D., Sallares, V., Zitellini, N., De Franco, R., 2013. Early-stage rifting of the northern Tyrrhenian Sea Basin: Results from a combined wide-angle and multichannel seismic study. Geochemistry, Geophys. Geosystems 14, 3032–3052. doi:10.1002/ggge.20180

Moulin, M., Klingelhoefer, F., Afilhado, A., Aslanian, D., Schnurle, P., Nouze, H., Rabineau, M., Beslier, M.-O., Feld, A., 2015. Deep crustal structure across a young passive margin from wide-angle and reflection seismic data (The SARDINIA Experiment) - I. Gulf of Lion's margin. Bull. La Soc. Geol. Fr. 186, 309–330. doi:10.2113/gssgfbull.186.4-5.309

Mutter, J.C., Talwani, M., Stoffa, P.L., 1982. Origin of seaward-dipping reflectors in oceanic crustl off the Norwegian margin by subaerail sea-floor spreading. Geology 10, 353–357. doi:10.1130/0091-7613(1982)10<353

Nelson, C.H., Maldonado, A., 1990. Factors controlling late Cenozoic continental margin growth from the Ebro Delta to the western Mediterranean deep sea. Mar. Geol. 95, 419–440. doi:10.1016/0025-3227(90)90127-6

Ortí, F., Vaquer Navarro, R., 1980. Volcanismo jurásico del sector valenciano de la Cordillera Ibérica. Distribución y trama estructural. Acta Geológica Hispánica 15, 127–130.

Palomeras, I., Thurner, S., Levander, A., Liu, K., Villasenor, A., Carbonell, R., Harnafi, M., 2014. Finite-frequency Rayleigh wave tomography of the western Mediterranean: Mapping its lithospheric structure. Geochemistry, Geophys. Geosystems 15, n/a-n/a. doi:10.1002/2013GC004861

Parés, J.M., Freeman, R., Roca, E., 1992. Neogene structural development in the Valencia trough margins from palaeomagnetic data. Tectonophysics 203, 111–124. doi:10.1016/0040-1951(92)90218-U

Pascal, G., Torné, M., Buhl, P., Watts, A. B., Mauffret, A., 1992. Crustal and velocity structure of the Valencia trough (western Mediterranean), Part II. Detailed interpretation of five Expanded Spread Profiles. Tectonophysics 203, 21–35. doi:10.1016/0040-1951(92)90213-P

Pascal, G.P., Mauffret, A., Patriat, P., 1993. The ocean-continent boundary in the Gulf of Lion from analysis of expanding spread profiles and gravity modelling. Geophys. J. Int. 701–726. doi:10.1111/j.1365-246X.1993.tb04662.x

Peddy, C., Pinet, B., Masson, D., Scrutton, J., Sibuet, J.C., Warner, M.R., Lefort, J.P., Shroeder, I.J., 1989. Crustal structure of the Goban Spur continental margin , Northeast Atlantic , from deep seismic reflection profiling. J. Geol. Soc. London. 146, 427–437.

Perez-Gussinye, M., Reston, T. J., Morgan, J.P., 2001. Serpentinization and magmatism during extension at non-volcanic margins : the effect of initial lithospheric structure. Geol. Soc. London 551–576. doi:0305-8719/01/

Phillips, J.D., Forsuth, D., 1972. Plate Tectonics, Paleomagnetism, and the Opening of the Atlantic. Geol. Soc. Am. Bull. 83, 1579–1600. doi:10.1017/CBO9781107415324.004

Pitman, W.C., Talwani, M., 1972. Sea-Floor Spreading in the North Atlantic. Geol. Soc. Am. Bull. 83, 619–646.

Platt, J.P., Vissers, R.L.M., 1989. Extensional collapse of continental lithosphere, a working hypothesis for the Alborean Sea and Gibraltar Arc. Geology 17, 540–543. doi:10.1130/0091-7613(1989)017<0540:ECOTCL>2.3.CO;2

Prada, M., Sallares, V., Ranero, C.R., Vendrell, M.G., Grevemeyer, I., Zitellini, N., De Franco, R., 2014. Seismic structure of the Central Tyrrhenian basin: Geophysical constraints on the nature of the main crustal domains. J. Geophys. Res. Solid Earth 119, 52–70. doi:10.1002/2013JB010527

Prada, M., Sallares, V., Ranero, C.R., Vendrell, M.G., Grevemeyer, I., Zitellini, N., de Franco, R., 2015. The complex 3-D transition from continental crust to backarc magmatism and exhumed mantle in the Central Tyrrhenian basin. Geophys. J. Int. 203, 63–78. doi:10.1093/gji/ggv271

Ranero, C.R., Pérez-Gussinyé, M., 2010. Sequential faulting explains the asymmetry and extension discrepancy of conjugate margins. Nature 468, 294–9. doi:10.1038/nature09520

Rehault, J.-P., Boillot, G., Mauffret, A., 1984. The western mediterranean basin geological evolution. Mar. Geol. 55, 447–477.

Reston, T.J., Pennell, J., Stubenrauch, A., Walker, I., Perez-Gussinye, M., 2001. Detachment faulting, mantle serpentinization, and serpentinite-mud volcanism beneath the Porcupine Basin , southwest of Ireland. Geol. Soc. Am. 29, 587–590.

Reston, T.J., Gaw, V., Pennell, J., Klaeschen, D., Stubenrauch, A., Walker, I., 2004. Extreme crustal thinning in the south Porcupine Basin and the nature of the Porcupine Median High: implications for the formation of non-volcanic rifted margins. J. Geol. Soc. London. 161, 783–798. doi:10.1144/0016-764903-036

Reston, T.J., 2007. The formation of non-volcanic rifted margins by the progressive extension of the lithosphere: the example of the West Iberian margin. Geol. Soc. London, Spec. Publ. 282, 77–110. doi:10.1144/SP282.5

Reston, T.J., Pérez-Gussinyé, M., 2007. Lithospheric extension from rifting to continental breakup at magma-poor margins: Rheology, serpentinisation and symmetry. Int. J. Earth Sci. 96, 1033–1046. doi:10.1007/s00531-006-0161-z

Reston, T.J., 2009. The structure, evolution and symmetry of the magma-poor rifted margins of the North and Central Atlantic: A synthesis. Tectonophysics 468, 6–27. doi:10.1016/j.tecto.2008.09.002

Roca, E., Desegaulx, P., 1992. Analysis of the geological evolution and vertical movements in the Valencia Trough area , western Mediterranean. Mar. Pet. Geol. 9.

Roca, E., 1996. La evolución geodinámica de la Cuenca Catalano-Balear y áreas adyacentes desde el Mesozoico hasta la actualidad. Acta Geol. Hisp. 29, 3–25.

Roca, E., Sans, M., Cabrera, L., Marzo, M., 1999. Oligocene to Middle Miocene evolution of the central Catalan margin (northwestern Mediterranean). Tectonophysics 315, 209–233. doi:10.1016/S0040-1951(99)00289-9

Rodriguez-Perea, A. , Ramos-Guerrero, E. , Pomar, L., Paniello, X., Obradorr, A. , Martí, J., 1987. El triásico de las Baleares. Cuad. Geol. Ibérica 11, 295–321.

Rollet, N., De, J., Beslier, M., Guennoc, P., Re, J., Sosson, M., Truffert, C., 2002. Back arc extension, tectonic inheritance, and volcanism in the Ligurian Sea, Western Mediterranean. Tectonics 21, doi: 10.1029/2001TC900027

Rosenbaum, G., Lister, G.S., Duboz, C., 2002. Reconstruction of the tectonic evolution of the western Mediterranean since the Oligocene. J. Virtual Explor. 8. doi:10.3809/jvirtex.2002.00053

Sàbat, F., Roca, E., Muñoz, J.A., Vergés, J., Santanach, P., Sans, M., Massana, E., Estévez, A., Santisteban, C., 1997. Role of extension and compression in the evolution of the eastern margin of Iberia: the ESCI-València Trough seismic profile. Rev. Soc. Geol. España, 8 (4), 1995: 431-448

Sàbat, F., Gelabert, B., Rodríguez-Perea, A., Giménez, J., 2011. Geological structure and evolution of Majorca: Implications for the origin of the Western Mediterranean. Tectonophysics 510, 217–238. doi:10.1016/j.tecto.2011.07.005

Sage, F., Pontoise, B., Mascle, J., Basile, C., Arnould, L., 1997. Crustal structure and ocean–continent transition at marginal ridge: the Côte d'Ivoire–Ghana marginal ridge. Geo-Marine Lett. 17, 40–48. doi:10.1007/PL00007206

Salas, R., Casas, A., 1993. Mesozoic extensional tectonics, stratigraphy and crustal evolution during the Alpine cycle of the eastern Iberian basin. Tectonophysics 228, 33–55. doi:10.1016/0040-1951(93)90213-4

Salas, R., Guimerà, J., Mas, R., Martín-Closas, C., Meléndez, A., Alonso, A., 2001. Evolution of the Mesozoic Central Iberian Rift System and its Cainozoic inversion (Iberian Chain). In: P.A. Ziegler, W. Cavazza, A.H.F. Robertson, S. Crasquin-Soleau (eds), Pre-Tethys Memoir 6: Peri-Tethyan Rift/Wrench Basins and Passive Margins. Mém. Mus. natn. Hist. nat., 186 : 145-185. Paris ISBN : 2-85653-528-3.

Sallarès, V., Martínez-Loriente, S., Prada, M., Gràcia, E., Ranero, C., Gutscher, M.A., Bartolome, R., Gailler, A., Dañobeitia, J.J., Zitellini, N., 2013. Seismic evidence of exhumed mantle rock basement at the Gorringe Bank and the adjacent Horseshoe and Tagus abyssal plains (SW Iberia). Earth Planet. Sci. Lett. 365, 120–131. doi:10.1016/j.epsl.2013.01.021

Sallarès, V., Meléndez, A., Prada, M., Ranero, C.R., McIntosh, K., Grevemeyer, I., 2013. Overriding plate structure of the Nicaragua convergent margin: Relationship to the seismogenic zone of the 1992 tsunami earthquake. Geochemistry, Geophys. Geosystems 14, 3436–3461. doi:10.1002/ggge.20214

Schettino, A., Turco, E., 2006. Plate kinematics of the Western Mediterranean region during the Oligocene and Early Miocene. Geophys. J. Int. 166, 1398–1423. doi:10.1111/j.1365-246X.2006.02997.x

Seber, D., Barazangi, M., Ibenbrahim, A., Demnati, A., 1996. Geophysical evidence for lithospheric delimination beneth the Alboran Sea and Rif-Betic mountains. Nature 379, 785–779.

Seranne, M., 1999. The Gulf of Lion continental margin (NW Mediterranean) revisited by IBS: an overview. Geol. Soc. London, Spec. Publ. 156, 15–36. doi:10.1144/gsl.sp.1999.156.01.03

Smith, A.G., 1971. Alpine deformation and the oceanic areas of the Tethys, Mediterranean, and Atlantic. Bull. Geol. Soc. Am. 82, 2039–2070. doi:10.1130/0016-7606(1971)82[2039:ADATOA]2.0.CO;2

Spakman, W., Wortel, M.J.R., Spakman, W., Wortel, R., 2004. Tomographic View on Western Mediterranean Geodynamics Chapter 2 A Tomographic View on Western Mediterranean Geodynamics 31–52.

Tandon, K., Lorenzo, J.M., de La Linde Rubio, J., 1998. Timing of rifting in the Alboran Sea basin - correlation of borehole (ODP Leg 16 1 and Andalucia A- 1) to seismic reflection data: implications for basin formation. Mar. Geol. 144200403, 275–294.

Thurner, S., Palomeras, I., Levander, A., Carbonell, R., Lee, C.-T., 2014. Ongoing lithospheric removal in the western Mediterranean: Evidence from Ps receiver functions and thermobarometry of Neogene basalts (PICASSO project). Geochemistry Geophys. Geosystems 15, 1113–1127. doi:10.1002/2013GC005124

Torné, M., Banda, E., 1992. Crustal thinning from the Betic Cordillera to the Alboran Sea. Geo-Marine Lett. 12, 76–81. doi:10.1007/BF02084915

Torné, M., Pascal, G., Buhl, P., Watts, A.B., Mauffret, A., 1992. Crustal and velocity structure of the Valencia trough (western Mediterranean), Part I. A combined refraction/ wide-angle reflection and near-vertical reflection study. Tectonophysics 203, 1–20.

Turcotte, D. L., and Schubert, G. (2002), Geodynamics, Second Edition, Cambridge University Press, Cambridge, United Kingdom, 456 pp.

Urgeles, R., Camerlenghi, A., Garcia-Castellanos, D., De Mol, B., Garcés, M., Vergés, J., Haslam, I., Hardman, M., 2011. New constraints on the Messinian sealevel drawdown from 3D seismic data of the Ebro Margin, western Mediterranean. Basin Res. 23, 123–145. doi:10.1111/j.1365-2117.2010.00477.x

Van Hinsbergen, D.J.J., Vissers, R.L.M., Spakman, W., 2014. Origin and consequences of western Mediterranean subduction, rollback, and slab segmentation. Tectonics 33, 393–419. doi:10.1002/2013TC003349

Vázquez, J.T., Alonso, B., Fernández-Puga, M.C., Gómez-Ballesteros, M., Iglesias, J., Palomino, D., Roque, C., Ercilla, G. and Díaz-del-Río, V., 2015. Seamounts along the Iberian Continental Margins. Boletín Geológico y Minero, 126 (2-3): 483-514 ISSN: 0366-0176

Vegas, R., 1992. The Valencia trough and the origin of the western Mediterranean basins. Tectonophysics 203, 249–261. doi:10.1016/0040-1951(92)90226-V

Vergés, J., Sàbat, F., 1999. Constraints on the Neogene Mediterranean kinematic evolution along a 1000 km transect from Iberia to Africa. Geol. Soc. London, Spec. Publ. 156, 63–80. doi:10.1144/GSL.SP.1999.156.01.05

Vergés, J., Fernàndez, M., 2012. Tethys–Atlantic interaction along the Iberia–Africa plate boundary: The Betic–Rif orogenic system. Tectonophysics 579, 144–172. doi:10.1016/j.tecto.2012.08.032

Vidal, N., 1995. Estructura Litosférica en el Margen Oriental de la Península Ibérica a partir de datos de Sísmica de Reflexión Vertical y de Gran Ángulo (Doctoral dissertation, Tesis Doctoral, Univ. Barcelona).

Vidal, N., Gallart, J., Dañobeitia, J., 1997. Contributionof the ESCI-València Trough wide-angle data to a crustal transect in the NE Iberian margin. Rev. la Soc. Geológica España 8, 417–429.

Vidal, N., Gallart, J., Dañobeitia, J.J., Neus Vidal, Josep Gallart, J.J.D., 1998. A deep seismic crustal transect from the NE Iberian Peninsula to the Esatern Mediterranean. J. Geophys. Res. 103, 12381. doi:10.1029/98JB00076

Villaseñor, A., Chevrot, S., Harnafi, M., Gallart, J., Pazos, A., Serrano, I., Córdoba, D., Pulgar, J.A., Ibarra, P., 2015. Subduction and volcanism in the Iberia-North Africa collision zone from tomographic images of the upper mantle. Tectonophysics 663, 238–249. doi:10.1016/j.tecto.2015.08.042

Wang, Y., 2003. Multiple subtraction using an expanded multichannel matching filter. Geophysics 68, 346–354.

Wang, X., Xia, C., Liu, X., 2012. A case study: Imaging OBS multiples of South China Sea. Mar. Geophys. Res. 33, 89–95. doi:10.1007/s11001-012-9148-2

Watts, A.B., Torné, M., Buhl, P., Mauffret, A., Pascal, G., Pinet, B., 1990. Evidence for reflectors in the lower continental crust before rifting in the Valencia trough. Nature 348, 631–635.

Watts, A. B., Torné, M., 1992. Subsidence history, crustal structure, and thermal evolution of the Valencia Trough: A young extensional basin in the western Mediterranean. J. Geophys. Res. 97, 20021. doi:10.1029/92JB00583

Watts, A.B., Platt, J.P., Buhl, P., 1993. Tectonic evolution of the Alboran Sea basin. Basin Res. 5, 153–177. doi:10.1111/j.1365-2117.1993.tb00063.x

Wessel, P., W. H. F. Smith, R. Scharroo, J. Luis, and F. Wobbe, Generic Mapping Tools: Improved Version Released, EOS Trans. AGU, 94(45), p. 409-410, 2013. doi:10.1002/2013EO450001.

Wessel, P., and W. H. F. Smith, New, improved version of Generic Mapping Tools released, EOS Trans. AGU, 79(47), p. 579, 1998. doi:10.1029/98EO00426.

Wessel, P., and W. H. F. Smith, New version of the Generic Mapping Tools released, EOS Trans. AGU, 76(33), 329, 1995. doi:10.1029/95EO00198.

Wessel, P., and W. H. F. Smith, Free software helps map and display data, EOS Trans. AGU, 72(41), 445–446, 1991. doi:10.1029/90EO00319.

White, R., McKenzie, D., 1989. Magmatism at rift zones: The generation of volcanic continental margins and flood basalts. J. Geophys. Res. 94, 7685. doi:10.1029/JB094iB06p07685

White, R.S., McKenzie, D., O'Nions, R.K., 1992. Oceanic crustal thickness from seismic measurements and rare earth element inversions. J. Geophys. Res. 97, 19683. doi:10.1029/92JB01749

White, R.S., Smith, L.K., Roberts, A. W., Christie, P. a F., Kusznir, N.J., Roberts, A. M., Healy, D., Spitzer, R., Chappell, A., Eccles, J.D., Fletcher, R., Hurst, N., Lunnon, Z., Parkin, C.J., Tymms, V.J., 2008. Lower-crustal intrusion on the North Atlantic continental margin. Nature 452, 460–464. doi:10.1038/nature06687

Whitmarsh, R.B., Manatschal, G., Minshull, T. a, 2001. Evolution of magma-poor continental margins from rifting to seafloor spreading. Nature 413, 150–154. doi:10.1038/35093085

Wortel, M.J., Spakman, W., 2000. Subduction and slab detachment in the Mediterranean-Carpathian region. Science 290, 1910–1917. doi:10.1126/science.290.5498.1910

Yilmaz, O., (2001). Seismic data processing. Society of exploration geophysicists, ed.:Doherty, S., Tulsa, US, 522 pp.

Zeck, H.P., 1997. Mantle peridotites outlining the Gibraltar Arc — centrifugal extensional allochthons derived from the earlier Alpine, westward subducted nappe pile. Tectonophysics 281, 195–207. doi:10.1016/S0040-1951(97)00067-X

Zelt, C.A., Forsyth, D.A., 1994. Modeling wide-angle seismic data for crustal structure: J. Geophys. Res. 99.

Ziegler, P.A., 1992. European Cenozoic rift system. Tectonophysics 208, 91–111. doi:10.1016/0040-1951(92)90338-7

Annex

Figure index

Chapter 1: Introduction

Chapter 2: Motivation and Objectives

Chapter 3: Methods

Chapter 5: Data processing and modelling

Chapter 6: Valencia Trough Basin

Chapter 8: Algero-Balearic Basin

Table index

Chapter 4: Dataset and acquisition parameters

Chapter 5: Data processing and modelling